AD-A274 326

Sound Speed, Reflectivity, Absorption, and Thermal Diffusivity Measurements in Arctic Ice in 1990

by G.R. Garrison, K.L. Williams, P.D. Mourad, R.E. Francois, T. Wen, and W.J. Felton

S DTIC
ELECTE
DEC 3 0 1993
A

Technical Report
APL-UW TR 9208
November 1993

93-31188

93 12 23 043

Sound Speed, Reflectivity, Absorption, and Thermal Diffusivity Measurements in Arctic Ice in 1990

by G.R. Garrison, K.L. Williams, P.D. Mourad, R.E. Francois, T. Wen, and W.J. Felton

Accesion For		
NTIS CRA&I		✓
DTIC TAB		☐
U announced		☐
Justification		
By		
Distribution /		
Availability Codes		
Dist	Avail and/or Special	
A-1		

Technical Report
APL-UW TR 9208
November 1993

DTIC QUALITY INSPECTED 3

Applied Physics Laboratory   University of Washington
1013 NE 40th Street   Seattle, Washington 98105-6698

Acknowledgment

This work was supported by the Office of Naval Technology (now ONR-T).

ABSTRACT

Detailed measurements of internal properties of Arctic ice were made in Spring 1990 to relate acoustic properties to the physical properties of the ice. This report presents the procedures, analyses, and results of those studies. Some basic parameters measured in previous field studies were remeasured; consistency between individual experiments strengthens our confidence in the results and the techniques used. Novel techniques were used to measure properties of growing ice, which was later cored, submerged, and remeasured. Results reported here have been summarized in the open literature [Williams et al., *J. Acoust. Soc. Am.*, *92*, 2075, 1992]. The basic data and their processing are described here in detail.

In the ice-growth and submergence study, a 2-m-square hole was cut though the ice canopy. Strings of hydrophones and thermistors were then suspended vertically in the hole, and the water froze around them. Frequent monitoring of ice temperature and the receipt of sound pulses from below, along with salinities determined from ice cores obtained a short distance away, gave insight into the freezing process and the formation of a skeletal layer above the ice/water interface. Periodic measurements of the reflectivity of the growing ice at 37–150 kHz gave further information on the skeletal structure. The sound speed in the skeletal layer varied from that of the water at the ice/water interface to that of bulk ice at about 3 cm into the ice. Absorption of sound (in decibels per meter) was about three times greater near the interface, decreasing to that for bulk ice at 15–20 cm into the ice. When an ice block was cored from the new ice and forced downward 1 m, it warmed to the water temperature in about 3 days. During this time, sound speed, absorption, and reflectivity were monitored and showed effects of the added pressure and higher temperature. The average thermal diffusivity of the ice was between 0.0015 and 0.0035 cm^2/s, with the lower values being obtained when more of the ice was at a temperature near the melting point.

TABLE OF CONTENTS

I. EXECUTIVE SUMMARY

A. Sound Speed in the Ice

An area of flat Arctic ice in the Beaufort/Chukchi Sea was selected for several experiments.

1. Average sound speeds for the ice canopy were obtained by reflecting sound off the ice from below and timing the interval between the echoes from the lower and upper surfaces. Using three different transducers, at different times, we determined the average vertical sound speed in the canopy to be 3842 m/s, with 1% accuracy.

2. In another experiment, sound was transmitted upward from below the ice and received by hydrophones embedded at various depths within the ice. Accurate timing of the received pulse gave a sound speed profile in the ice, with a definitely slower sound speed in the skeletal layer. In the bottom 15 cm, the average sound speed was about 3300 m/s compared with an average speed of 3820 m/s in the canopy.

3. For an independent measurement, an ice core was taken nearby and sawed into sections. The temperature of each section was measured by inserting a probe into a drilled hole. The sound speed in each section was determined by timing the travel of short pulses of 800-kHz sound through the section. Salinities were determined by melting the ice and measuring the conductivity of the water. These measurements gave both a directly measured sound speed profile and one calculated from measured temperatures and salinities using theory involving the brine volume. There was general agreement between measurement and theory.

4. The most accurate sound speed profile was obtained by suspending strings of thermistors and hydrophones in an open hole and transmitting sound upward to the hydrophones from below as the sensors were successively frozen into the ice. Temperatures were also recorded. Time intervals between arrivals at hydrophones a known distance apart gave detailed sound speed profiles as freezing progressed until the ice was 42 cm thick. By choosing a hydrophone pair that bracketed the undersurface of the freezing ice, we were able to measure sound speed for several thicknesses of new ice, primarily skeletal layers. The sound speed in the lower 3 cm of new ice increased smoothly from the water sound speed to an average value for the ice canopy.

5. Measurements continued as a block of ice containing the sensors was cored out and pushed 1 m downward. The ice gradually warmed to the water temperature in 4 days. Although the sound speed increased in the lower 5 cm of the ice, it decreased in the remainder of the ice as its temperature increased. The sound speed peaked 8–10 cm above the bottom because the increased pressure forced water into the brine channels and reduced the bulk salinity.

6. In summary, the average sound speed in a 200-cm-thick ice canopy was 3820 ± 20 m/s. In comparison, measurements in 1988 in a 140-cm-thick canopy gave 3670 ± 30 m/s. In the lower 3 cm, which is primarily skeletal layer, the speed dropped off, gradually approaching the speed in the water below.

B. Ice Canopy Reflectivity

1. The 1990 measurements near normal incidence verify that the reflectivity of the bottom of the canopy decreases at higher frequencies (10–300 kHz) as shown in the 1988 measurements. Below 20 kHz the reflectivity appeared to approach the value (0.41) calculated for typical average (bulk) properties of the ice. For higher frequencies, it decreased to about 0.05 at 200–300 kHz.

2. There appear to be interference effects between reflections from the "top" and bottom of the skeletal layer which cause anomalously low values near 50 kHz and high ones near 100 kHz. These are discussed in Ref. 1 (Section VII.B). If we assume from our measurements that the sound speed in the skeletal layer averages 2000 m/s, the layer thickness needed to give the observed interference is 1 cm, which is about the thickness of fragile ice observed in this skeletal layer.

3. A theoretical calculation discussed in Refs. 1 and 2 predicts that the sound speed profile measured here would produce the measured reflectivities.

C. Absorption of Sound in the Ice

We used the frequency and temperature dependence of sound absorption in ice given by McCammon and McDaniel[3] for horizontal transmissions:

$$\alpha = k f (-6/T)^{2/3} \quad \text{dB/m} , \tag{1}$$

where their k is 0.06, f is frequency in kilohertz, and T is temperature in degrees Celsius. Our analysis has been directed toward determining a value of k for vertical transmissions through the canopy using in-situ measurements. We made three different measurements of absorption.

1. Reflections obtained from the lower and upper surfaces of the ice canopy with three different transducers gave values of 0.18, 0.24, and 0.12 for k. These values average 0.18, compared with the value of 0.19 ± 0.02 measured in 1988.

2. In recordings of the intensity at hydrophones in the ice, k varied from 0.3 in the solid portion of the 42-cm-thick ice to 1–3 at the lower interface. The variation of k near the interface indicates that Eq. (1) is not valid for the skeletal layer. The total absorption in the skeletal layer was 4–6 dB (1–2 dB/cm), considerably higher than that for solid ice.

3. After the same ice was submerged and slowly warmed by the surrounding seawater, the k measured for the solid portion was 0.31 ± 0.11. This fairly constant k means

that the absorption decreased with increasing temperature about as assumed in Eq. (1). This is considerably higher than the average k of 0.18 measured for the ice canopy. The ice in the canopy may have hardened with time, causing the absorption to decrease correspondingly.

D. Thermal Diffusivity of the Ice

The thermal diffusivity in 2-m-thick ice of varying temperature averaged between 0.0015 and 0.0035 cm². This spread is thought to be due to the temperature variation in the ice. For ice only slightly above the freezing point, the measured diffusivity was low; i.e., such ice is a poor conductor of heat.

II. INTRODUCTION

Acoustic and physical measurements of Arctic sea ice were made in the spring of 1990 at an ice camp in the Beaufort/Chukchi Sea. The study was primarily of the acoustic properties of the ice canopy. The variation of sound speed and absorption in the ice with depth was measured in detail. The acoustic reflectivity of the underside of the canopy was measured at several locations, and the distributions of ice temperature and salinity in blocks from the canopy were monitored. Cylindrical ice blocks were cored out and submerged, and their temperature and acoustic properties were monitored to study the effect of the skeletal layer properties on sound speed, reflectivity, and absorption.

Many of the measurements were similar to those made during a previous study in 1988.[1] As a new feature of the 1990 experiment, strings of hydrophones and strings of thermistors were suspended in a newly opened hole, where they were gradually encompassed by the ice as the hole froze over and the ice thickened. Monitoring the thermistors gave temperature profiles in the ice. Monitoring the transmissions from a transducer suspended below the refreezing hole gave sound speed and absorption profiles. After the ice froze to a thickness of 42 cm, a cylindrical block was cored from the new ice and forced downward 1 m. The resulting warming of the block and accompanying changes in acoustic properties were monitored for 4 days. Throughout the experiment, acoustic pulses at 37–150 kHz were transmitted and received from below to measure the reflectivity of the ice.

Many of the studies reported here were summarized in a recent paper.[4] This report describes the basic data and their processing in detail.

Figures and tables appear after the text and are paginated according to content. For example, Figures 1 and 2 appear on page F1,2, etc.

UNIVERSITY OF WASHINGTON • APPLIED PHYSICS LABORATORY

III. TRANSDUCERS

Three different transducers were employed during the experiment to give independent checks on the results and provide some variations in the transducer beam pattern.

A. ITC 1042 Transducer

The ITC 1042, a 2.5-cm-diameter sphere with a nearly omnidirectional beam pattern, was calibrated during the experiment by measuring the reflections from a level air/water interface. This interface was obtained by installing a flat metal pan with a diameter about the same as that of the ice block, open end down, just below the ice and then filling the pan with air. This was done on 28 March after the ice-block reflection measurements were completed. Pans 60 and 40 cm in diameter were installed in turn, and their reflections measured while the transducer was moved in each direction until the return dropped off, to assure we had obtained the maximum at normal incidence. For the 60-cm pan, there was enough variation to plot a pattern and verify the maximum. For the 40-cm pan, however, only six measurements were taken at each frequency. We made a few informal plots to see if the returns showed a maximum. In some cases, the falloff on one side was not obtained because we did not move the transducer far enough. However, the flatness at the top indicated that we were near the maximum.

The calibration number, CAL, is defined as the sum of the transmitting response and the receiving sensitivity. For reflection from a circular water/air interface, it is calculated by

$$CAL = 20 \log E/V + 40 \log R + 2\alpha R - G - 20 \log A \, f/c \, , \qquad (2)$$

where E/V is the ratio of received to transmitted amplitudes, R is the range, α is the absorption coefficient of water, G is the gain of the receiving system, A is the area of the block face, f is the frequency, and c is the sound speed in the water. The last term is the target strength of the circular area. The received amplitude was read as an average in the steady-state portion of the return. The gain was 40 dB for the preamplifier plus 20 dB for the master gain.

The return from the bottom of the inverted, air-filled pan was read at several positions of the transducer to give variations in incident angle. The peak was fairly well defined, and the results for the 40- and 60-cm pans were in good agreement, differing by no more than 0.5 dB. The values selected for CAL are plotted in Figure 1 along with the 1988 field values and the values obtained during calibrations in Lake Union (Seattle) in both years. Compared with 1988, the 1990 values are 2 dB higher at the lower frequencies and 1 dB higher at 60 and 80 kHz. (The 1988 field experiment used no frequencies above 80 kHz with this transducer.) The Lake Union values are much lower, probably because of the higher temperatures.

TR 9208   5

B. Platter Transducer

The platter transducer was a narrowbeam, multielement array arranged within a 28-cm-diameter disk. The beam patterns are shown in Ref. 1.

In calibrating the platter, we sometimes used a K&H filter, which was calibrated using a strong ac signal with very little noise. Table 1 shows the amount that should be added to the signal to correct for the effect of the filter, based on the average of two separate measurements.

The platter was calibrated on 19 March by stationing it below a newly opened 2-m-square hole and making five sets of measurements. After taking an average at each frequency, we applied the filter correction and computed the *CAL* values shown in Table 2 with

$$CAL = 20\log V/T + 20\log 2R + 2\alpha R - G + \text{Filter Loss} . \tag{3}$$

The platter was also calibrated using the spherical reflector described in Section III.E. One set of measurements was taken directly below the sphere at a range of 6.6 m. With the sphere target strengths determined in 1990 (shown in Figure 4), we determined the *CAL* values given in Table 3 using the equation

$$CAL = 20\log V/T + 40\log R + 2\alpha R - G - TS , \tag{4}$$

where *TS* is target strength.

Similar measurements of the sphere's target strength were made in 1988. However, they were unsatisfactory, especially at the higher frequencies. For better comparison between 1988 and 1990, we used the 1990 sphere target strengths in the 1988 calibration measurements of the sphere to determine the *CAL* values shown in Table 4.

The platter calibration values in both years and the values selected for 1990 are compared in Table 4 and plotted in Figure 2. The results obtained with the sphere are considered the most reliable because they were observed at the same time as the ice reflections. Unfortunately, the values obtained using the air/water interface are much lower, and would result in unrealistically high reflection coefficients.

C. 22 × 22 Transducer

This transducer consisted of an array of 22 × 22 elements built at APL from an 8.26-cm-square ceramic plate. When potted in polyurethane and mounted for use, it had a beamwidth (between −3 dB points, one-way) of 8° at 100 kHz. The beam patterns are shown in Ref. 1.

The transducer was calibrated in the field on 22 March with the spherical reflector described in Section III.E. The returns from the sphere were measured on the same pings used to measure surface reflections. About half the records were made with a K&H filter; its effect was shown in Table 1.

The results of the 22×22 calibrations are listed in Table 5 and plotted in Figure 3. Runs 1–3 agreed very well, whereas Run 4 was much lower, at least at the higher frequencies; it was also noisier. For these reasons, it was not included in averaging the *CAL* values to obtain those to use in the 1990 analysis. When the 22×22 transducer was mounted on an arm, we used the "on-arm" values listed in Table 5.

D. 22×22 Transducer on Arm

For some of the measurements, the 22×22 transducer was mounted on a hinged arm that could be passed through a hole in the ice. A wire was then used to pull the arm to a horizontal position about 1 m below the ice. Turning a hinged handle above the ice caused the transducer to move along a 3.6-m-diameter circle. Acoustic pulses were transmitted upward, and the returns received at the transducer and passed by cable to the recording station.

In preparation for these measurements, the transducer was calibrated in the field under the same conditions and with the same accessory equipment used in the reflection measurements. To do so, the apparatus was lowered through a large open hole which had been prepared for other purposes, and the arm suspended and turned so that the transducer projected sound directly upward toward the air/water interface. Pulses 0.5 ms long were projected at five frequencies, and the returns recorded. The set was then repeated. The results are shown in Table 6.

The *CAL* values calculated at each frequency with

$$CAL = 20\log V/T + 20\log 2R + 2\alpha R - G \qquad (5)$$

are plotted on Figure 3 for comparison with the 22×22 calibrations using a sphere. The on-arm values are 5–7 dB lower except at the higher frequencies, 160 and 220 kHz, where the difference is much greater. The cause of the discrepancy is discussed in Section VI.C.

E. Spherical Reflector

To calibrate the transducers, a 20-cm-diameter stainless steel sphere filled with Freon TF was placed 3.7 m below the ice near the center of the measurement area, where its reflection was measured whenever ice reflections were measured.

Some sphere returns were filtered with a K&H filter, which lowered the return by the following amounts:

7.3 dB at   20 kHz
7.6 dB at   30 kHz
7.2 dB at   40 kHz
6.2 dB at   60 kHz
6.2 dB at   80 kHz
6.2 dB at 100 kHz
7.0 dB at 120 kHz.

The target strength of the sphere was determined using the ITC 1042 transducer and the relation

$$TS = 20\log E/V - CAL + 40\log R + 2\alpha R - G .$$ (6)

Returns from the sphere were measured at the same time as those from the air-filled calibration pans as well as at other times. The TS values selected for 1988 and 1990 are shown in Figure 4. They are in fair agreement, except that the 1988 results drop off at 60–80 kHz. The values selected in 1988 were influenced by the calibration measurements in Seattle, which dropped off at the higher frequencies. In the 1990 measurements, the target strength increased for frequencies up to 100 kHz.

IV. ONE-WAY TRANSMISSION EXPERIMENT

This experiment consisted of positioning a sound source beneath the ice, placing a receiver in a shallow hole in the top of the ice above it, and measuring the travel time and intensity of the sound transmitted from the source to the receiver. By deepening the hole, the distance the sound traveled through the ice was decreased. By comparing the transit time with the actual separation between the source and the receiver, and knowing the depth of the ice, we were able to calculate the sound speed profile in the ice.

For these measurements, the 22×22 transducer was supported on three lines in a 30-m triad (an equilateral triangle with each vertex 30 m from the center) as shown in Figure 5. We made three sets of measurements, transmitting 0.2 ms pulses from the 22×22 transducer at frequencies of 30, 40, 60, 80, 100, 120, 160, and 200 kHz. For set 1 we used a Sipre corer to core out the ice one increment at a time. Snapping off the core was difficult. A special reamer was used to smooth out the bottom, and a high-powered vacuum cleaner to clean out the cuttings; however, the hose was small and chunks of ice often plugged the end. A bottle of compressed air was helpful for blowing loose the ice in the bottom of the hole so the vacuum could pick it up.

The signal was received on an ITC 1042 transducer mounted inside an aluminum tube about 3 m long, with the transducer flush with the end of the tube. Unfortunately, slight downward pressure on the tube increased the received amplitude, and slight movement of the transducer in the hole changed it considerably. For acoustic coupling, we tried first grease and then water. Water coupling gave varied results, some higher, some lower. Nothing seemed to work well. We managed to get down about 1 m with a dry hole. We started a second hole alongside the first with the intention of using water as a coupler. We tried at two depths in this hole, but the data looked poor.

The next day, we drilled the previous hole through and took a measurement with the transducer in the water. We then started two holes about 1 m apart at a different location. At each depth increment, we reamed the hole to obtain a smooth bottom and then used a small amount of water for coupling. When both holes were about 1 m deep, we drilled one on through to provide a source of water for the other. Hole preparation consisted of (1) augering, (2) using the Sipre corer to give a flat surface near the periphery, and (3) reaming out the bottom with a special tool.

A. Sound Speed

We expected the timing measurements would be accurate despite the coupling problems. For each incremental lowering of the receiver, we compared depth-scale readings to get the depth increment. At each frequency, we timed the same feature of the first positive peak of the return. We then took each depth increment and divided it by the time difference to get the sound speed.

At each receiver depth, sound speed measurements were made at all eight frequencies (30, 40, 60, 80, 100, 120, 160, and 200 kHz). The data showed good agreement. In some cases, however, the data for the lowest frequency (30 kHz) and the two highest frequencies (160 and 200 kHz) were omitted because the distortion was so great that we could not determine the time of a selected feature in the return. Measurements at four different transducer positions in the bottom of the hole gave consistent travel times. We then averaged the sound speeds for all frequencies that gave a usable signal, usually five or six of the eight available.

The sound speed profiles obtained from the three sets of measurements are listed in Table 7 and plotted in Figure 6. The deepest reading, for set 2, was taken 7 cm above the bottom. The sound speed appears to decrease at the bottom.

Figure 6 shows much variation with little correspondence between runs. We think the largest error might be an undetected change in the depth of the transmitting transducer between data sets. (There is some indicatio.. of such a change during a few of the sets.) This change could be caused by currents which, when strong, would lift the transducer slightly. A 2-cm vertical variation would account for most of the scatter.

The dropoff in sound speed at the bottom of the ice appears to be valid because two consecutive points show a decrease.

B. Absorption

The data did not show the expected increase in intensity as the receiving transducer was placed lower and lower in the ice. We looked first at steady-state averages, then at the first cycle only, and finally at the first few cycles—and in each attempt found no satisfactory results. It appears that much of the sound was lost when it entered the ice. Within the ice the intensity fluctuated greatly, with the average about the same at all distances into the ice. Apparently the coupling in the bottom of the hole was poor and very erratic. We therefore consider these absorption measurements to be invalid.

V. ICE BLOCK REFLECTIONS

During some earlier measurements of reflections from a submerged ice block,[5] there was some indication that the reflectivity changed in the first minutes after submersion. One purpose of the 1990 experiment was to record this change.

A. Time Series at Normal Incidence

An ice block 58 cm in diameter was cored out of the canopy on 26 March and depressed 1.31 m. We estimated that its center was at frame position N20/E30. We took reflection measurements using the ITC 1042 transducer as soon as possible. Unfortunately, the transducer was located 0.7 m (1.4°) from the block's center, and the readings were low. It took 17 minutes to move the transducer around and find the maximum response, at N22/E27. A set of readings at normal incidence was then taken at all frequencies and repeated 14 times during the next 21 hours. Figure 7 shows the target strengths computed at each frequency.

Some cancellation of the signal was observed at 40 and 120 kHz. After one or two cycles, the amplitude dropped and then rose again at the end of the pulse. This interference is believed to be between returns from the bottom of the ice and from about 1.3 cm into the skeletal layer (1/4 wavelength at 40 kHz and 3/4 wavelength at 120 kHz).

One and one-half hours after the block was depressed, the target strength at 40 kHz and above dropped sharply, the more so the higher the frequency. In the next hour, the target strength recovered and leveled off for the rest of the experiment except for a small drop near the end at 80 kHz and above. At the right of Figure 7 we show the target strengths determined in 1988 for a 58-cm block shortly after it was cored out and depressed; the vertical lines show the variation in target strength during 15 hours after submergence. The 1990 results at 30 kHz were about 5 dB higher than the 1988 results. Perhaps the skeletal layer was thicker in 1988, and thus the interference occurred at 30 kHz instead of 40 kHz. To produce interference at 30 kHz, the second return must have come from 1.7 cm into the skeletal layer in 1988 compared with 1.3 cm in 1990.

The increasing dropoff with frequency at 1.5 h suggests that the transducer beam might have moved off the axis of the block. This could be due to either block tilt or transducer movement. The block was solidly fixed in the ice when we tried to adjust it for a small tilt; therefore tilt seems unlikely. Movement of a transducer suspended on three lines about 30 m long seems a possibility, if there was a change in the current that caused the lines to bow and raise the transducer. To investigate this possibility, we measured the travel time of the reflections. The results are plotted in Figure 8. The travel time is shorter, indicating a rise in the transducer, for the fourth, fifth, and sixth measure-

ments. This dip coincides with the dips in target strength at 1700 h.* The implication is that the transducer's position was a little off center, so that a slight upward movement of the transducer brought the block off the response pattern, the more so the higher the frequency. This effect is difficult to separate from temporal changes in the reflections.

During the first hour after submersion (the first three points in Figure 7), the target strength at frequencies of 60 kHz and above dropped 3–5 dB. This does not agree with the 1988 results,[5] which showed a much larger drop for an 84-cm block and no appreciable drop for a 58-cm block; however, in 1988 there was an uncertain delay after submersion before the measurements began. A small decrease in reflectivity is not surprising considering the changes observed in the temperature and sound speed near the lower surface after submersion (see Section VIII).

B. Returns From an Artificially Formed Ice Block

An artificial ice block was formed by filling a container with seawater and leaving it exposed to the cold air. Because a rigid container would not allow horizontal expansion, and the ice surface would bulge in the middle, we made the container in such a way that it could expand as the water froze. The resulting surface was fairly flat, but we had to protect it from the sun, flying snow, and changes in air temperature. At times we added water to maintain a flat surface.

After obtaining a block about 15 in. thick, 58 cm in diameter, and fairly flat on top, we turned it over and installed a three-legged stand that would accept a 5-cm-diameter pole. This pole was required for pushing the block down in the water and for indicating, when it was vertical, that the face of the block was horizontal. When the block was turned over, we noticed that some brine had drained out; further smoothing was necessary.

This block was forced downward, as was done with the natural block, and its reflection measured. A few trials showed that the maximum return was near frame position N22/E25. Reflections were measured with the transducer at this location and at several adjacent locations. Two measurements at N22/E25 appeared to give a maximum at all frequencies. The results are plotted in Figure 9 along with the 1988 results for a natural ice block with the skeletal layer sawed off. The artificial ice block did not reflect nearly as well as the sawed-off block of cold, hard ice used in 1988. Freezing a good solid block with a flat surface was more difficult than we expected.

C. Incidence Angle Dependence

The variation in the target strength of the depressed 58-cm block as a function of incidence angle was measured by moving the transducer in various directions (see

---

*All times mentioned in this report are local.

Table 8). A comparison of the skeletal layer reflection at normal incidence in 1990 with that for 1988 is given in Figure 10; the results are about the same.

The measured target strengths as a function of incidence angle are plotted in Figures 11–14 along with the patterns computed by numerical integration. The maximum target strengths are nearly the same as in 1988,[5] but the lobes are less well developed.

D. Temperature Change After Submersion

To measure temperature changes in the ice block after submersion, two vertical arrays of thermistors were installed in the ice canopy within the 58-cm-diameter cylinder that was to be cored out. The arrays were built in-house using Yellow Springs Instrument (YSI) precision thermistors with impedance-to-temperature calibrations matched to 0.2°C. Each thermistor was encased in marine epoxy. One array was close to the axis of the cylinder; the other was 20 cm away, 9 cm from the outer surface.

To calibrate the thermistors, we relied on the resistance and temperature readings provided by YSI at every degree from −80°C to 100°C. We used the readings from −40°C to 40°C and fitted them with the following equation suggested by Doebelin,[6] whose source was Sachse[7]:

$$1/\theta = a + b\ln R + c(\ln R)^3 , \tag{7}$$

where θ is the absolute temperature in degrees Kelvin, R is the resistance in ohms, and a and b are constants.

The least-squares fit to these data is given by

$$1/\theta = 1.328401 \times 10^{-3} + 2.8726 \times 10^{-4}\ln R + 1.25087 \times 10^{-7}(\ln R)^3 , \tag{8}$$

and this was used as the calibration curve for all thermistors. The curve is plotted in Figure 15. A few check measurements were made on two different thermistors; the points fall close to the curve.

The resistance of the thermistors was read at four times prior to melting out the block: 1200 h on 24 March, 1415 h on 25 March, 1001 h on 26 March, and 1323 h on 26 March. The thermistors' locations within the block and their corresponding temperatures are shown in Figure 16. Temperature decreased with distance from the lower face. The four sets, taken over 3 days, are consistent to 0.2°C in the lower two-thirds of the block. In the upper third, there are some changes of 0.5–0.8°C which may be related to changes at the surface, but they are not relatable to the surface temperatures (Figure 66 of Section IX).

The temperature profiles in the ice for the last three sets of measurements prior to melt-out are shown in Figure 17. In the upper plot, least-squares fits have been made to each thermistor string. In the lower, data from both strings have been used to calculate a

least-squares line. The data fall very close to a straight line. The outer string (triangles) shows only a slightly warmer temperature than the central one (circles).

The block was melted out during 1445–1515 h on 26 March. Figure 18 shows three sets of readings taken within 1 h after melt-out but before submergence of the block at 1725 h. Figure 19 shows nine more sets of readings taken from 1725 h to 1630 h on the following day as the block warmed.

At 1521 h, 36 minutes after melt-out started and 6 minutes after the block was completely melted out, the profile changed as shown at the left of Figure 20. After about 20 h, the temperature was close to that of the water. The temperatures of the center string lagged those of the other string by several hours.

The temperature change of the thermistors in each string is shown in Figure 21a. The readings of the two strings are combined in Figure 21b for comparison.

The gradual change in the temperature profile, from a uniform gradient at first to a constant temperature in about 20 h, roughly corresponds to the changes in reflectivity shown in Figure 7 if the dip at 1.5 h is ignored. The reflectivity decreases as the temperature gradient in the ice decreases. There are additional comparisons in Section VIII.

VI. UNDER-ICE REFLECTIONS

With a sound source and receiver mounted below the ice, we measured the reflectivity of the under-ice surface with three transducers: the ITC 1042, the platter, and the 22×22. In addition to detecting the return from the lower surface, we also detected the one from the upper surface, giving a measure of the sound speed and absorption within the ice.

A. Sound Speed Determined from Internal Reflections

We made many under-ice surface-reflection measurements in which the return from the back face (upper surface) was also detected. The time between these reflections was easy to measure. These time measurements, combined with measurements of the ice thickness, give its sound speed. The accuracy of this determination, however, is limited by that of the thickness measurements, which were not very accurate, and because the thickness changed gradually with time.

The following method was used to measure the time difference between reflections from the lower and upper faces: (1) We picked a distinguishable feature in the displayed pulse, such as the peak value of the first full-strength cycle of the lower face return, at each frequency; (2) we measured the time from this peak to several possible corresponding peaks in the upper face return, at each frequency; (3) we looked for a constant time difference between the lower- and upper-face peaks at all frequencies to confirm that we were using the same cycle of the two returns. Because of the 180° phase shift at the upper surface, negative peaks in the upper-face return were matched with positive peaks in the lower-face return.

The ice thickness measurements were made at three locations:

Date	Location	Depth
19 March	Small triad	198 cm
21 March	Large triad	212 cm
26 March	Ice block	213 cm

The ice may have been generally thinner at the small triad; it wouldn't have increased in thickness 14 cm in 2 days. Between 21 and 26 March, we assume a linear increase in thickness between the two values shown for the vicinity of the large triad, which included the ice block.

1. ITC 1042

Measurements of surface reflections from both faces of the ice canopy were made at 12 locations in the large triad. At seven of these locations, our recording was too short and the return from the back face was cut off. The sound speeds calculated for the other five locations are 3876, 3852, 3963, 3760, and 3718 m/s, for an average sound speed of 3834 ± 43 m/s.

2. Platter Transducer

Measurements of surface reflections from both faces were made at eight locations in the small triad. The transducer was mounted 8.7 m below the bottom of the ice, and the ring was moved to 2 m from the center of the triad in eight directions. The corresponding movement of the transducer below the ice was about 40% greater. The results are 3824, 3824, 3986, 3873, 3907, 3881, 3806, and 3942 m/s, for an average sound speed of 3880 ± 22 m/s.

3. 22 × 22 Transducer

Measurements of surface reflections from both faces were made at eight locations in a 12 × 14 m area in the large triad. The results are 3896, 3996, 3787, 3669, 3871, 3767, 3767, and 3765 m/s, for an average sound speed of 3813 ± 35 m/s. No back-face reflections were available for on-arm measurements with the 22 × 22 because the recording was too short.

The average sound speed for the three transducers is 3842 ± 35 m/s.

B. Reflectivity at a Range of 9 m

When a pulse is transmitted at voltage T and the return from the surface at range R has voltage V, we can compute the amplitude reflection coefficient R_a using

$$20\log R_a = 20\log V/T + 20\log 2R + 2\alpha R - CAL - G, \tag{9}$$

where α is the absorption coefficient in seawater, CAL is the sum of transmitting response and receiving sensitivity of the transducer, and G is the receiving system gain in decibels.

1. Platter Transducer

The platter transducer was installed at the small triad and, prior to cutting the 2-m-square holes for the experiment described in Section VII, the topside ring was placed 2 m from the center of the triad at azimuthal intervals of 45° (N, NE, E, etc.). At each of these eight locations, the return from the surface was measured, and the transmit voltage recorded.

The results are summarized in Table 9 and plotted in Figure 22. The N reading was very high at all frequencies; we presume there was some major irregularity in the surface. We have omitted the N set in the averaging. The R_a averages for the other seven measurements are plotted in Figure 23 to show how they compare with the 1988 results. Except at 220 kHz, the 1990 values are lower than those measured in 1988.

2. 22 × 22 Transducer

At the large triad, the 22 × 22 transducer was moved to eight positions corresponding to the ring locations shown in Table 10; this placed the transducer about 6 m from the ice block's (future) position in directions about 45° apart. A high-pass filter was used for

the latter half of the data. Its effect was measured later in conjunction with the reflection measurements with the ITC 1042 (see Table 11). The measurements at each location are summarized in Table 10. A comparison with 1988 results is shown in Figure 24; the results are in fair agreement.

3. ITC 1042

The effect of the filter was measured using a cw signal with a low noise level (see Table 11). Surface reflection measurements with the ITC 1042 were made in the same eight locations used for the 22×22. These locations were numbered 1 to 8 in the same order as for the 22×22. At four locations farther out from the center, reflection measurements were made using two pulse lengths, 0.2 ms (as before) and 1.0 ms. The results are summarized in Table 12. The values for locations 4 and 10 were very high and were omitted when calculating the averages. The averages are plotted in Figure 25 along with the 1988 results.

The R_a value at 120 kHz is very high. This may be partly due to constructive interference between reflections from the top and bottom of the skeletal layer.

C. Reflectivity at a Range of 2 m

1. 22×22 Transducer on Arm

The 22×22 transducer was calibrated by placing it on the arm beneath a man-made hole so that it recorded reflections from the open surface. The results were presented earlier in Section III.D. The CAL values were 7, 5, 8, 19, and 17 dB lower than for the earlier longer-range calibration using a sphere. When we used the sphere calibration, the measured reflection coefficients for the rotating arm were in good agreement with other R_a measurements. Had the open-surface calibration been used, the results would have been very high (above $R_a = 0.2$). Also, the averages of the open-surface returns, for two successive sets of measurements, varied by 3, 5, 6, 1, and 11 dB for frequencies of 80, 100, 120, 160, and 200 kHz, respectively, which seems excessive and indicates a problem. Perhaps the open surface was partially frozen over or rippled to give a low return, especially at the higher frequencies. We decided to use the sphere calibration, as we did for the 22×22 measurements at long range.

Measurements of under-ice surface reflections were made at two holes. At each, the transducer arm was swung around and stopped every 10° for measurements. Averages of the measurements at each frequency, along with the standard deviations, are shown in Table 13 and plotted in Figure 26. The results for the two holes are similar, both showing a peak at 120 kHz.

The combined R_a distribution for both holes is shown in Figure 27. Also shown are the Rice probability functions computed for three values of γ, where γ is the ratio of the coherently reflected echo intensity to the incoherently scattered intensity. The best fit

appears to be one of the three, and a more refined selection would not be worthwhile. The dropoff in γ at high frequencies would be expected because of increased scattering as the frequency increases. The low value for γ at 80 kHz may indicate that a single parameter distribution is inadequate to account for all the physics of the present situation, which involves frequency dependent transmission as well as rough surface scattering.

2. ITC 1042 on Arm

The ITC 1042 transducer was placed on the same arm used for the 22×22 transducer, and measurements were taken every $20°$ at hole 2. No calibration measurements were made at this time.

The results are plotted in Figure 28 for comparison with 1988 results. The amplitude reflection coefficient was calculated using the transducer calibration value obtained in Section III.A. The rise with frequency is puzzling but seems to occur for both measurements at 2-m range.

D. Summary of Reflectivity Results

The measurements of under-ice reflectivity with three different transducers show considerable variation, especially at the higher frequencies. Because several hours passed between measurements, temporal changes may have contributed to the variation. The platter transducer gave quite low R_a values; the 22×22 gave results close to those obtained in 1988; the ITC 1042 gave slightly high results. At close range, 2 m, the 22×22 values were in general agreement with those of the other transducers, except for a low value at 80 kHz. Calibration at this range was questionable. The spot size is probably too small for good averaging.

E. Absorption

When reflections from both the front and back faces are measurable, the absorption in the ice can be calculated. The results will include the loss at the upper-face reflection, but this can be considered negligible since it is from an ice/air interface.

The equation for the loss[1] is

$$\text{Loss} = 20\log[(1 - R_a^2)(-R_b)V_1/(R_a V_2)/(1 + s N /R)] , \qquad (10)$$

where

$$
\begin{aligned}
R_a &= \text{lower-face reflection coefficient} \\
R_b &= \text{upper-face reflection coefficient} \\
V_1/V_2 &= \text{ratio of amplitude of lower-face return to upper-face return} \\
s &= \text{thickness} \\
N &= \text{ratio of sound speed in water to speed in ice} \\
R &= \text{range.}
\end{aligned}
$$

We now use Eqs. (16)–(20) from Section VII.D for the absorption dependence on temperature, the temperature factor q, and the total loss, which includes a loss p at the interface. For an assumed constant temperature gradient from T_1 in the water to T_2 at the surface of the ice,

$$q = 3(6^{2/3})[(-T_2)^{1/3} - (-T_1)^{1/3}]/(T_1 - T_2) . \qquad (11)$$

To evaluate q, we use $T_1 = -2°C$ and $T_2 = -20°C$. The latter is a good average for the week of the measurements and is assumed to be the temperature at the top of the ice. These temperatures give $q = 0.80$. If we had used $T_2 = -25°C$, as it was a few days earlier, we would obtain $q = 0.71$, and the absorption results would be proportionally higher, by 13% in this case.

For Eq. (10) we use the R_a value from Section VI.B and assume $R_b = -1$. The loss for each transducer is calculated in the following subsections and plotted against the product fqs. The slope of the best line is equal to the absorption coefficient k.

1. ITC 1042

Diskettes of data collected with the ITC 1042 were examined to measure the ratio of lower-face reflection to upper-face reflection. (The reflection coefficients were determined in Section VI.B.) The results are shown in Table 14. The parameters used in Eq. (10) were

$$
\begin{aligned}
s &= 2.1 \text{ m} \\
N &= 2.5 \\
R &= 29 \text{ m} \\
1 + sN/R &= 1.18 .
\end{aligned}
$$

The computed absorption loss (one-way) is plotted versus fqs in Figure 29. For 18 points, $p = 4.3$ dB and $k = 0.18$, with a correlation coefficient r of 0.85.

2. Platter Transducer

The results for the platter transducer were computed in the same manner as above, and are tabulated in Table 15. The loss is plotted versus fqs in Figure 30. The best line, for 24 points, is $p = 16.3$ dB and $k = 0.12$, with $r = 0.76$.

3. 22×22 Transducer

Similar computations for the 22×22 transducer are tabulated in Table 16. The loss is plotted versus fqs in Figure 31. The best line, for 30 points, is $p = 5.0$ dB and $k = 0.24$, with $r = 0.94$.

In summary, the average of the three sets of measurements is $p = 8.5$ dB and $k = 0.18$. As is explained in Section VII.D, the measured boundary loss p will include the effect of the change in the hydrophone's sensitivity when it is frozen into the ice.

VII. GROWING-ICE EXPERIMENT

By installing sensors in the water and waiting for the ice to form around them, we were able to measure temperatures and the sound field within the ice.

A. Equipment Installation

Two 2-m-square holes were made in the ice by coring out, with a thermal melter, four 84-cm cylinders and then melting out the cusps with a perforated straight section of copper tubing. The first hole was the "main hole" used for the experiment, and the other hole was the "monitor hole," a duplicate hole from which core samples could be taken without disrupting the experiment. A few hours elapsed between construction of the main hole and the monitor hole. To offset this, the surface of the main hole was kept free of ice until measurements started at the monitor hole; thus the two holes are considered to have begun freezing at the same time (even though the ice surrounding the main hole would have been warmed somewhat by the water).

While the surface was free of ice, instrumentation was suspended from a pair of 2×4's placed across each hole. A hydrophone string (described in Section VII.C) was suspended in the water at the center of the main hole, and a string of thermistors was suspended in the water near the centers of both holes. Both types of sensors were attached to a 5/8-in.-diameter plastic rod as shown in Figure 32. Later, in January 1992, the rods were suspended in air, and the positions of the sensors were measured with a ruled tape. The results are shown in Table 17 and Figure 33.

The platter transducer was suspended on three lines in a small triad (see Figure 5 for triad configuration). The lines passed through short lengths of pipe extending through the ice 10 m away and were attached above the ice to a small ring. Movement of the transducer was controlled by moving the ring over a small frame fitted with pegs which was placed on the ice near the main hole. As the ring was moved from peg to peg, the transducer remained at nearly constant depth 10 m below the ice. The platter was used to transmit pulses which were received by the hydrophones and as a transmitter-receiver for measuring reflections off the ice.

A transducer that had been used to measure under-ice erosion in an earlier experiment was mounted beneath the free surface on a pole and arm so that it could be swung out of the way when a block of ice was cored out of the refrozen surface and depressed. This transducer was used to measure reflections from the lower surface of the freezing ice at 92 kHz and thus monitor the downward progression of the newly frozen surface.

B. Temperature Changes

Temperature readings were taken at the times listed in Table 18. All measured resistances of the thermistors were converted to temperature using Eq. (8). The measured temperatures are listed in Table 19. The change in the temperature at each

thermistor throughout freezing is shown in Figure 34a for the main hole and in Figure 34b for the monitor hole. The two are compared in Figure 34c. (Note: In comparing the temperatures at the two holes, care must be taken to compare time-coincident profiles.) The temperature data for the main hole are plotted as vertical profiles in Figure 35. Similar profiles for the monitor hole are plotted in Figure 36. A comparison between the profiles for the two holes is given in Figure 37. Groups of profiles (labeled a, b, c, and d in Figure 37) are plotted at an enlarged scale in Figures 38a–38c. Figure 38 shows that the temperature variations at the two locations were nearly the same.

The changes in air temperature at the surface of the ice, obtained from readings of the thermistor at the top of the string in the main hole, are shown in Figure 39. The air temperature monitored at the camp is shown for comparison. The surface temperatures measured at the two holes are in good agreement. The agreement between the surface temperature and the air temperature is only fair in general, but very good during warming periods.

C. Incremental Sound Speed

1. Instrumentation

To measure sound speed in the refreezing hole, 12 hydrophones were attached to a stiff plastic rod; the vertical spacing was 2.5 cm for the lower six and 5 cm for the upper six. The hydrophones and thermistors are shown in Figure 32; their spacings are listed in Table 17 and plotted in Figure 33. After the main hole was cored and while the water surface was ice-free, the string of hydrophones was suspended so that No. 12 was a little below the water surface. The thermistor string was also suspended at this time, 15 cm away. The platter transducer was suspended below the main hole from three lines as described earlier (see Figure 5). Short (0.2 ms) pulses at 92 kHz were transmitted upward to the string of receiving hydrophones, and the received signals recorded on diskettes with a dual-channel Nicolet oscilloscope. Readings from two adjacent hydrophones were recorded at the same time, giving an accurate measure of the difference in the travel time of the pulse from one hydrophone to another. Acoustic measurements were taken immediately after installation to obtain an estimate of the hydrophone spacing, based on the known sound speed in the near-freezing water. Later measurements after ice began forming gave the sound speed in the ice at various stages of freezing, both in the skeletal layer and, later, in the more-solid ice.

2. The Experiment

The hole was cleared and the strings installed at 1910 h on 19 March. The time differences were first read at 2320 h. A second set was read at 1207 h on 20 March.

After return of the equipment to APL, the spacing between the hydrophones was measured with a tape. A comparison between the spacings determined acoustically and those measured directly is shown in Table 20. The maximum difference (for hydrophones 2–3) was 3 mm; the total distance (hydrophones 1–12) differed by only 1 mm.

The first time differences were used as reference times, based on a sound speed (obtained from CTD profiles) of 1436 m/s in the water. However, it appears that before the first time measurement some ice had formed, reducing the travel time. The tape-measured spacings shown in Table 20 indicate that the travel times for intervals 10–11 and 11–12 should have been about 35 μs. Every few hours another set of readings was taken and compared with the first (in-water) reading. The sound speed ratio with respect to a water sound speed of 1436 ms was assumed to be inversely proportional to the ratio of time differences. Table 21 shows the measured time intervals and calculated sound speeds for the ice growth period. The sound speeds in the ice during the ice growth period are summarized in Table 22.

We determined the depth of the under-ice surface from acoustic data taken with two transducers: the platter transducer suspended on three lines below the main hole at a depth of 10 m, and the ice-erosion sonar transducer (see Section VII.G) mounted on a pole beneath the main hole at a depth of 1.5 m. The difference in reflection time when the hole was open and when new ice was forming gave a measure of the distance the ice surface had lowered.

There was always one hydrophone interval that contained both a layer of ice and a layer of water. For a known sound speed in the water of 1436 m/s, we calculated the average sound speed in the ice that would produce the measured average travel time for that interval. Figure 40 defines the symbols used in calculating the average sound speed in the ice portion of the interval and in a larger interval including the next hydrophone above.

$$
\begin{aligned}
F_1, F_2 &= \text{sound travel time between hydrophones, in water} \\
G_1, G_2 &= \text{sound travel time between hydrophones, when ice present} \\
A &= 1436\,F_1 \\
E &= 1436\,F_2 \\
T_6 &= \text{difference between travel time of initial surface reflection} \\
&\quad \text{and ice reflection for sonar (see Figure 49)} \\
D_6 &= 1436\,T_6 \\
D_5 &= \text{measured depth of hydrophone from Table 20} \\
B_1 &= D_6 - D_5 \\
D_4 &= E - B_1 \\
T_2 &= G_2 - D_4/1436.
\end{aligned}
$$

The average speed in the ice portion of the lower interval is

$$C_2 = B_1/T_2 .$$

The in-ice travel time across the three-hydrophone interval is

$$T_3 = G_1 + G_2 - D_4/1436 .$$

The average speed in the ice portion of these two intervals is

$$C = (A + B_1)/T_3 .$$

Results are shown in Table 23 for both the interface interval and the ice interval above. At first, the value calculated for B_1, the ice thickness below the middle hydrophone, was sometimes negative, indicating that the T_6 values should be about 1 cm higher. One centimeter corresponds to a 14 μs reduction in sonar return time and may be just a matter of interpretation of the start of the pulse. This adjustment was made and provided more consistent results.

We obtained the average sound speed for a thicker layer of ice by using the next higher hydrophone in the ice as the upper hydrophone; the results are given in Table 24.

All results are plotted in Figure 41. A fourth-degree power curve was fitted to the points:

$$\overline{C}_I(s) = 1490 + 480.93s - 55.670s^2 + 3.2548s^3 - 0.071579s^4 , \qquad (12)$$

which is a good fit for $s = 0$ to 15 cm. The total travel time through the ice can be expressed either as an integral or in terms of the average speed given in Eq. (12). Taking the derivative of this travel time equality with respect to s gives

$$\frac{d}{ds} \left[\int_0^s \frac{dx}{C_I(x)} \right] = \frac{d}{ds} \left[\frac{s}{\overline{C}_I(s)} \right] \qquad (13)$$

or

$$C_I(s) = \frac{\overline{C}_I^2(s)}{[\overline{C}_I(s) - s\dfrac{d}{ds} \overline{C}_I(s)]} , \qquad (14)$$

which is plotted as a solid line in Figure 41. Beyond $s = 7$ cm, the fit becomes uncertain because we have only sparse data for the large s values in the fourth-order fit of Eq. (12). This method assumes that the profile in the lower 10–20 cm of ice is the same at all stages of freezing, i.e., for ice of any thickness from 10 to 42 cm. The validity of this assumption can be judged from the spread of the data in Figure 41.

Figure 42 shows the average sound speed in each interval in Table 21 in which the speed appeared to have reached a plateau. These points have been added to Figure 41 as open circles, extending the profile beyond the end of the solid line. The solid line shows an "acoustic" skeletal layer thickness of about 3 cm.

In Figure 43, the raw sound speed data for each interval in Table 22 have been plotted as a function of time of month. The sound speed increases slowly at first as the skeletal layer fills the interval and then quickly as the ice hardens.

The sound speed profile in the lower few centimeters of ice is important in understanding acoustic reflections off the lower surface of growing ice.

D. Incremental Absorption

The 92-kHz transmissions from the platter transducer suspended below the refreezing hole provided an opportunity to measure the absorption of sound in the ice under varying temperatures. We recorded each ping on two adjacent hydrophones simultaneously to compare the amplitudes of the sound arriving at two hydrophones a known distance apart. By recording signals in the ice-free water where absorption was negligible, we in effect calibrated the receiving circuits. For adjacent hydrophones a distance s apart with amplitude readings of A' and B' in water and A and B in ice, the measured absorption coefficient would be

$$\alpha = 1/s[20\log(AB'/BA')] \quad \text{dB/m} . \tag{15}$$

For ice of varying absorption within thickness s, we can express the absorption loss as

$$\text{Loss} = p + \int_0^s \alpha(s)ds', \tag{16}$$

where p is the loss at the interface between water and ice.

For the frequency and temperature dependence of absorption of sound in the ice, we use the McCammon-McDaniel equation[3]

$$\text{Absorption} = kf(-6/T)^{2/3} , \tag{17}$$

where f is the frequency in kilohertz, T is the temperature in degrees Celsius, and k is a coefficient given by McCammon and McDaniel as 0.06.

With this expression for α, the integration in Eq. (16) becomes an integration of $(1/-T)^{2/3}$ over the thickness s. If we assume a constant temperature gradient across s from T_1 to T_2, then

$$T = T_1 + (T_2 - T_1)s'/s \qquad (18)$$

at distance s' from the lower surface, and the absorption loss is given by

$$\text{Loss} = kf\int_0^s (-6/T)^{2/3} ds' \qquad (19)$$

$$= kf(6)^{2/3}[-3(-T)^{1/3}]_{T_1}^{T_2}[s/(T_2 - T_1)]$$

$$= kf(6)^{2/3}(-3)[(-T_2)^{1/3} - (-T_1)^{1/3}[s/(T_2 - T_1)]\,.$$

If we let the temperature terms be expressed by Eq. (11), i.e., by

$$q = 3(6^{2/3})[(-T_2)^{1/3} - (-T_1)^{1/3}]/(T_1 - T_2)\,,$$

then the total loss is

$$L_t = p + kfqs\,. \qquad (20)$$

A plot of measured loss vs fqs should show a linear variation with slope k. If some temperatures along the path between the hydrophones are measured, the q for the hydrophone interval can be determined by summing qs contributions for each increment between thermistors.

Another approximation would be to determine the temperature at each hydrophone by interpolating between the thermistors above and below it; then q could be determined from Eq. (11), using T_1 and T_2 as the interpolated temperatures at the hydrophones.

1. Effect on Hydrophone Sensitivity When Frozen in Ice

We do not know how freezing the hydrophones into the ice affects their sensitivity but would expect the sensitivity squared to change inversely with the longitudinal impedance of a liquid medium. Application to a solid may be problematic; however, if this relation is applied to ice with a density of 0.93 and a sound speed of 3500 m/s, the hydrophone sensitivity would be about 3.5 dB less in the ice than in air, and thus account for a major part of the loss at the boundary (evaluated as 4.56 dB in Section VII.D.3). The sensitivity change may not be abrupt but gradual over the 3 cm that the sound speed changed. This means that the two effects—the sensitivity change of the transducer and the absorption in the skeletal layer—cannot be separated with the measurements taken in this experiment.

2. *Absorption Loss as Freezing Progressed*

The data for hydrophones 10–12 are unusable for two reasons: (1) Hydrophone 10 was not recorded much of the time, and (2) some ice had already formed when intervals 10–11 and 11–12 were initially recorded, and thus there was no calibration of the receiving circuits.

The next four intervals (8–9, 7–8, 6–7, and 5–6) were used to evaluate absorption because these hydrophones were in the ice the longest. The readings for interval 6–7 were not valid for the skeletal layer transition, and have therefore been omitted. The amplitude readings in the other three intervals and their ratios are shown in Tables 25–27. Figure 44 shows the absorption loss and calculated sound speeds. The average ratio of the readings taken at each hydrophone pair before any ice appeared in the interval sets the 0 dB reference for the receiving circuits. The calibration ratio is plotted (in decibels) as points at the left of the first hydrophone arrow in each graph. The ratios are fairly consistent, showing that the equipment was capable of consistent amplitude measurements (on the same ping).

Figure 44 shows high absorption at the same time as a sharp increase in sound speed. We believe these changes are an effect of the skeletal layer. After the sound speed levels off, we would expect to be measuring the absorption in solid ice. The loss in interval 8–9 is lower than that in 7–8, perhaps because the lower interval did not freeze as solidly as the one farther into the ice. The loss shown in Figure 44 is highly variable. This variability is caused mainly by variation in the amplitude of the signal during the first two or three cycles. We preferred not to average over the whole pulse because some other paths might be included.

The measured losses for some of the later runs are given in Table 28 and in Figure 45. Run 2 is included in the table to give a hydrophone sensitivity calibration; in the analysis, however, all the in-water measurements were averaged to give the calibration for each interval. For these later runs, the ice should have been fairly solid, but the plot shows that the loss for a given interval was sometimes inconsistent between the four runs. (The losses for the wider intervals are divided by 2 to give a true comparison.) The very low absorption recorded on all runs for interval 5–6 is puzzling. Note also that all the losses for hydrophone interval 6–7 are quite high. This could result if hydrophone 6 moved as the ice froze around it, but this seems unlikely, and there was no marked change in the time between arrivals to hydrophones 5, 6, and 7. It is possible that the ice structure in this hydrophone interval changed, perhaps because of changes in the atmospheric temperature. Or perhaps ray bending caused some interference, or there was some shading by another hydrophone. The peak resulting from the high absorption in the skeletal layer varies from run to run because the skeletal layer was moving downward as the ice thickness was increasing. We suspect an error in the reading for interval 2–3 for Run 31 because it is so much lower than that of the other runs and, being negative, indicates a gain, which seems unlikely.

3. Absorption in the Skeletal Layer

For every run, the lower surface of the ice lies between some pair of hydrophones (see Figure 46). In the space between the hydrophones, there is a layer of ice, and below it a layer of water. Temperature T_2 at the hydrophone just above the ice interface can be interpolated, assuming a constant gradient between thermistors. This is used to compute q for the ice layer. The measured transmission loss from the lower to the upper hydrophones occurs predominately in the ice, which has a thickness s. Because the loss in the ice was measured for many runs, and thus many values of s, we obtained a relationship between loss and s. Some additional data points were obtained by taking an interval involving more hydrophones, summing the intervening losses, and thus obtaining some values for larger s. The results are summarized in Table 29.

All data from Tables 28 and 29 are plotted in Figure 47. A second-degree least-squares line for the loss is

$$L_t = 4.56 + 0.981 fqs - 0.0164(fqs)^2 \tag{21}$$

with s in meters. The slope of the line at any point is the value of k, and varies from 1.0 to 0.3. A k of 1.0 at the interface corresponds to an absorption loss of 2 dB/cm, at 92 kHz.

Figure 48 compares the results of these and other measurements of k for the ice canopy. It appears that the absorption is high at the bottom of the skeletal layer and then decreases gradually as the ice hardens with age. Figure 44 showed a continuing trend toward lower absorption for the upper, and older, layers of ice.

E. Under-Ice Reflectivity

1. Time of Returns

The platter transducer was supported by three lines beneath the recently made 2-m-square hole. At 2100 h on 19 March, the water surface was swept clear of ice crystals and the first reflections were measured, at frequencies of 37, 52, 92, 150, and 220 kHz. Some reflections that arrived earlier than the surface reflections were identified as returns from the bottom of the ice canopy, from the arm that supported the ice-erosion sonar, and from the lower end of the sensor strings.

At the beginning of the reflection measurements, the digital recording window did not include the transducer arm. Therefore, at first we compared the ice reflection time with the reflection time for the sensor string. Table 30 shows the measured reflection times for the ice and the sensors at 220 kHz, the computed difference, and the change in this difference as freezing progressed.

Later on, when the arm's reflection was recorded, we compared the ice reflection times with the arm reflection times at 92 kHz. The results are shown in Table 31. We have overlapped the data in Tables 30 and 31 to get the offset between the arm and the sensor string.

The two-way travel times in both tables, along with similar data from the ice-erosion sonar, have been plotted in Figure 49 to give the ice depth as freezing progressed. The best-fit curve gives the distance from the initial water surface to the lower surface of the ice, to an accuracy of about 0.5 cm.

2. Amplitude of Returns

The amplitudes of the returns from the freezing ice before and after submergence of the block were tabulated. The amplitude reflection coefficients for the main return prior to submergence are listed in Table 32 and plotted for each frequency in Figure 50.

Some of the returns had a short initial portion with a lower amplitude. At 1115 h on 21 March, for example, the 37-kHz return showed an 88-μs region with an amplitude only 1/3 that of the following pulse. The total return was elongated by this amount, indicating that there were two pulses, one slightly delayed. This was not apparent at the higher frequencies, where the main pulse started at the same time as the first (low-amplitude) portion of the 37-kHz return. This could indicate that returns from the top of the ice were important at 37 kHz only. At the higher frequencies, absorption may have reduced the reflection from the back face sufficiently that its effect was not appreciable. In calculating the reflection coefficients at 37 kHz, we used the low-amplitude portion of the initial pulse and ignored the amplitude of the main pulse. However, the reflection coefficient was also calculated for the main pulse, and is plotted in Figure 50 as the filled circles.

On the eighth set of readings, on 21 March at 1115 h, the returns appeared to be 20 dB higher. These values would have indicated reflection coefficients greater than unity. At the same time, the Nicolet oscilloscope scale for the return changed by 20 dB while the scale for the transmitted pulse remained the same. This could have been an operator response to a 20-dB-higher signal resulting from the unknown addition of a 20-dB gain, but the operators cannot conjecture what this gain change could have been. We considered checking for a 20-dB shift in the return from the sonar arm, but unfortunately the return was chopped off the recording for all runs before the sudden change. We have shifted the returns by −20 dB starting with the eighth set of readings.

On 27 March at 1311 h, the readings at all five frequencies dropped about 20 dB and then rose back on the next set. The return from the sonar arm showed a decrease of 22 dB at the same time. Close examination of the sensor return just prior to the ice return showed that it also dropped about 20 dB. In Table 32 and Figure 50, this set of readings has therefore been corrected by +20 dB relative to the adjacent data sets.

The amplitude reflection coefficients shown in Figure 50 and Table 32 for 220 kHz appear too high. Some other echoes are present at this frequency, but they would not interfere because the beam is so narrow. Even when the 220 kHz data and the combined direct and reflected pulses at 37 kHz are removed (Figure 51), the daily variations are still very high. To see the trends, we have plotted the daily averages in Figure 52. There appears to be an increase with time for the lower frequencies and a decrease with time for the higher frequencies.

The averages of the reflection coefficients measured during freezing are plotted in Figure 53b along with the 1988 results. The coefficients, and the decrease with frequency, agree well with the 1988 results. Included is a theoretical curve based on the measured sound speed profile shown in Figure 53a. The theoretical calculation is discussed in Section IV of Ref. 2.

3. Phase of the Returns

At times, the difference in phase between the signals received at adjacent hydrophones was measured with a phasemeter and recorded throughout the pulse as an alternative method of measuring the time difference between arrivals. The phase difference fluctuated during the first part of the pulse and then became more steady, but it did not reach a constant value until near the end of the pulse. The amplitude also varied during the first quarter of the pulse and then settled to a constant value. It appears that the returns arrived via several paths, and only when all had arrived did the amplitude and phase settle down. Because of the depth offset, however, these paths may not have been the same for each hydrophone. Therefore the final phase may not be a good measure of the time difference. We used the time of arrival of the first positive peak, which gave more consistent results.

F. Ice Core Data

Prior to the ice-growth experiment, an ice core was taken from the canopy nearby and sawed into sections; the temperature of each section was then measured by drilling a small hole and inserting a thermistor probe. The sections were later melted, and the salinities of the melt water were measured with a conductivity probe. The sound speed in some of the sections was measured directly by transmitting sound through the short length of core.

Figure 54 shows the measured temperatures and salinities of the sectioned ice core along with the computed sound speed and porosity. Also shown are the results for a core taken in the monitor hole on the last day of the ice growth experiment.

G. Ice Depth Monitored by Ice-Erosion Sonar Transducer

In addition to measuring reflections from the under-ice surface with the platter transducer, we employed a sonar transducer that had been used in earlier years to measure erosion in the under-ice surface. It was used here to monitor the increase in the

depth of the under-ice surface as additional ice froze. This sonar transducer was mounted on a horizontal arm which was fastened to a vertical pole located at one edge of the melted-out hole. The transducer was swung around until it was approximately under the center of the hole, with its beam directed upward.

The system transmitted short (0.5 ms) cw pulses at 92 kHz. The return was recorded on a Nicolet oscilloscope about twice per day. For analysis, we compared the return times with those recorded for returns from the air/water interface at the start of the experiment. The results are tabulated in Table 33 and were used to plot Figure 49.

VIII. CHANGES IN THE ICE AFTER SUBMERGENCE

A 58-cm-diameter block was cored from the newly formed ice containing the thermistors and hydrophones used for the ice-growth experiment and pushed downward 1 m as diagramed in Figure 55. The objective was to observe changes in the sound speed and absorption within the ice, and in the reflectivity of the bottom surface, as the ice was warmed by the surrounding water.

A. Temperature

The temperature readings in the ice block after it was submerged are shown in Table 34 and the profiles plotted in Figure 56. By the time of the last set of readings, the entire block was near the temperature of the water.

B. Incremental Sound Speed

Table 35 summarizes the sound speeds computed for the hydrophone intervals after the ice block was submerged. Data of type AB should be more accurate because the arrival times at the two hydrophones were compared for the same ping. At most depths there was an immediate change, presumably due to temperature, followed by a slow drift as the block's temperature gradually approached that of the surrounding water. The submerged time was divided into five intervals, and an average sound speed was computed for each time interval, for each hydrophone interval. These averages are plotted in Figure 57. The profiles for the five time intervals are plotted individually in Figure 58 and as a composite in Figure 59. The time-interval numbers are plotted at the computed average for each hydrophone interval. The connecting lines, drawn from the top and bottom of the numbers, provide a simple approximation to the profiles that would give these averages. The lowest hydrophone interval shows an increase in sound speed with time because this interval was not all ice at submergence, and more ice formed after submergence because heat continued to pass into the cold ice above. At the upper levels, the sound speed decreases as the ice warms.

After we calculated the sound speeds from the measured arrival time differences at the hydrophones, we compared each time difference with the time difference measured before any ice had frozen. We used only the first in-water measurement, although there were many more during the next hours. We compared some initial time interval readings with the average of several and found the discrepancy was less than 1%. Ignoring the first interval (1–2), the maximum correction varied from +0.7% to –0.7%. This appears to be small enough to ignore.

We now compare the sound speeds in the submerged ice with the measured temperatures. The sound speeds and the temperatures were not measured individually at the same time and depth, so some averaging is required. For the sound speed, we have divided the submerged time into five periods, as was done for Figure 57. The averages

for each hydrophone interval in each period are tabulated in Table 36 along with the standard deviations of the data.

To obtain Table 36, we first averaged the temperature readings shown in Table 34 for each thermistor over each of the five time periods and then estimated the average temperature in each hydrophone interval. The corresponding values of sound speed versus temperature are plotted in Figure 60 along with theoretical curves for selected salinities based on the sound speed calculated from brine volume/Young's Modulus relationships. The data points for the entire block (Figure 60a) generally fall within the lines for salinities of 0–8 ppt, the range usually found in Arctic ice. Those for only the interior of the block (Figure 60b), where the pressure effects would be small, show less variability and fall close to the line for a salinity of 5 ppt.

Some information on the salinity at this locality was obtained from measurements on a core sample taken from the adjacent monitor hole. These data are presented in Figure 61 (profile S1). These salinities are for newly frozen ice before the block in the main hole was cored out. Both Figures 60 and 61 show that salinities of 4–8 ppt could account for the measured sound speed, except for hydrophone interval 5–6. As the block warmed above –5°C, the sound speed in this interval was exceptionally high (see Figure 59). This interval had a low absorption loss (Figure 45) and a lower salinity during submergence (Figure 61, profile S2).

These anomalies may result from a disruption of the hydrostatic equilibrium of the block due to submergence, which may have forced seawater into the block, reducing the salinity in the brine drainage channels. After the block was submerged and warmed, the salinity may have decreased owing to brine drainage. This pressure effect probably occurred within a short time. With the salinity reduced, and the block still cold, more ice would have formed, increasing the frame rigidity of the ice, which would account for the reduced porosity, the higher sound speed, and the lower absorption.

C. Under-Ice Reflectivity

After the block was melted out and depressed, readings were taken of acoustic returns from its lower surface to determine the effect of the surrounding water. The returns were converted to target strength and compared with the theoretical target strength of a 58-cm-diameter rigid plate. The difference was $20\log R_a$. The R_a values computed are listed in Table 37 and plotted in Figure 62. Although the variation is very large, R_a appears to decrease as the block warms, except for a large peak at all frequencies on 30 March.

Figure 63 shows the amplitude reflection coefficient versus frequency for the submerged ice in 1990 compared with the ice canopy in 1988. The reflectivity of the submerged block becomes much lower as the ice warms and the boundary transition becomes less abrupt. Again, we have used the measured sound speed profile,

approximated by the smooth line in Figure 63(a), to calculate the theoretical amplitude reflection coefficient, shown by the solid line in Figure 63(b). The line is a fair match to the measurements, except at 150 kHz where the measured refection coefficient is high with respect to the values at the other frequencies.

D. Absorption

1. Amplitude Readings

As mentioned previously, we continued to transmit sound pulses into the ice block from below after it was cored out and submerged at the end of the ice growth experiment. For a selected ping, we compared the amplitudes at two adjacent hydrophones and corrected them by the in-water ratio obtained for those hydrophones before the ice began to freeze. For another ping, we made the same comparison for the next two adjacent hydrophones, and so on.

We first tried using the average amplitude for the entire pulse length. However, the first few cycles were often erratic, and the amplitude varied considerably before settling to a steady state, as if additional out-of-phase paths were included as time progressed and interfered sufficiently to change the amplitude sum. We decided that the amplitude of the first cycle would be free of this interference and would give a better measure of absorption.

We do not have amplitude comparisons for every run, because on alternate runs we recorded the amplitude of the ping at only one hydrophone and the phase difference between arrivals at the two hydrophones. We had hoped that the phase difference would be useful in measuring the time difference between arrivals, but it was found to be inferior to measuring the time differences directly.

2. Temperature Effect

During submergence, temperatures were measured every few hours. There were generally two thermistors closely bracketing the depth of each hydrophone, so that the temperature at each hydrophone was well known. As discussed in Section VII.D, we assumed the temperature dependence of McCammon and McDaniel[3] given in Eq. (17), i.e.,

$$\text{Absorption} = kf(-6/T)^{2/3} ,$$

with the total loss, including the loss at the interface, expressed as Eq. (20),

$$L_t = p + k\,fqs ,$$

where s is the distance the sound travels through the ice. For these calculations, we assumed a constant temperature gradient between hydrophones. For a constant

temperature gradient between temperatures T_1 and T_2, q can be calculated from Eq. (11),

$$q = 3(6^{2/3})[(-T_2)^{1/3} - (-T_1)^{1/3}]/(T_1 - T_2).$$

We calculated the absorption loss from the amplitude ratio A_r (with Loss = $20\log A_r$) and determined the average value of the absorption coefficient k that was the best fit to all the submerged ice measurements.

3. In-Water Measurements

The in-water measurements are shown in Table 38. We used only a few of the available runs, making sure no ice was present. The average amplitude ratios (A/B) for the first eight hydrophone pairs are given at the bottom of the table. These ratios reflect differences in the receiving circuitry for individual hydrophones. The ratios seemed to be fairly consistent over several pings.

4. Absorption Loss

Absorption loss was determined by measuring the change in amplitude as the sound progressed through the ice. We compared use of the first cycle with use of the steady-state portion of the pulse, and decided use of the first cycle would give better results. The first-cycle amplitude measurements are shown in Table 39. Below the two ampli-tude readings, we have calculated the ratio and then corrected by dividing by the in-water ratio. The corrected ratios are summarized in Table 40. Because the readings for hydrophone 10 were faulty, we give ratios only through hydrophones 8–9.

5. Absorption Coefficient k

Table 41 shows the values used in calculating absorption. We take 20 log of the amplitude ratios, determine q from the interpolated temperatures at the hydrophones at each end of the interval, and then sum these items as we progress upward through the ice. This sum indicates the cumulative absorption loss for various cumulative fqs values. A plot of the sum of the losses versus the sum of fqs will have a slope equal to the absorp-tion coefficient k.

The cumulative absorption losses are tabulated in Table 42 and plotted in Figure 64, which includes one graph for each run. The values of k, determined from the slope of a least-squares line for all the data, are summarized in Table 43, which gives the y-intercept, the slope, and the standard deviation for each run. The y-intercept varies greatly because (1) the ice around hydrophone 1 melted, and (2) the data for hydro-phones 1 and 2 were sometimes erratic and were therefore omitted. If we weight the k values for each run by $1/\sigma$, we get an average of 0.31 ± 0.11. This is about twice the k value determined for the canopy (Section VI), but about the same as the thick-ice limit

determined in Section VII for the newly frozen ice shortly before it was cored. The variation of k with time is shown in Figure 65. Individual k values are quite erratic. There is no noticeable trend with time (and thus temperature), which means that the temperature dependence given by McCammon-McDaniel, Eq. (17), does not need modification. This test of the temperature dependence is a moderately good one because the $T^{2/3}$ dependence predicts a doubling of the absorption for the 4-day temperature change from an average of −6°C to −2°C.

IX. ENVIRONMENT

Environmental measurements at the ice camp are detailed in Ref. 8. Some the results pertinent to these studies are included here.

A. Weather

Air temperature, barometric pressure, and wind properties during the experiment are shown in Figure 66. A histogram of wind vectors, Figure 67, shows the prevailing wind direction to be about 225° True. A plot of wind vectors, Figure 68, shows the wind direction was highly variable, again with some predominance from the southwest.

B. Currents

The measured currents during run 1 at 1103 h on 29 March and during run 3 at 1137 h on 3 April are shown in Figures 69 and 70, respectively. For each measurement, we have plotted both the current relative to the floe and the current relative to the Earth, the latter being obtained by combining the current measurement with the measured floe movement (see next paragraph).

C. Floe Drift

The position of the floe was monitored with both the Global Positioning System and the NAVSAT system. Figure 71 shows the path of the floe during the experiment, with some averaging to smooth out the jitter in the readings. From these readings, we calculated the drift speed and direction shown in Figure 72. A comparison of the drift data with the wind data (Figure 73) shows a close relationship if a ratio of 40 is used in the speed scales.

D. Ice Properties

Three ice cores were obtained to measure ice properties. After the cores were removed, the temperature was measured every few centimeters along the core by inserting a small probe containing a thermistor into a drilled hole. The cores were then sawed into small sections. For some of these sections, the sound speed was measured by transmitting an 800-kHz pulse through the ice and recording the transit time. The core sections were then melted, and their salinities were determined by measuring the conductivity of the melt water. Sound speeds were also usually calculated, using equations involving the void ratio and Young's Modulus.

One of these ice cores was taken in the area of the 30-m triad; another was taken in the monitor hole ice at the end of the ice-growth experiment. These results are tabulated in Table 44 and were plotted in Figure 54.

The third core was taken from the ice block used at the end of the ice-growth experiment after it had warmed for 4 days and been brought to the surface. Figure 61 compares the salinities measured before submergence of the ice block with those measured after it had been submerged for 4 days an. shows the porosity calculated from temperature and salinity. Figure 58(b) shows the average sound speed after submergence.

X. THERMAL DIFFUSIVITY

A. Previous Analysis

The homogeneous equation of heat conduction is

$$\frac{\partial^2 \bar{T}}{\partial z^2} = \frac{1}{\kappa} \frac{\partial \bar{T}}{\partial t} , \tag{22}$$

where z is the vertical coordinate in the ice, t is the time from a selected initial condition, and κ is the diffusivity. We use the freezing point of the seawater as the reference temperature, i.e.,

$$\bar{T} = T + 1.8 . \tag{23}$$

In Ref. 4 we developed theoretical equations for the temperature distribution in the ice for the boundary conditions of various ice configurations. For two configurations, we compared the theoretical results for various values of κ with measured results to estimate κ.

In one case, the ice in the 2-m-square hole had frozen to a thickness of 42 cm, and a rise in ambient temperature caused a warming of the ice (Figure 35). A comparison of theoretical and measured temperature profiles for the last temperature profile measured during the ice-growth experiment indicated a diffusivity of 0.0080 cm^2/s .

In the other case, a 58-cm-diameter ice block was cored from the same ice and submerged in seawater that was at the freezing temperature. The resulting warming of the ice block is shown in Figure 56. Comparisons between theory and measurements were made 8 h and 16 h after the block was submerged and indicated a diffusivity between 0.0013 and 0.0018 cm^2/s.

B. An Ice Block from the Canopy

Prior to the ice-growth experiment, strings of thermistors were placed in the ice canopy by drilling a small vertical hole, inserting a string of thermistors, and refilling the hole with water, which quickly froze. Two strings of eight thermistors each were installed, one at the center of a planned 58-cm-diameter block and the other 20 cm from the center. The initial temperature readings are presented in Figures 16 and 17.

After several sets of temperature measurements were taken, a 58-cm-diameter block was cored out by melting a circular groove in the ice. The block was depressed 1.31 m, where it was surrounded by seawater at the freezing temperature. However, there was 70 cm of overlap between the block and the canopy where the water circulation was poor; some freezing of the water in this narrow slot (about 3 cm) may have occurred. The temperature changes within the block after it was depressed are shown in Figures 19–21.

We now use the changing temperature profile in the block to provide a third determination of the diffusivity κ. For initial conditions, we examine the center profile from the measurements taken 2 h after submersion (Figure 19, at left). We approximate the profile primarily as two straight-line segments: (1) from -2°C at the upper surface of the ice to -13°C 60 cm below the surface, and (2) from there to -2°C at the bottom, as shown in the upper graph of Figure 74. In the same manner as for the ice growth experiment, theoretical predictions were made of the temperature profile in the ice as a function of time. In Figure 74, predicted profiles in the center of the block for various trial values of κ are compared with measured profiles to determine the effective κ. Comparisons are made 305 and 1055 minutes after submersion of the block (5.1 and 17.6 h, respectively). To indicate the accuracy of κ, theoretical results are shown for two values that appear to fit the data. They indicate a diffusivity of 0.0030–0.0035 cm²/s. This analysis supersedes the one in Ref. 4, where smaller values were obtained.

For completeness, similar comparisons should be made for the other string 20 cm from the center of the block, but this has not been done owing to the complexity of the calculation.

In developing the equations in the appendix of Ref. 4, we assumed that the initial temperature varied linearly from the center of the ice block to the edge, since this assumption greatly simplified the calculations. The extra string of thermistors 20 cm from the center (9 cm from the edge) of the 58-cm-diameter block allowed a check on this assumption. The temperatures at the center and 20 cm from the center, taken (or interpolated) from Figure 19 at three depths for a time just after submersion, are compared in Figure 75. The temperature at the edge of the block was assumed to be that of the adjacent water. The variation shown in the figure is certainly not linear. For rigorous results, the calculation should be made with a more accurate knowledge of the initial radial variation and with a diffusivity that varies with temperature, but this would require a much more complex treatment.

C. Discussion of Results

Three different calculations of diffusivity were made from ice temperature changes measured under widely differing circumstances:

(1) a block of ice that had grown to 42 cm thick and was subjected to air temperature—0.0080 cm²/s

(2) a block from this ice that was later submerged in near-freezing seawater—0.0013 to 0.0018 cm²/s

(3) a 58-cm-diameter block cut from the 212-cm-thick canopy and submerged—0.0030 to 0.0035 cm²/s.

For (1), the final temperature at the top was known, and we were merely looking at changes in the shape of the profile, involving 2°C at most, for various values of κ. For the other measurements, the interior of the ice changed by 8°C and these measurements give a more accurate κ.

For (3), the 58-cm-diameter block cut from the ice canopy was still in close proximity to the canopy ice; thus the temperature gradient from center to edge would not be as great near the top, and less heat would penetrate, giving a lower apparent κ. On the other hand, κ is known to be smaller at temperatures near freezing; thus more heat could enter from above, giving a higher apparent κ. If the latter effect is greater, the measured value of 0.0030–0.0035 cm²/s would be erroneously high, and the lower value may be more reliable.

In summary, the thermal diffusivity was measured in ice of considerable thickness and varying temperature. The average diffusivity varied between 0.0015 and 0.0035 cm²/s, and this spread is thought to be due to the temperature variation in the ice. When much of the ice was only slightly above the freezing point, the measured diffusivity was low, indicating that such ice is a poor conductor of heat.

REFERENCES

1. T. Wen, G. R. Garrison, R. E. Francois, R. P. Stein, and W. J. Felton, Sound Speed, Reflectivity, and Absorption Measurements in Arctic Ice in 1988, APL-UW TR 9005, Applied Physics Laboratory, University of Washington, Seattle, March 1991.

2. G. R. Garrison, R. E. Francois, and T. Wen, "Acoustic reflections from arctic ice at 15–300 kHz," *J. Acoust. Soc. Am., 90,* 973–984 (1991).

3. D. A. McCammon and S. T. McDaniel, "The influence of the physical properties of ice on reflectivity," *J. Acoust. Soc. Am., 77,* 499–507 (1985).

4. K. L Williams, G. R. Garrison, and P. D. Mourad, "Experimental examination of growing and newly submerged sea ice including acoustic probing of the skeletal layer," *J. Acoust. Soc. Am., 92,* 2075–2092 (1992).

5. G. R. Garrison, R. E. Francois, T. Wen and W. J. Felton, Acoustic Reflections from Cylindrical Blocks of Arctic Ice, 1988, APL-UW TR 8815, Applied Physics Laboratory, University of Washington, Seattle, January 1990.

6. E. O. Doebelin, *Measurement Systems: Application and Design,* McGraw-Hill, New York, 1983.

7. H. B. Sachse, *Semiconductor Temperature Sensors,* Wiley, New York, 1975.

8. T. Wen, F. W. Karig, W. J. Felton, J. C. Luby, and K. L. Williams, Environmental Measurements in the Beaufort Sea, Spring 1990, APL-UW TR 9105, Applied Physics Laboratory, University of Washington, Seattle, December 1990.

FIGURES

LIST OF FIGURES

Figure 1.   Calibrations of ITC 1042 transducer in 1988 and 1990.

Figure 2.   Calibrations of platter transducer in 1988 and 1990. The calibration using the sphere is preferred.
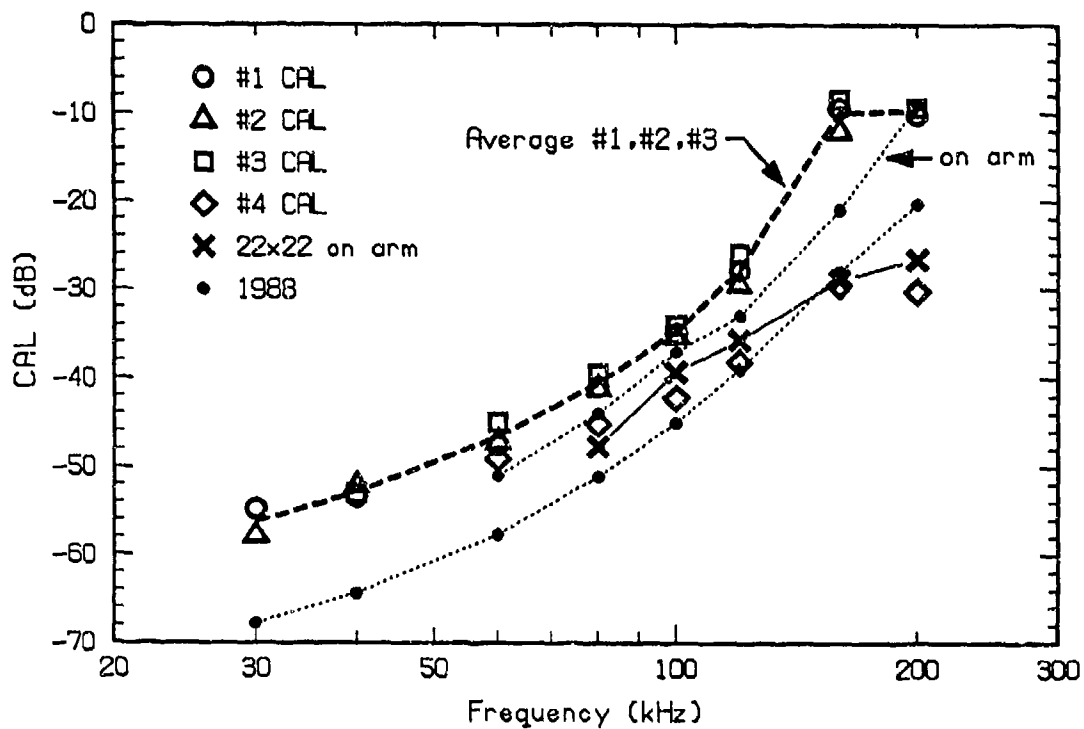
Figure 3.   Calibrations of 22×22 transducer in 1988 and 1990.
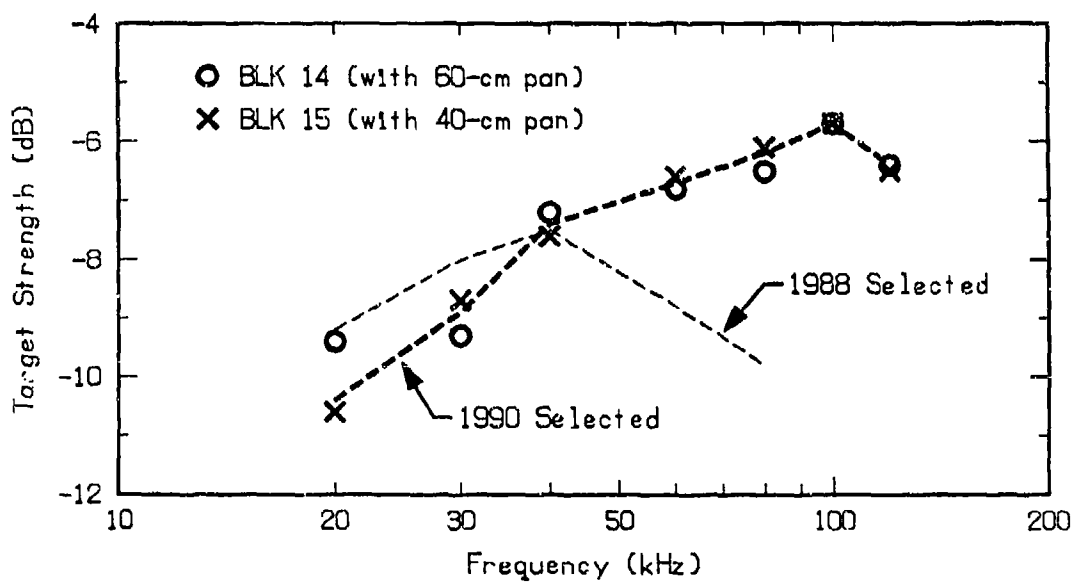
Figure 4.   Measured target strength of Freon-filled sphere in 1988 and 1990.

F3, 4

To Instrumentation

(a)

Cable to Transducer

N

Ring

Not to Scale

Transducer
Below

(b)

1.36 m

Ring

30 m

30 m

ICE

11 m

Line

Cable
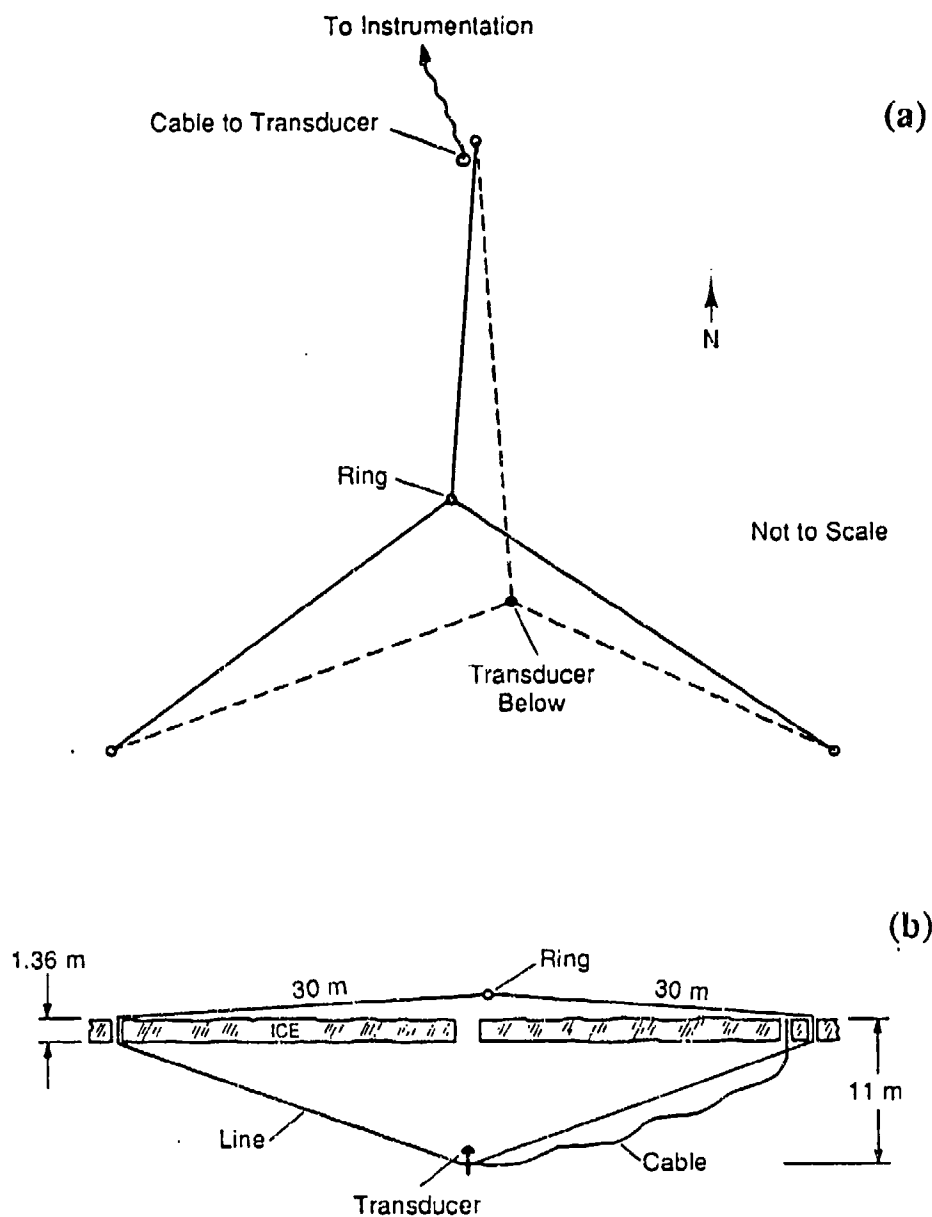
Transducer

Figure 5. Triad suspension system used to support and move the transducer below the
ice. Movement of the ring on top of the ice controls the movement of the
transducer below. The ring is positioned on a frame with wooden pegs to
ensure accurate movement. (a) Plan view, (b) elevation view (two-
dimensional simplification). This is called the large triad. A similar system,
the small triad used for the ice-growth experiment, was one-third the size
(10 m versus 30 m).

F5
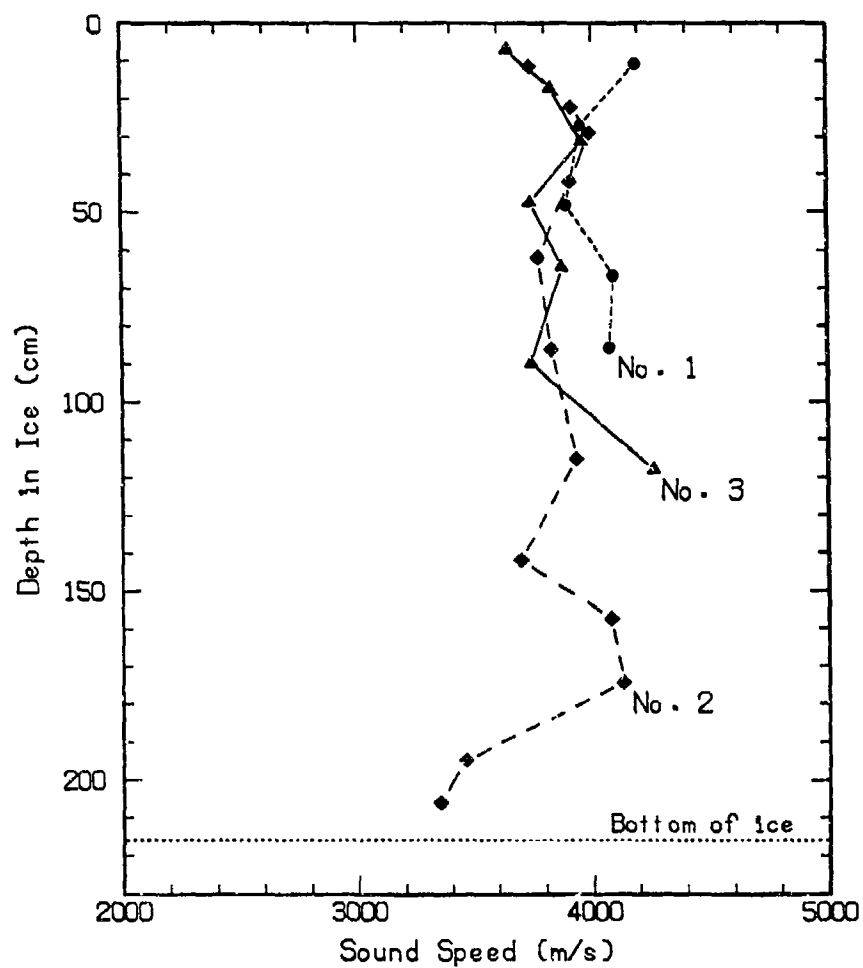
Figure 6. Sound speed profiles obtained from three sets of vertical one-way transmissions through the ice at frequencies of 30–200 kHz.
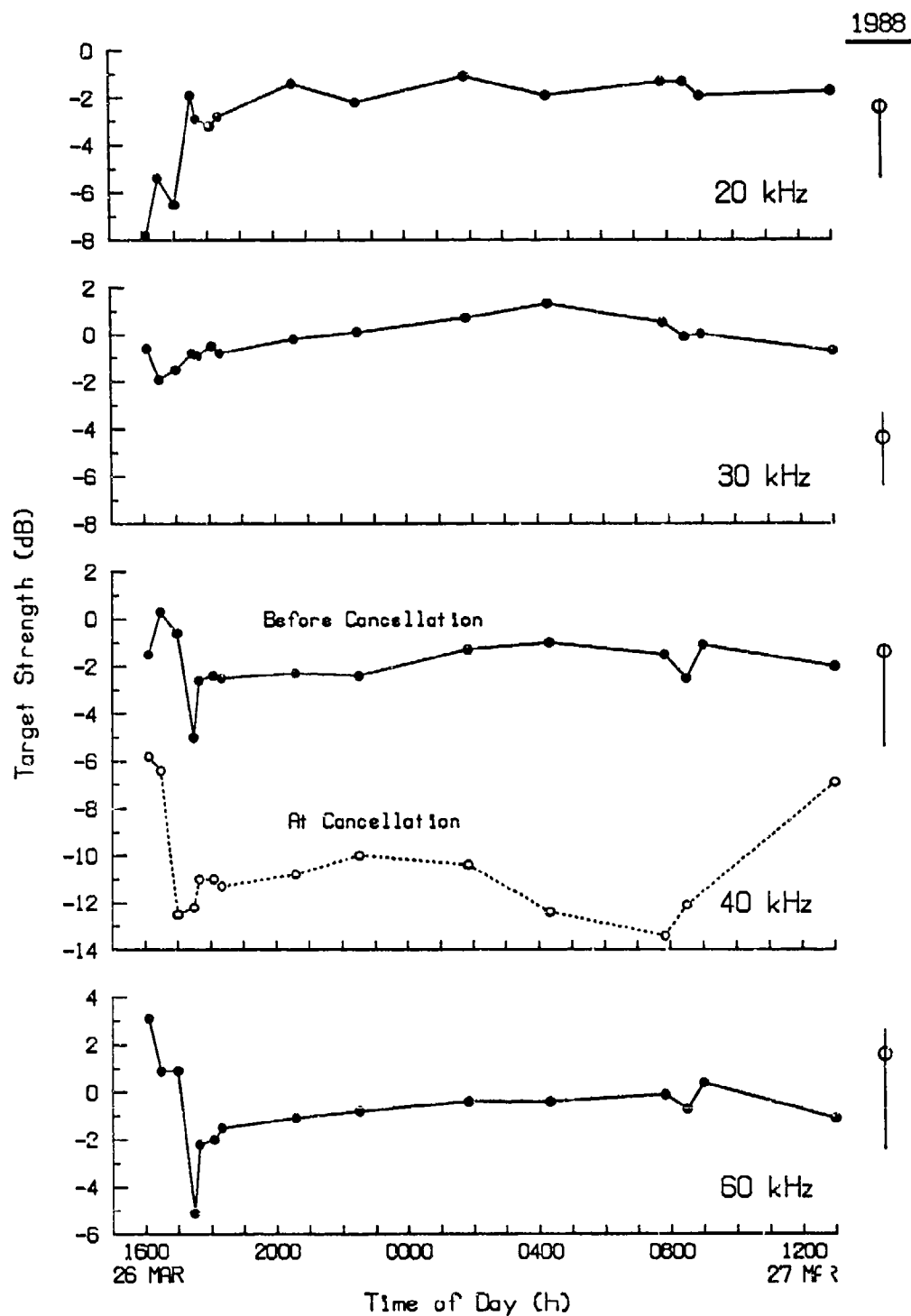
Figure 7. Measured target strength of the bottom of a 58-cm-diameter ice block after it was submerged and then warmed by the water for several hours. The 1988 average and spread are shown at the right. At 40 and 120 kHz, there were two returns at slightly different times.

F7a

Figure 7, cont.

F7b
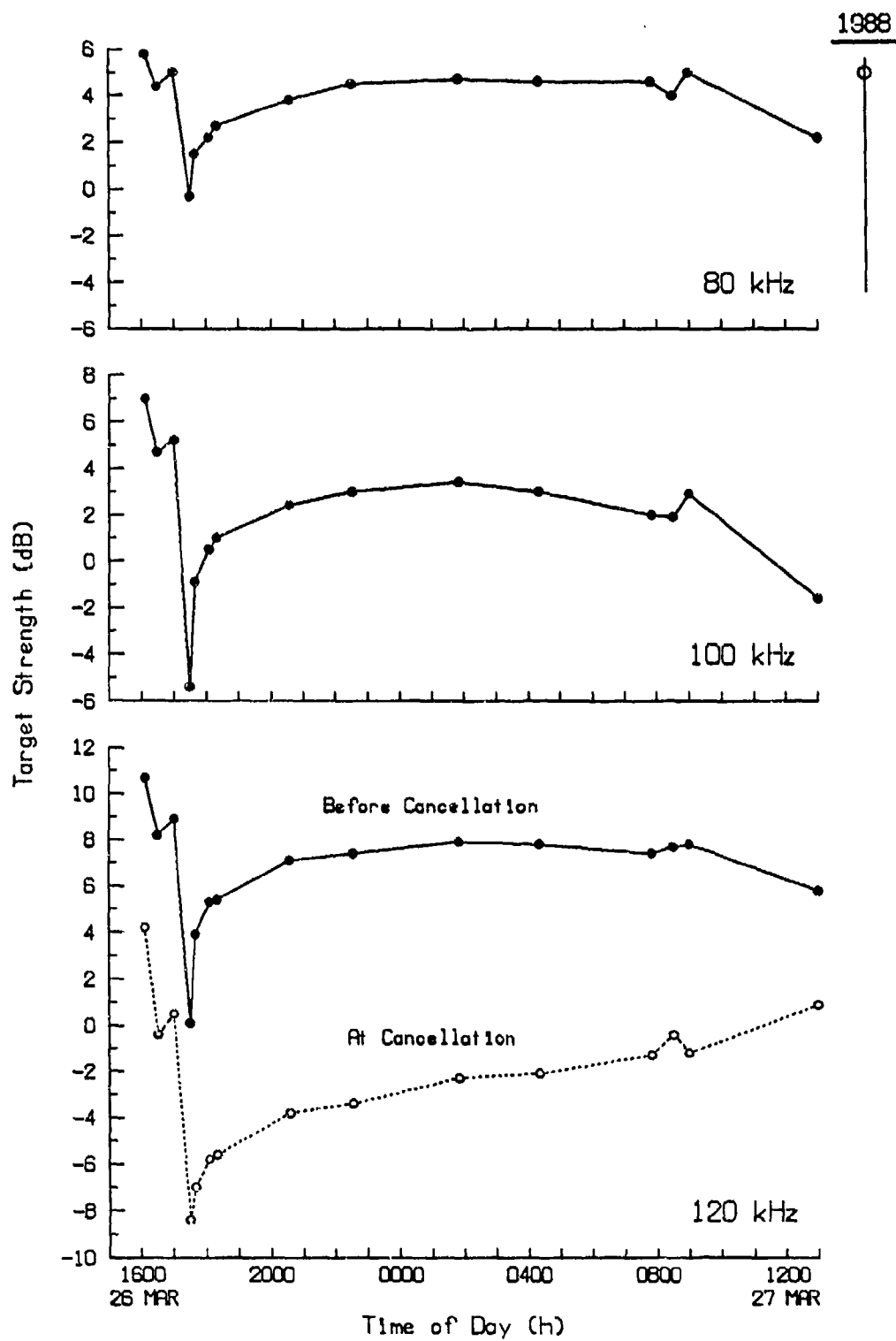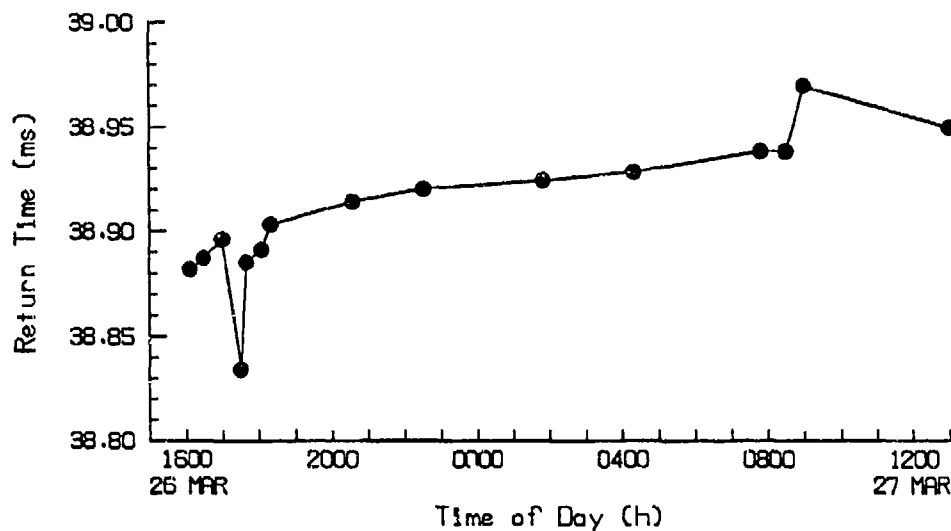
Figure 8. Monitoring the time of the return during the period of the measurements presented in Figure 7.
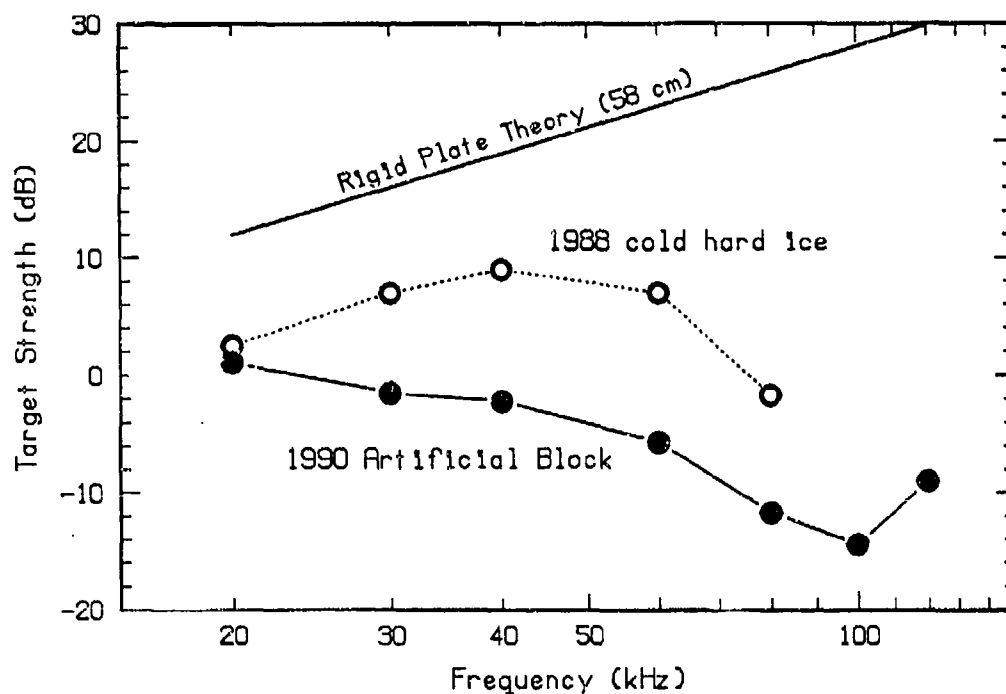
Figure 9. Target strength of an ice block prepared by freezing a container of water on the surface.
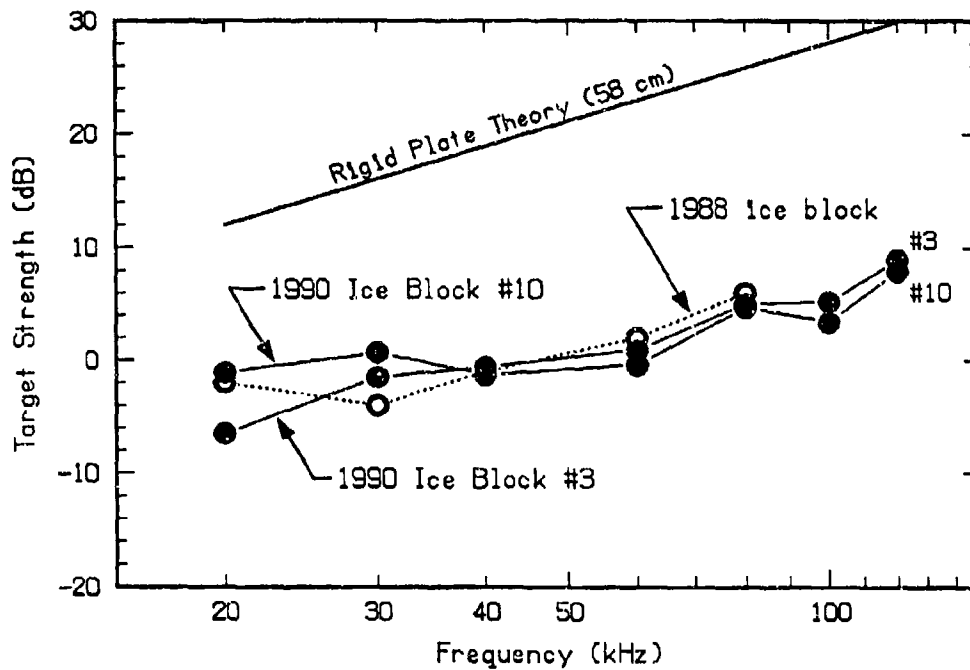
Figure 10. Target strength of the lower faces of two ice blocks compared with 1988 measurements.
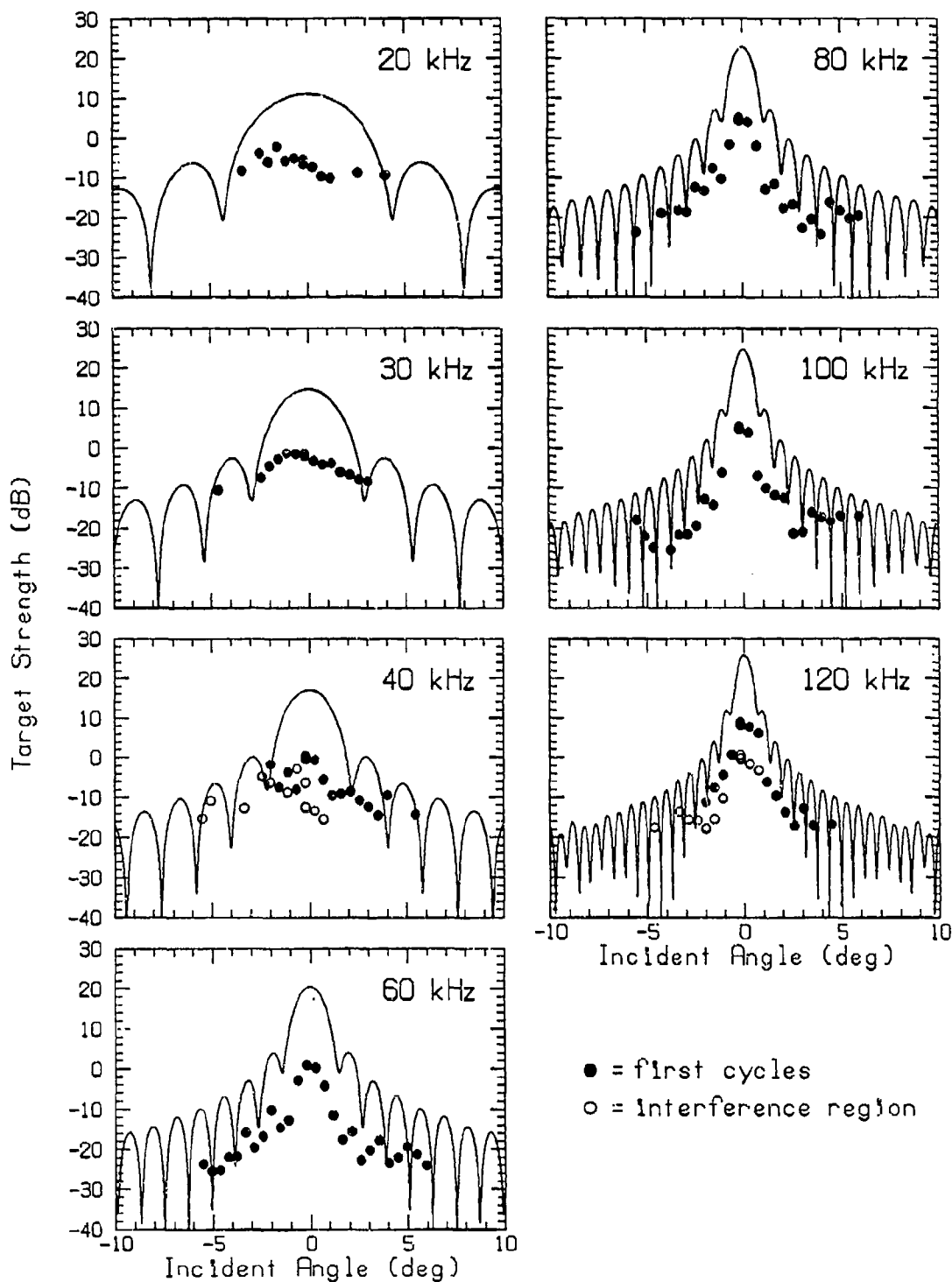
Figure 11. Target strength versus angle of incidence for a submerged ice block, north–south traverse.

F11
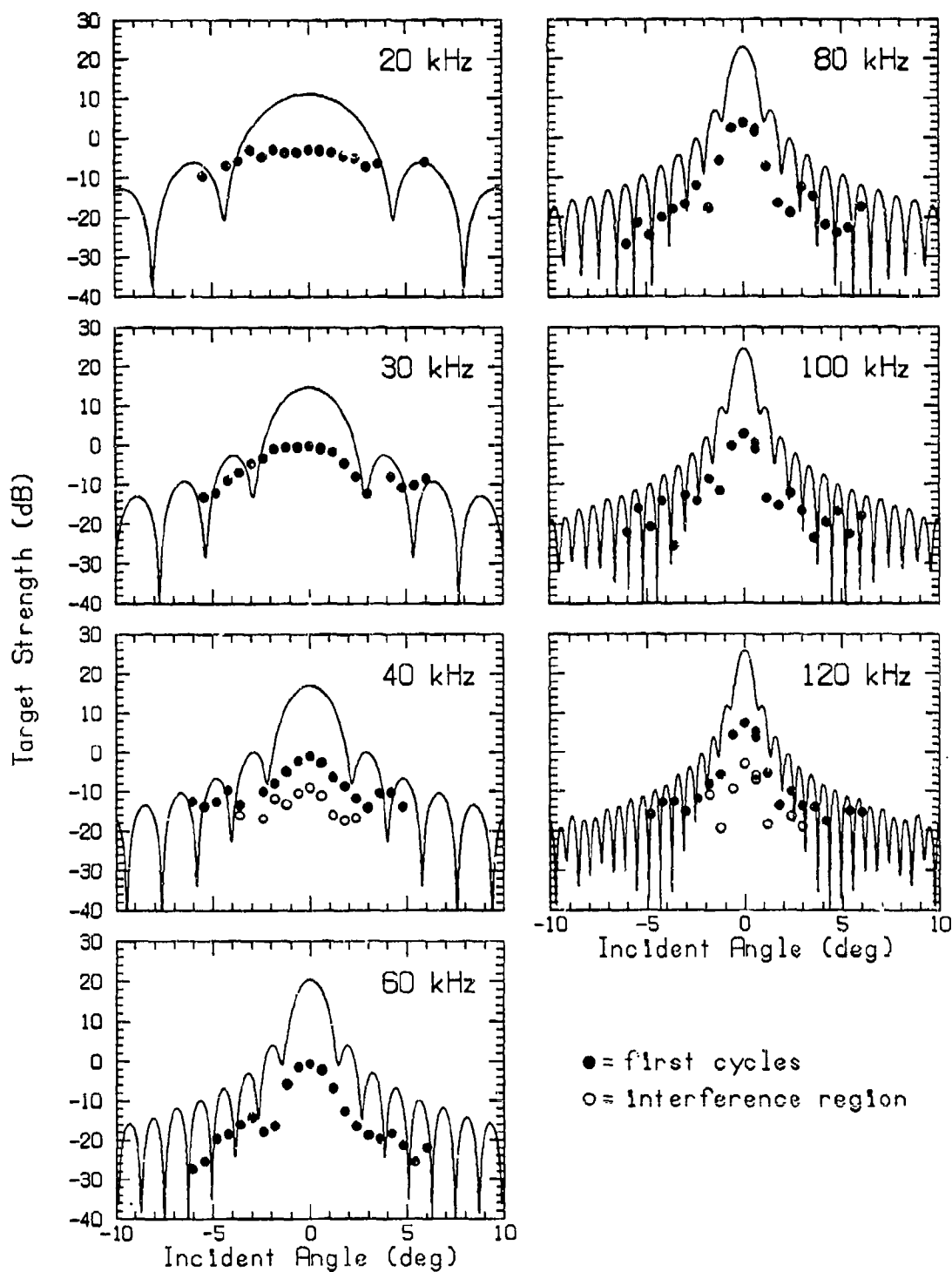
Figure 12. Target strength versus angle of incidence for a submerged ice block, east–west traverse.

F12
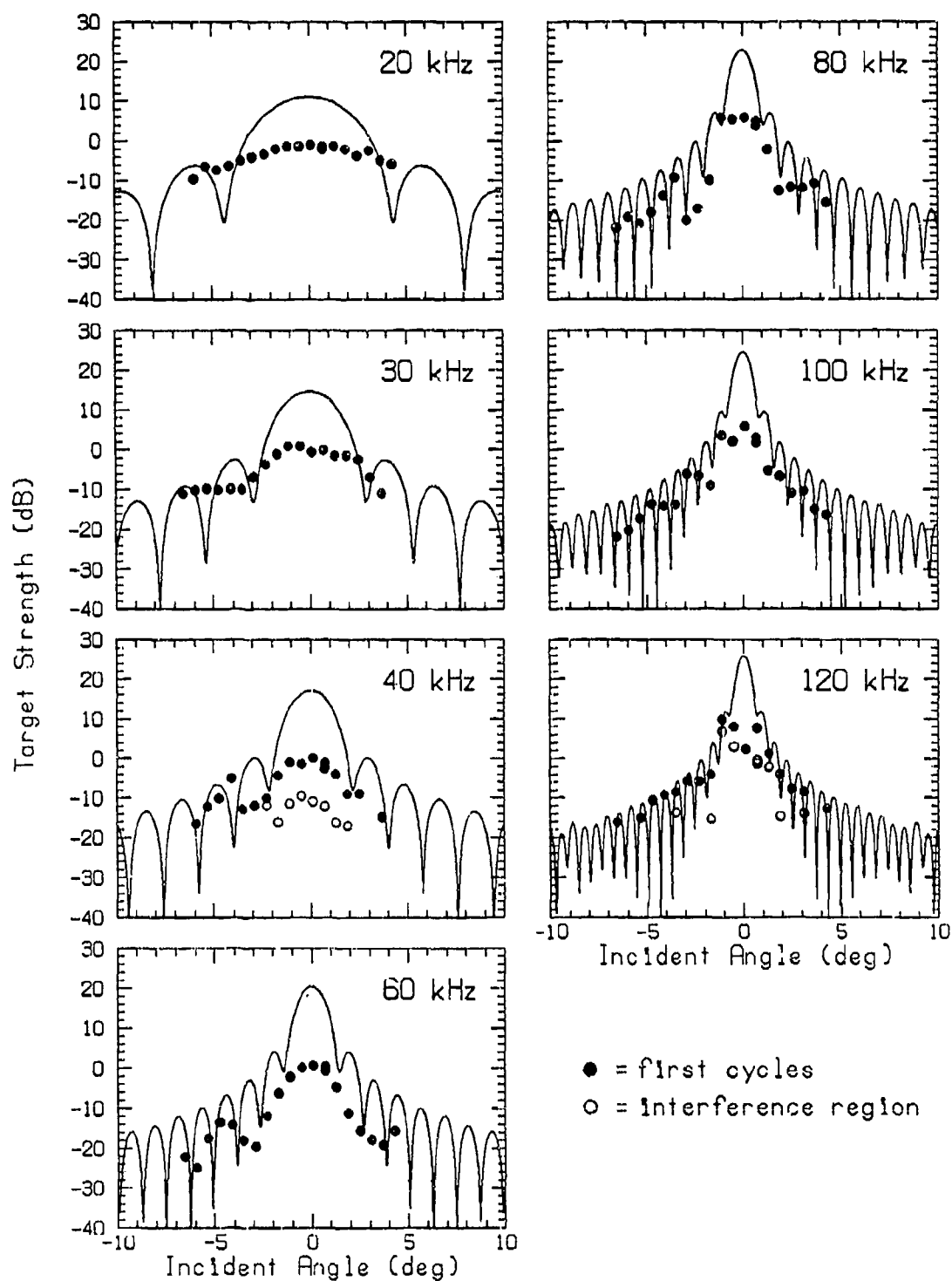
Figure 13. Target strength versus angle of incidence for a submerged ice block, second east–west traverse.
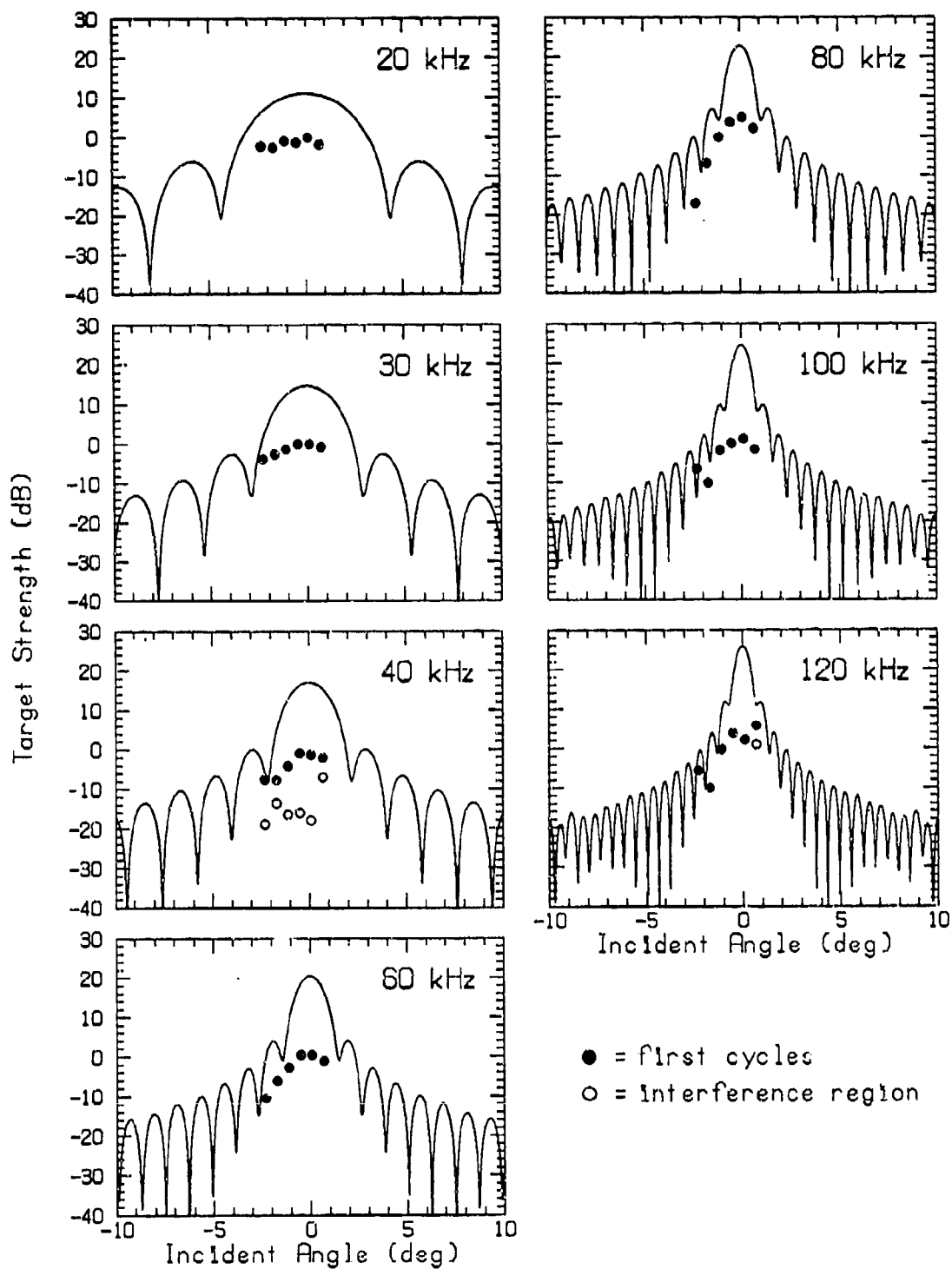
Figure 14. *Target strength versus angle of incidence for a submerged ice block, center—west traverse.*

F14
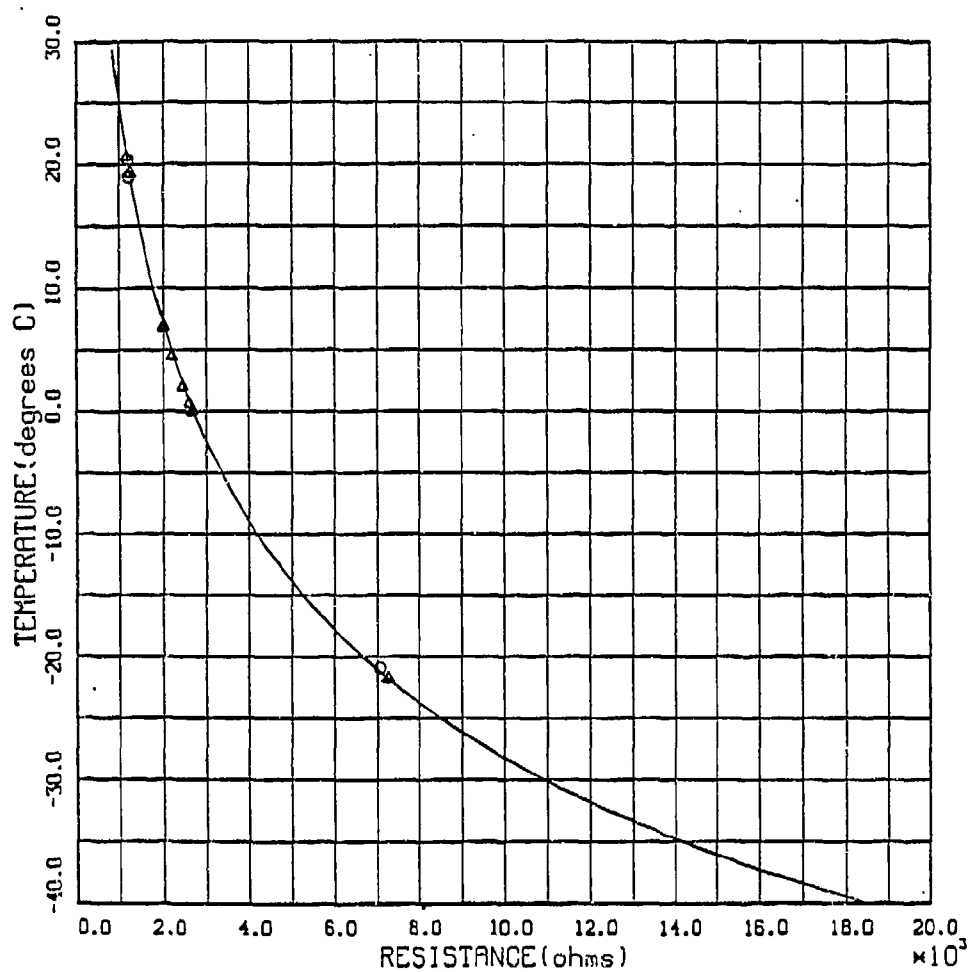
Figure 15. Calibration curve for the thermistors. The curve was checked at several temperatures for two thermistors (circles and triangles).

F15
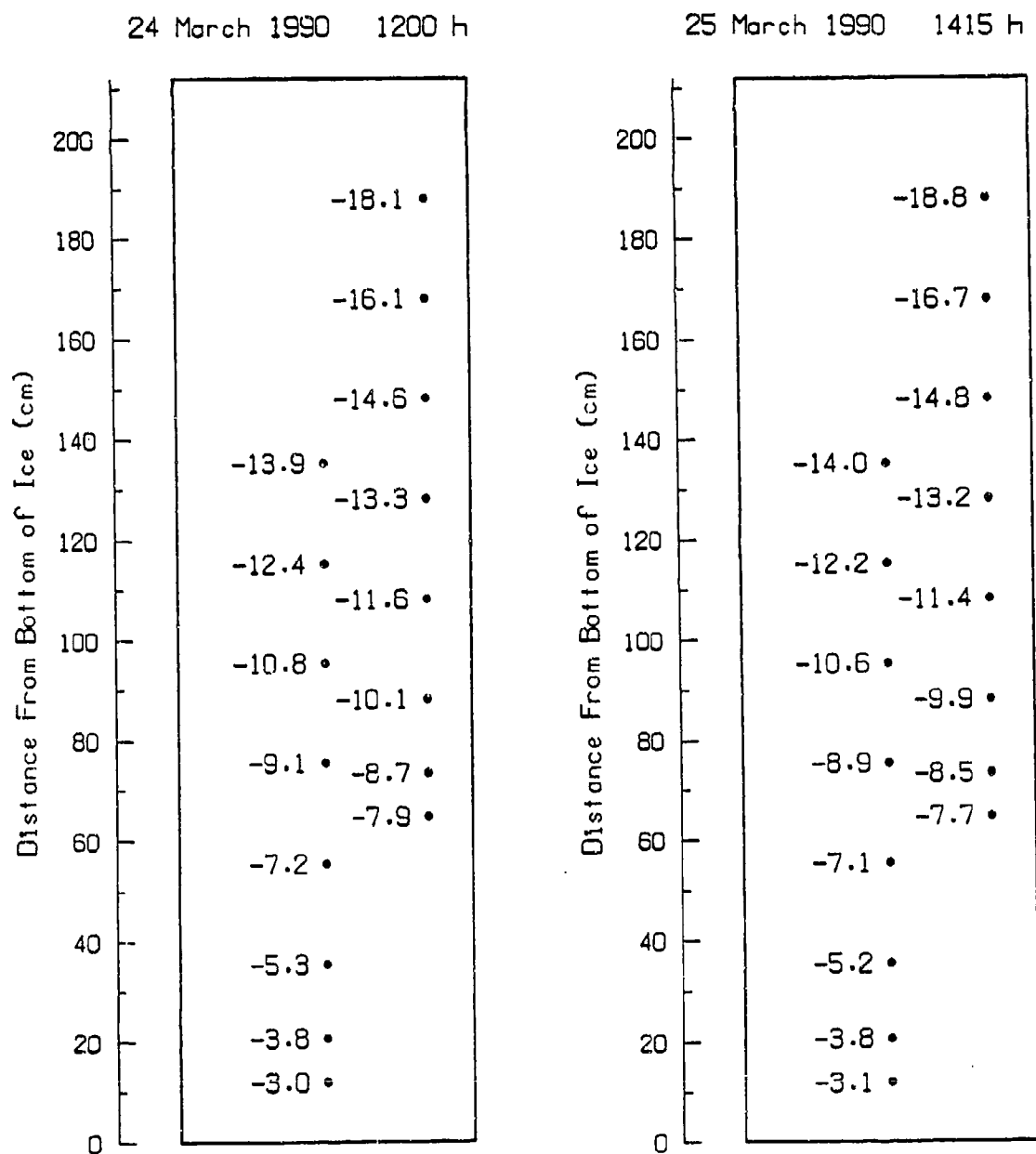
Figure 16. *Temperature readings (°C) within a (future) ice block before it was cored by melting a circular groove around it.*

26 March 1990   1001 h

26 March 1990   1323 h
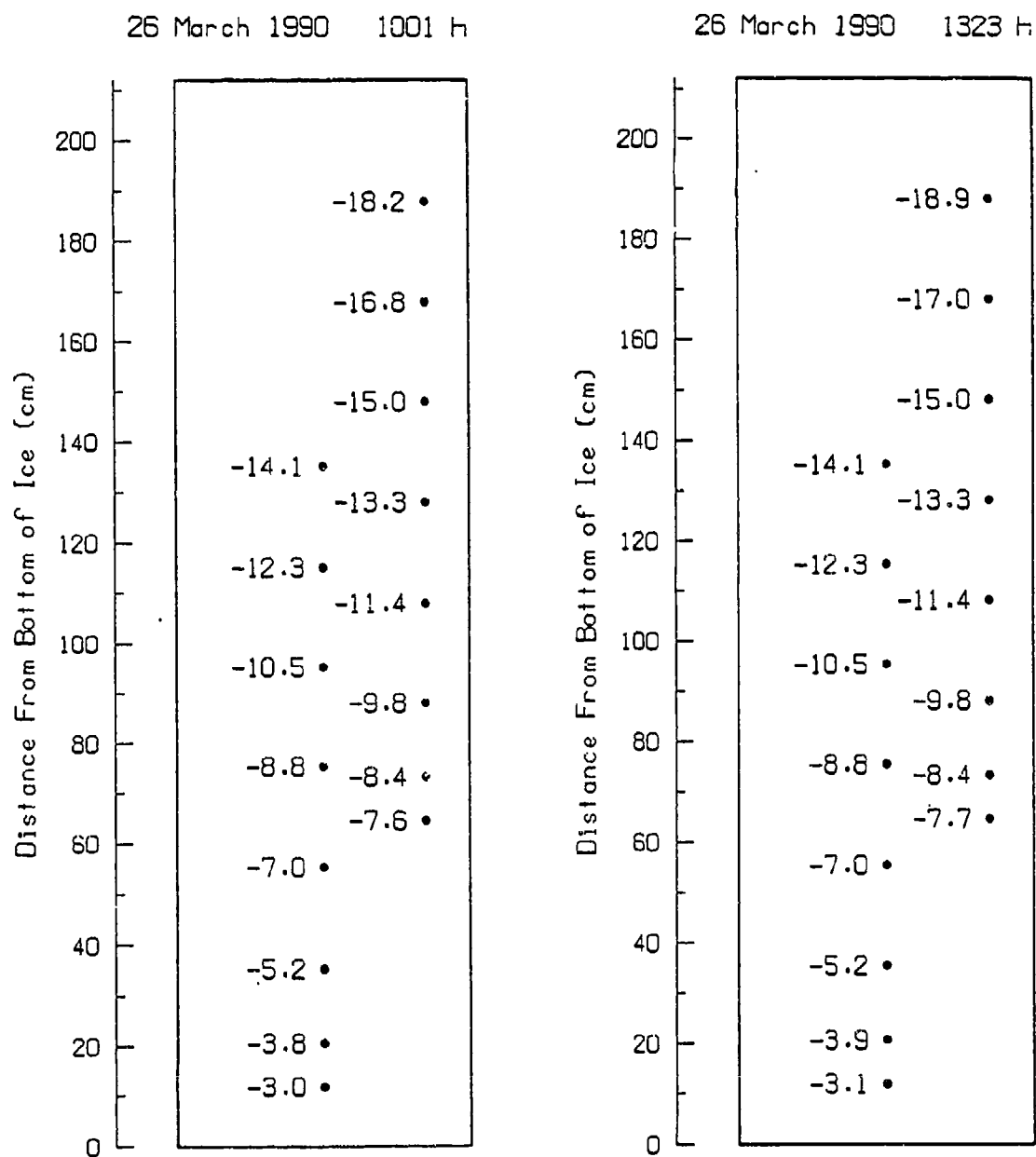
Figure 16, cont.
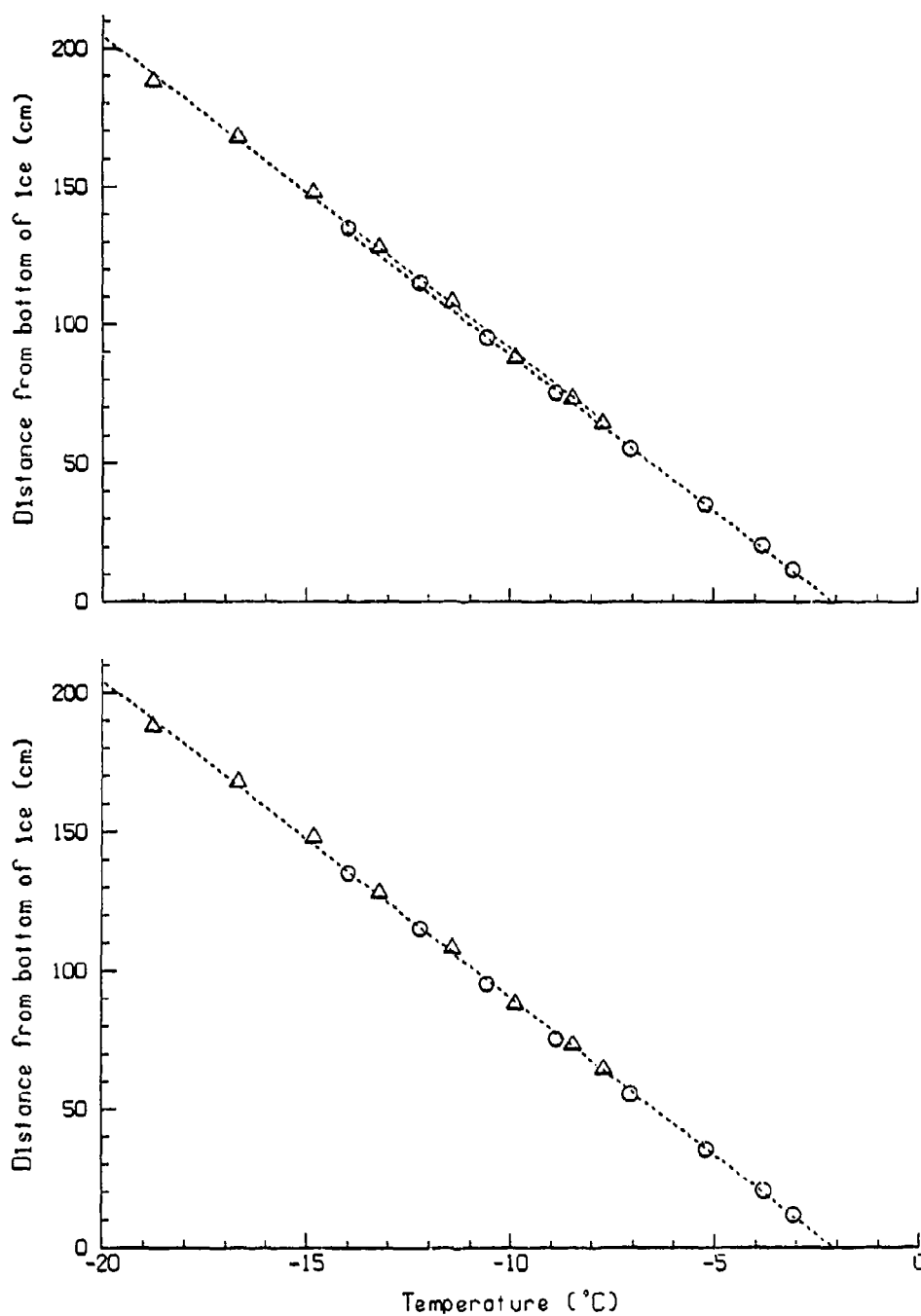
Figure 17a. Temperature profiles in the (future) ice block before coring, measured at 1415 h on 25 March 1990; circles for central string, triangles for outer string. In the upper graph, a best-fit line has been drawn for each thermistor string; in the lower graph, one line has been fitted to all points.
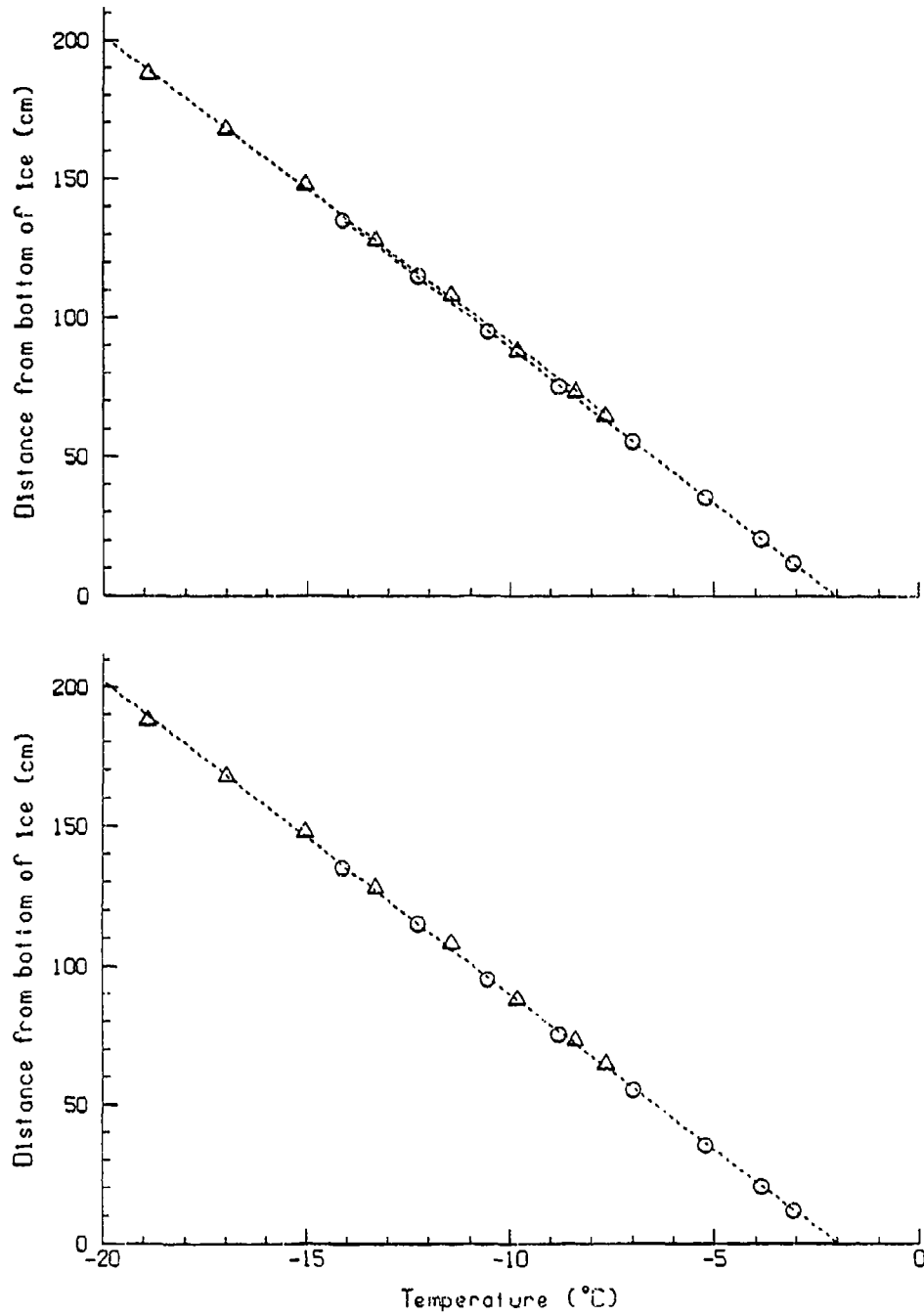
Figure 17b. Same as Figure 17a but measured at 1001 h on 26 March 1990.
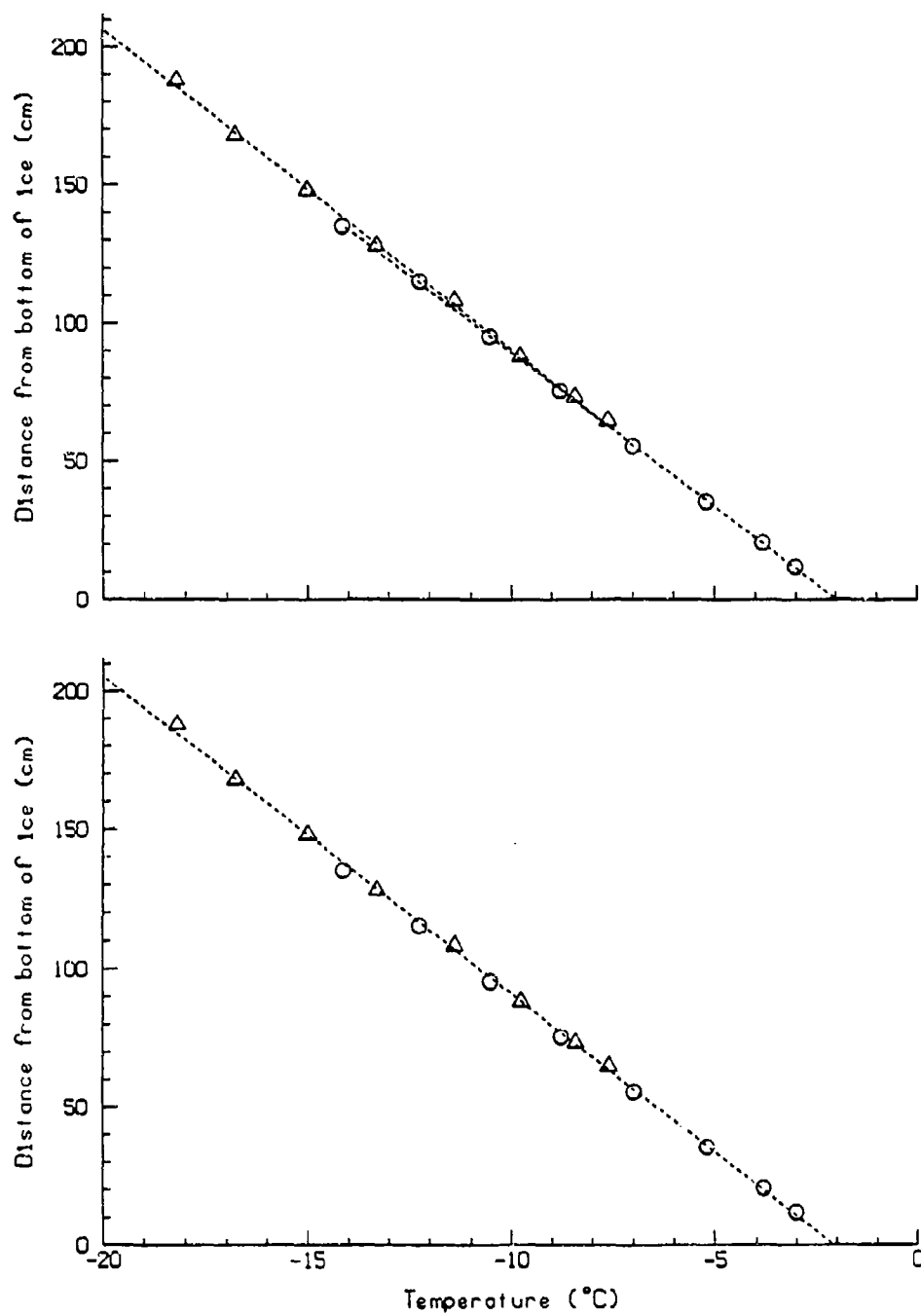
Figure 17c. Same as Figure 17a but measured at 1323 h on 26 March 1990.

F17c

26 March 1990   1521 h
0.1 h after melting out

26 March 1990   1600-1609 h
0.8 h after melting out

26 March 1990   1610-1614 h
0.9 h after melting out
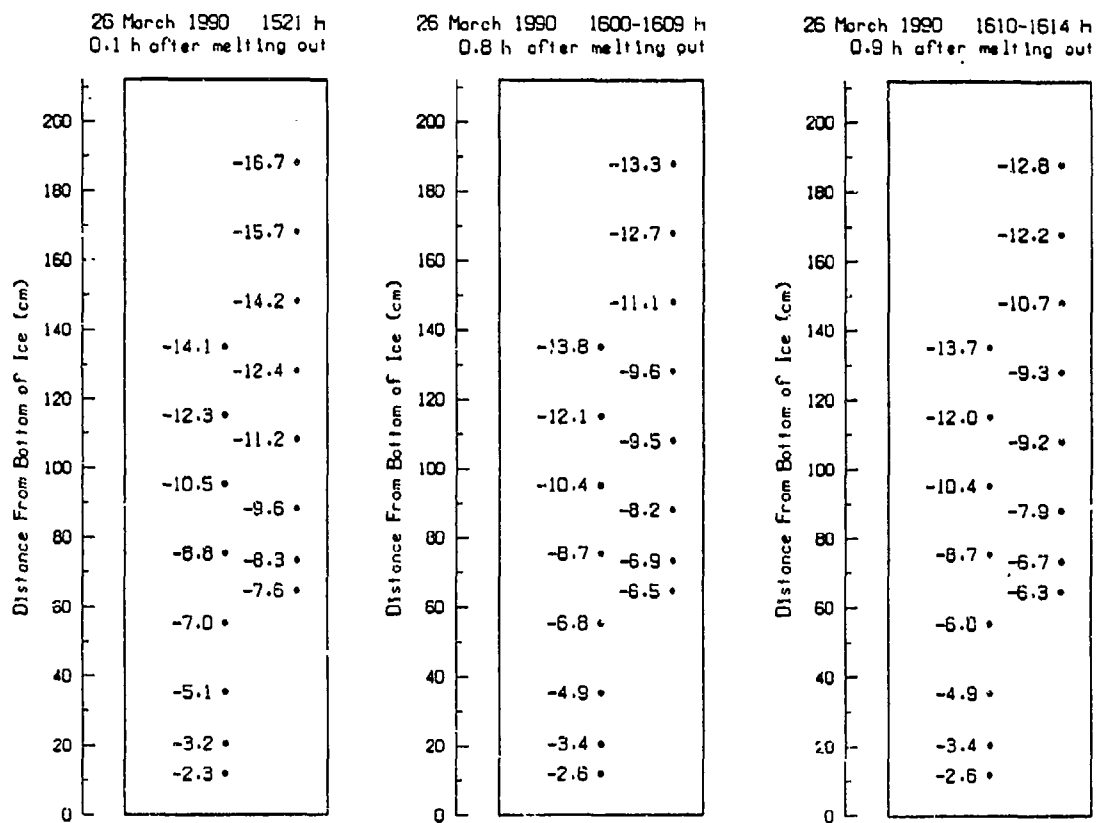
Figure 18. Temperature readings within the ice block after it was cored out (but not depressed).
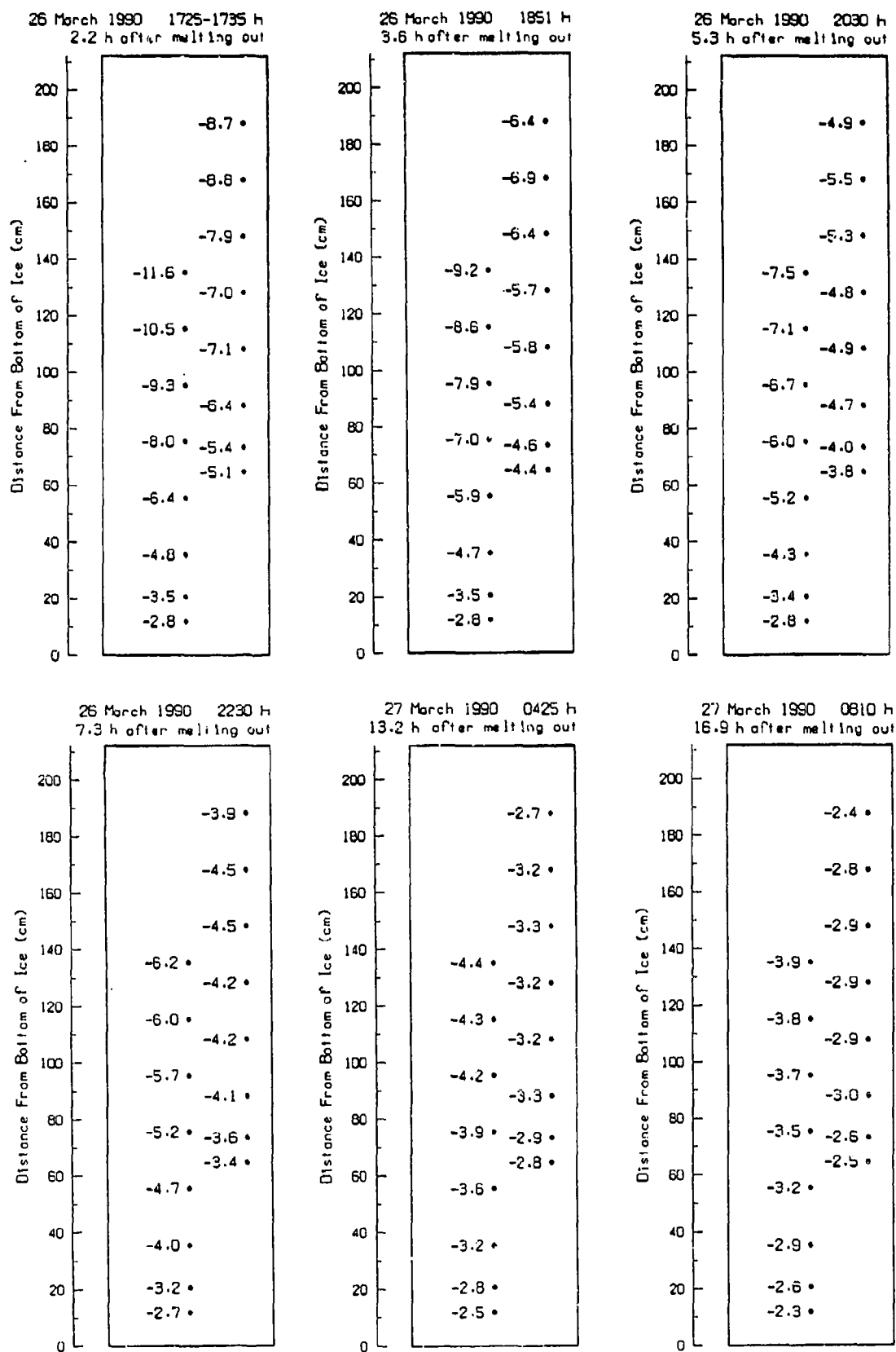
Figure 19. Temperature readings within the ice block after it was depressed at 1725 h.
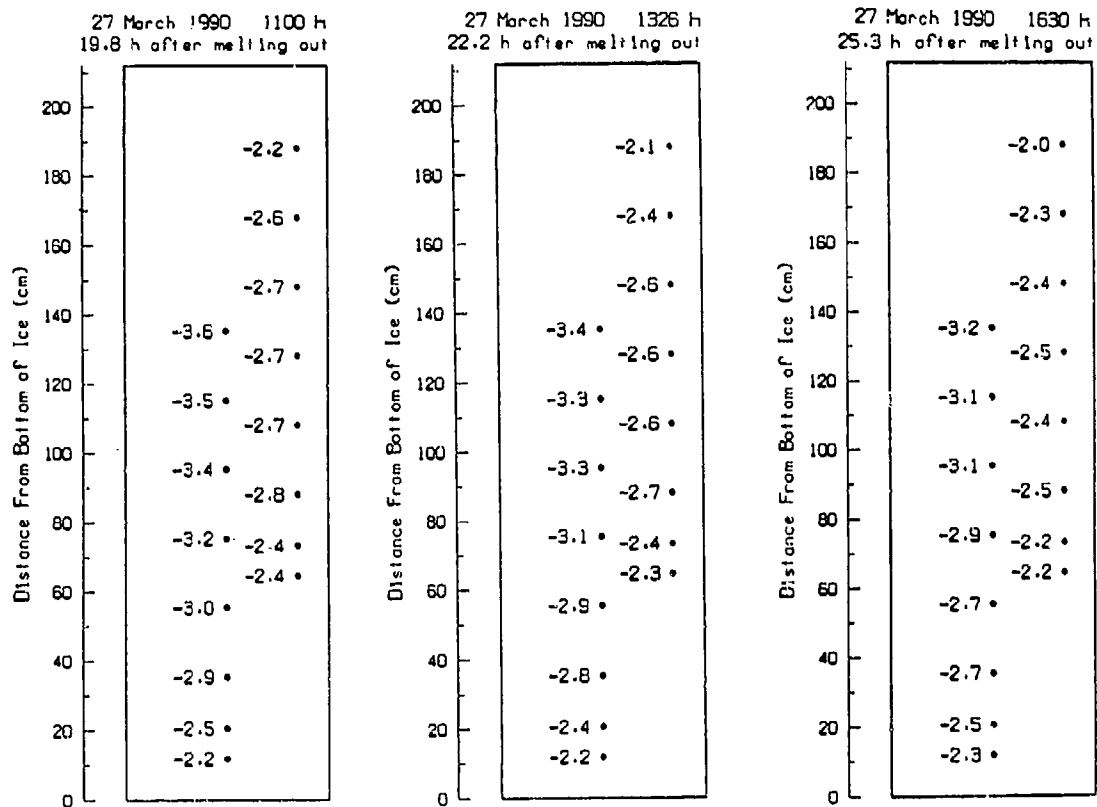
Figure 19, cont.
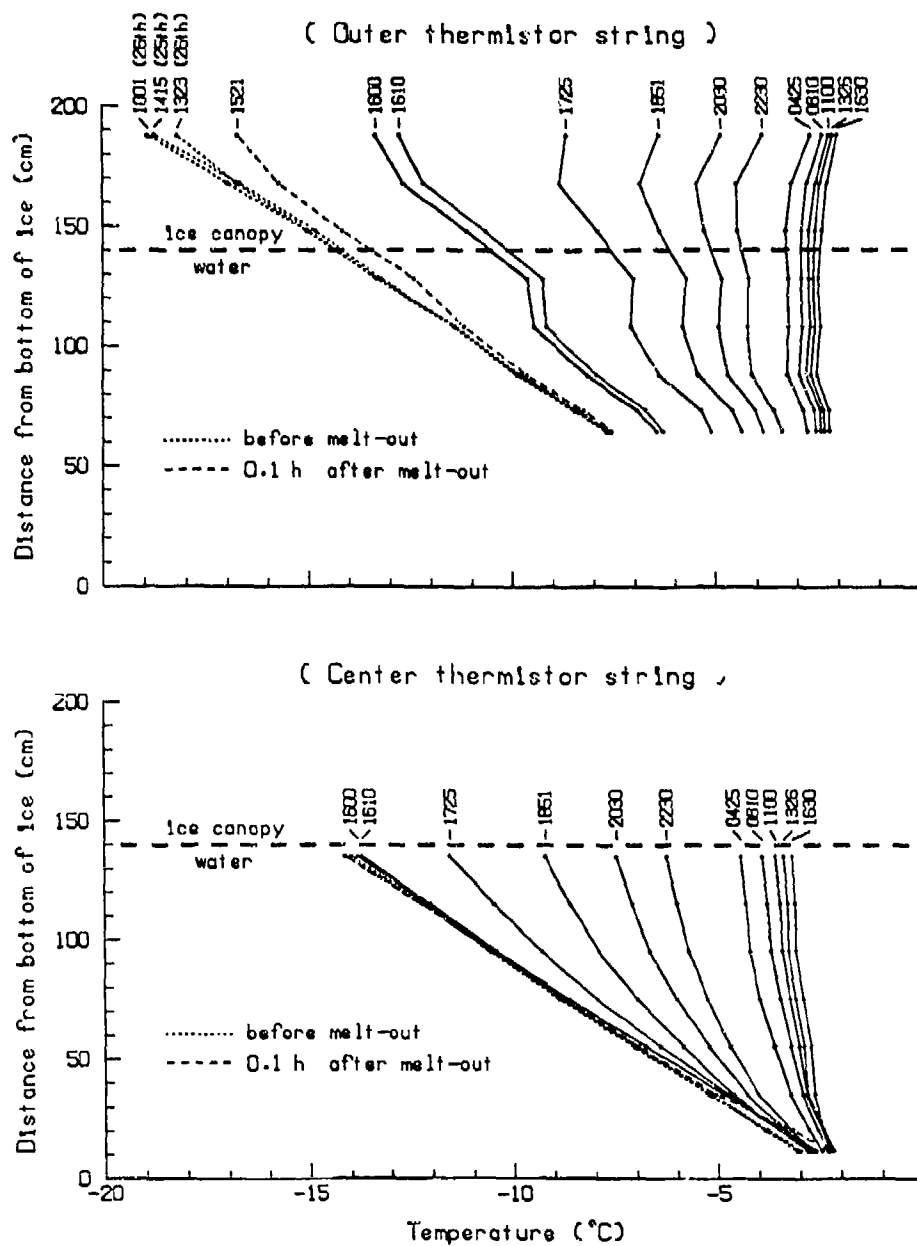
Figure 20. · *Temperature profiles recorded during warming of the ice block on 26 and 27 March 1990. The block was melted out at 1515 h on 26 March and depressed at 1725 h.*
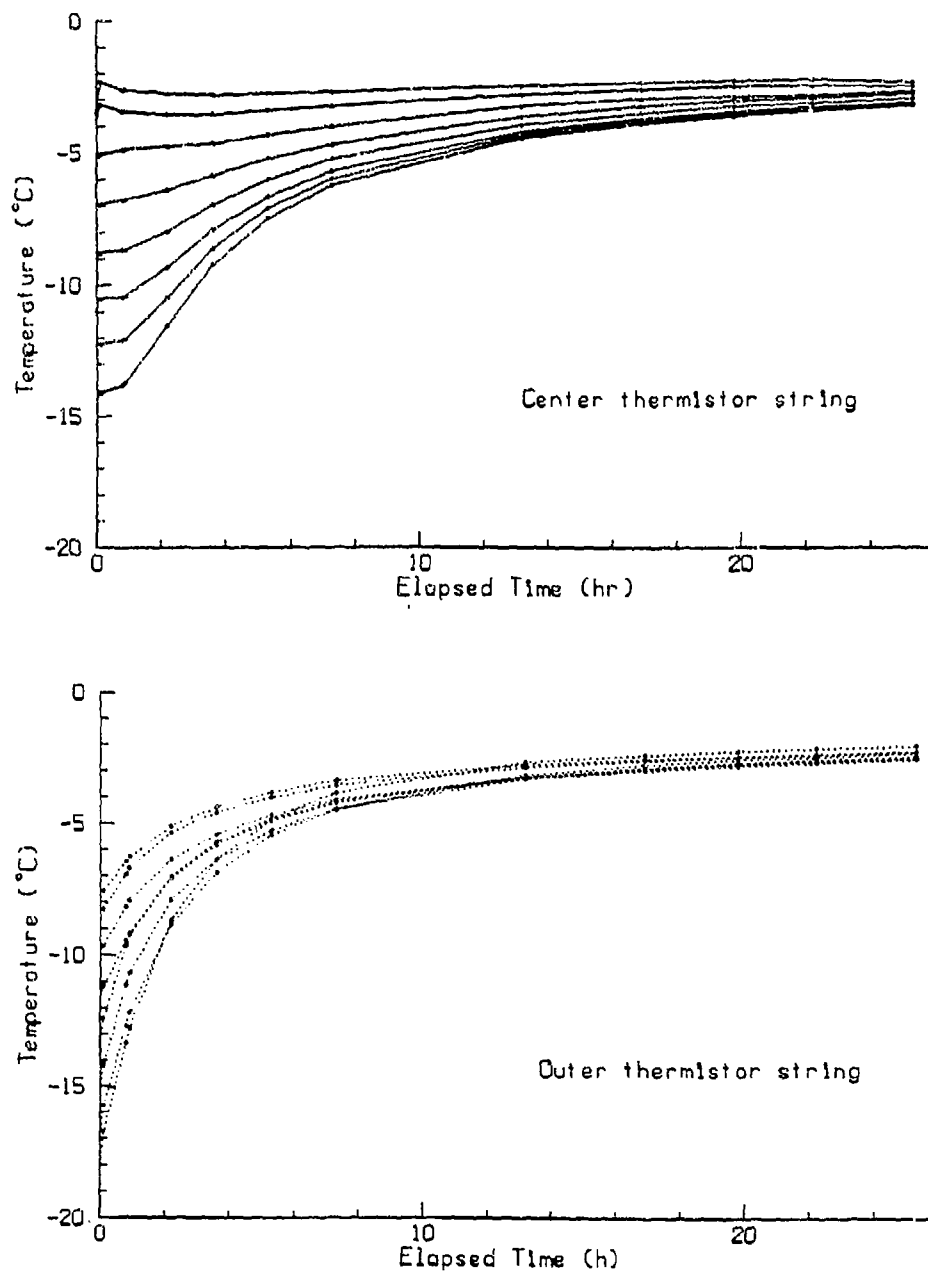
Figure 21a. Variation of temperature at each thermistor as the block warmed. The time was measured from melt-out at 1515 h on 26 March. The block was depressed 2.2 h after melt-out.
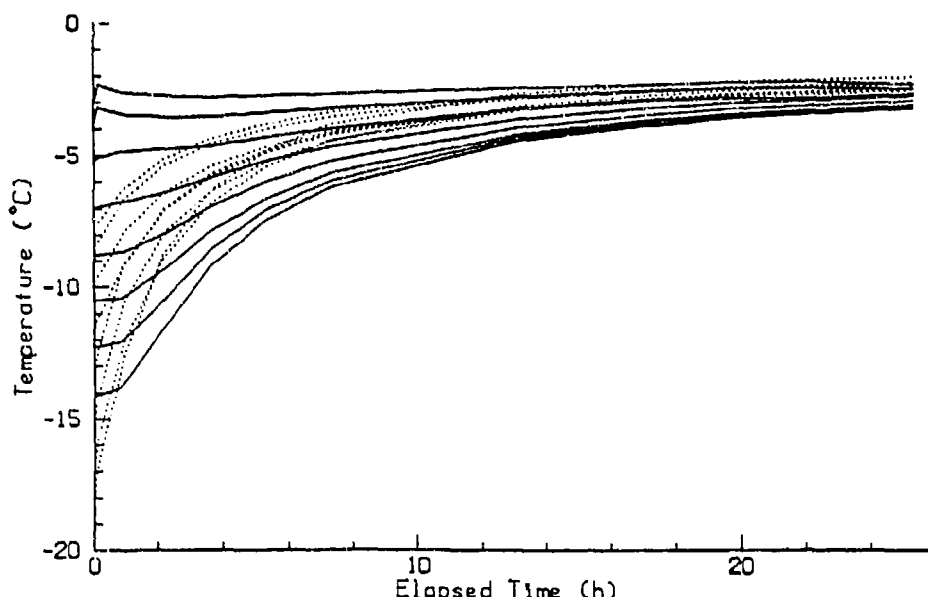
Figure 21b. A comparison of the temperatures at the two strings. Dotted lines are for the outer string.
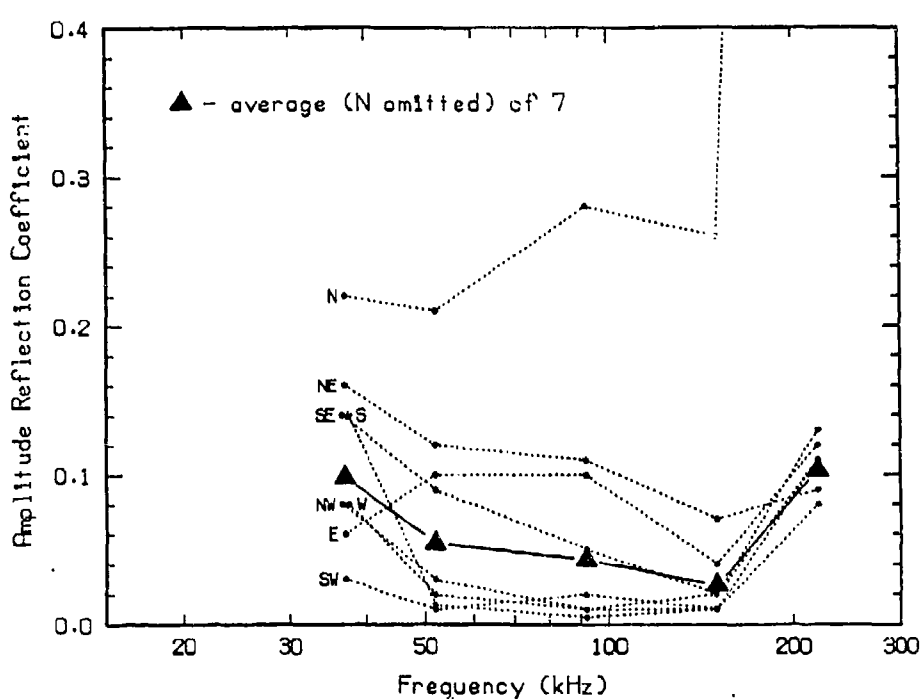
Figure 22. Measured reflectivity at several locations within the small triad, using the platter transducer.
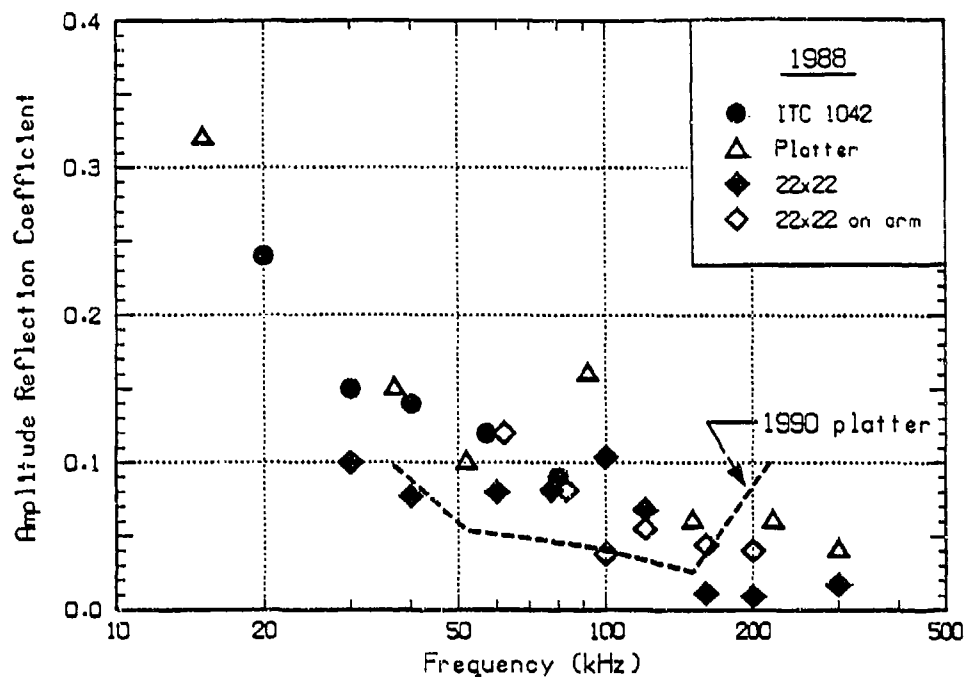
Figure 23. Measurements of the reflectivity of the underside of the ice canopy using the platter transducer, and comparison with 1988 measurements.
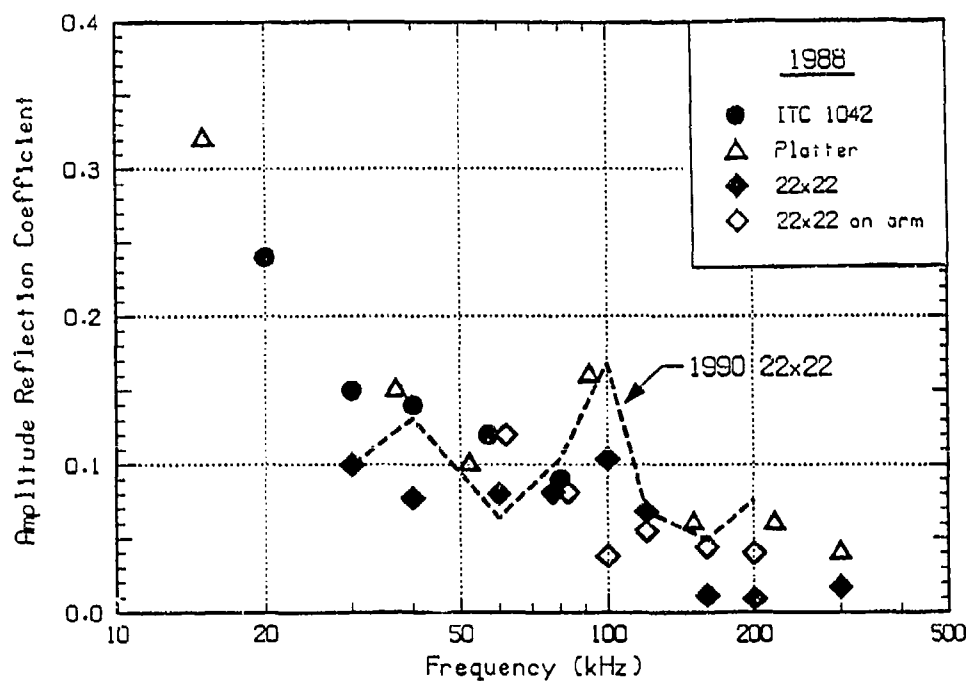
Figure 24. Measurements of the reflectivity of the underside of the ice canopy using the 22 × 22 transducer, and comparison with 1988 measurements.

F23, 24
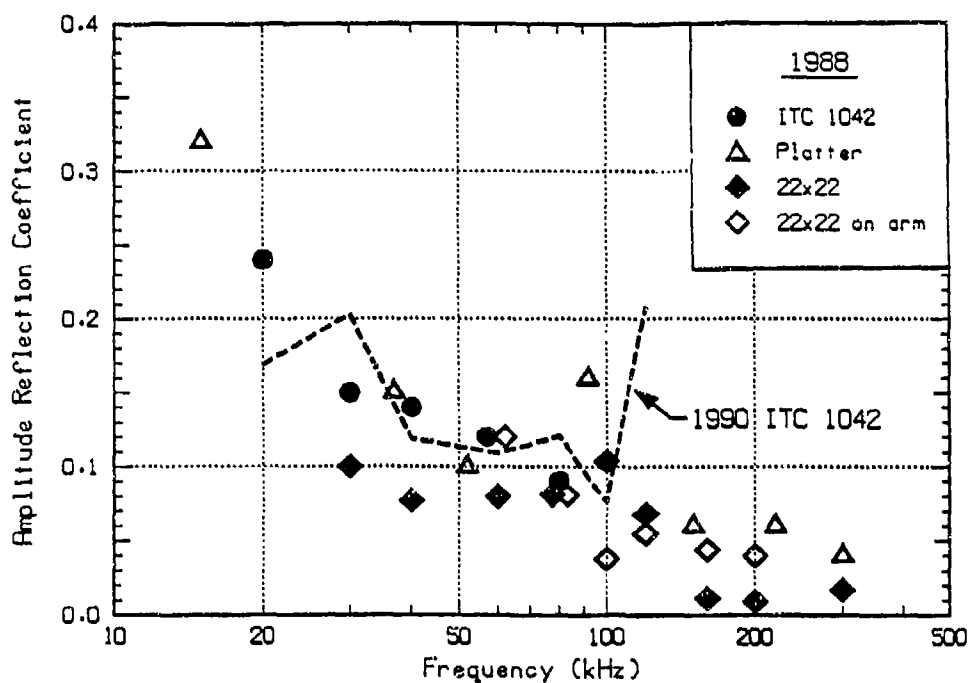
Figure 25. Measurements of the reflectivity of the underside of the ice canopy using the ITC 1042 transducer, and comparison with 1988 measurements.
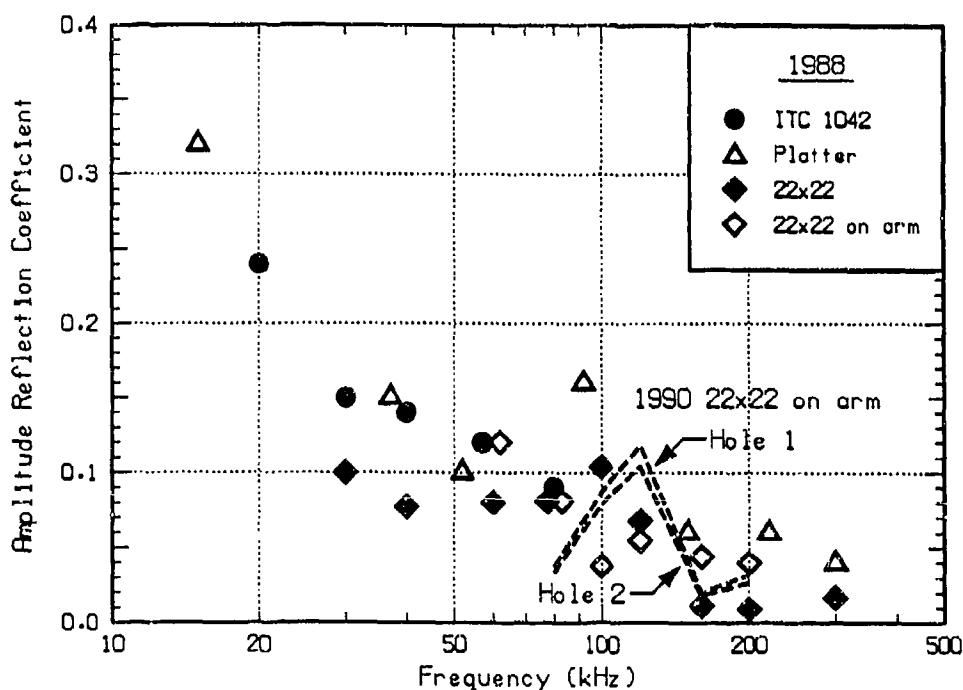
Figure 26. Measurements of the reflectivity of the underside of the ice canopy using the 22×22 transducer on an arm at short range, and comparison with 1988 measurements. The values are based on the transducer calibration obtained using the sphere.

F25, 26
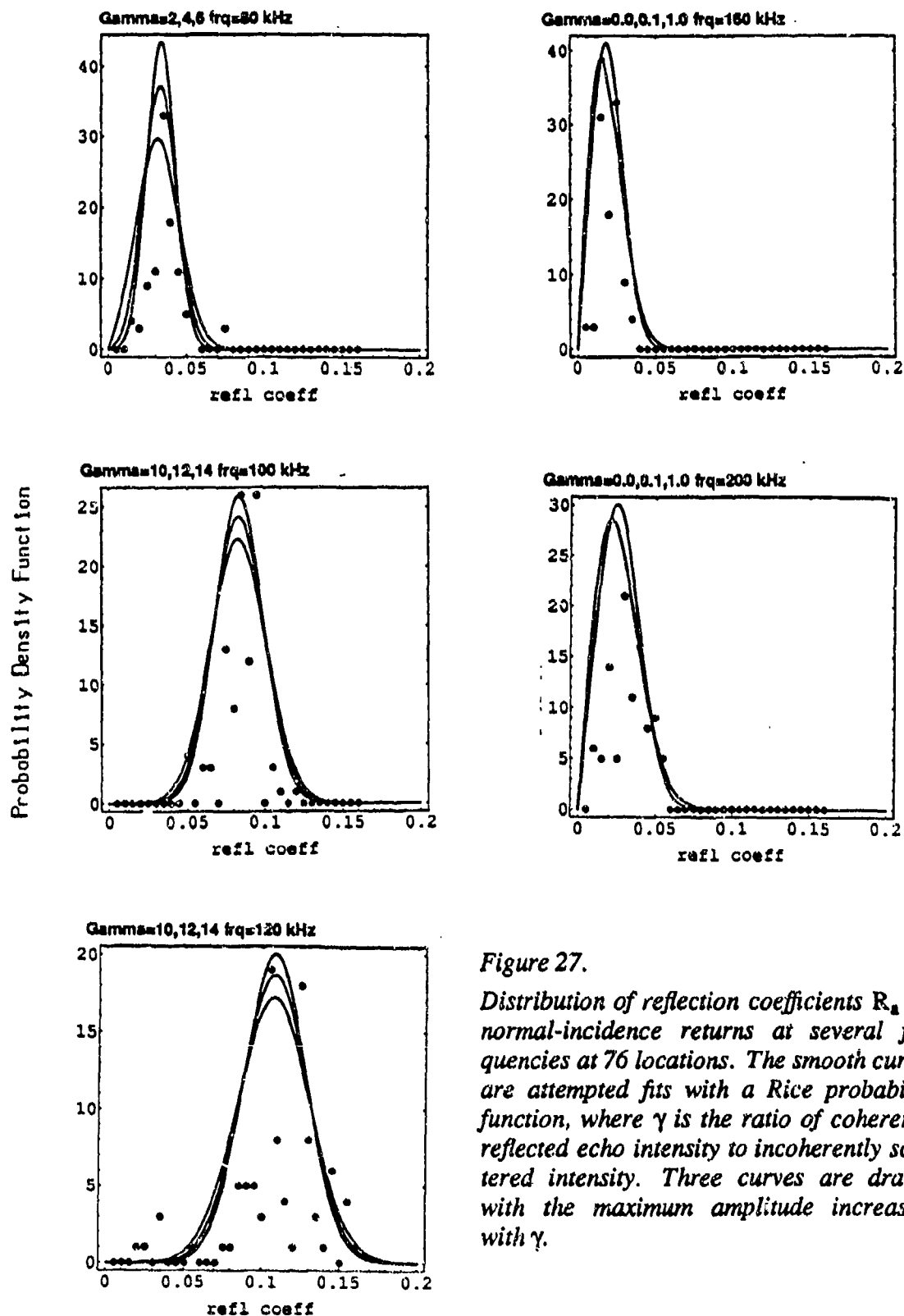
Figure 27.

Distribution of reflection coefficients R_a for normal-incidence returns at several frequencies at 76 locations. The smooth curves are attempted fits with a Rice probability function, where γ is the ratio of coherently reflected echo intensity to incoherently scattered intensity. Three curves are drawn, with the maximum amplitude increasing with γ.

F27
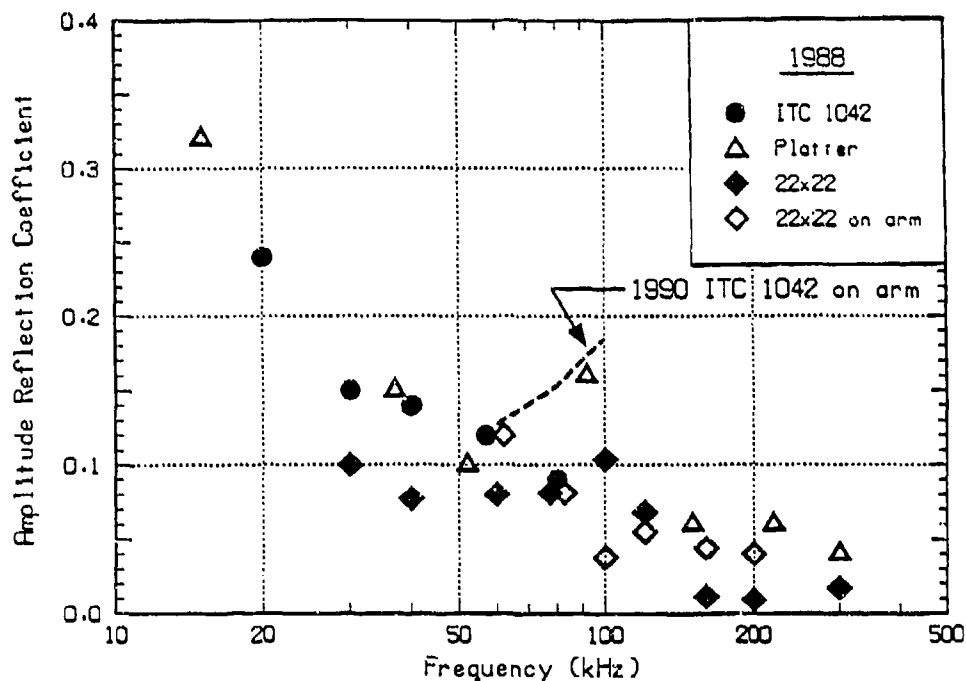
Figure 28. *Measurements of the reflectivity of the underside of the ice canopy using the ITC 1042 transducer on an arm at short range, and comparison with 1988 measurements.*
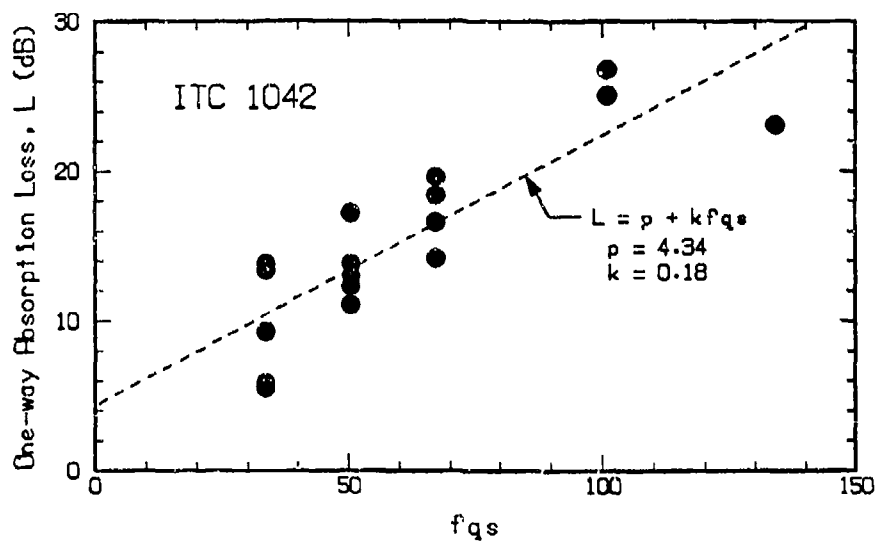
Figure 29. *Absorption loss obtained by comparing reflections obtained from the lower and upper faces of the ice canopy using the ITC 1042 transducer. The dashed line represents a loss at the boundary and a constant absorption coefficient* k.
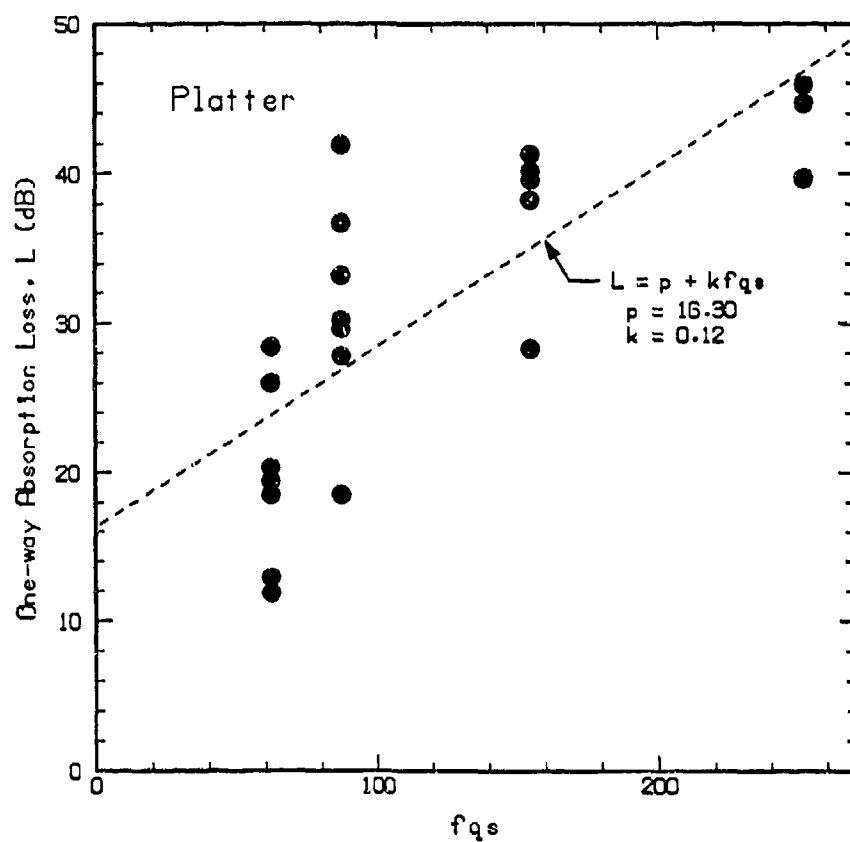
Figure 30. Absorption loss obtained by comparing reflections obtained from the lower and upper faces of the ice canopy using the platter transducer. The dashed line represents a loss at the boundary and a constant absorption coefficient k.
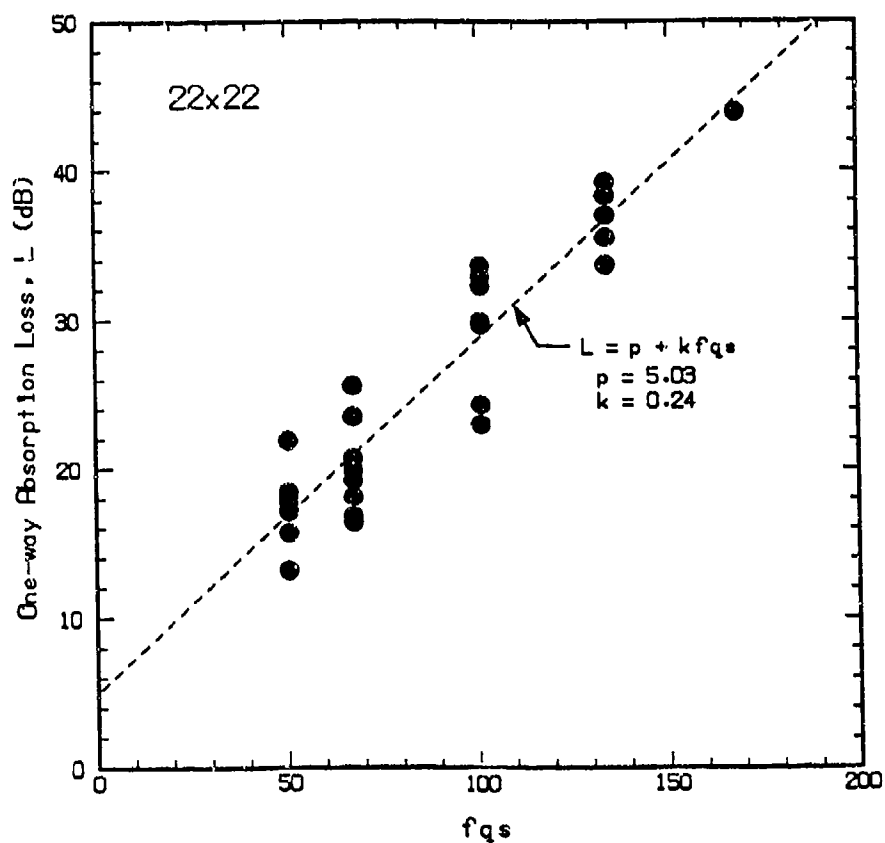
Figure 31. Absorption loss obtained by comparing reflections obtained from the lower and upper faces of the ice canopy using the 22×22 transducer. The dashed line represents a loss at the boundary and a constant absorption coefficient k.
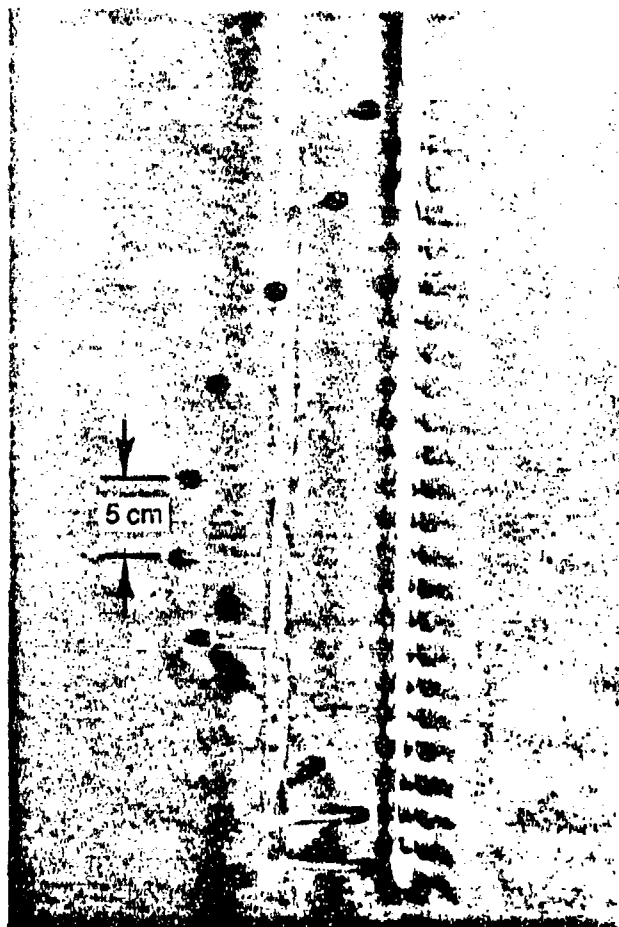
Figure 32. Arrays of hydrophones (left) and thermistors (right) that were suspended in the center of a 2-m-square hole in the ice. Both arrays were suspended from a wooden 2×4 placed across the hole.
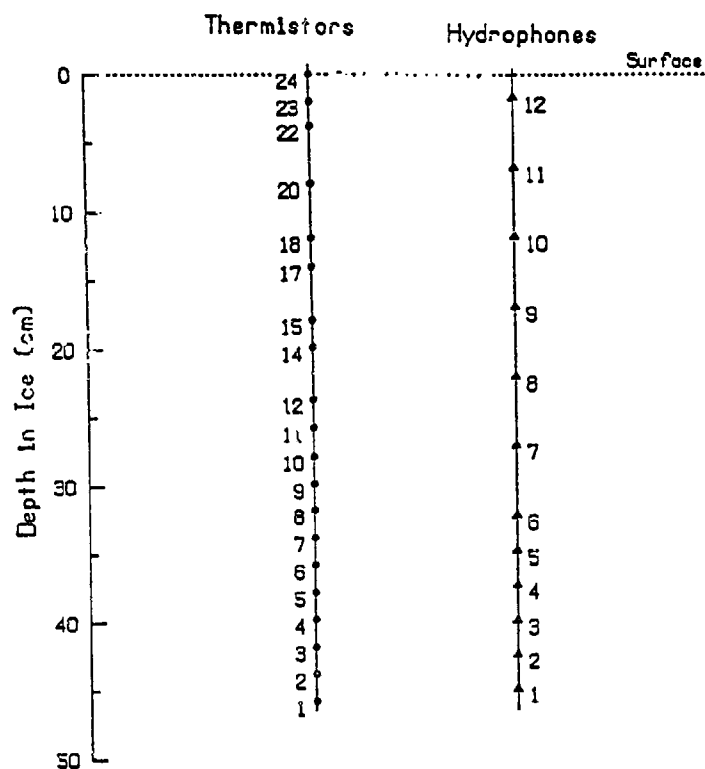
Figure 33. Depths of hydrophones and thermistors suspended in the main 2-m-square hole in the ice. The top thermistor was placed at the surface of the water. Note that the numbering starts at the bottom. Thermistors that were not operable have been omitted.
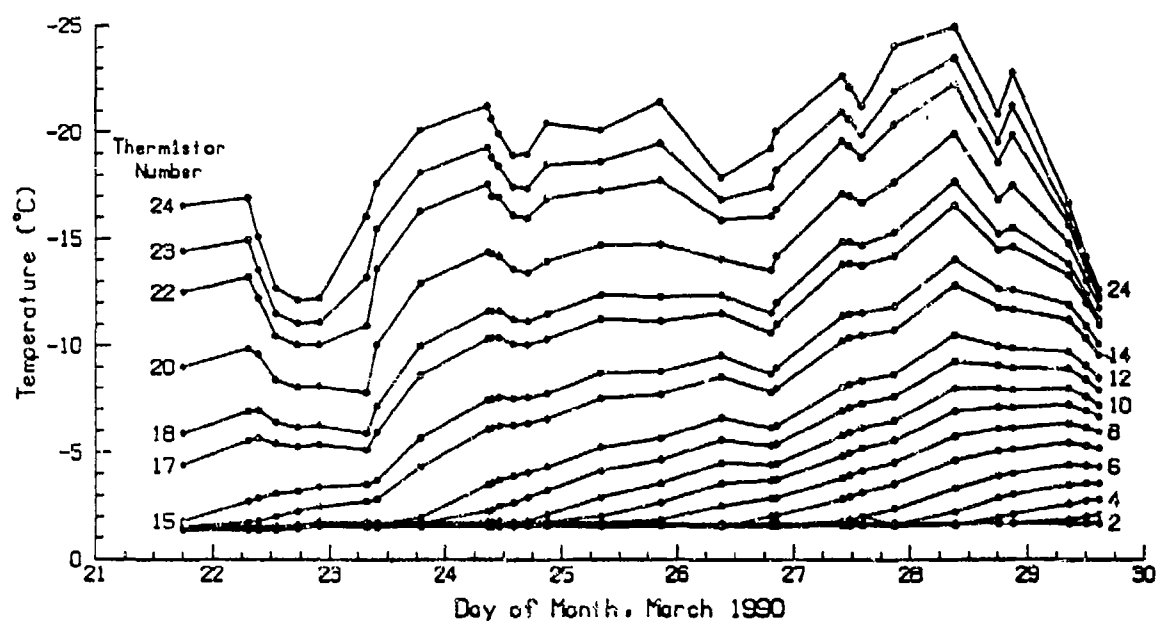
Figure 34a. Variation of temperature with time for all thermistors in the main hole during ice growth.
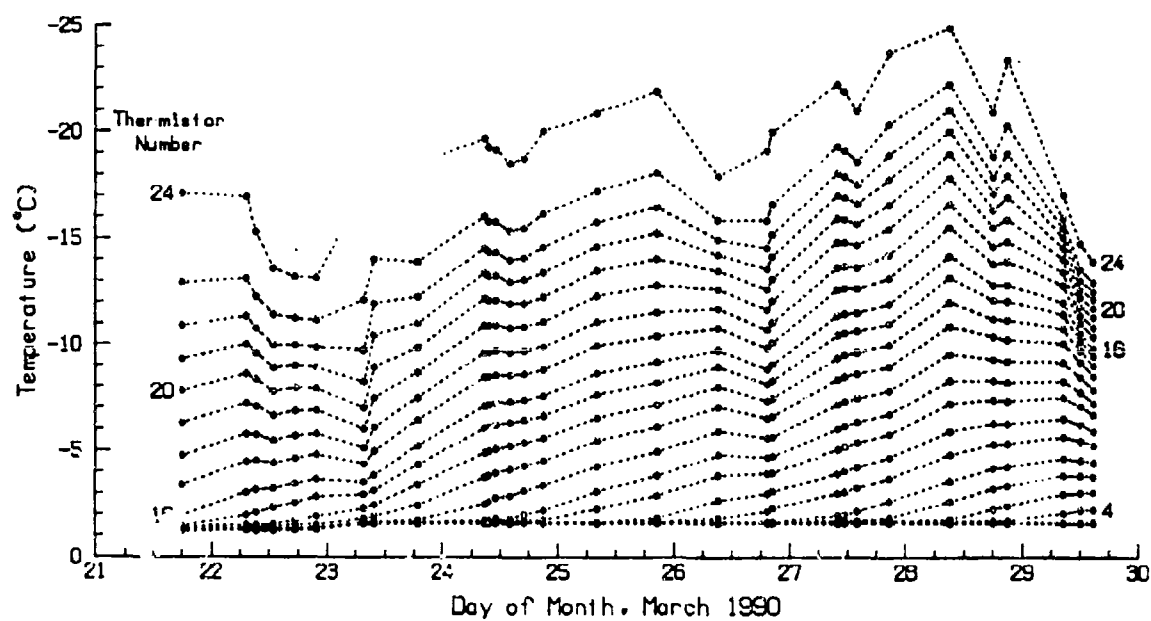
Figure 34b. Variation of temperature with time for all thermistors in the monitor hole during ice growth.
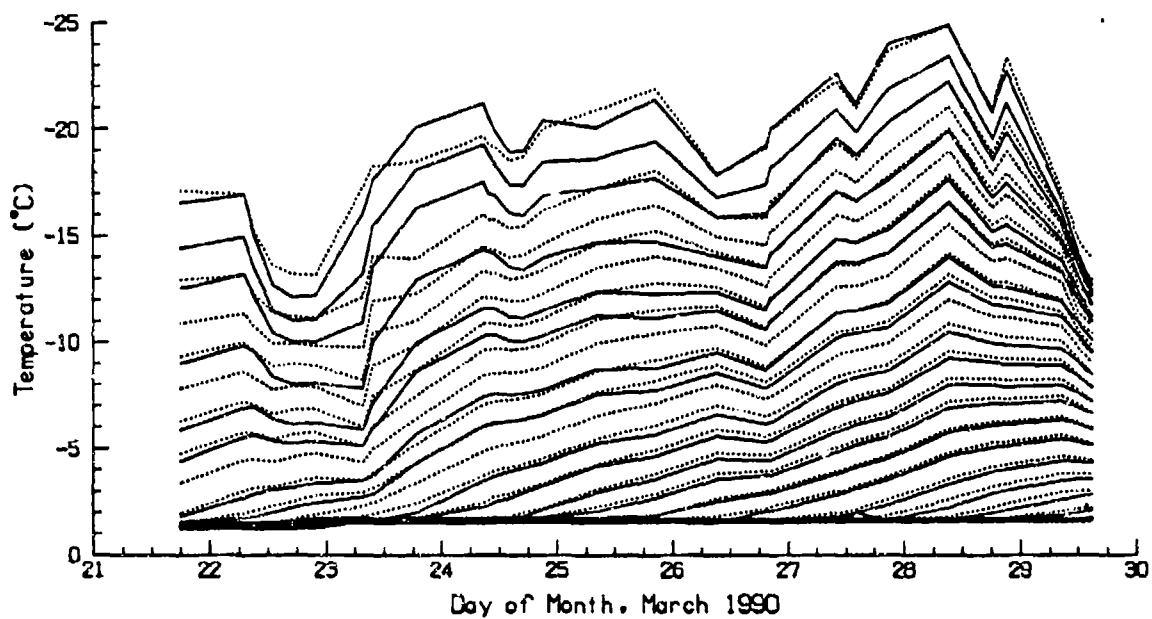
Figure 34c. *Comparison of temperature variations in the main hole (solid lines) and monitor hole (dashed lines) during ice growth. The close match observed at the lower right is misleading because it is between thermistors one number different (e.g., the curve for sensor 3 in the main hole lies near that for sensor 4 in the monitor hole).*
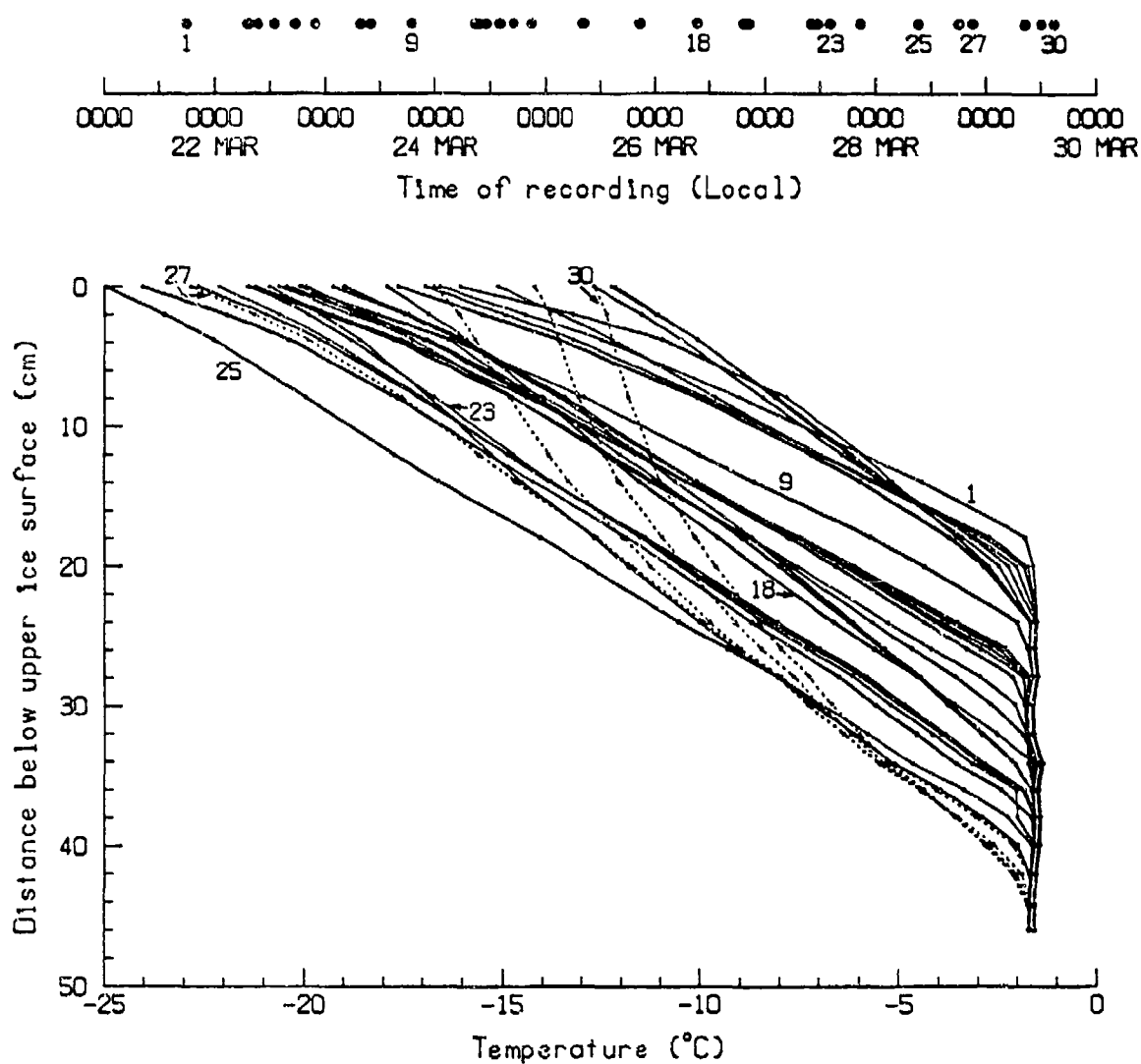
Figure 35. Temperature profiles for the main hole, computed from data in Table 19. Several profiles are labeled by run number; the graph at the top of the figure relates run number with local time. The dotted lines show the effect of a 12°C rise in ambient temperature on 29 March 1990.
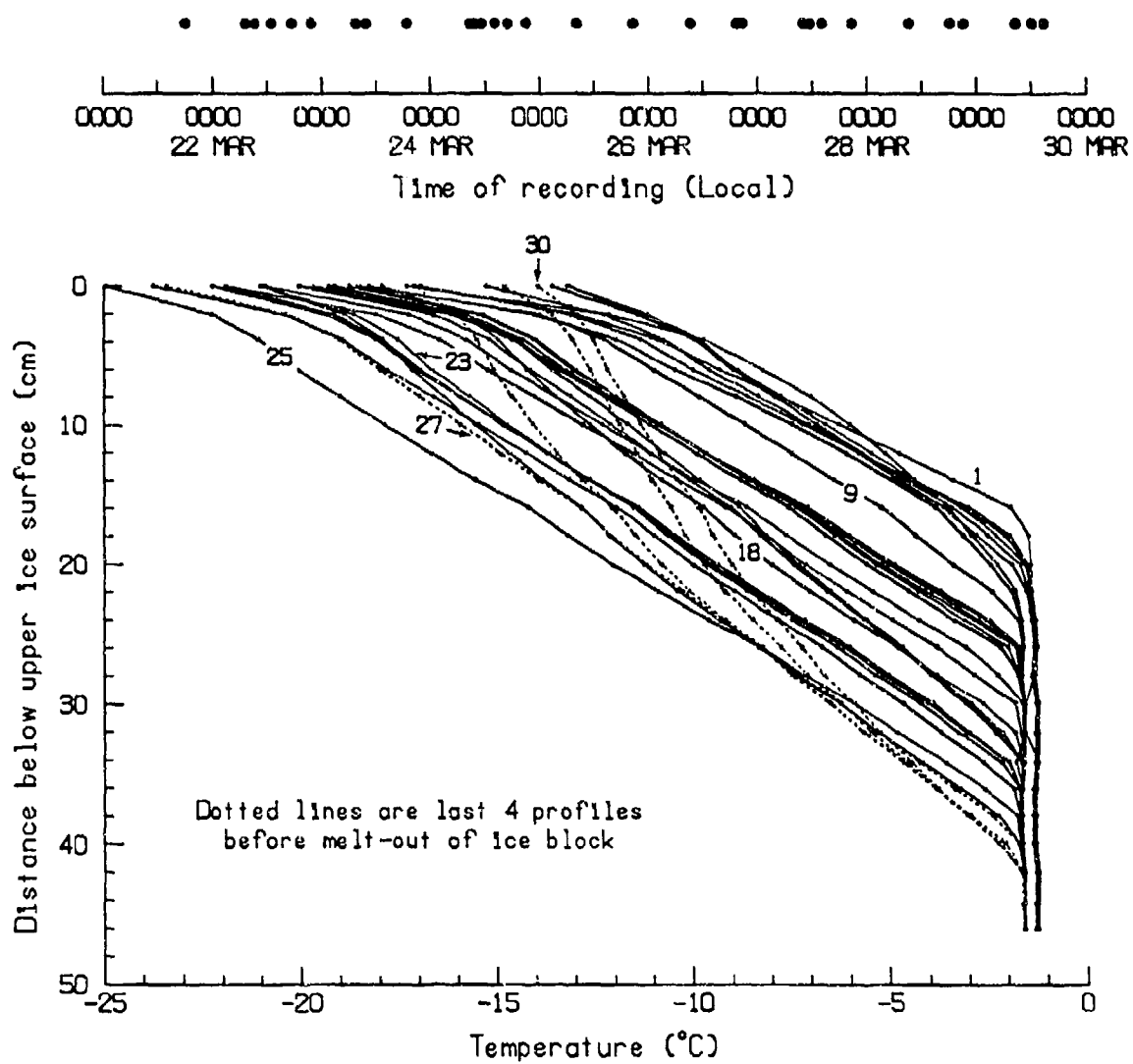
Figure 36. Same as Figure 35, but for measurements in the monitor hole.
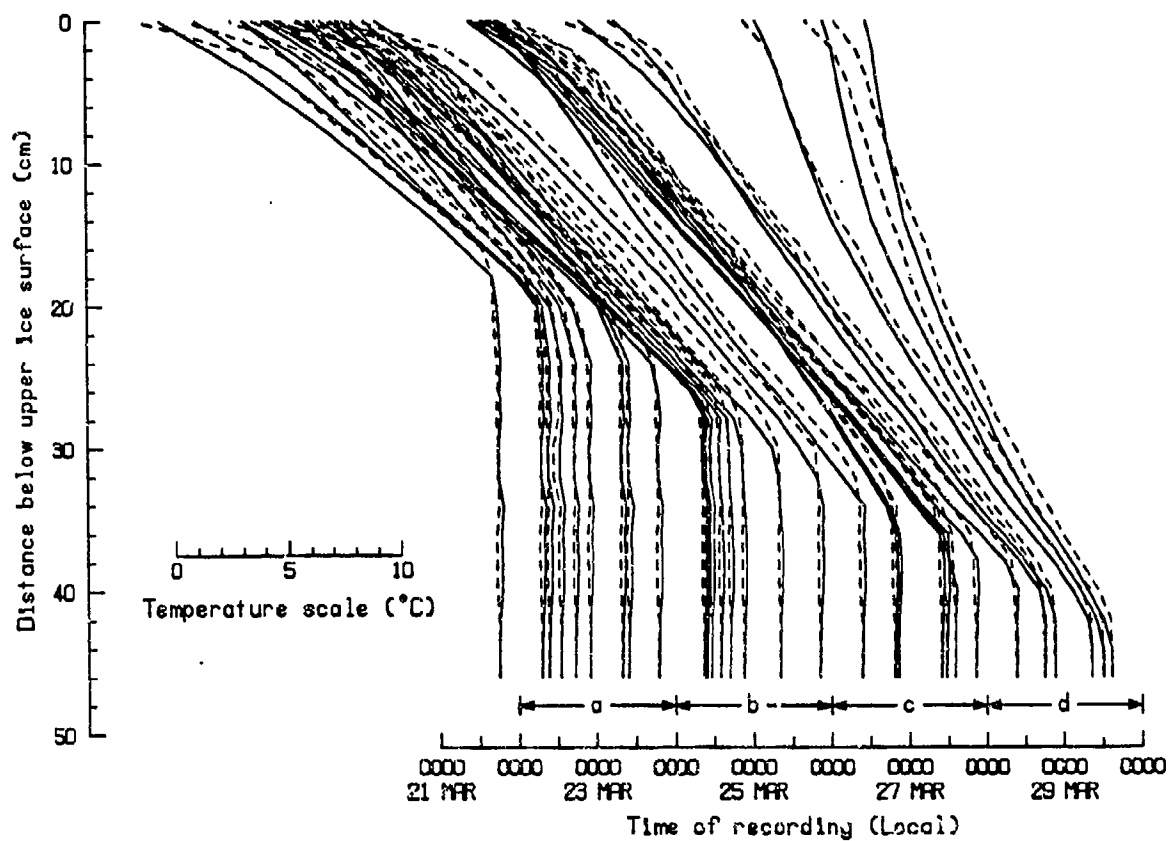
Figure 37. *Comparison of temperature profiles recorded in the two holes during ice growth. Dashed lines are for the monitor hole. See Figure 38 for expanded views of the comparisons.*

F37
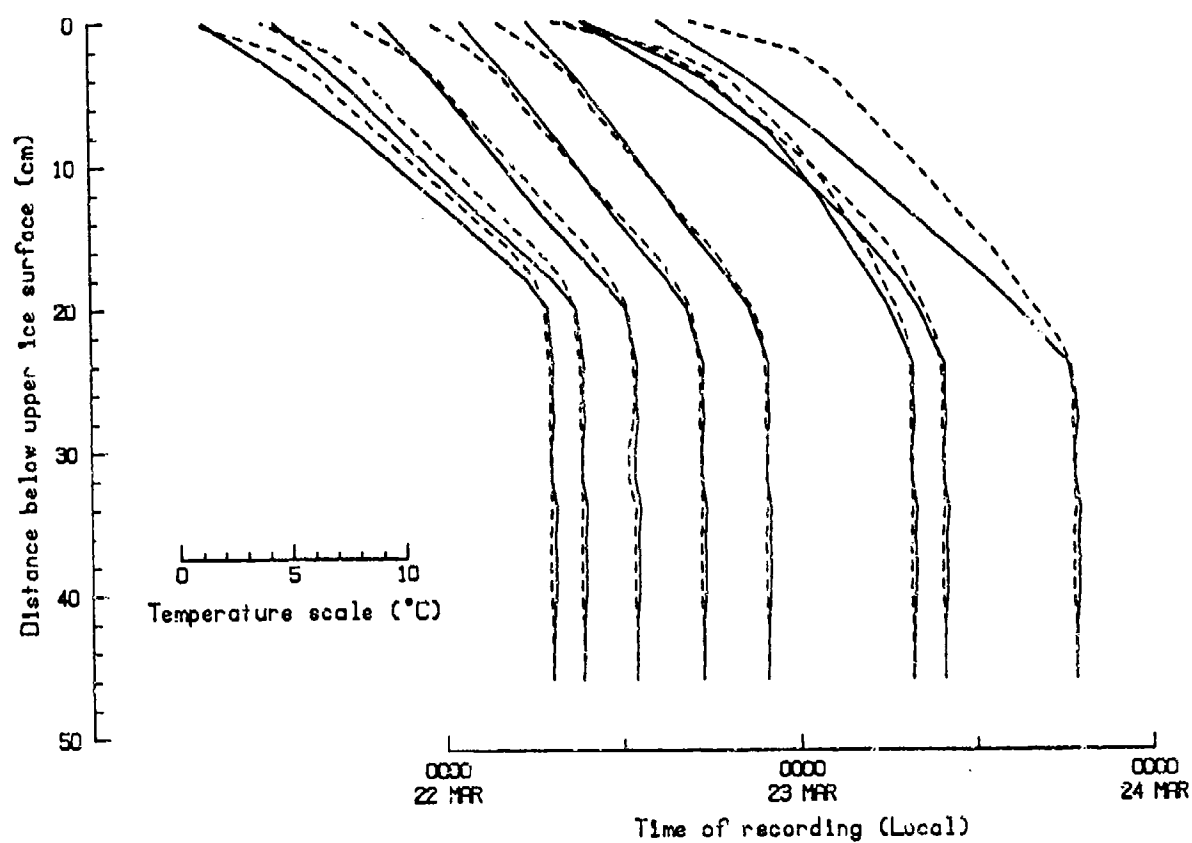
Figure 38a. A more detailed comparison of the profiles designated "a" in Figure 37. Dashed lines are for the monitor hole.
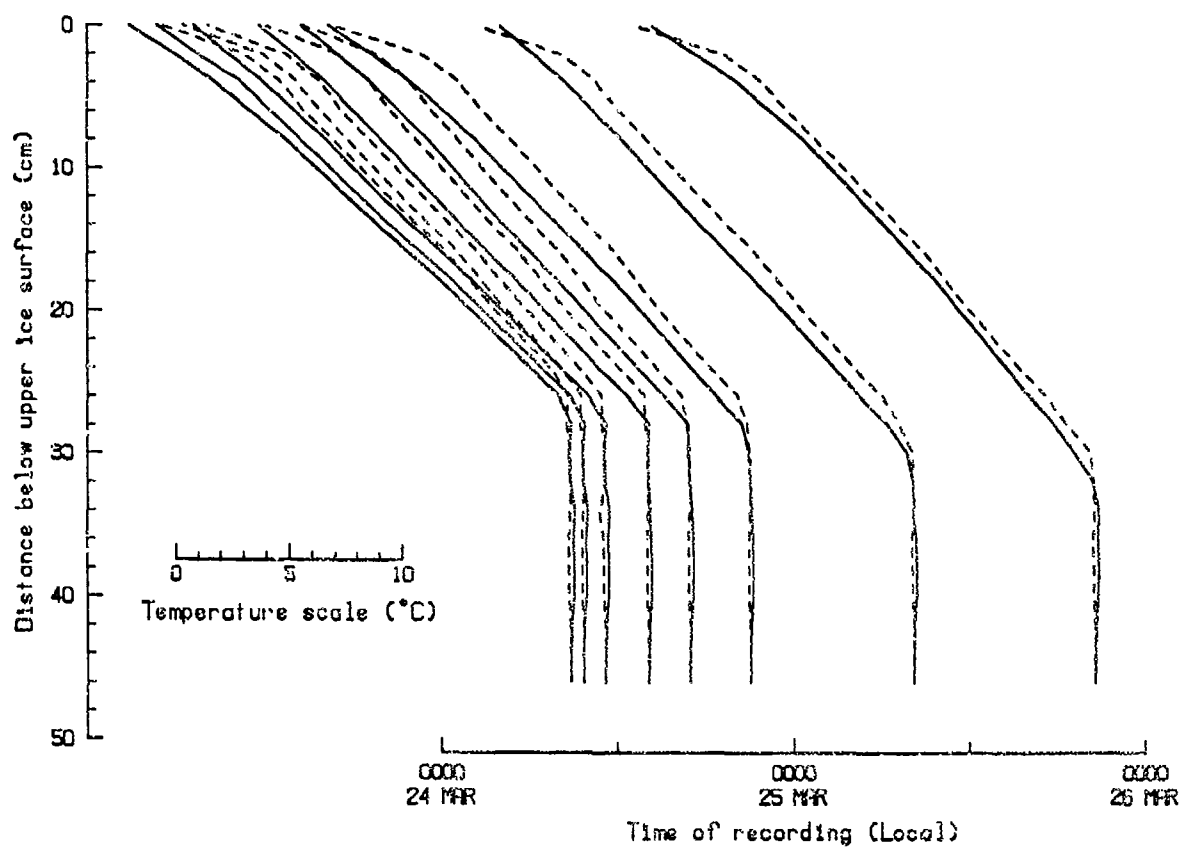
Figure 38b.   Same as Figure 38a, but for the profiles designated "b" in Figure 37.

F38b
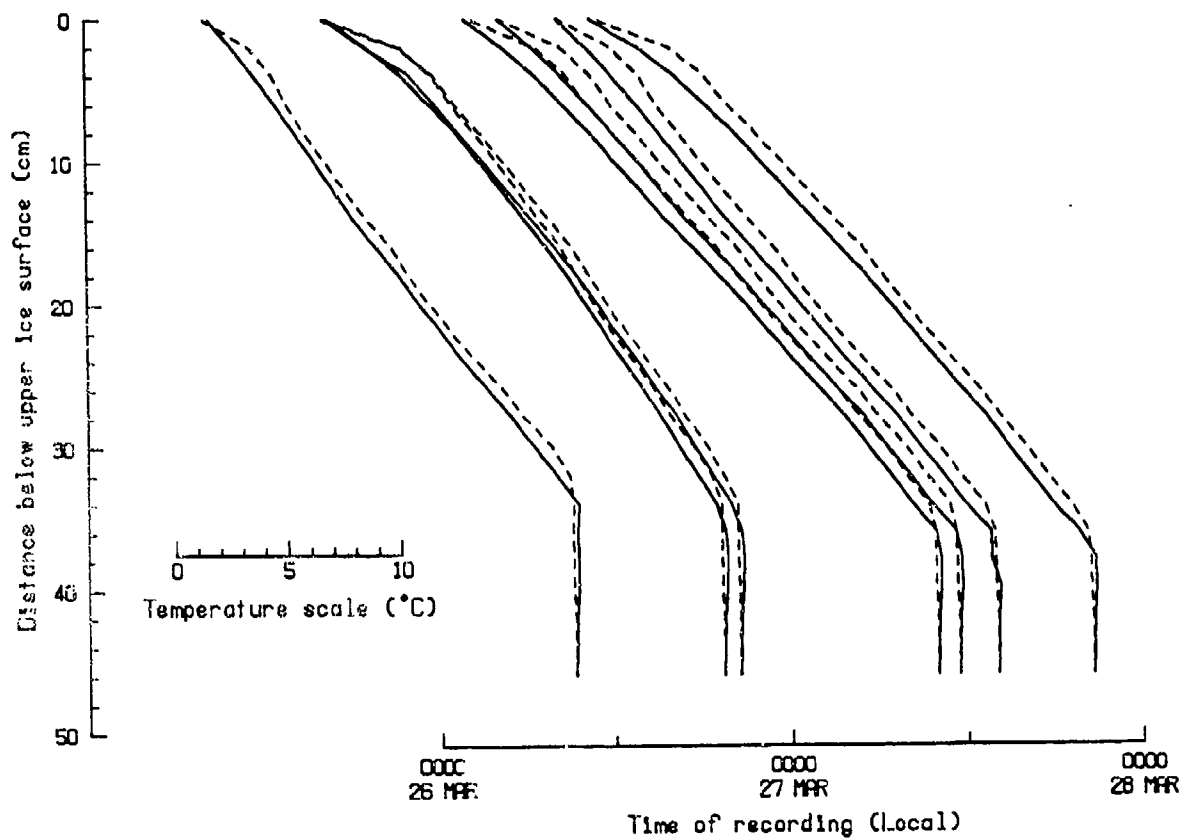
Figure 38c. Same as Figure 38a, but for the profiles designated "c" in Figure 37.

F38c
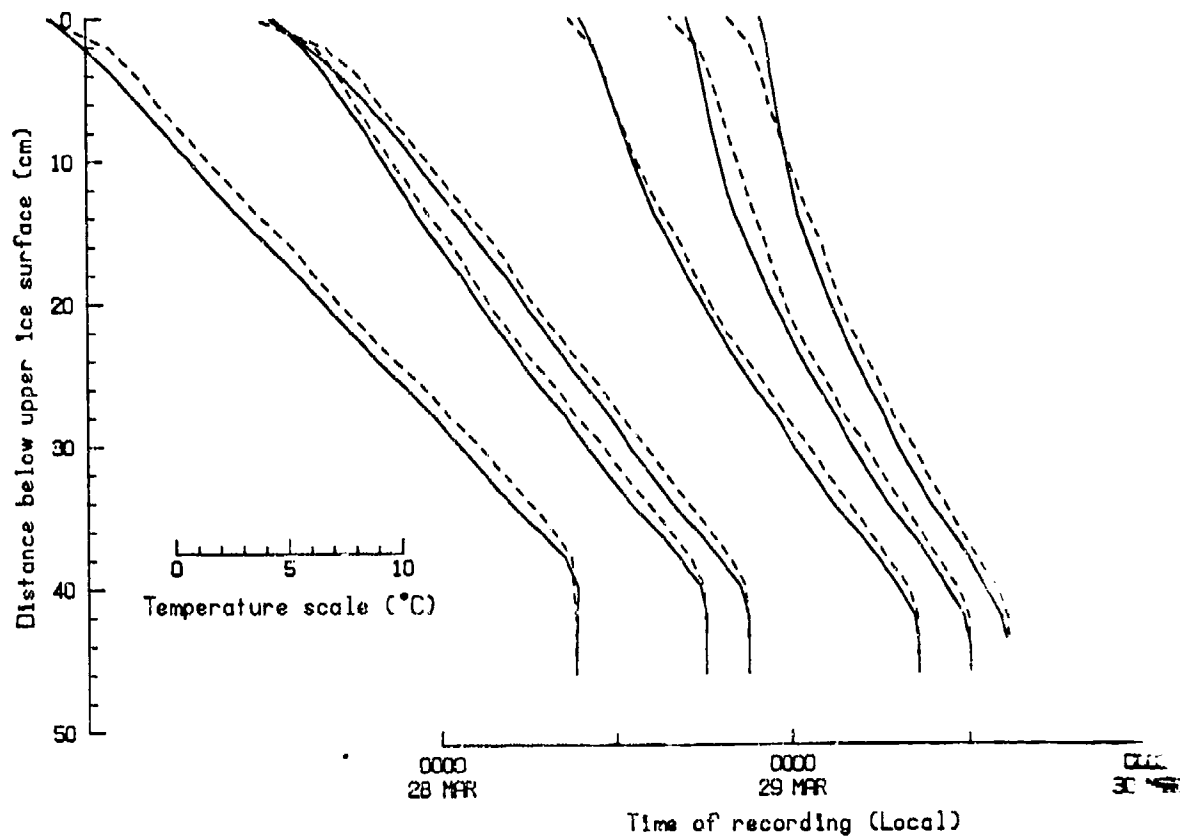
Figure 38d.   Same as Figure 38a, but for the profiles designated "d" in Fig   7

F38d
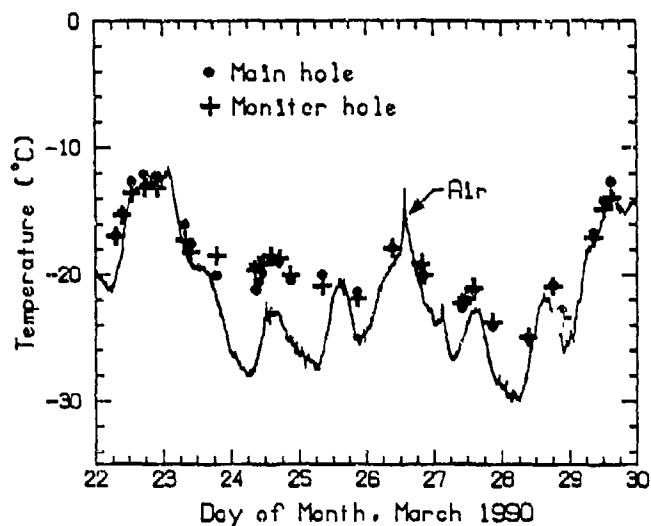
Figure 39. *Comparison of temperatures recorded at the upper thermistors of the arrays (data points) and air temperatures measured at the camp's portable weather station (line). The array temperatures tend to be higher, probably because of protection by snow cover.*
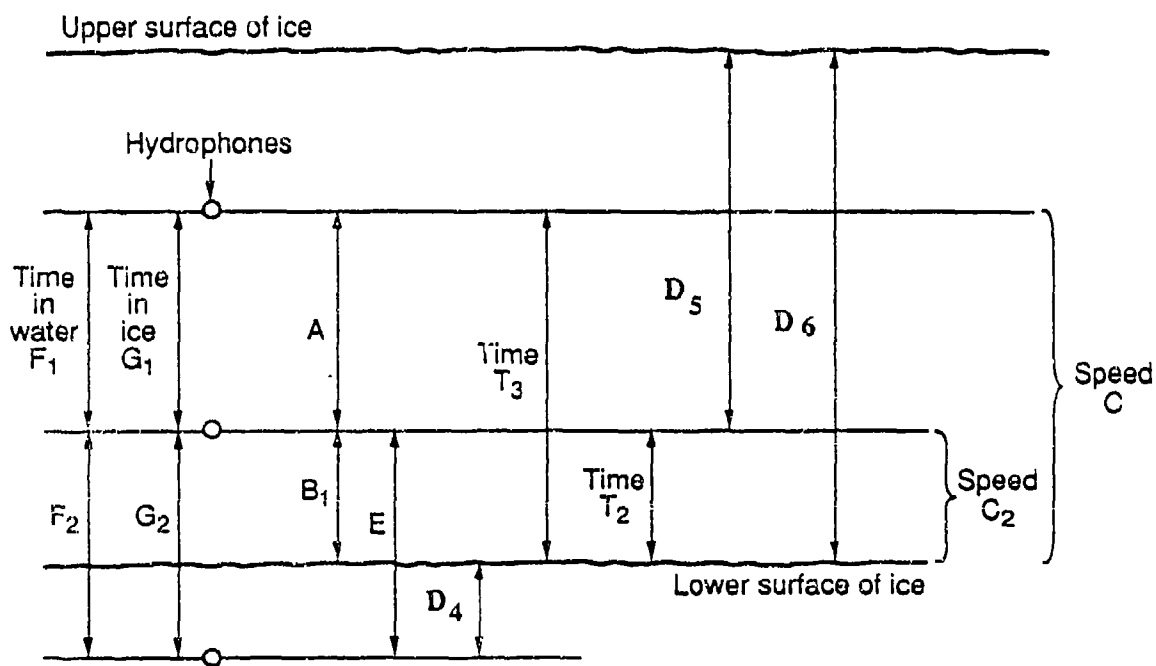
Figure 40. *Vertical distances and travel times used to calculate sound speeds for the ice. The ice surface lies between the lower two hydrophones in the figure. The sound speed in the water is known to be 1436 m/s from routine oceanographic measurements. "Time" is the transit time for an acoustic pulse.*
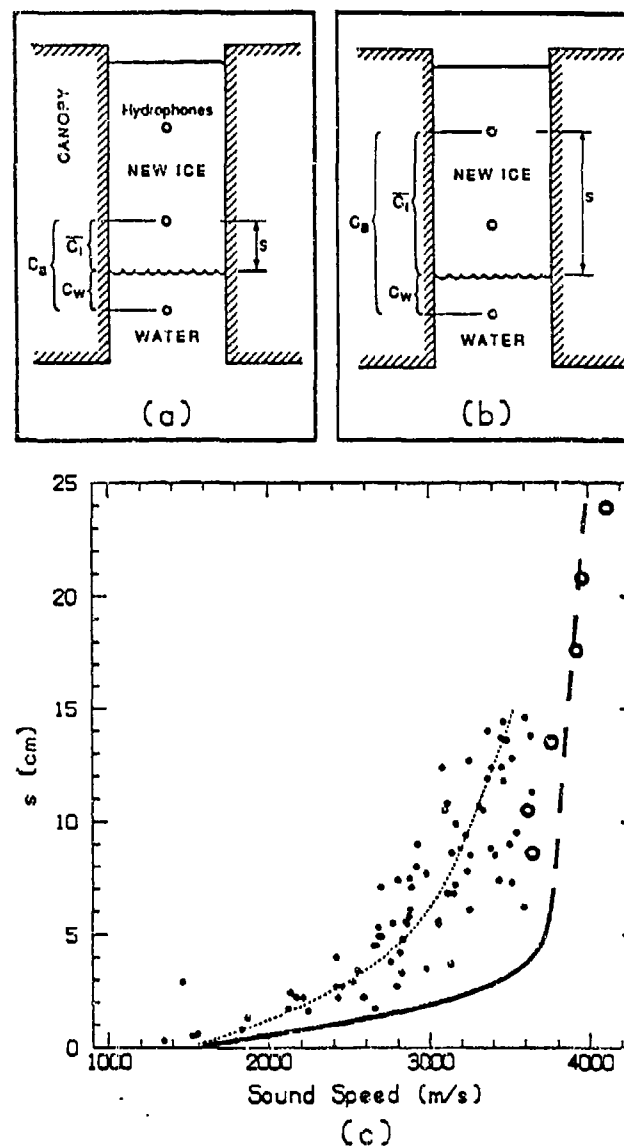
Figure 41. The average sound speed for a short distance s into the ice as calculated from the measured travel times between a hydrophone just below the ice and one just above it, as in (a). To obtain values for larger s, the second hydrophone above the ice was substituted for the upper one, as in (b). This gives two values of average sound speed versus s for every set of measurements during the ice-growth experiment; these are plotted as dots in (c). The solid line is the profile in the ice calculated using Eq. (14). The line is extended to fit some sound speed measurements obtained from hydrophone pairs well into the ice.
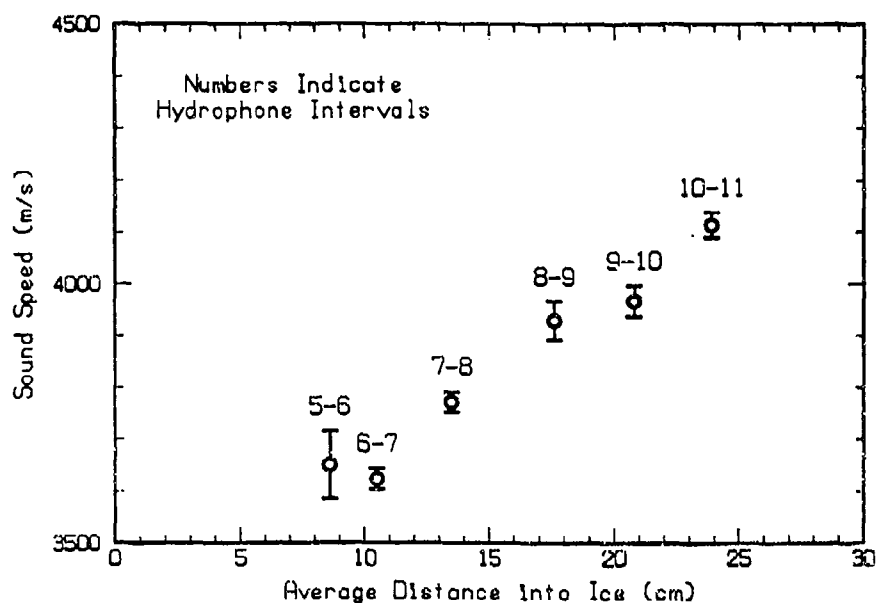
Figure 42. Some acoustically measured sound speeds for intervals where the hydrophones have been in the ice long enough that the sound speed has reached a fairly steady value.
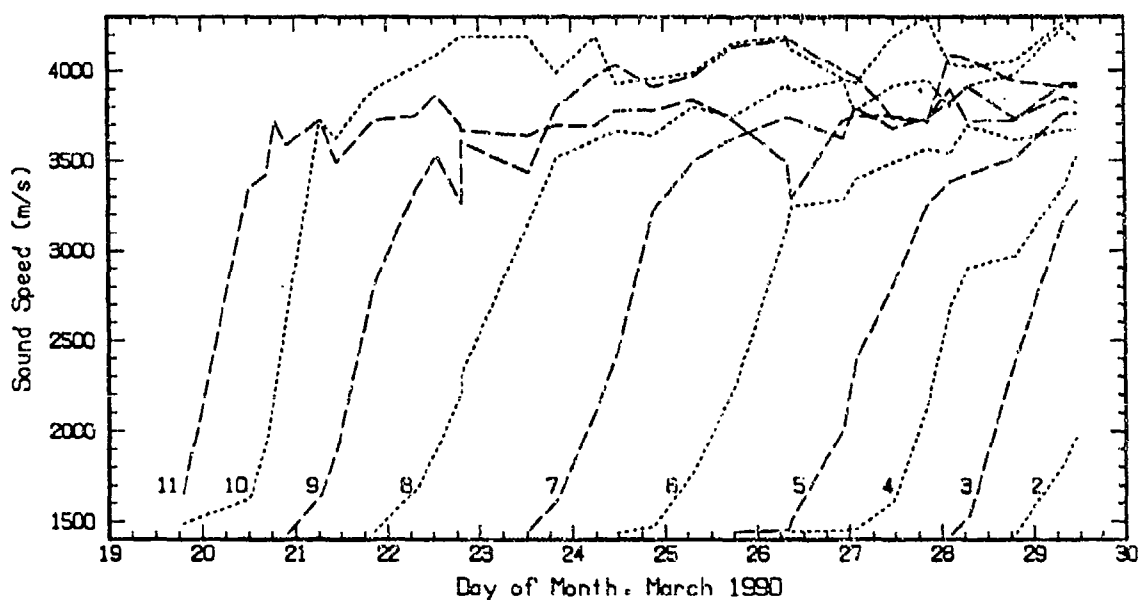
Figure 43. The change in sound speed calculated from acoustic travel time for each hydrophone pair as the ice formed, covering one hydrophone after another. The number of the deeper of the pair is given.
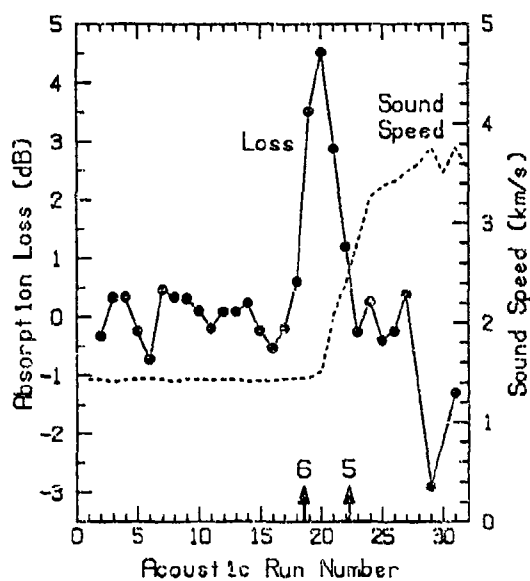
(a) Hydrophones 5-6
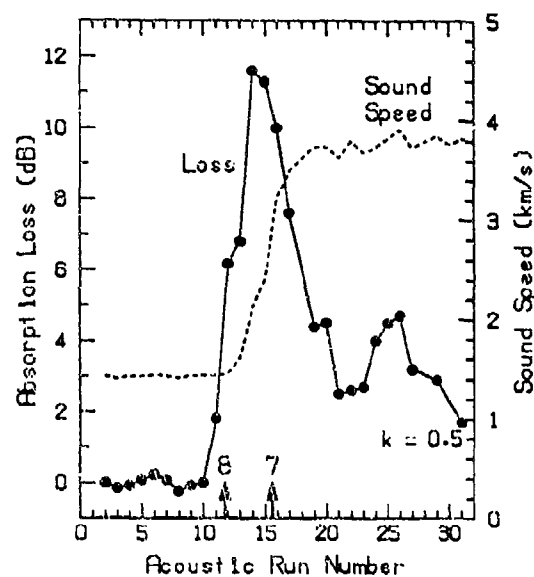
(b) Hydrophones 7-8
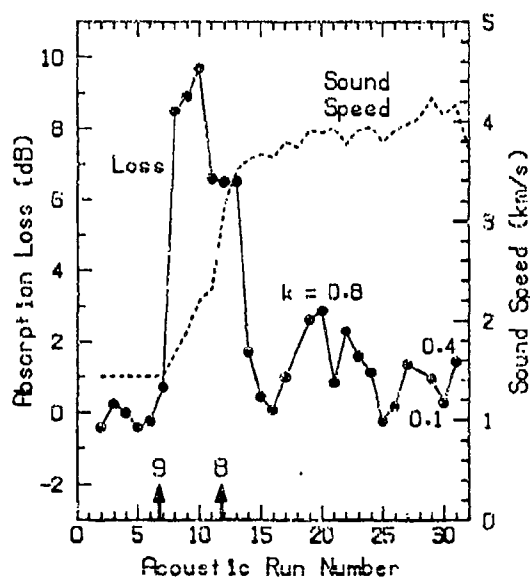
(c) Hydrophones 8-9

Figure 44. *Absorption loss and sound speed in the interval between hydrophone pairs. The arrows indicate when each hydrophone was frozen into the ice. When a hydrophone pair is sampling the skeletal layer, the loss is large and may include effects due to boundary loss or sensitivity change. As the ice advances, the hydrophones are left in solid ice which has a low absorption. The sound speed increases as more and more of the interval is filled with ice and this ice hardens.*
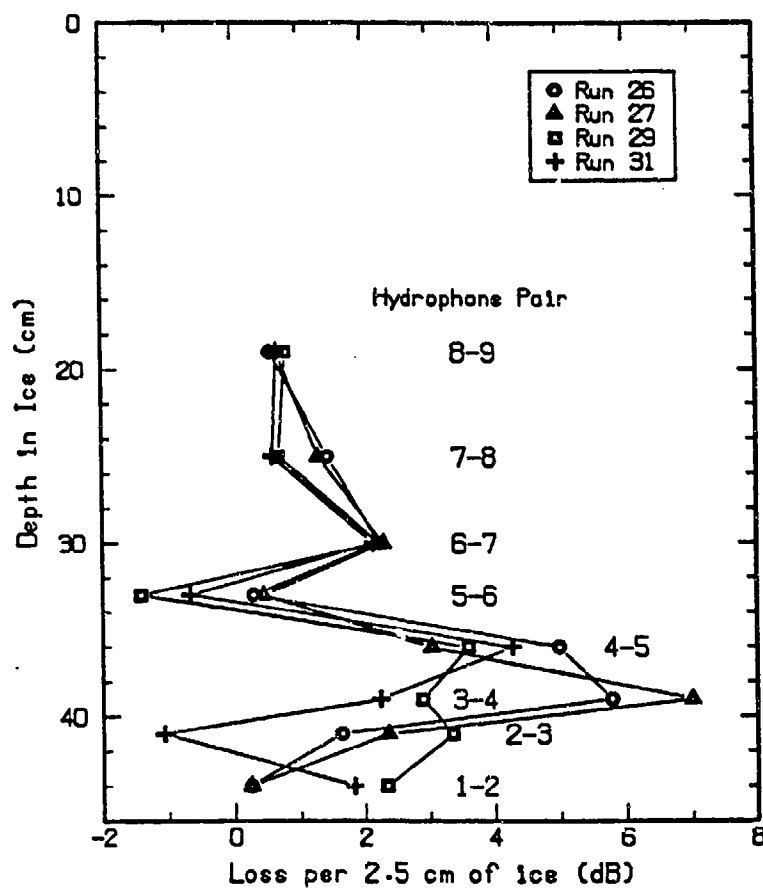
Figure 45. Absorption loss profiles for four acoustic runs, from readings of the amplitude of the signal at each hydrophone.
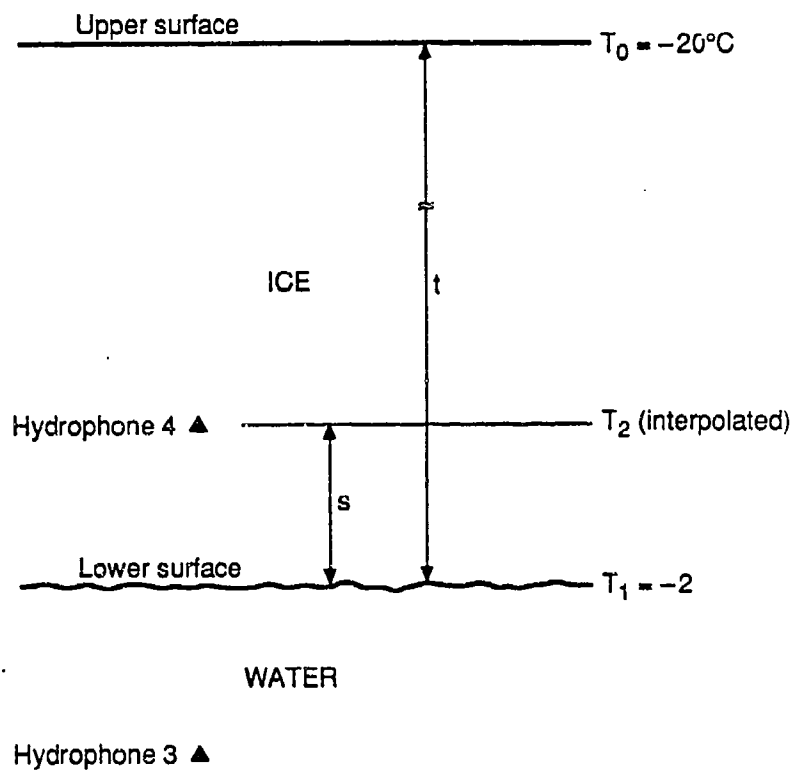
Figure 46. *Values used to calculate the absorption loss in a thickness s of the skeletal layer when the ice extends somewl at below a hydrophone (hydrophone 4 is shown in the example). The temperature gradient across thickness s is assumed to be constant. The temperature T_2 is interpolated between the air and water temperature or determined from the thermistor readings.*
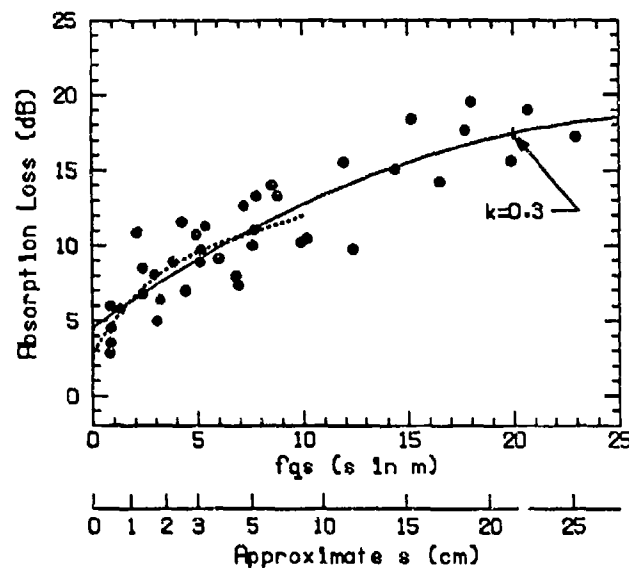
Figure 47. *Signal loss between hydrophones for various distances s (see Figure 46).*
The loss is plotted versus the integral of fqs where f is the frequency and q
includes the temperature dependence of the absorption. The slope in this
plot is the absorption constant k in Eq. (20). A second-degree best-fit curve
shows that k is high in the skeletal layer and then drops off farther into the
ice (to 0.3 at fqs = 20). A fourth-degree curve (dotted) gives a better fit for
the 3-cm skeletal layer.
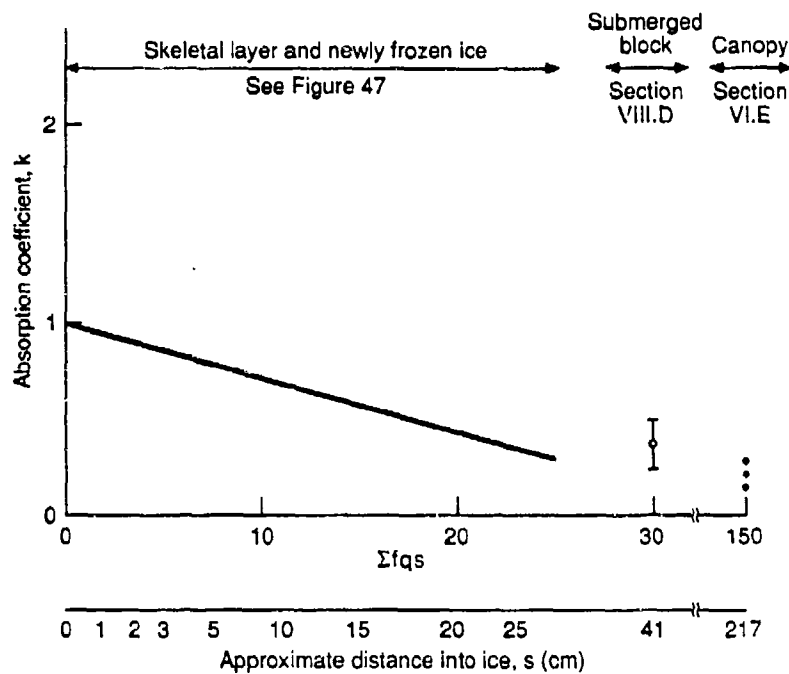
Figure 48. *Summary of absorption coefficients measured in the skeletal layer, in the*
submerged ice block, and in the ice canopy.
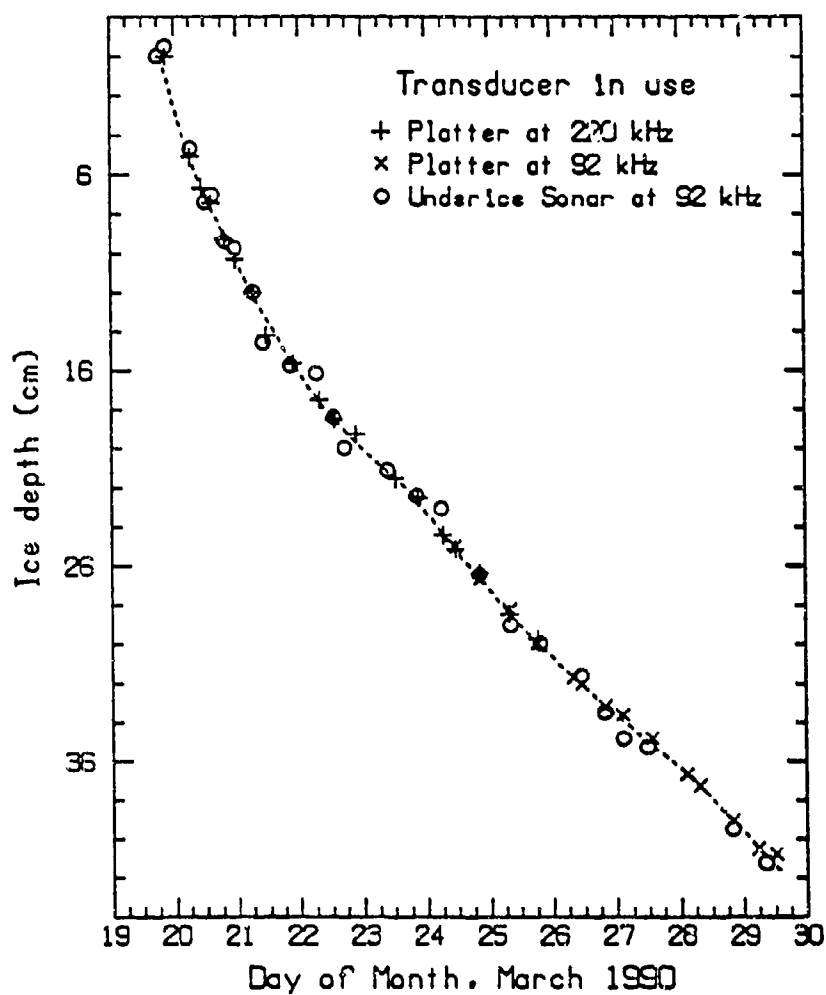
Figure 49. Ice depth during the ice growth phase as determined acoustically from two different transducers suspended below the hole. Initially, reflections from the water surface were used as the reference for returns to the platter transducer; later, because the platter's depth varied, reflections from the bottom of the sensor array and the arm for the ice-erosion sonar transducer were used.
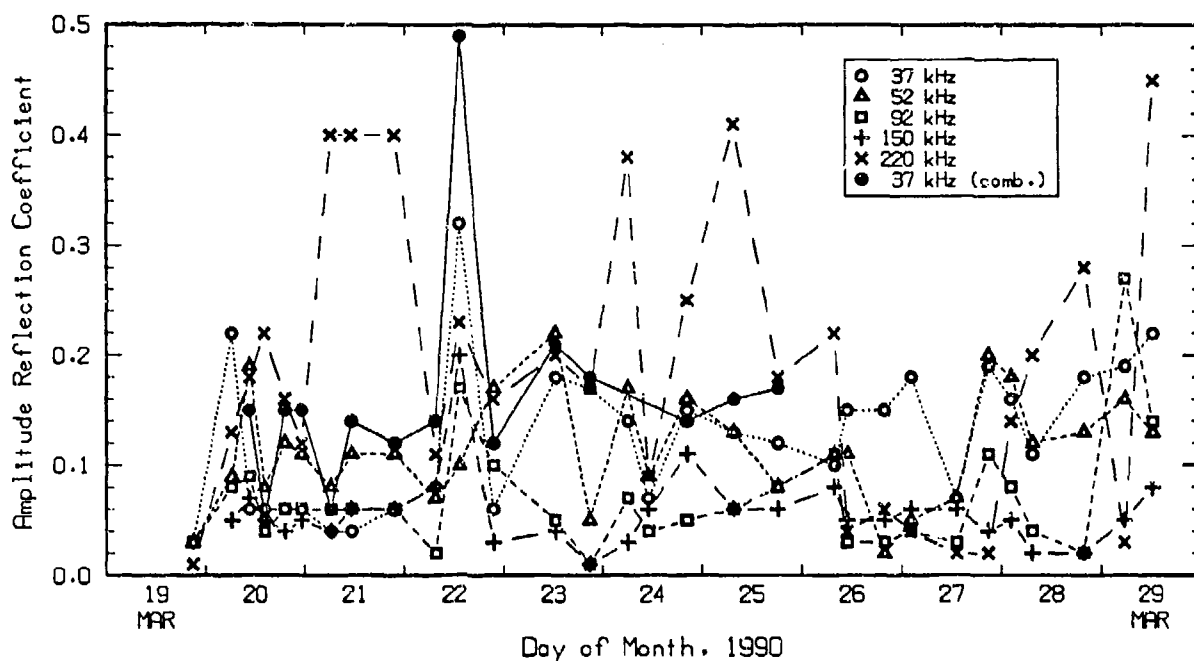
Figure 50. Amplitude reflection coefficients calculated from reflection measurements during the ice-growth phase of the experiment.
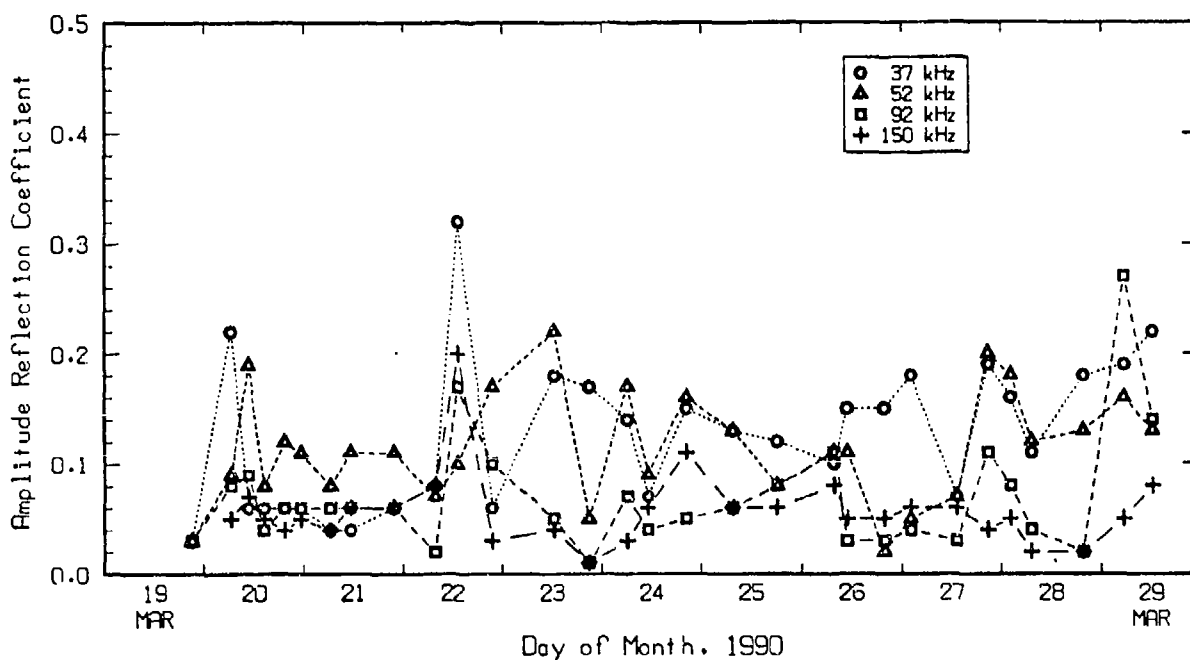
Figure 51. Amplitude reflection coefficients during the ice-growth phase after omitting the highly variable results at 220 kHz and the combined pulses at 37 kHz.
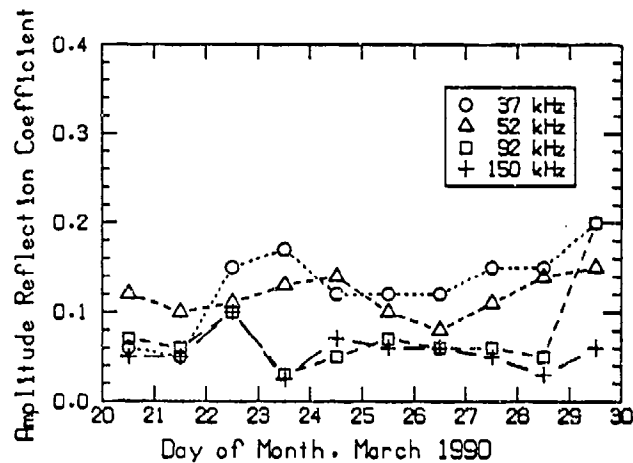
Figure 52. *Daily averages of the amplitude reflection coefficients measured during the ice-growth phase of the experiment.*
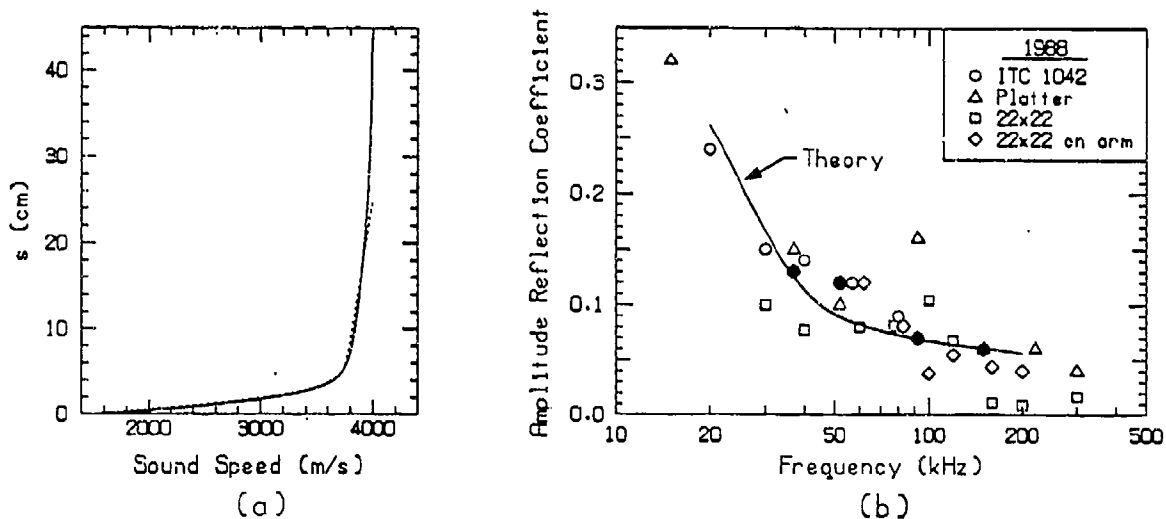
Figure 53. *(a) Sound speed profile (dotted line) derived from measurements, and the best fit (solid line) of a special equation, Eq. (9) in Ref. 4, that is suitable for predicting a curve such as the solid line in (b). (b) Average amplitude reflection coefficients for all measurements during ice growth (filled circles) compared with ice canopy reflectivities measured in 1988 and the theoretical curve corresponding to the sound speed profile (solid line in (a)).*
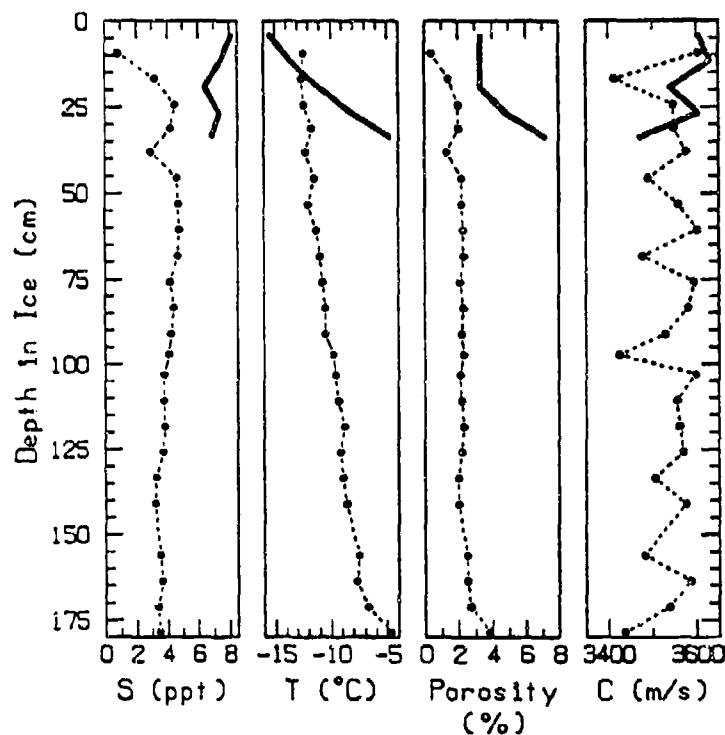
Figure 54. Temperature and salinity measured in a core taken from the ice canopy in the vicinity of the ice-growth experiment along with the calculated porosity and sound speed profiles. The dotted line is for a core taken near the 30-m triad; the heavy solid line near the top of the graphs is for a core taken from the monitor hole on the last day of the ice-growth experiment.
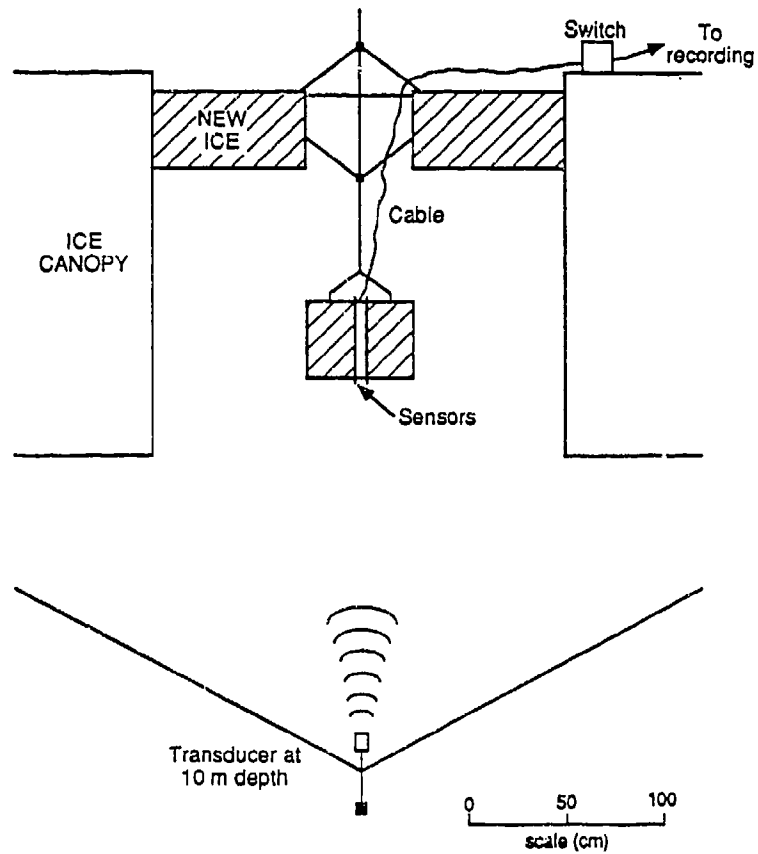
Figure 55. Arrangement after the ice in the 2-m hole had frozen to 42 cm and a block of the new ice had been cored out and submerged.

F55
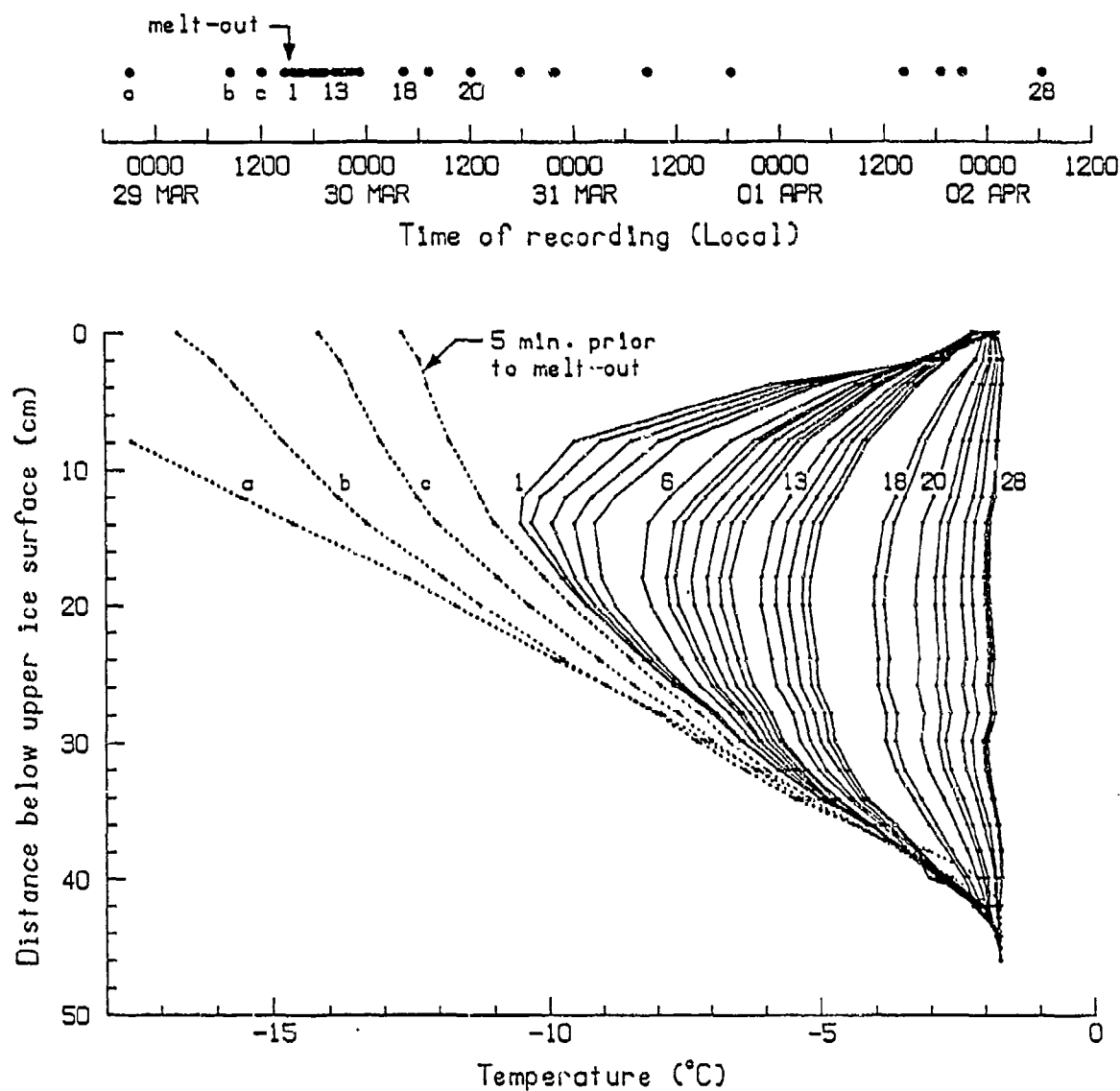
Figure 56. *Temperature profiles in the submerged ice block during the 3 days it took for the block to warm to the temperature of the water. The four profiles taken prior to melt-out are shown as dotted lines in Figure 36. As in Figure 36, several profiles are labeled by run number after submergence. The graph at the top of the figure associates run number with local time.*
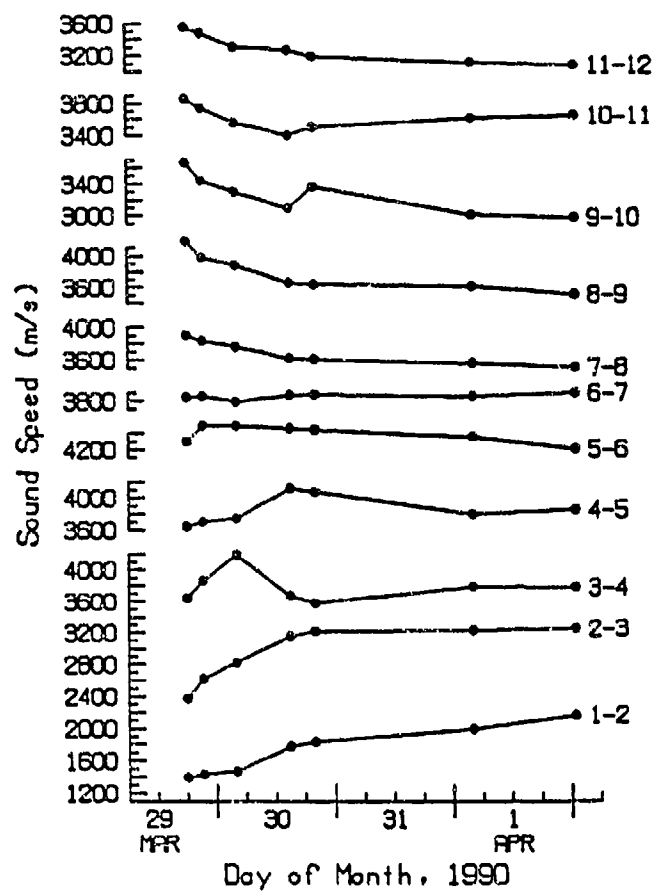
Figure 57. *Sound speed measured in each of the hydrophone intervals during the submerged part of the experiment. The first measurement took place 2 h and 20 min after the block was submerged.*
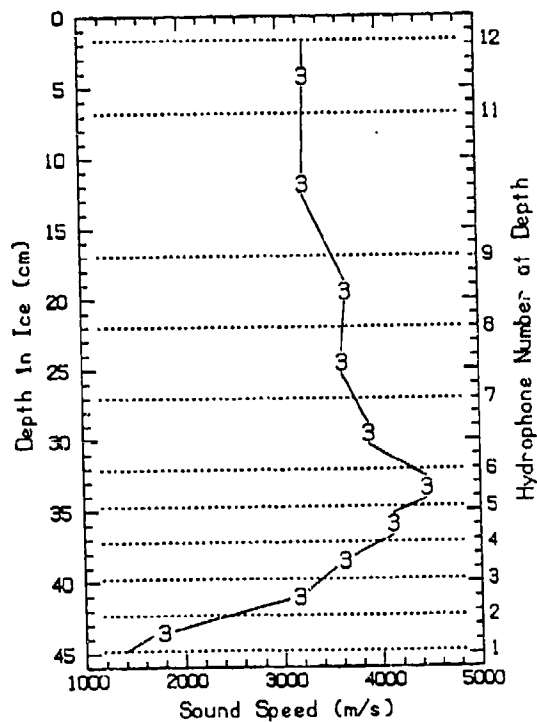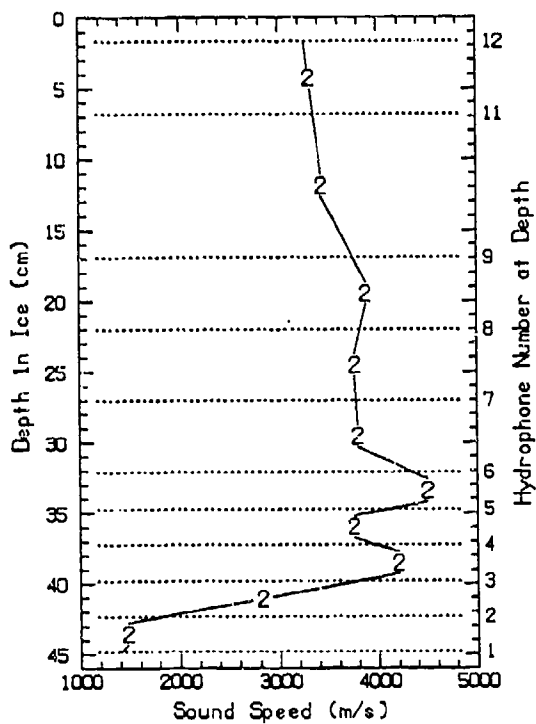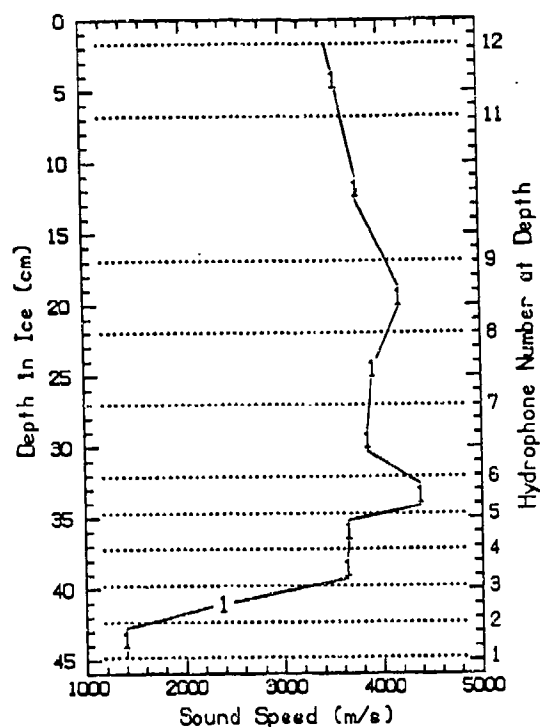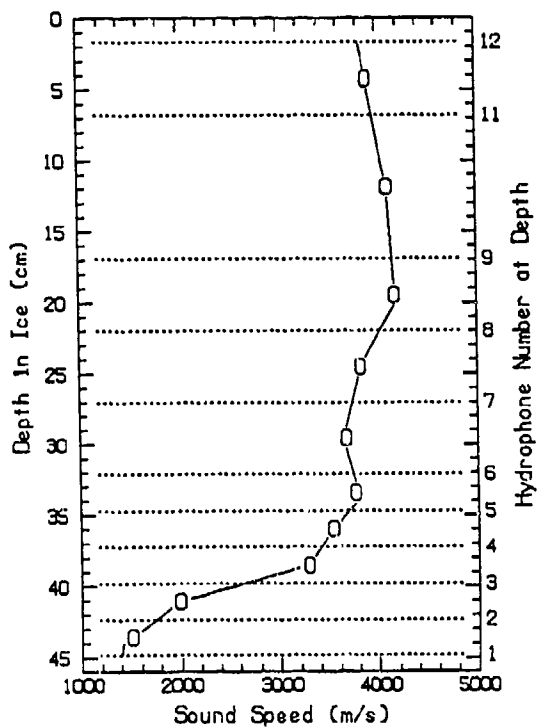
Figure 58a. Sound speed averages for the last profile taken before coring of the block (0), and after 5 h (1), 12 h (2), and 1 day (3) of submergence and warming.

F58a
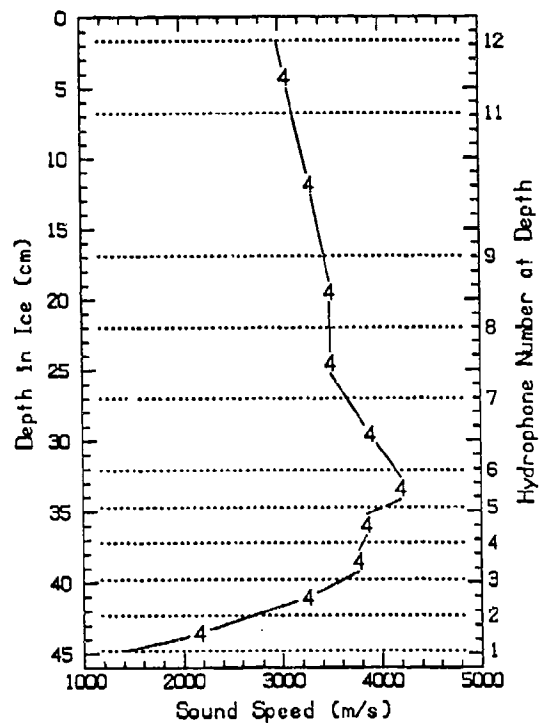
Figure 58b.   Sound speed averages after 4 days of submergence and warming.
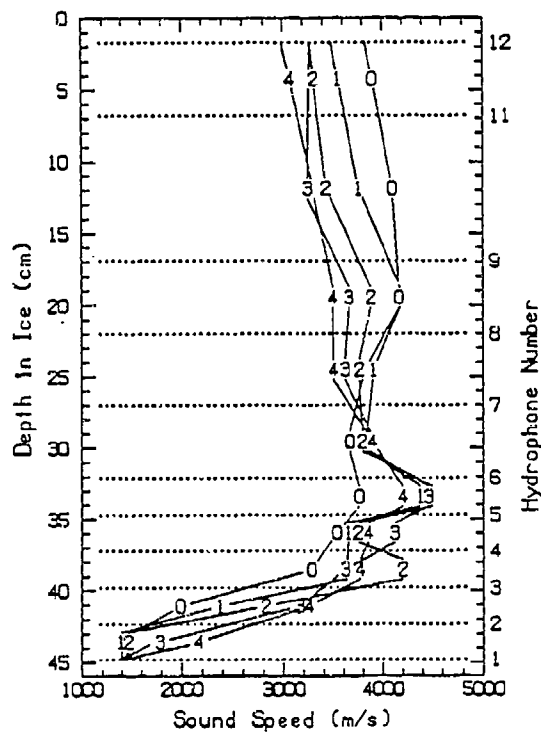
*Figure 59.   Comparison of all profiles shown in Figure 58 for various times after sub-
mergence of the ice block.*

F58b, 59
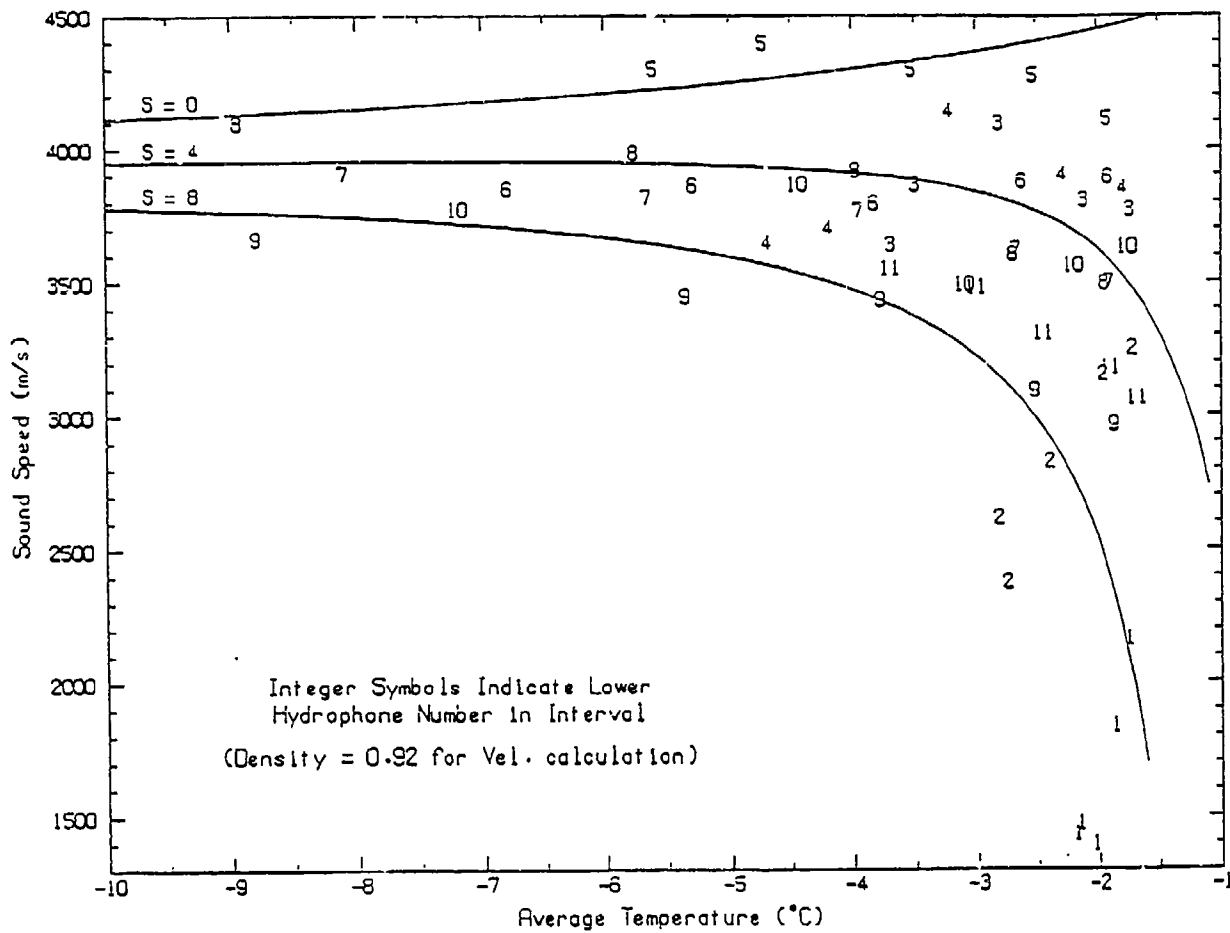
Figure 60a. *Sound speed versus temperature during warming of the ice block. Theoretical lines are plotted for several typical salinities.*
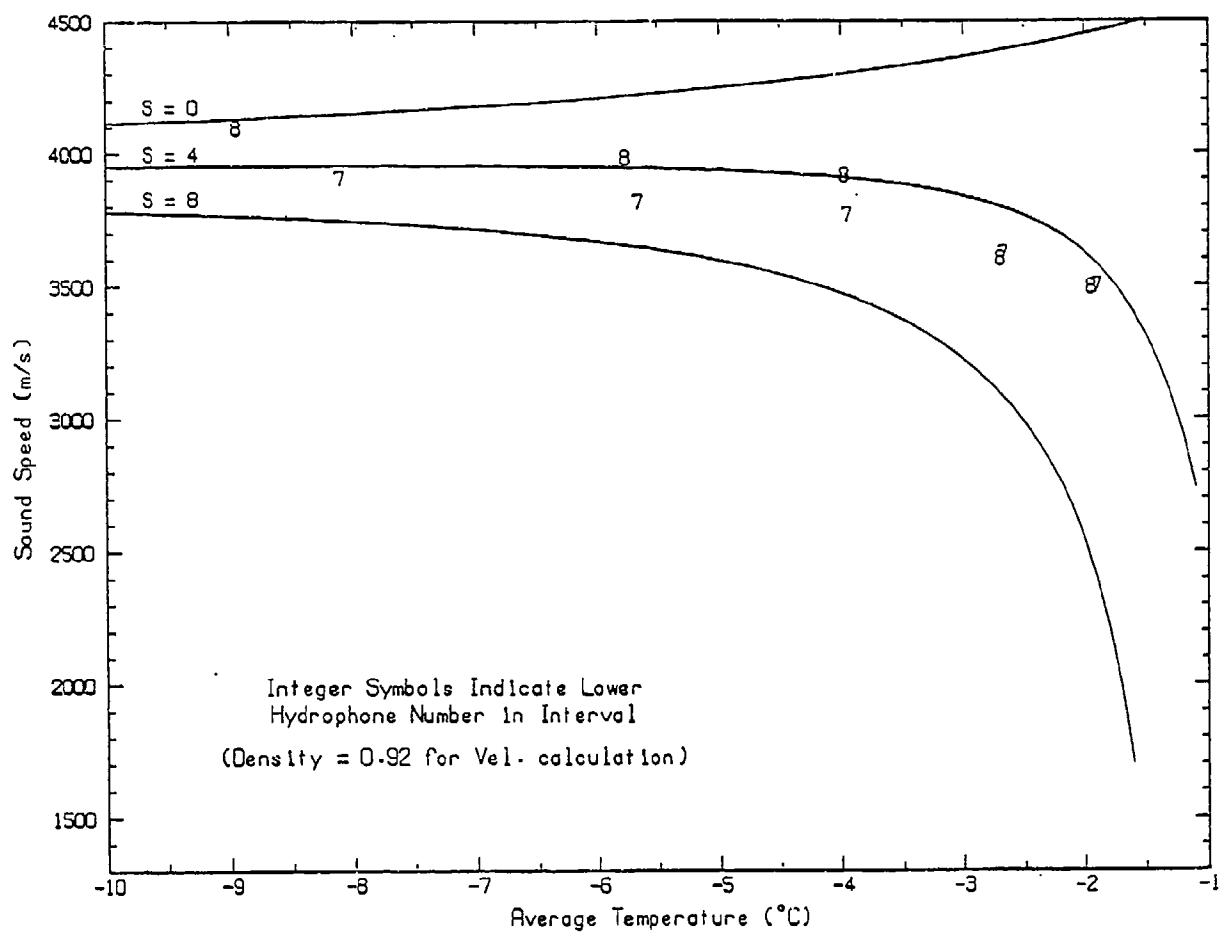
Figure 60b.   Same as Figure 60a, but for hydrophone intervals 7–8 and 8–9 only, where pressure effects should be minimum.

F60b
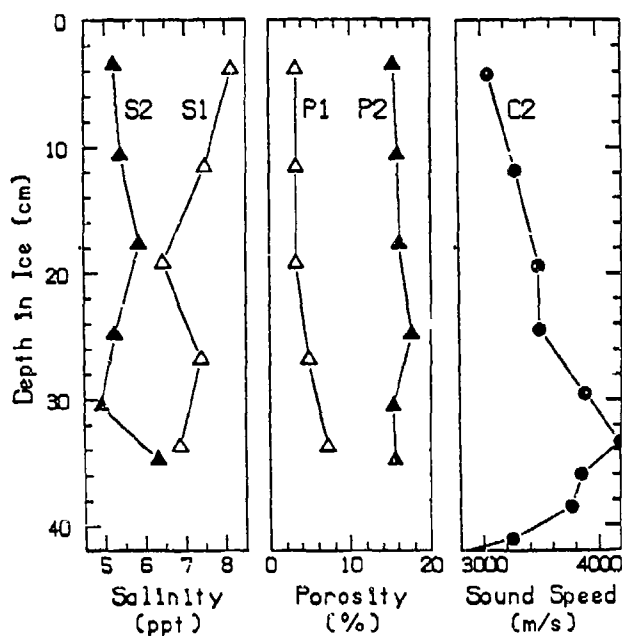
Figure 61. *Measured salinities of the ice cores before submersion (S1) and after warming (S2), and the porosities calculated, respectively, from these data. Also shown is the sound speed profile from Figure 58b to show how the peak at 32 cm corresponds to a low salinity.*
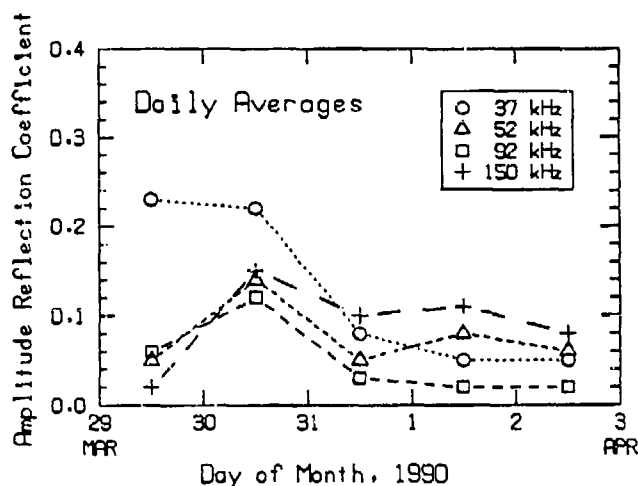
Figure 62. *Amplitude reflection coefficients measured during the warming phase. Although the scatter of individual measurements is large, averages for each day show a decreasing trend after the initial increase when the block was submerged.*
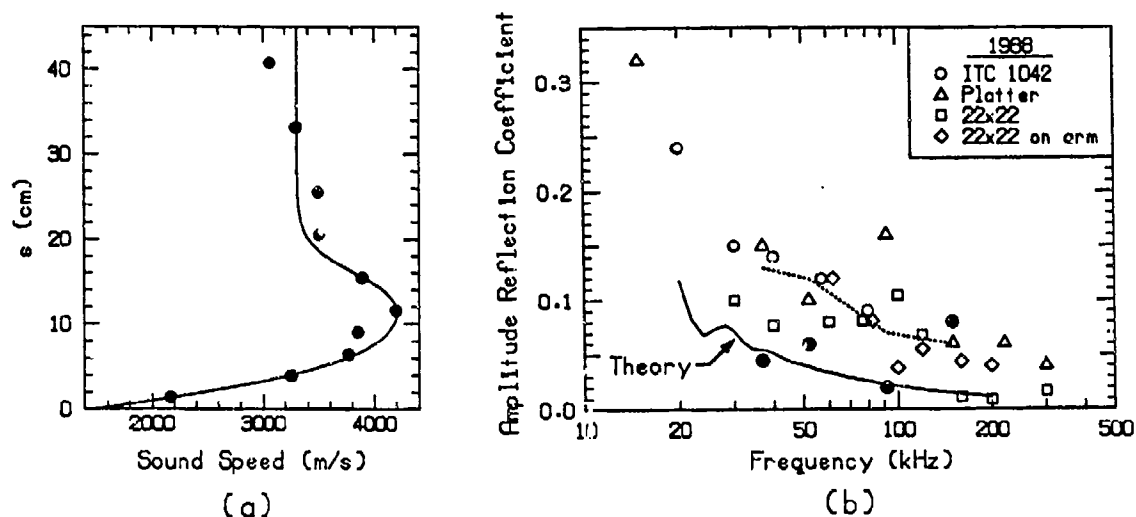
Figure 63. *(a) Sound speed data from Figure 58b for the end of the submerged phase (solid dots), and the best fit (line) of Eq. (9) in Ref. 4, which was used to predict the theoretical results in (b). (b) Average amplitude reflection coefficients for all measurements during the submerged phase (filled circles) compared with ice canopy reflectivities measured in 1988. The solid line is the theoretical results predicted from the best-fit line in (a). The dotted line represents the data from Figure 53 for the ice-growth phase.*
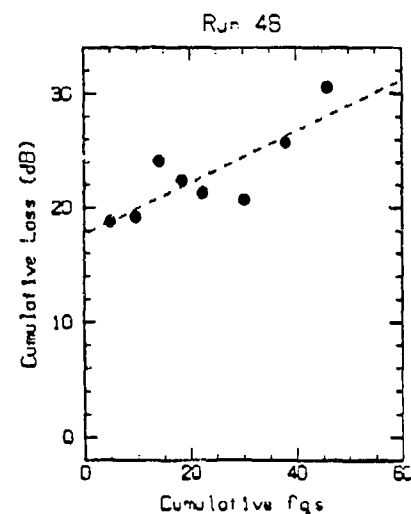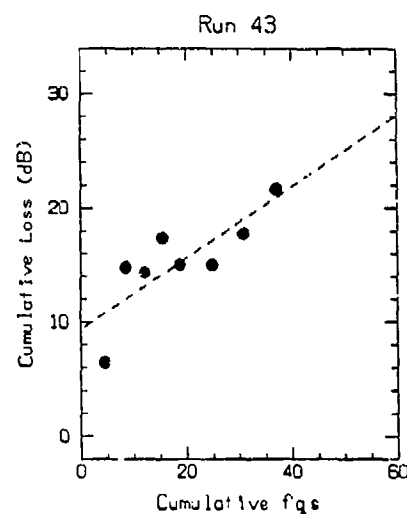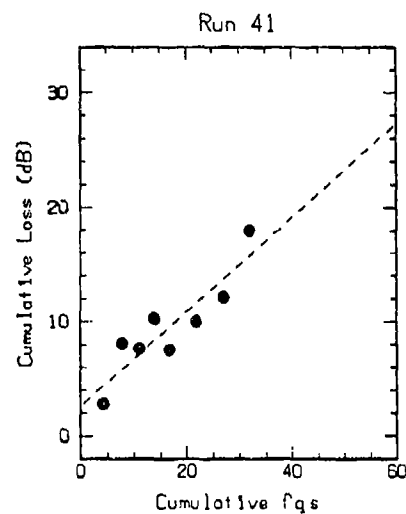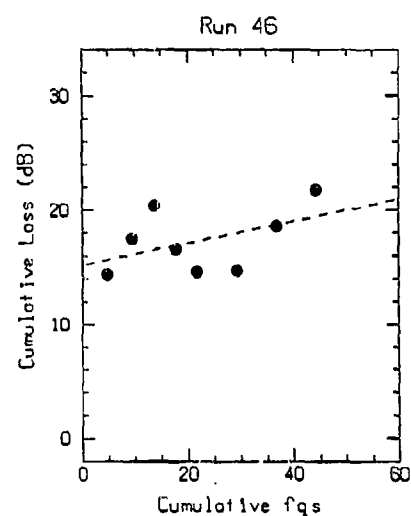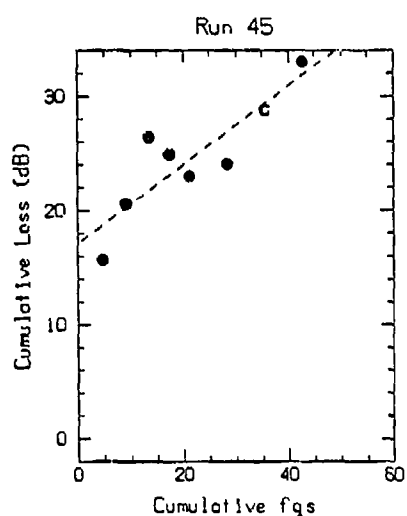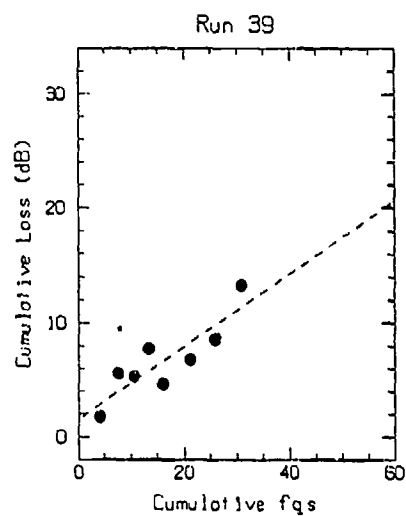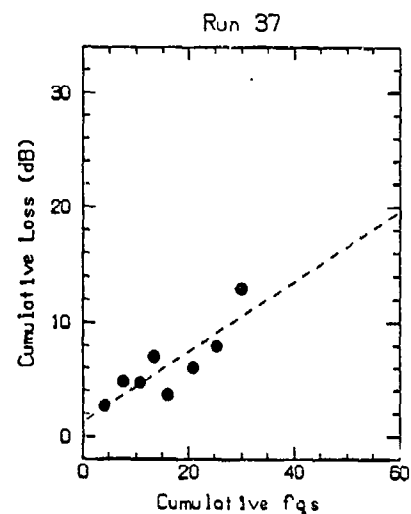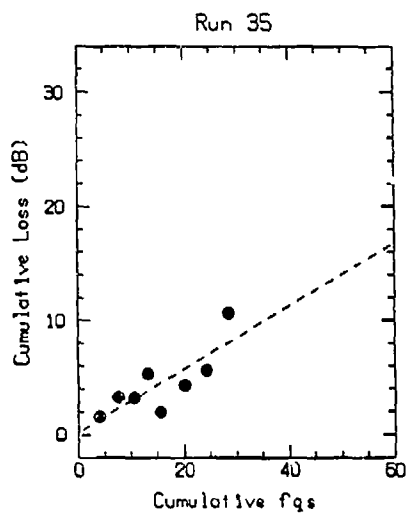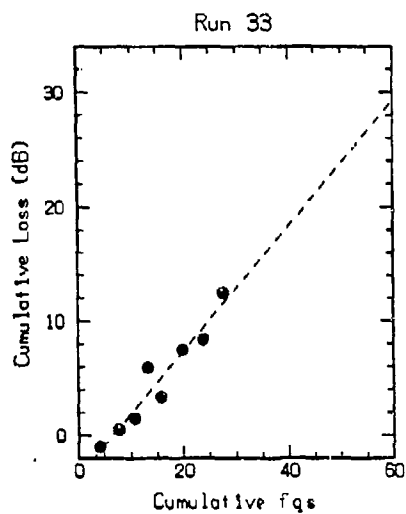
Figure 64. *Cumulative loss at each hydrophone for acoustic measurements made after the block had been submerged.*

Run 51

Run 52

Run 54

Run 56

Run 57
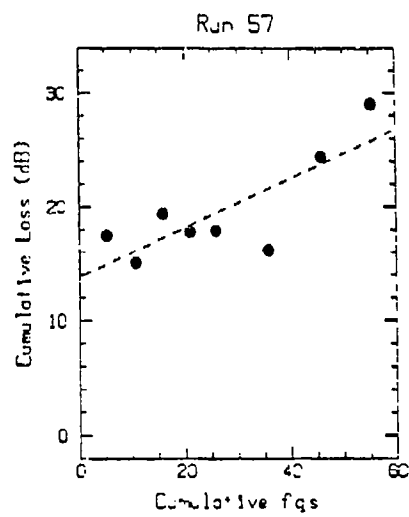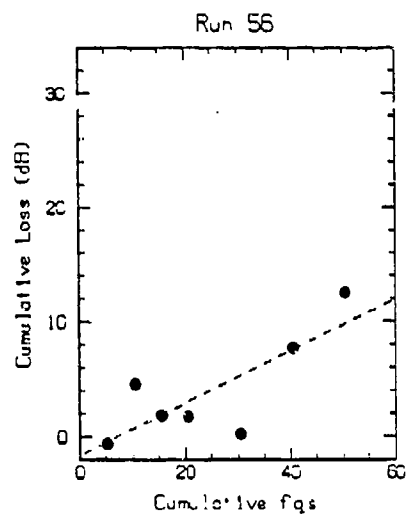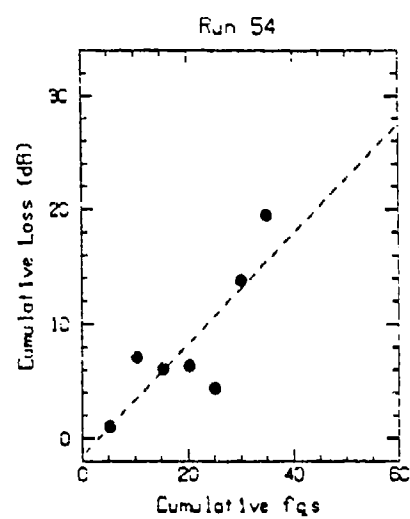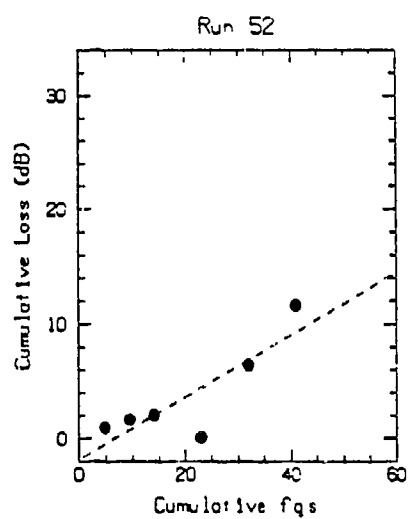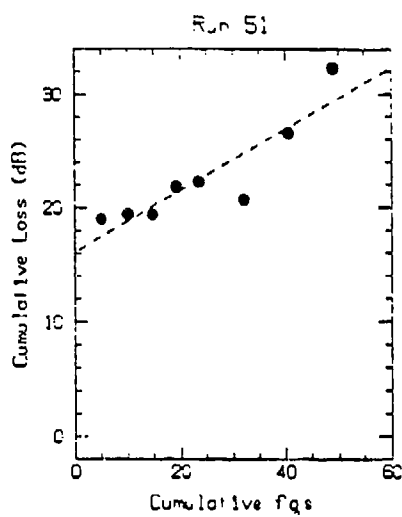
Figure 64, cont.
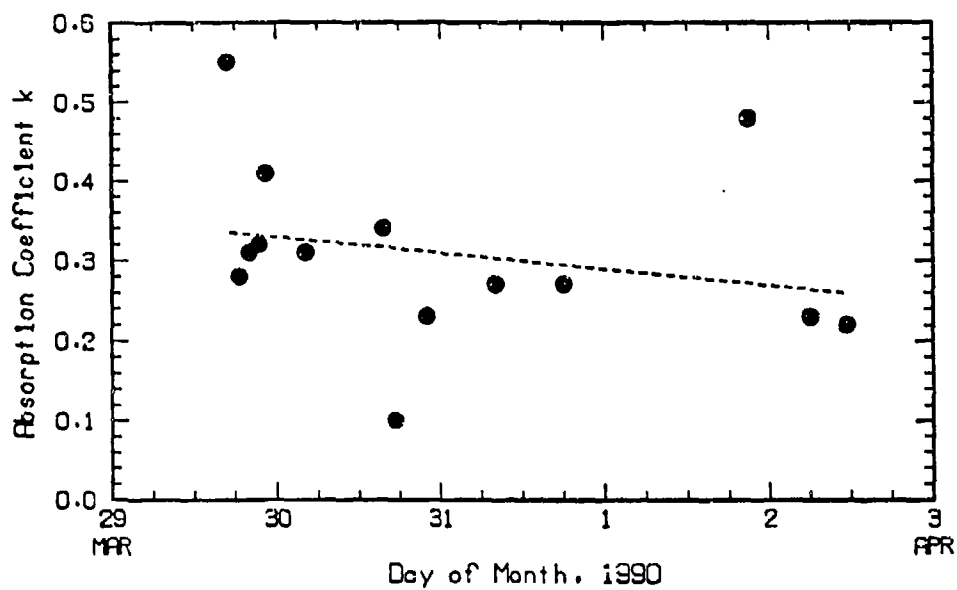
Figure 65. Absorption coefficients k *measured for the ice block during the 4 days after submergence;* k = 0.335 − 0.0201 D, *where* D *is the time (in days) after the first data point.*
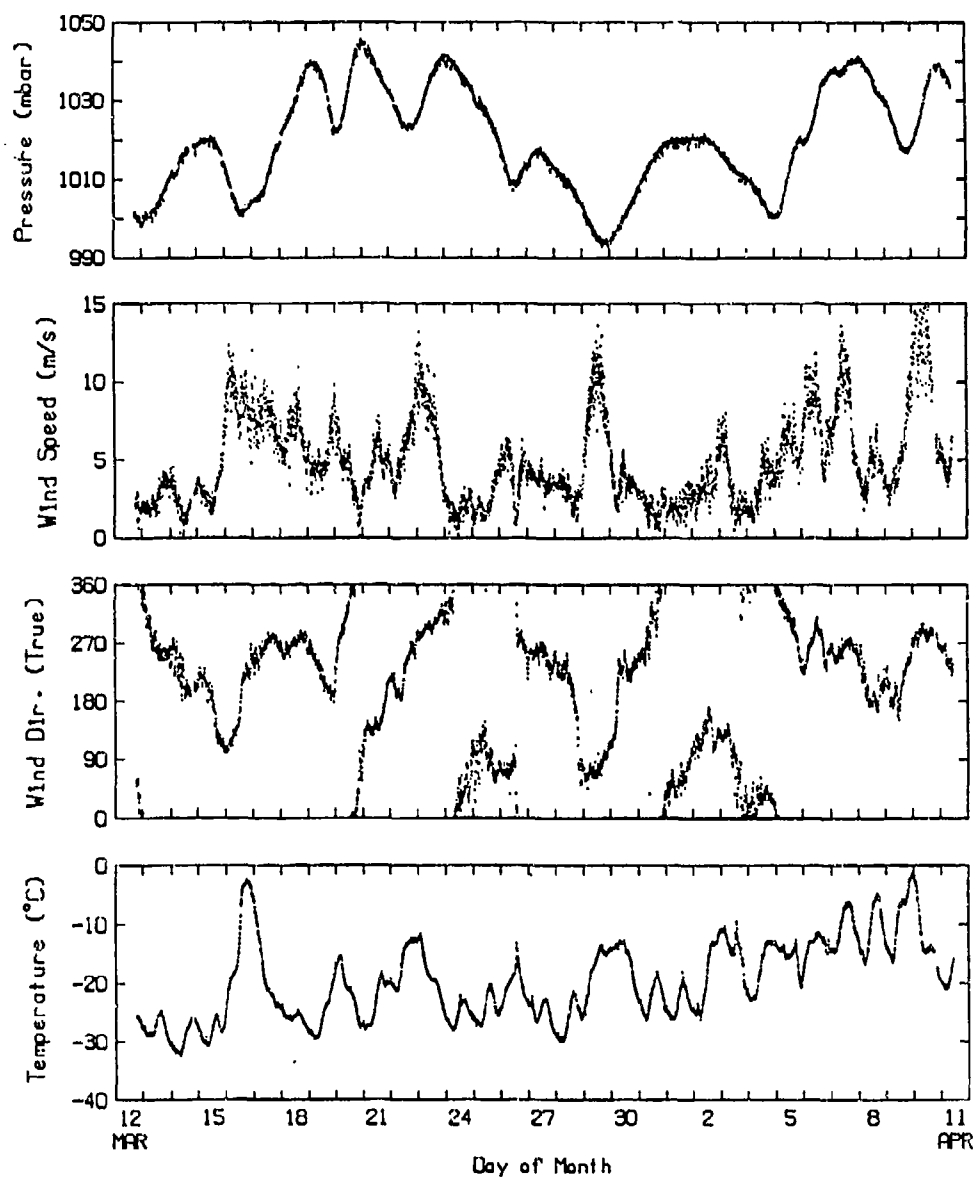
Figure 66. Weather measurements at the ice camp during its occupancy.
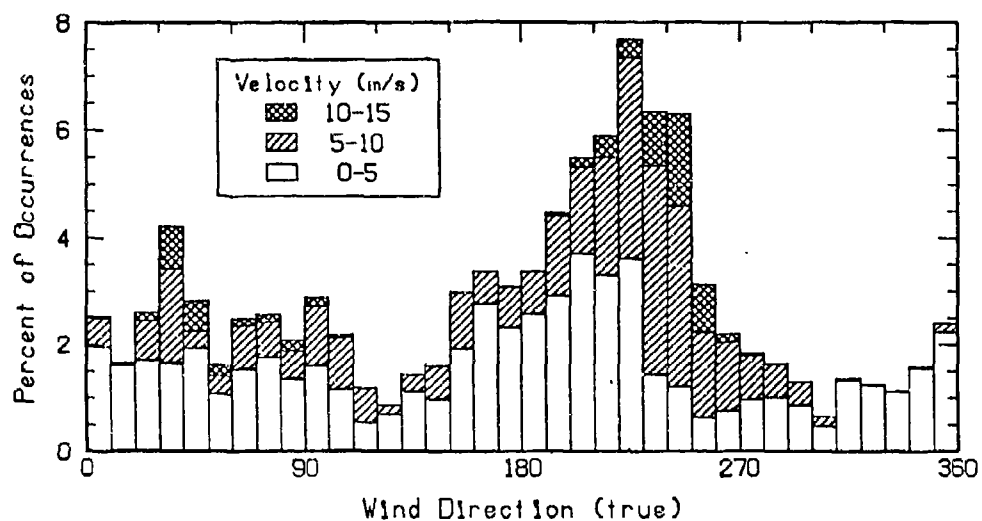
Figure 67. Histogram of wind vectors at the ice camp.
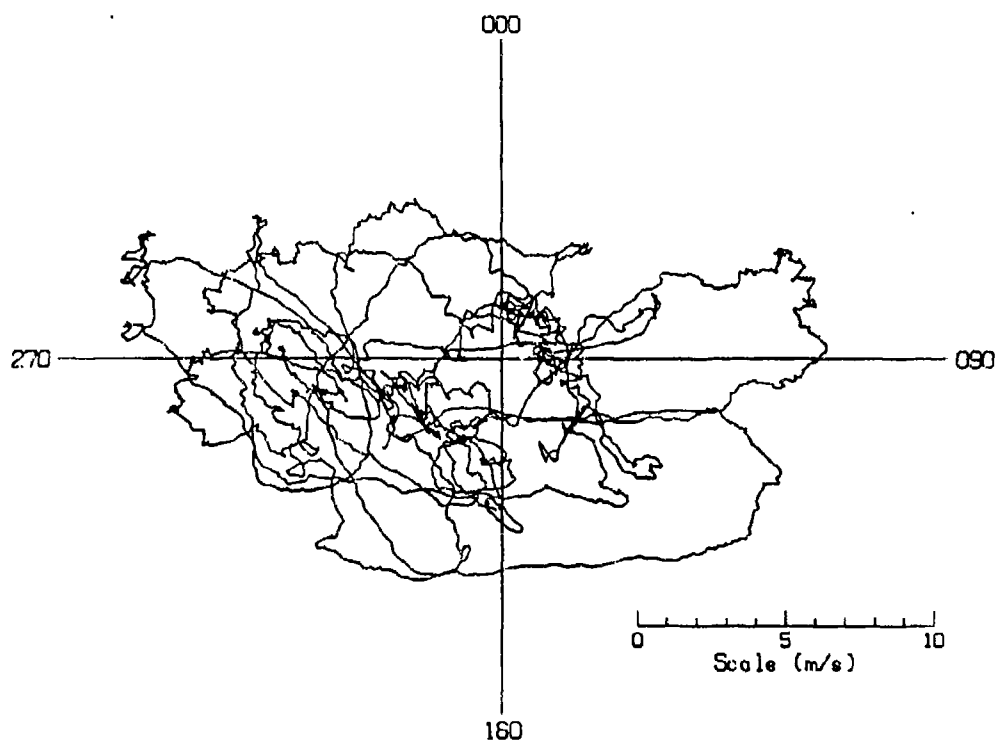
Figure 68. Wind vector diagram for all measurements at the ice camp.
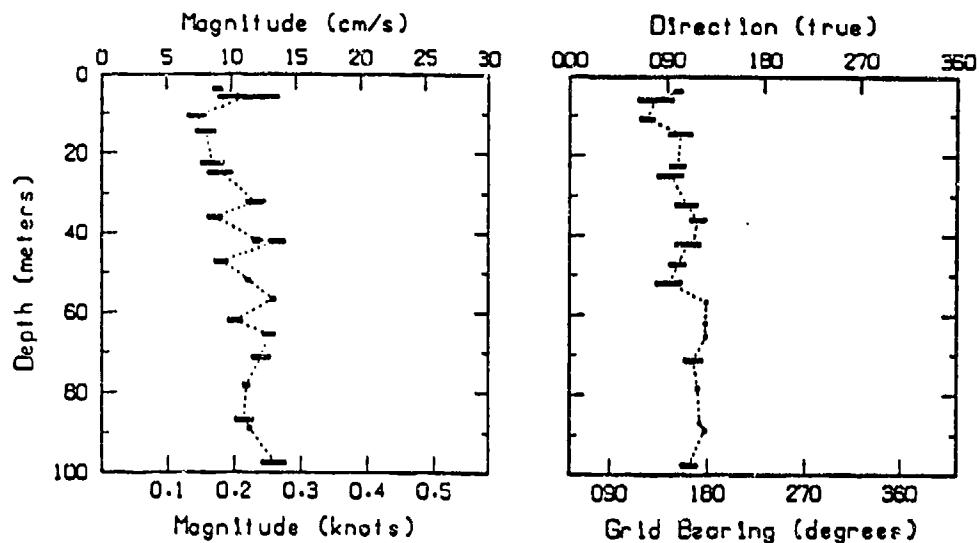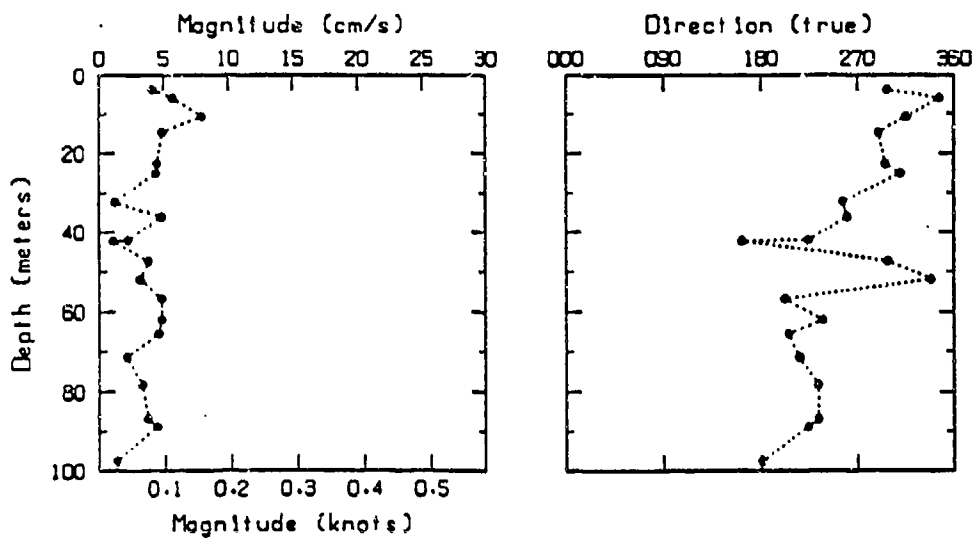
Figure 69. Current magnitude and direction relative to the floe (upper) and relative to the earth (lower) for run 1. Horizontal bars indicate standard deviation of the measurements at each depth.

F69
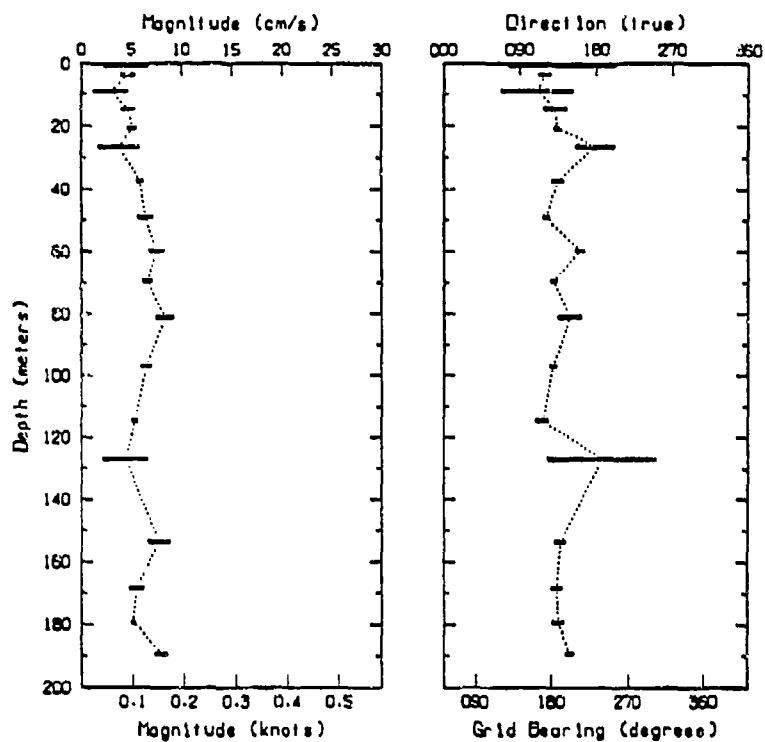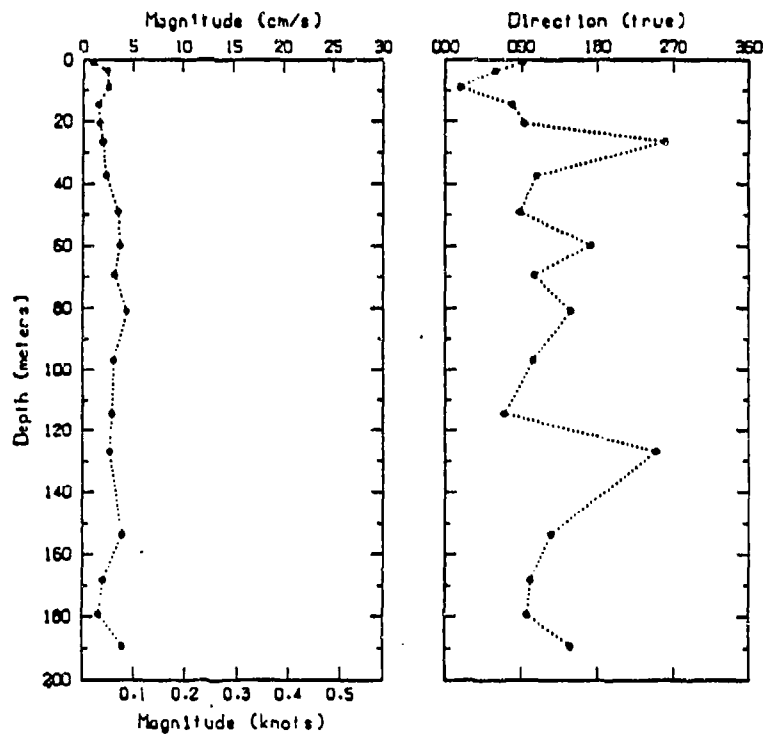
Figure 70. Current magnitude and direction relative to the floe (upper) and relative to the earth (lower) for run 3. Horizontal bars indicate standard deviation of the measurements at each depth.

F70
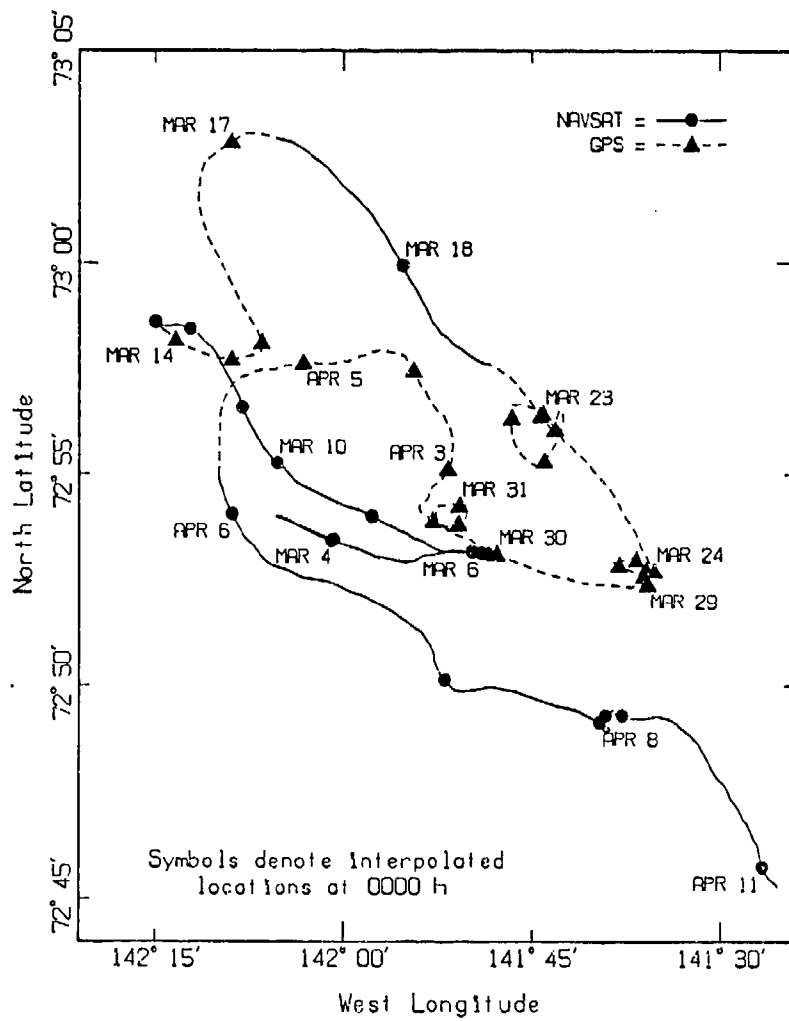
Figure 71.   Positions of the floe during the ice camp occupancy.
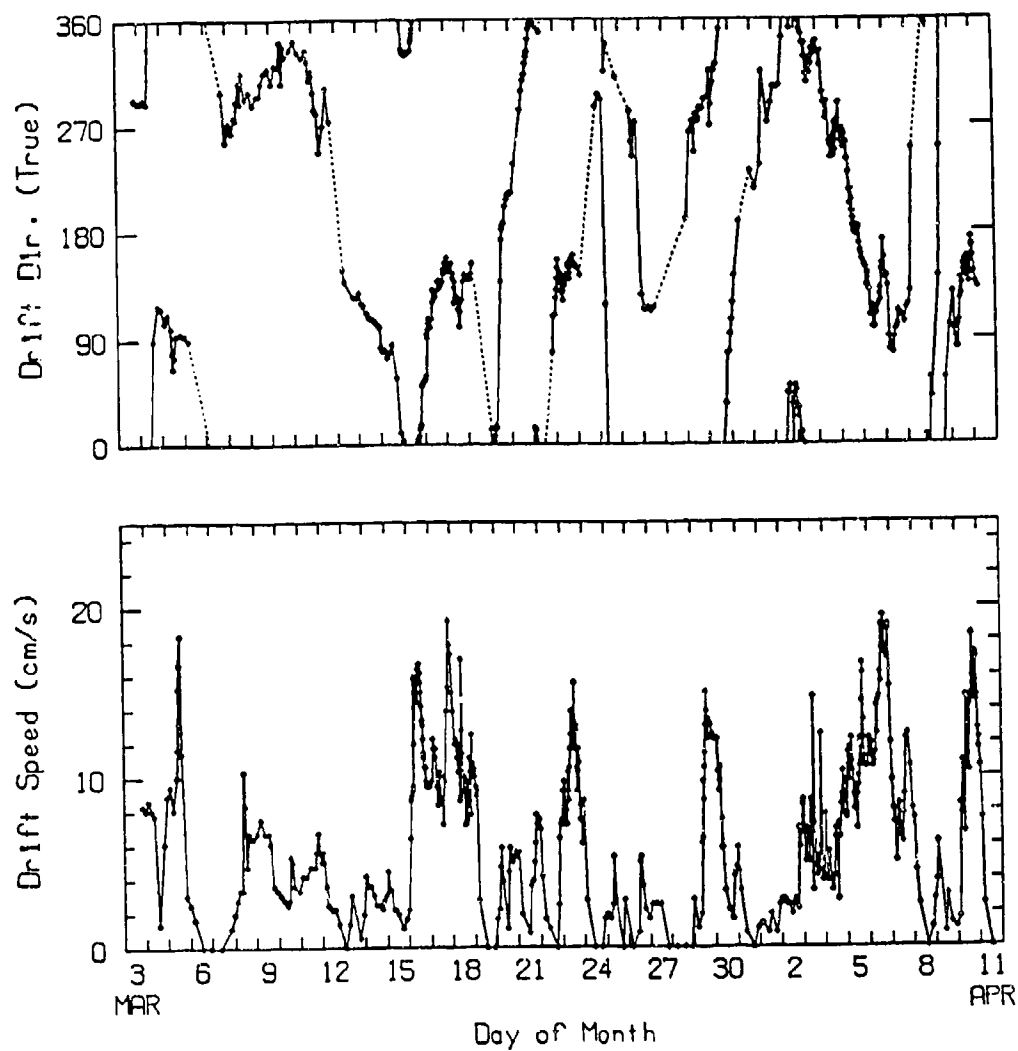
Figure 72. Speed and direction of floe drift during the ice camp occupancy.

F72
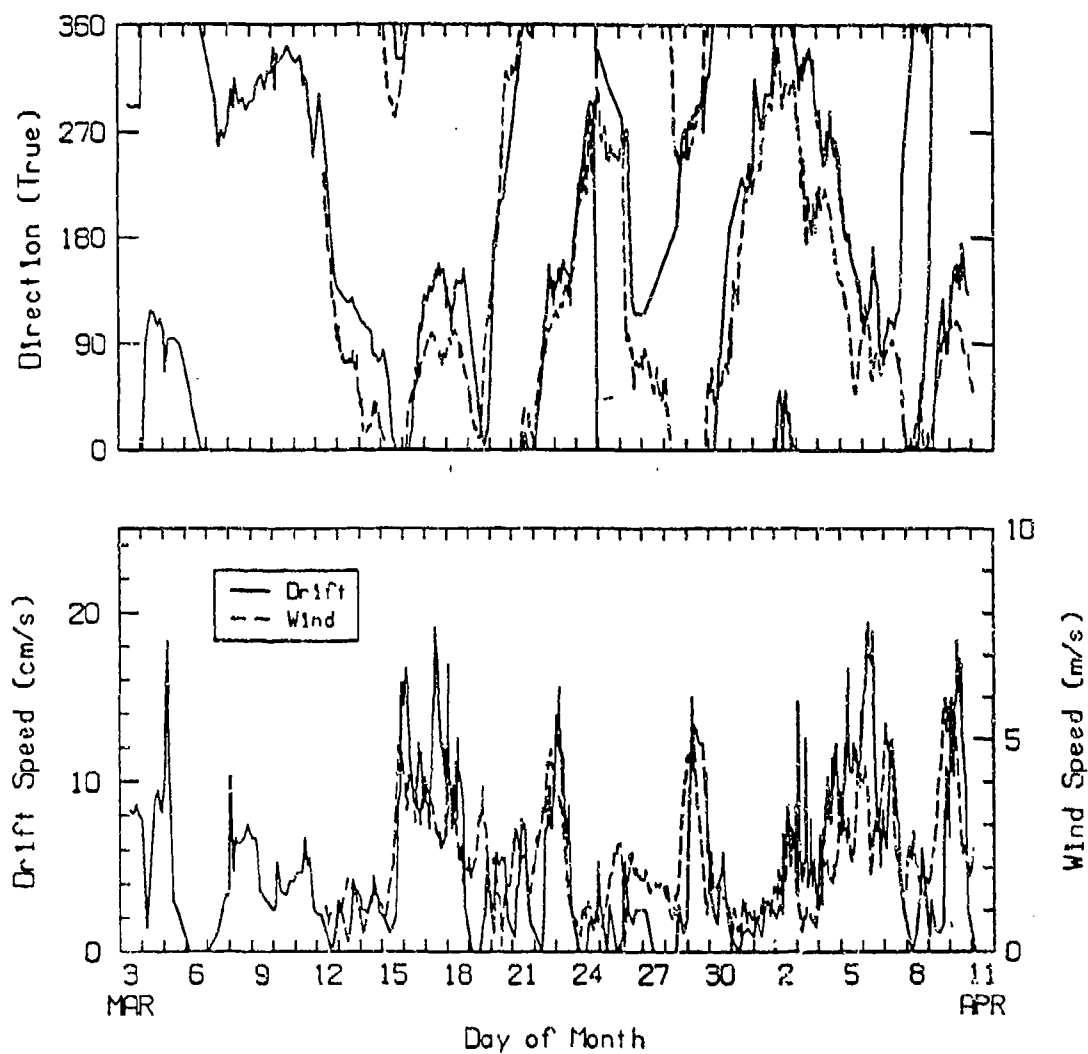
Figure 73. Comparison of the speed and direction of the floe drift with the speed and direction of the wind (normalized for best fit with a ratio of 40).
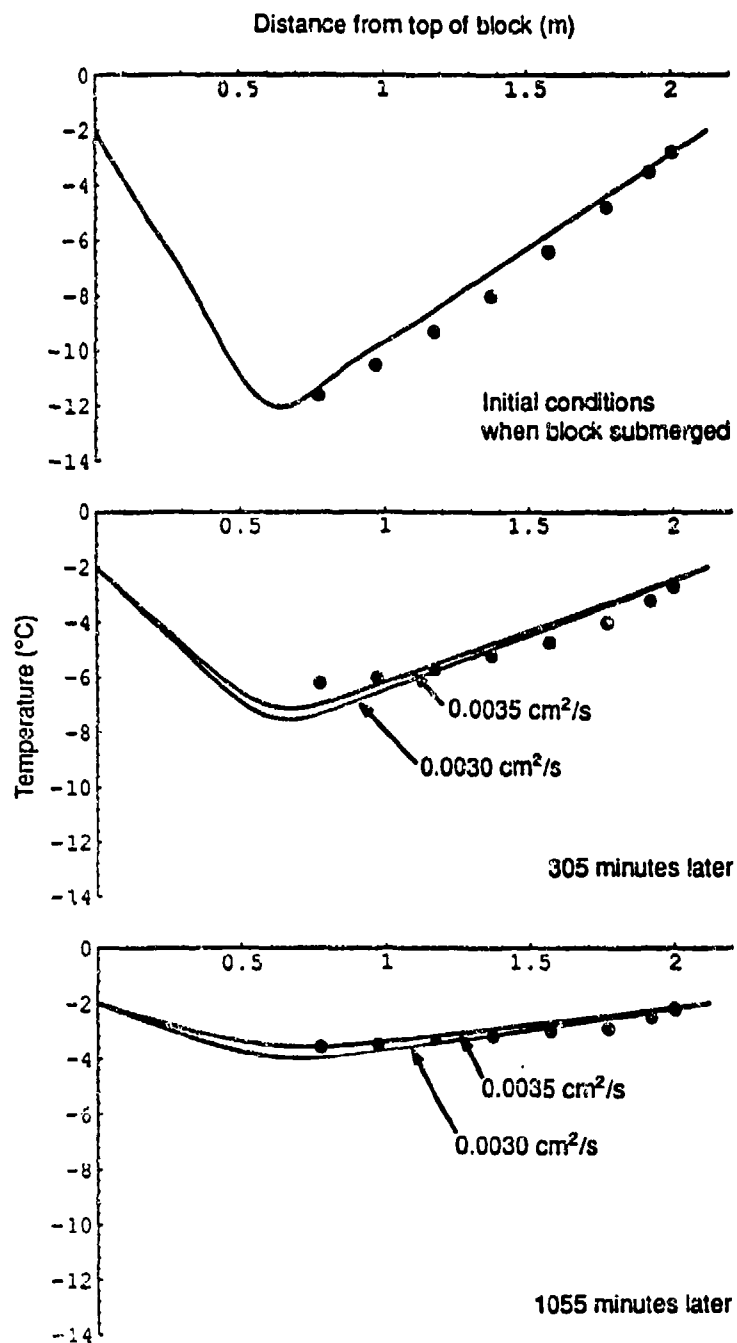
Figure 74. *Comparison of measured temperature profiles in a 58-cm-diameter ice block cut from the canopy with profiles predicted for various diffusivity values. The selection of the best fit is done visually.*
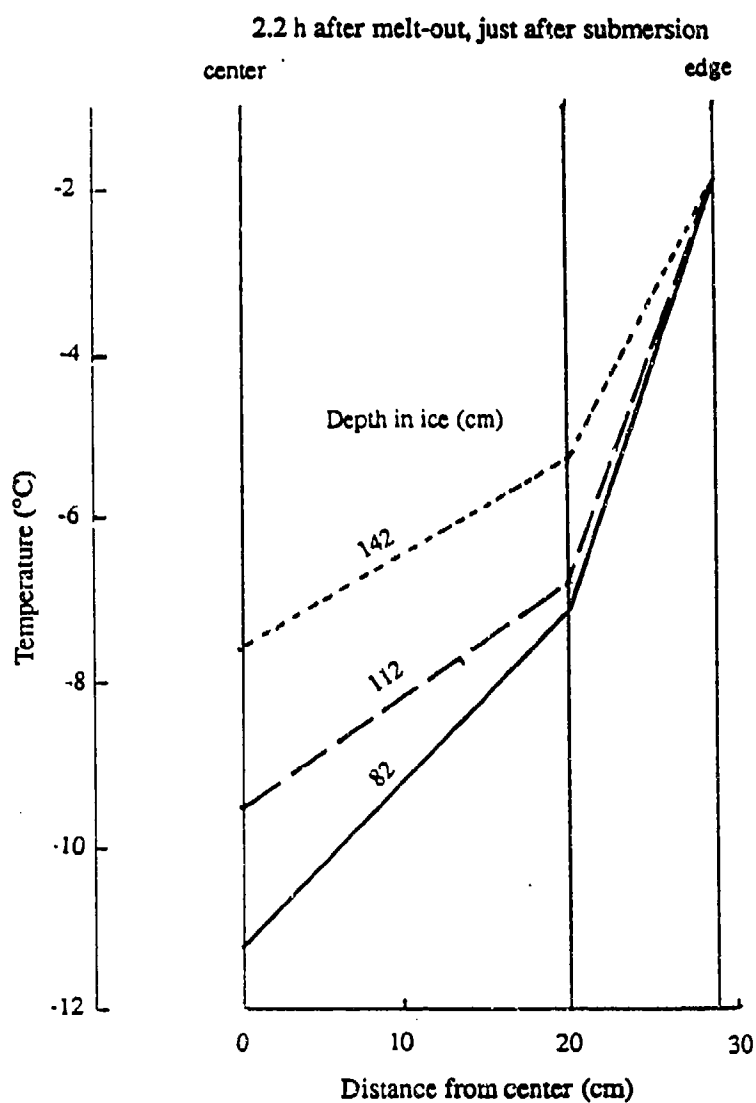
Figure 75. *The measured temperature variation from the center to the edge of a 58-cm-diameter ice block cut from the canopy, at various times after submersion. Our assumption of a linear change appears to be inaccurate during the early stages.*

TABLES

LIST OF TABLES

Table 1. *Calibration of (K&H) filter for measurements with the platter transducer.*

Frequency (kHz)		Received Signal				Received Signal			
	Frame	Without Filter (V)	With Filter (V)	Ratio (dB)	Frame	Without Filter (V)	With Filter (V)	Ratio (dB)	Average Correction (dB)
37	1	1.986	0.887	7.0	6	1.976	0.893	6.9	6.95
52	2	1.984	0.848	7.4	7	1.970	0.847	7.3	7.35
92	3	1.964	0.912	6.7	8	1.966	0.849	7.3	7.00
150	4	1.943	0.785	7.9	9	1.951	0.711	8.8	8.35
220	5	1.924	0.907	6.5	10	1.923	0.917	6.4	6.45

Table 2. *Platter transducer calibration using the water surface as a reflector.*

Frequency (kHz)	Average $20 \log V/T$ (dB)	$20 \log 2R$ (dB)	$2\alpha R$	Gain (dB)	Filter Loss (dB)	CAL (dB)
37	−50.9	26.2	0.2	20	6.9	−37.6
52	−35.6	26.2	0.2	20	7.3	−21.9
92	−46.6	26.2	0.4	20	7.0	−33.0
150	−64.1	26.2	0.6	20	8.3	−48.9
220	−39.6	26.2	0.9	20	6.4	−26.2

Table 3. *Platter transducer calibration using a spherical reflector.*

Frequency (kHz)	20 log V/T	Sphere Target Strength (dB)	Cal (dB)	Cal Average of Two Sets (dB)
First set (PLA-1; R = 6.6 m; Gain = 20 dB)				
37	−54.7	−7.8	−33.9	
52	−34.0	−7.0	−14.0	
92	−38.0	−5.9	−18.9	
150	−44.1	−6.0	−24.7	
220	−31.4	--	--	
Second set (PLA-3; R = 6.7 m; Gain = 20 dB)				
37	−53.7	−7.8	−32.8	−33.4
52	−32.8	−7.0	−12.8	−13.4
92	−38.4	−5.9	−19.2	−19.1
150	−43.2	−6.0	−23.7	−24.2
220	−29.8	--	--	--

Table 4. *Summary of platter transducer calibrations.*

Frequency (kHz)	Air/water interface 1988 (dB)	1990 (dB)	Using sphere with 1990 target strength 1988 (dB)	1990 (dB)	Selected for use in 1990 (dB)
15	--	--	--	--	−37
37	−38.1	−37.6	−31.7	−33.4	−34
52	−20.2	−21.9	−13.3	−13.4	−14
92	−33.1	−33.0	−26.1	−19.1	−19
150	−33.6	−48.9	−20.0	−24.2	−25
220	−15.1	−26.0	--	--	−22
300	--	--	--	--	−22

Table 5. *Summary of 22 × 22 transducer calibrations, in decibels. All calibrations used a spherical reflector except for the on-arm calibration, which was from an air/water interface.*

Frequency (kHz)	Run 1	Run 2	Run 3	Run 4	1988	On arm	Average for Runs 1–3
30	−54.8	−57.8	--	--	−67.8	--	−56.3
40	−53.4	−52.2	−53.0	--	−64.4	--	−52.9
60	−47.6	−47.2	−45.0	−49.1	−57.7	--	−46.6
80	−41.0	−41.2	−39.5	−45.2	−51.1	−47.7	−40.6
100	−34.9	−35.3	−34.0	−42.2	−45.0	−39.3	−34.7
120	−27.9	−29.4	−26.0	−38.2	−39.0	−35.7	−27.8
150	--	--	--	--	−30.5	--	--
160	−9.4	−12.0	−8.4	−29.5	−28.0	−28.9	−9.9
200	−10.1	--	−9.3	−30.2	−20.3	−26.6	−9.7

Table 6. *Calibration of 22 × 22 transducer on an arm at short range below an air/water interface.*

Frequency (kHz)	20 log V/T 1st set (dB)	2nd set (dB)	Average CAL (dB)
80	−20.10	−17.40	−47.7
100	−12.70	−8.09	−39.3
120	−3.50	−10.00	−35.7
160	−0.58	0.54	−28.9
200	−3.19	7.73	−26.6

Note: Range = 1.77 m; gain = 40 dB

Table 7. *Sound speeds calculated from one-way vertical transmissions through the ice.*

No. 1			No. 2; Hole 1			No. 3; Hole 2		
Depth (cm)	Sound speed (m/s)	Std. dev. of mean (m/s)	Depth (cm)	Sound speed (m/s)	Std. dev. of mean (m/s)	Depth (cm)	Sound speed (m/s)	Std. dev. of mean (m/s)
10.8	4189	23	11.4	3739	26	6.9	3643	26
27.1	3954	17	22.2	3917	75	17.1	3828	18
48.1	3893	10	29.1	3994	70	31.3	3960	7
66.7	4093	25	42.0	3910	19	47.5	3739	32
85.7	4075	27	62.0	3772	20	64.5	3875	30
			86.3	3828	27	89.9	3740	16
			115.1	3933	19	117.9	4261	8
			141.9	3694	18			
			157.4	4080	11			
			174.4	4128	64			
			194.8	3456	68			
			206.0	3346	62			

Table 8. *Summary of measurements of target strength versus angle of incidence for a submerged ice block.*

Figure No.	Movement of Transducer	Time interval After Submergence (h)
11	center to north; center to south	1.3 – 2.2
12	center to east; center to west	2.3 – 3.1
13	center to east; center to west	17.3 – 18.0
14	center to west	21.8 – 22.0

Table 9. *Reflection coefficients* R_a *measured from the underside of the ice canopy using the platter transducer.*

Location	Frequency (kHz) 37	52	92	150	220
S	0.14	0.01	--	0.01	0.08
SW	0.03	0.01	0.02	0.01	0.08
W	0.08	0.02	0.01	0.01	0.11
NW	0.08	0.03	0.01	0.02	0.13
N	0.22	0.21	0.28	0.26	1.72
NE	0.16	0.12	0.11	0.07	0.09
E	0.06	0.10	0.10	0.04	0.12
SE	0.14	0.09	0.05	0.02	0.11
Average (omitting north set)					
R_a	0.10	0.05	0.05	0.03	0.03
Std dev	0.05	0.05	0.05	0.02	0.05

Table 10. *Reflection coefficients* R_a *measured from the underside of the ice canopy using the* 22×22 *transducer.*

Ring Location	Frequency (kHz) 30	40	60	80	100	120	160	200
N12/E56	0.11	0.14	0.10	0.10	0.15	0.04	0.10	0.08
N27/E56	0.09	0.13	0.06	0.09	0.16	0.07	0.05	0.06
N51/E40	0.07	0.09	0.04	0.07	0.10	0.04	0.03	0.06
N51/E16	0.13	0.12	0.05	0.10	0.17	0.06	0.04	0.04
Filter installed								
N27/E0	0.11	0.16	0.08	0.13	0.22	0.11	0.04	0.07
N12/E0	0.08	0.12	0.06	0.09	0.17	0.07	0.04	0.09
N12/E16	0.10	0.14	0.06	0.12	0.18	0.07	0.04	0.12
N12/E40	0.11	0.15	0.06	0.13	0.19	0.08	0.05	0.09
Average	0.100	0.131	0.064	0.104	0.168	0.068	0.049	0.076
Std dev of mean	0.007	0.008	0.006	0.007	0.012	0.008	0.008	0.008

Table 11. *Filter corrections for the ITC 1042 transducer, measured using a zero-noise signal.*

Frequency (kHz)	Output amplitude (V)		Correction (dB)
	Unfiltered	Filtered	
20	2.000	0.869	7.2
30	1.998	0.837	7.6
40	1.997	0.928	6.7
60	1.992	0.951	6.4
80	1.987	0.981	6.1
100	1.988	0.972	6.2
120	1.982	0.888	7.0

Table 12. *Reflection coefficients R_a measured for the ice canopy using the ITC 1042 transducer. The first eight locations are the same as those for the 22×22 measurements.*

Location Number	Filter used?	Frequency (kHz)						
		20	30	40	60	80	100	120
1	yes	0.21	0.27	0.15	0.13	0.17	0.10	0.23
2	yes	0.11	0.19	0.12	0.10	0.12	0.04	0.17
3	no	0.12	0.15	0.11	0.08	0.09	0.05	0.10
4	no	0.24	0.43	0.09	0.17	0.34	0.26	0.39
5	no	0.19	0.25	0.16	0.14	0.15	0.07	0.15
6	no	0.15	0.18	0.14	0.09	0.11	0.05	0.14
7	no	0.17	0.22	0.13	0.11	0.12	0.04	0.22
8	no	0.21	0.28	0.18	0.14	0.14	0.07	0.20
9	no	0.15	0.16	0.06	0.10	0.10	0.12	0.31
10	no	0.39	0.42	0.16	0.20	0.31	0.35	0.60
11	no	0.15	0.15	0.08	0.10	0.07	0.08	0.28
12	no	0.23	0.18	0.06	0.10	0.14	0.14	0.28
Average of all locations except 4 and 10								
R_a		0.17	0.20	0.12	0.11	0.12	0.08	0.21
Std dev of mean		0.01	0.02	0.01	0.01	0.01	0.01	0.03

Table 13. *Amplitude reflection coefficients* R_a *for the ice canopy using the* 22×22 *transducer on-arm. The special short-range calibration using the air/water interface was considered erroneous; instead, the calibration obtained using a sphere was employed.*

Frequency (kHz)	Hole 1 R_a	Std dev	Hole 2 R_a	Std dev
80	0.038	0.003	0.034	0.001
100	0.087	0.002	0.079	0.002
120	0.118	0.004	0.104	0.003
160	0.020	0.001	0.018	0.001
200	0.032	0.002	0.027	0.002

Note: Because of overlap, there were 38 measurements at Hole 1 and 39 at Hole 2.

Table 14. *Values used to determine the absorption coefficient* k *from reflections measured with the ITC 1042 transducer.*

Location	Frequency (kHz)	R_a	V_1/V_2	Loss (dB)	fqs
1	20	0.21	0.49	5.5	33.6
	30	0.27	1.42	12.3	50.4
	40	0.15	1.73	19.6	67.2
9	20	0.15	0.85	13.4	33.6
	30	0.16	1.40	17.2	50.4
	40	0.06	0.48	16.6	67.2
10	20	0.39	1.06	5.8	33.6
	30	0.42	2.17	11.1	50.4
	40	0.16	0.99	14.2	67.2
11	20	0.15	0.89	13.8	33.6
	30	0.15	0.91	13.8	50.4
	40	0.08	0.79	18.4	67.2
	60	0.10	2.14	25.1	101
	80	0.07	1.19	23.1	134
12	20	0.23	0.84	9.3	33.6
	30	0.18	0.98	13.0	50.4
	40	0.06	0.48	16.6	67.2
	60	0.10	2.60	26.8	101

Table 15. *Values used to determine absorption coefficient* k *from reflections measured with the platter transducer.*

Location	Frequency (kHz)	R (m)	R_a	$1+sN/R$	V_1/V_2	Loss (dB)	fqs
S	37	8.68	0.14	1.60	1.01	12.9	62.2
	52	8.68	0.01	1.60	1.10	36.7	87.4
SW	37	8.35	8.03	1.60	1.26	28.4	62.2
	52	8.35	0.01	1.60	1.98	41.9	87.4
W	37	8.23	0.08	1.64	2.64	26.0	62.2
	52	8.23	0.02	1.64	1.50	33.2	87.4
NW	37	7.78	0.08	1.67	1.38	20.3	62.2
	52	7.78	0.03	1.62	1.67	30.2	87.4
	92	7.78	0.01	1.67	1.71	40.2	155
N	37	7.34	0.22	1.72	1.56	11.9	62.2
	52	7.34	0.21	1.72	3.19	18.5	87.4
	92	7.34	0.28	1.72	13.5	28.3	155
	150	7.34	0.26	1.72	46.5	39.7	252
NE	37	7.75	0.16	1.68	2.58	19.4	62.2
	52	7.75	0.11	1.68	5.01	27.8	87.4
	92	7.75	0.12	1.68	15.3	38.3	155
	150	7.75	0.07	1.68	23.4	45.9	252
E	37	8.24	0.06	1.64	0.83	18.5	62.2
	52	8.24	0.10	1.64	4.07	27.8	87.4
	92	8.24	0.10	1.64	15.8	39.6	155
	150	8.24	0.04	1.64	11.3	44.7	252
SE	37	8.49	0.14	1.62	2.39	20.3	62.2
	52	8.49	0.09	1.62	4.43	29.6	87.4
	92	8.49	0.05	1.62	9.38	41.3	155

Table 16. Values used to determine the absorption coefficient k from reflections measured with the 22 ×22 transducer.

Ring Location	Frequency (kHz)	R_a	V_1/V_2	R (m)	1 + sN/R	Loss (dB)	fqs
N12/E56	30	0.11	0.60	28.5	1.18	13.2	50.4
	40	0.14	1.16			16.8	67.2
	60	0.10	1.69			23.0	101
	80	0.10	5.76			33.7	134
N27/E56	30	0.09	0.83	28.2	1.19	17.7	50.4
	40	0.13	1.27			18.1	67.2
	60	0.06	2.20			29.7	101
N51/E40	30	0.07	0.68	26.5	1.20	18.1	50.4
	40	0.09	1.63			23.5	67.2
	60	0.04	1.50			29.9	101
N51/E16	30	0.13	1.32	26.6	1.20	18.4	50.4
	40	0.12	2.79			25.6	67.2
	60	0.05	1.84			29.7	101
	80	0.10	7.25			35.5	134
N27/E0 Filtered	30	0.11	0.96	28.1	1.19	17.2	50.4
	40	0.16	2.12			20.7	67.2
	60	0.08	4.60			33.6	101
	80	0.13	13.0			38.3	134
N12/E0 Filtered	30	0.08	1.18	28.4	1.18	21.9	50.4
	40	0.13	1.54			19.9	67.2
	60	0.06	2.93			32.3	101
N12/E16 Filtered	30	0.10	0.85	28.7	1.18	17.1	50.4
	40	0.14	1.54			19.2	67.2
	60	0.06	1.16			24.3	101
	80	0.12	10.2			37.0	134
	100	0.18	34.5			43.9	168
N12/E40 Filtered	30	0.11	0.80	28.8	1.18	15.7	50.4
	40	0.15	1.19			16.4	67.2
	60	0.06	3.15			32.9	101
	80	0.13	14.3			39.2	134

Table 17. Thermistor and hydrophone spacings, measured in air on 27 January 1992.

	Thermistors			Hydrophones	
No.	Depth (cm)	Difference (cm)	No.	Depth (cm)	Difference (cm)
24	0.00		12	1.7	
23	1.95	1.95	11	6.8	5.1
22	3.85	1.9	10	11.8	5.0
21	5.95	2.1	9	16.9	5.1
20	7.95	2.0	8	22.0	5.1
19	9.95	2.0	7	27.0	5.0
18	11.90	1.95	6	32.1	5.1
17	13.95	2.05	5	34.7	2.6
16	15.95	2.0	4	37.2	2.5
15	17.90	1.95	3	39.8	2.6
14	19.90	2.0	2	42.3	2.5
13	21.90	2.0	1	44.8	2.5
12	23.70	1.8			
11	25.85	2.15			
10	27.90	2.05			
9	29.90	2.0			
8	31.80	1.9			
7	33.85	2.05			
6	35.85	2.0			
5	37.80	1.95			
4	39.80	2.0			
3	41.80	2.0			
2	43.75	1.95			
1	45.80	2.05			

Table 18. Times of readings of thermistor string suspended in the main hole.

Date	Time (local)	Date	Time (local
21 March	in pm	25 March	0815 h
22 March	0715 h		2035 h
	0918 h	26 March	0916 h
	1257 h		1926 h
	1725 h		2031 h
	2149 h	27 March	1000 h
23 March	0740 h		1128 h
	0949 h		1406 h
	1848 h		2042 h
24 March	0848 h	28 March	0915 h
	0941 h		1810 h
	1110 h		2106 h
	1407 h	29 March	0835 h
	1658 h		1205 h
	2103 h	31 March	1446 h

Note: The block was cored out at 1510 h local time on 31 March 1990.

T18

Table 19. Temperatures recorded in the main hole during ice growth (99.00 indicates that the thermistor failed).

			(Depths of thermistors)				
46.0	44.2	42.0	39.9	37.9	36.0	34.1	32.0
29.9	27.9	25.9	24.0	21.9	20.0	17.9	15.9
13.9	12.0	9.9	7.9	6.0	3.8	2.0	0.0

21 March 1990   (afternoon)   No. 1

-1.55	-1.53	-1.50	-1.41	-1.40	-1.43	-1.36	-1.57
-1.58	-1.45	-1.52	-1.47	99.00	-1.60	-1.79	99.00
-4.40	-5.87	99.00	-8.98	99.00	-12.49	-14.41	-16.55

22 March 1990   0715 HR   No. 2

-1.57	-1.55	-1.53	-1.43	-1.41	-1.44	-1.36	-1.59
-1.60	-1.46	-1.53	-1.49	99.00	-1.73	-2.70	99.00
-5.53	-6.91	99.00	-9.84	99.00	-13.19	-14.93	-16.90

22 March 1990   0918 HR   No. 3

-1.56	-1.53	-1.51	-1.42	-1.40	-1.43	-1.34	-1.57
-1.58	-1.45	-1.51	-1.48	99.00	-1.81	-2.87	99.00
-5.66	-6.96	99.00	-9.58	99.00	-12.21	-13.53	-15.08

22 March 1990   1257 HR   No. 4

-1.56	-1.54	-1.52	-1.42	-1.41	-1.44	-1.35	-1.58
-1.58	-1.45	-1.52	-1.49	99.00	-2.00	-3.07	99.00
-5.40	-6.41	99.00	-8.39	99.00	-10.45	-11.47	-12.67

22 March 1990   1725 HR   No. 5

-1.60	-1.58	-1.56	-1.47	-1.45	-1.49	-1.41	-1.62
-1.63	-1.50	-1.57	-1.53	99.00	-2.22	-3.17	99.00
-5.25	-6.15	99.00	-8.04	99.00	-10.04	-11.04	-12.12

22 March 1990   2149 HR   No. 6

-1.72	-1.70	-1.68	-1.59	-1.57	-1.60	-1.52	-1.74
-1.75	-1.61	-1.68	-1.64	99.00	-2.46	-3.38	99.00
-5.36	-6.24	99.00	-8.09	99.00	-10.04	-11.09	-12.21

23 March 1990   0740 HR   No. 7 0.5 hr after snow removal

-1.71	-1.69	-1.66	-1.57	-1.56	-1.59	-1.51	-1.73
-1.75	-1.60	-1.68	-1.65	99.00	-2.72	-3.52	99.00
-5.13	-5.88	99.00	-7.80	99.00	-10.94	-13.19	-16.03

23 March 1990   0949 HR   No. 8

-1.71	-1.69	-1.66	-1.57	-1.56	-1.59	-1.49	-1.73
-1.74	-1.60	-1.68	-1.66	99.00	-2.83	-3.71	99.00
-5.94	-7.16	99.00	-10.04	99.00	-13.58	-15.47	-17.60

23 March 1990   1848 HR   No. 9

-1.72	-1.70	-1.67	-1.58	-1.57	-1.60	-1.53	-1.73
-1.75	-1.61	-1.72	-1.97	99.00	-4.33	-5.68	99.00
-8.61	-9.99	99.00	-12.93	99.00	-16.29	-18.10	-20.10

T19a

Table 19, cont.

```
24 March 1990   0848 HR        No. 10
    -1.71     -1.69    -1.66     -1.57    -1.56    -1.59    -1.53    -1.74
    -1.77     -1.66    -2.25     -3.50    99.00    -6.08    -7.45    99.00
   -10.30    -11.61    99.00    -14.37    99.00   -17.56   -19.28   -21.22

24 March 1990   0941 HR        No. 11
    -1.71     -1.69    -1.67     -1.57    -1.56    -1.59    -1.52    -1.74
    -1.77     -1.66    -2.32     -3.57    99.00    -6.13    -7.49    99.00
   -10.35    -11.61    99.00    -14.28    99.00   -16.97   -18.81   -20.60

24 March 1990   1110 HR        No. 12
    -1.71     -1.69    -1.66     -1.57    -1.56    -1.59    -1.52    -1.74
    -1.78     -1.67    -2.48     -3.71    99.00    -6.22    -7.56    99.00
   -10.35    -11.61    99.00    -14.16    99.00   -16.94   -18.40   -19.92

24 March 1990   1407 HR        No. 13
    -1.71     -1.69    -1.66     -1.57    -1.56    -1.59    -1.64    -1.74
    -1.77     -1.69    -2.68     -3.91    99.00    -6.30    -7.54    99.00
   -10.09    -11.23    99.00    -13.58    99.00   -16.11   -17.46   -18.94

24 March 1990   1658 HR        No. 14
    -1.72     -1.70    -1.67     -1.58    -1.57    -1.60    -1.64    -1.75
    -1.79     -1.82    -2.92     -4.07    99.00    -6.37    -7.58    99.00
   -10.04    -11.14    99.00    -13.41    99.00   -15.96   -17.36   -18.97

24 March 1990   2103 HR        No. 15
    -1.72     -1.70    -1.67     -1.59    -1.57    -1.60    -1.66    -1.75
    -1.80     -2.10    -3.26     -4.33    99.00    -6.57    -7.76    99.00
   -10.30    -11.47    99.00    -13.95    99.00   -16.87   -18.49   -20.42

25 March 1990   0815 HR        No. 16
    -1.70     -1.68    -1.66     -1.57    -1.55    -1.59    -1.72    -1.76
    -2.03     -2.93    -4.16     -5.26    99.00    -7.54    -8.73    99.00
   -11.25    -12.37    99.00    -14.72    99.00   -17.27   -18.62   -20.10

25 March 1990   2035 HR        No. 17
    -1.72     -1.70    -1.67     -1.58    -1.57    -1.60    -1.57    -1.85
    -2.66     -3.55    -4.65     -5.65    99.00    -7.70    -8.77    99.00
   -11.14    -12.26    99.00    -14.73    99.00   -17.73   -19.47   -21.39

26 March 1990   0916 HR        No. 18
    -1.71     -1.68    -1.66     -1.58    -1.57    -1.61    -1.55    -2.52
    -3.57     -4.51    -5.60     -6.62    99.00    -8.55    -9.52    99.00
   -11.52    -12.35    99.00    -14.04    99.00   -15.88   -16.83   -17.87

26 March 1990   1926 HR        No. 19
    -1.72     -1.70    -1.67     -1.59    -1.57    -1.64    -2.03    -2.86
    -3.70     -4.43    -5.32     -6.14    99.00    -7.82    -8.66    99.00
   -10.60    -11.52    99.00    -13.53    99.00   -16.03   -17.43   -19.25

26 March 1990   2031 HR        No. 20
    -1.72     -1.70    -1.67     -1.59    -1.57    -1.64    -2.07    -2.89
    -3.74     -4.47    -5.40     -6.24    99.00    -7.99    -8.94    99.00
   -10.99    -11.99    99.00    -14.16    99.00   -16.36   -18.20   -20.04
```

T19b

```
27 March 1990    1000 HR        No. 21
   -1.71     -1.69    -1.66     -1.58    -1.58    -1.79    -2.82    -3.80
   -4.83     -5.78    -6.94     -8.03    99.00   -10.19   -11.38    99.00
  -13.79    -14.85    99.00    -17.11    99.00   -19.59   -20.94   -22.63

27 March 1990    1128 HR        No. 22
   -1.71     -1.69    -1.66     -1.58    -1.59    -1.85    -2.93    -3.92
   -4.97     -5.93    -7.09     -8.18    99.00   -10.35   -11.47    99.00
  -13.83    -14.85    99.00    -17.01    99.00   -19.38   -20.60   -22.11

27 March 1990    1406 HR        No. 23
   -1.71     -1.69    -1.67     -1.59    -1.99    -2.00    -3.14    -4.14
   -5.19     -6.13    -7.28     -8.35    99.00   -10.45   -11.52    99.00
  -13.75    -14.69    99.00    -16.69    99.00   -18.81   -19.89   -21.22

27 March 1990    2042 HR        No. 24
   -1.72     -1.70    -1.68     -1.60    -1.65    -2.39    -3.55    -4.54
   -5.58     -6.49    -7.62     -8.66    99.00   -10.74   -11.85    99.00
  -14.20    -15.32    99.00    -17.66    99.00   -20.37   -21.93   -24.04

28 March 1990    0915 HR        No. 25
   -1.72     -1.70    -1.68     -1.64    -2.23    -3.33    -4.64    -5.76
   -6.94     -8.01    -9.26    -10.50    99.00   -12.84   -14.04    99.00
  -16.58    -17.70    99.00    -19.95    99.00   -22.27   -23.48   -24.96

28 March 1990    1810 HR        No. 26
   -1.72     -1.71    -1.70     -1.98    -2.89    -3.91    -5.09    -6.12
   -7.13     -8.01    -9.09     -9.99    99.00   -11.80   -12.67    99.00
  -14.49    -15.24    99.00    -16.83    99.00   -18.59   -19.56   -20.85

28 March 1990    2106 HR        No. 27
   -1.72     -1.71    -1.71     -2.10    -3.05    -4.03    -5.14    -6.13
   -7.10     -7.93    -8.95     -9.89    99.00   -11.71   -12.62    99.00
  -14.65    -15.55    99.00    -17.53    99.00   -19.89   -21.25   -22.81

29 March 1990    0835 HR   No. 28  before melt-out (A)   -6.6 hr
   -1.72     -1.72    -1.88     -2.61    -3.50    -4.43    -5.47    -6.37
   -7.26     -8.01    -8.94     -9.73    99.00   -11.23   -11.94    99.00
  -13.32    -13.83    99.00    -14.81    99.00   -15.66   -16.07   -16.69

29 March 1990    1205 HR   No. 29  before melt-out (B)   -3.1 hr
   -1.72     -1.72    -2.01     -2.76    -3.56    -4.40    -5.34    -6.18
   -6.97     -7.61    -8.42     -9.09    99.00   -10.35   -10.94    99.00
  -12.03    -12.40    99.00    -13.06    99.00   -13.58   -13.79   -14.16

29 March 1990    1446 HR   No. 30  before melt-out (C)   -0.4 hr
   -1.72     -1.73    -2.11     -2.83    -3.57    -4.34    -5.20    -5.97
   -6.67     -7.22    -7.93     -8.49    99.00    -9.58   -10.09    99.00
  -10.99    -11.23    99.00    -11.80    99.00   -12.21   -12.35   -12.67
```

Table 20. Acoustic measurements of the spacings of the hydrophones, before freezing started. The first timing measurement was on 19 March at 2320 h. The second was on 20 March at 1207 h.

Transducer Interval	Acoustic Timing 1st (µs)	Acoustic Timing 2nd (µs)	Cumulation of Average Time (µs)	Cumulation of Average Time (mm)	Measured with Rule at APL (mm)	Difference (Acoustic–Rule) (mm)
11–12	30.4[a]	15.0[a]	35	50	51	−1
10–11	33.8[a]	31.0[a]	70	101	101	0
9–10	35.4	35.4	105	151	152	−1
8–9	36.0	35.8	141	202	203	−1
7–8	34.6	34.4	176	253	253	0
6–7	35.0	35.0	211	303	304	−1
5–6	18.6	18.6	230	330	330	0
4–5	18.0	18.0	248	356	355	1
3–4	19.2	19.2	267	383	381	2
2–3	18.0	18.0	285	409	406	3
1–2	16.6	16.6	301	432	431	1

[a]It was apparent that some ice had formed on the surface, even to below hyrdrophone 11; therefore these times were estimated as 35.0 ms, based on the tape-measured spacings and times for hydrophones 8–10.

Table 21. Measured travel times (μs) between hydrophones, and calculated sound speeds (m/s) for the ice-growth period.

Run No.	Date and Time	1-2	2-3	3-4	4-5	5-6	6-7	7-8	8-9	9-10	10-11	11-12
		Hydrophone Interval										
0	3/19 1910 h	16.6	18.0	19.2	18.0	18.6	35.0	34.6	36.0	35.4	33.8[a]	30.4[a]
											1487	1653
1	3/20 1207 h	16.6	18.0	19.2	18.0	18.6	35.0	34.4	35.8	35.4	31.0[a]	15.0[a]
											1621	3351
2	1630 h	17.0	18.0	19.5	18.0	18.7	35.0	34.7	36.0	--	26.0	14.7
		1402	1436	1414	1436	1428	1436	1432	1436	--	1933	3419
3	1900 h	17.0	18.0	19.3	18.0	19.0	35.0	34.5	35.7	--	22.5	--
		1402	1440	1433	1436	1406	1436	1440	1448	--	2234	3723
4	2155 h	16.7	18.1	19.2	18.0	18.7	35.0	34.6	35.7	35.5	19.0	14.0
		1427	1432	1440	1436	1432	1436	1436	1448	1432	2645	3590
5	3/21 0635 h	16.8	17.9	19.3	18.2	18.6	35.0	34.5	35.7	31.0	13.7	13.8
		1419	1448	1433	1452	1436	1436	1440	1448	1640	3723	3723
6	1055 h	16.9	17.9	19.2	18.2	18.5	35.1	34.4	35.6	26.8	13.8	14.4
		1411	1448	1440	1420	1444	1432	1444	1452	1897	3642	3490
7	2030 h	17.0	18.3	19.3	18.0	18.6	34.9	35.0	35.8	18.1	12.9	13.5
		1402	1416	1433	1436	1436	1440	1420	1444	2809	3896	3723
8	3/22 0727 h	17.0	18.3	19.6	18.2	18.9	35.2	34.6	30.8	15.2	12.5	13.4
		1402	1416	1411	1420	1413	1428	1436	1678	3344	4021	3751
9	1300 h	16.9	18.1	19.4	18.0	18.6	35.0	34.4	27.1	14.4	12.3	13.0
		1411	1432	1425	1436	1436	1436	1444	1908	3530	4086	3866
10	1912 h	16.8	18.2	19.3	18.1	18.6	35.0	34.5	23.4	15.6	12.0	13.6
		1419	1424	1429	1428	1436	1436	1440	2209	3259	4188	3696
11	--	16.8	18.1	19.4	18.0	18.7	35.0	34.5	22.3	14.1[b]	12.0[b]	--
		1419	1432	1425	1436	1440	1436	1440	2318	3605	4188	3669
12	3/23 1240 h	16.8	18.0	19.4	18.0	18.6	35.0	34.3	16.4	14.8[b]	12.0[b]	13.8
		1419	1440	1425	1436	1436	1436	1449	3152	3435	4188	3642
13	2006 h	16.9	17.9	19.4	18.1	18.7	35.0	30.7	14.7	13.4	12.6	13.6
		1411	1448	1425	1432	1432	1436	1618	3517	3794	3989	3696
14	3/24 0615 h	16.8	18.3	19.4	18.2	18.9	35.0	23.4	14.3	12.8[b]	12.0[b]	13.6
		1419	1416	1425	1420	1413	1436	2123	3615	3971	4188	3696
15	1137 h	16.8	18.3	19.5	18.1	18.8	35.1	20.5	14.1	12.6	12.8	13.3
		1419	1416	1418	1432	1422	1432	2424	3666	4034	3927	3779
16	2110 h	16.9	18.2	19.4	18.2	18.8	34.1	15.4	14.2	13.0[b]	12.7[b]	13.3
		1411	1424	1425	1420	1422	1474	3226	3641	3910	3957	3779
17	3/25 0745 h	16.7	17.9	19.1	17.9	18.5	28.2	14.2	13.6	12.8	12.6	13.1
		1427	1448	1448	1440	1444	1782	3499	3801	3971	3989	3837

[a] Inaccurate because ice had already formed; see Table 20.

[b] Sum of 9–10 and 10–11 was determined and divided between the two for best results.

Run No.	Date and Time	Hydrophone Interval										
		1-2	2-3	3-4	4-5	5-6	6-7	7-8	8-9	9-10	10-11	11-12
18	3/25	16.8	18.1	19.4	18.0	18.5	22.4	13.7	13.8	12.3[b]	12.2[b]	13.5
	1820 h	1419	1432	1425	1436	1444	2244	3627	3746	4133	4154	3723
19	3/26	16.7	18.1	19.4	18.0	18.4	16.1	13.3	13.2	12.2[b]	12.0[b]	14.4
	0800 h	1427	1432	1425	1436	1451	3122	3736	3916	4167	4188	3490
20		16.8	18.1	19.4	17.9	17.7	15.5	13.3	13.3	12.3[b]	12.1[b]	15.3
	--	1419	1432	1425	1444	1509	3243	3736	3887	4167	4120	3285
21		16.7	18.1	19.4	17.8	13.2	15.3	13.7	13.1	13.1[b]	12.3[b]	13.5
	1042 h	1427	1432	1425	1452	2023	3285	3627	3946	4003	3957	3723
22	3/27	16.8	18.0	19.4	17.7	11.1	14.8	13.1	13.7	13.6[b]	12.0[b]	13.4
	0200 h	1419	1440	1425	1460	2406	3396	3793	3773	3971	3926	3751
23		16.5	17.9	19.4	16.0	9.5	14.4	13.5	13.2	13.6[b]	12.0[b]	13.4
	1145 h	1445	1448	1423	1615	2812	3490	3680	3916	3971	3927	3751
24		16.8	18.1	19.5	12.0	8.2	14.1	13.3	13.1	13.7[b]	11.7[b]	13.3
	2028 h	1419	1432	1414	2154	3257	3565	3736	3946	4003	3957	3923
25	3/28	16.7	18.1	19.3	9.9	7.9	14.2	13.0	13.6	13.4[b]	11.5[b]	12.9
	0230 h	1427	1428	1429	2664	3381	3539	3822	3801	4083	4037	3896
26		16.8	18.3	18.0	8.9	7.8	13.6	12.7	13.2	13.4	11.6	13.3
	0705 h	1419	1412	1532	2904	3424	3696	3912	3916	4067	4021	3723
27		17.0	18.2	11.5	8.7	7.6	13.9	13.3	13.0	12.9	12.4	13.3
	1918 h	1402	1420	2397	2971	3514	3616	3736	3977	4019	3973	3723
28[c]		16.6	17.9	10.6	8.4[b]	7.4[b]	13.6	13.1	12.8	12.7	12.1	--
	2029 h	1436	1444	2601	3077	3609	3696	3793	4039	4100	4053	--
29	3/29	16.1	14.2	8.7	7.7	7.1	13.7	12.9	12.2	13.0	11.8	12.8
	0754 h	1481	1820	3169	3357	3762	3669	3852	4237	4100	4053	3927
30[c]		16.6	14.2	8.8	9.3	7.6	14.1	13.2	12.7	13.4	11.7	--
	--	1436	1820	3133	2779	3514	3565	3764	4071	4051	4005	--
31		15.8	13.0	8.4	7.8	7.1	13.7	13.0	12.4	13.0	11.7	12.9
	1135 h	1509	1988	3282	3535	3762	3669	3822	4169	3910	4296	3896
32[c]		16.9	12.8	8.5	7.9	7.5	14.0	13.1	13.9	13.1	12.0	--
	--	1410	2019	3244	3490	3561	3590	3793	3719	3880	4188	--

[b]Sum of 9–10 and 10–11 was determined and divided between the two for best results.

[c]We did not compare two hydrophones on the same ping, and thus the accuracy is poor.

Table 22. *Summary of sound speeds in the ice (m/s), from Table 21.*

Run No.	Date March	Time (local)	Interval									
			11–12	10–11	9–10	8–9	7–8	6–7	5–6	4–5	3–4	2–3
0	19	1910	1653	1487								
1	20	1207	3351	1621								
2	20	1630	3419	1933								
3	20	1900	3723	2234								
4	20	2155	3590	2645								
5	21	0635	3723	3723	1640							
6	21	1055	3490	3624	1897							
7	21	2030	3723	3896	2809							
8	22	0727	3751	4021	3344	1678						
9	22	1300	3866	4086	3530	1908						
10	22	1912	3696	4188	3259	2209						
11	22	1917	3669	4188	3605	2318						
12	23	1240	3642	4188	3435	3152						
13	23	2006	3696	3989	3794	3517	1618					
14	24	0615	3696	4188	3971	3615	2123					
15	24	1137	3779	3927	4034	3666	2424					
16	24	2110	3779	3957	3910	3641	3226	1474				
17	25	0745	3837	3989	3971	3801	3499	1782				
18	25	1820	3723	4154	4133	3746	3627	2244				
19	26	0800	3490	4188	4167	3916	3736	3122	1451			
20	26	0900	3285	4120	4167	3887	3736	3243	1509			
21	26	2242	3723	3957	4003	3946	3627	3285	2023	1452		
22	27	0200	3751	3926	3971	3773	3793	3396	2406	1460		
23	27	1145	3751	3927	3971	3916	3680	3490	2812	1615		
24	27	2028	3923	3957	4003	3946	3736	3565	3257	2154		
25	28	0230	3896	4037	4083	3801	3822	3539	3381	2692		
26	28	0705	3723	4021	4067	3916	3912	3696	3424	2904	1532	
27	28	1918	3723	3973	4019	3977	3736	3616	3514	2971	2397	
29	29	0754	3927	4053	4100	4237	3852	3669	3762	3357	3169	1820
31	29	1135	3927	4296	3910	4169	3822	3669	3762	3535	3282	1988

Table 23. Values used to calculate sound speed in hydrophone intervals containing both ice and water. T_6 is the difference between the times of the sonar returns from the initial water surface and from the lower surface of the ice; $D_6 = 1436\,T_6$. See Figure 40 for definition of symbols.

March	Time (local)	Run No.	Mid Hyd No.	D_5 (cm)	T_6 (μs)	In Water		In Ice		Lower Int.		Both Int.	
						F_1 (μs)	F_2 (μs)	G_1 (μs)	G_2 (μs)	B_1 (cm)	C_2 (m/s)	$A+B_1$ (cm)	C (m/s)
20	1207	1	11	6.7	48	35.0	35.0	15.0	31.0	1.1	3012		
	1630	2			56			14.0	26.0	2.3	3381		
	1900	3			64			13.5	22.5	3.4	3046		
	2155	4			68			14.0	19.0	4.0	3409		
21	0635	5	10	11.8	84	35.0	35.4	13.5	31.0	1.2	3131		
	1055	6			92			13.8	26.8	2.4	3076		
	2030	7			107			12.9	18.1	4.5	3232		
22	0727	8	9	16.8	122	35.4	36.0	15.2	30.8	1.7	2658		
	1300	9			129			14.4	27.1	2.7	2794	7.8	3293
	1912	10			135			15.6	23.4	3.5	2981	8.6	3139
	1912	11			136			14.1	22.3	3.7	3130	8.8	3391
23	1240	12	8	21.9	150	36.0	34.6	16.4	34.3	0.6	1559	5.8	2872
	2006	13			157			14.7	30.7	1.6	2248	6.8	3111
24	0615	14			169			14.3	23.4	3.3	2823	8.5	3260
	1137	15			175			14.1	20.5	4.2	2814	9.4	3231
	2110	16	7	27.0	185	34.6	35.0	15.4	34.1	0.5	1979	5.5	3059
25	0745	17			197			14.2	28.2	2.2	2587	7.2	3158
	1820	18			208			13.7	22.4	3.8	2758	8.8	3193
26	0800	19	6	32.0	220	35.0	18.6	16.1	18.4	0.5	1524	5.6	2852
	0800	20			220			15.5	17.7	0.5	1941	5.6	3058
	2242	21			233			15.3	13.2	2.4	2137	7.4	2803
27	0200	22			235	18.6	18.0	11.1	17.7	2.7	2418	7.7	2980
	1145	23	5	34.7	244			9.5	16.0	1.3	1867	4.0	2422
	2028	24			250			8.2	12.0	2.2	2431	4.8	2833
28	0230	25	4	37.3	255			7.9	9.6	0.3	1349	2.9	1458
	0705	26			259	18.0	19.2	8.9	18.0	0.8	1832	3.4	2552
	1918	27			272			11.5	18.2	2.7	2455	5.3	2684
	2029	28	3	40.0	273			10.7	17.9	0.2	1657	2.9	2524
29	0754	29			284	19.2	18.0	8.7	14.2	1.7	2122	4.5	2669
	0754	30			284			8.8	14.2	1.7	2122	4.5	2653
	1135	31			287			8.4	13.0	2.2	2172	4.9	2686
	1135	32			287			8.5	12.8	2.2	2218	4.9	2701

Table 24.   Calculation of sound speed in thicker intervals of ice.

Run No.	Hydrophones Used	T_5 (μs)	T_6 (μs)	In Water F_1 (μs)	In Water F_2 (μs)	In Ice G_1 (μs)	In Ice G_2 (μs)	Upper Interval $A+B_1$ (cm)	Upper Interval C (m/s)
1									
2									
3									
4									
5	12-10-9	70	84	70.0	35.4	27.0	31.0		
6			92			28.2	26.8		
7			107			26.4	18.1		
8	11-9-8	105	122	70.4	36.0	27.7	30.8		
9			129			26.7	27.1	12.8	3527
10			135			27.6	23.4	13.7	3459
11			136			26.1	22.3	13.8	3644
12	10-8-7	141	150	71.4	34.6	31.2	34.3	10.8	3112
13			157			28.1	30.7	11.9	3372
14			169			27.1	23.4	13.6	3495
15			175			26.7	20.5	14.4	3475
16	9-7-6	176	185	70.6	35.0	29.6	34.1	10.7	3317
17			197			27.8	28.2	12.4	3399
18			208			27.5	22.4	14.0	3378
19	8-6-5	211	220	69.6	18.6	30.6	18.4	10.5	3098
20			220			28.8	17.7	10.5	3345
21			233			29.0	13.2	12.4	3084
22	7-5-4	230	235	53.6	18.0	25.9	17.7	12.7	3245
23			244			23.9	16.0	9.0	2925
24			250			22.3	31.5	9.9	3166
25	6-5-3		255	36.6	19.2	17.5	19.3	5.5	2860
26	6-4-3		259			16.7	18.0	6.1	2875
27			272			16.3	11.5	8.0	2916
28	5-3-2	248	273	37.2	18.0	19.0	17.9	5.5	2773
29			284			16.4	14.2	7.1	2886
30			284			18.1	14.2	7.1	2698
31			287			16.2	13.0	7.5	2874
32			287			16.4	12.8	7.5	2874

Note: See Figure 40 for definition of symbols; $D_5 = 1436T_5$, $D_6 = 1436T_6$.

T24

Table 25. Amplitude values used to calculate sound absorption at 92 kHz for hydrophone interval 5–6. The amplitude was averaged over the entire pulse.

	IN WATER					IN ICE				
Disk No.	Run No.	Hyd No.	Amp. (2×)	Ratio[a]		Disk No.	Run No.	Hyd No.	Amp. (2×)	Ratio	20 log (Ratio/Avg.)
1-Q1	2	5	4.64			5-Q1	18	5	4.41		
		6	4.26	1.089				6	3.64	1.212	0.61
1-Q3	3	5	4.78			5-Q3	19	5	3.98		
		6	4.07	1.174				6	2.35	1.694	3.52
1-Q2	4	5	4.89			5-Q2	20	5	3.67		
		6	4.16	1.175				6	1.93	1.902	4.52
1-Q4	5	5	4.90			5-Q4	21	5	2.44		
		6	4.46	1.099				6	1.55	1.574	2.88
2-Q1	6	5	4.70			6-Q1	22	5	1.92		
		6	4.52	1.040				6	1.48	1.298	1.20
2-Q3	7	5	4.52			6-Q2	23	5	2.90		
		6	3.79	1.193				6	2.64	1.098	−0.25
2-Q2	8	5	4.58			6-Q3	24	5	3.06		
		6	3.89	1.177				6	2.79	1.097	−0.26
2-Q4	9	5	4.42			6-Q4	25	5	1.74		
		6	3.77	1.172				6	1.61	1.081	−0.39
2-Q1	10	5	4.3			7-Q1	26	5	1.22		
		6	3.81	1.144				6	1.11	1.099	−0.24
3-Q2	11	5	4.3			7-Q2	27	5	2.34		
		6	3.96	1.106				6	1.98	1.182	0.39
3-Q3	12	5	4.1								
		6	3.67	1.142							
3-Q4	13	5	4.27			7-Q4	29	5	4.84		
		6	3.74	1.142				6	5.72	0.846	−2.5
4-Q1	14	5	4.16								
		6	3.58	1.162							
4-Q2	15	5	4.39			8-Q2	31	5	5.24		
		6	3.99	1.100				6	5.32	0.985	−1.19
4-Q3	16	5	25.0								
		6	23.5	1.064							
4-Q4	17	5	4.30								
		6	3.89	1.105							

[a]Average in-water ratio = 1.130 ± 0.045.

Table 26. *Same as Table 25 but for hydrophone interval 7–8.*

	IN WATER					IN ICE				
Disk No.	Run No.	Hyd No.	Amp. (2×)	Ratio[a]	Disk No.	Run No.	Hyd No.	Amp. (2×)	Ratio	20 log (Ratio/Avg.)
1-Q1	2	7	4.13		3-Q2	11	7	3.62		
		8	3.68	1.12			8	2.62	1.38	1.81
1-Q3	3	7	4.06		3-Q3	12	8	3.70		
		8	3.68	1.10			8	1.62	2.28	6.17
1-Q2	4	7	4.11		3-Q4	13	8	3.50		
		8	3.71	1.11			8	1.43	2.45	6.80
1-Q4	5	7	4.18		4-Q1	14	7	3.76		
		8	3.70	1.13			8	0.88	4.27	11.6
2-Q1	6	7	3.97		4-Q2	15	7	3.72		
		8	3.45	1.15			8	0.90	4.13	11.3
2-Q3	7	7	3.93		4-Q3	16	7	15.1		
		8	3.48	1.13			8	4.28	3.53	10.0
2-Q2	8	7	3.72		4-Q4	17	7	1.74		
		8	3.40	1.09			8	0.647	2.68	7.6
2-Q4	9	7	3.74		5-Q1	18	7			
		8	3.36	1.11			8	0.62		
3-Q1	10	7	3.60		5-Q3	19	7	1.316		
		8	3.22	1.12			8	0.712	1.85	4.4
					5-Q2	20	7	1.051		
							8	0.561	1.87	4.5
					5-Q4	21	7	0.800		
							8	0.534	1.50	2.5
					6-Q1	22	7	0.768		
							8	0.508	1.51	2.6
					6-Q2	23	7	3.81		
							8	2.51	1.52	2.7
					6-Q3	24	7	1.23		
							8	0.696	1.77	4.0
					6-Q4	25	7	0.884		
							8	0.468	1.89	4.5
					7-Q1	26	7	0.600		
							8	0.312	1.92	4.7
					7-Q2	27	7	3.94		
							8	2.43	1.62	3.2
					7-Q4	29	7	5.60		
							8	3.59	1.56	2.9
					8-Q2	31	7	4.57		
							8	3.60	1.27	1.09

[a] Average in-water ratio = 1.12 ± 0.02.

T26

Table 27. Same as Table 25 but for hydrophone interval 8–9.

	IN WATER					IN ICE				
Disk No.	Run No.	Hyd No.	Amp. (2×)	Ratio[a]	Disk No.	Run No.	Hyd No.	Amp. (2×)	Ratio	20 log (Ratio/Avg.)
1-Q1	2	8	4.032		2-Q2	8	8	3.73		
		9	3.760	1.072			9	1.25	2.984	8.5
1-Q3	3	8	4.176		2-Q4	9	8	3.808		
		9	3.620	1.154			9	1.216	3.132	8.91
1-Q2	4	8	4.19		3-Q1	10	8	3.621		
		9	3.73	1.123			9	1.056	3.429	9.7
1-Q4	5	8	4.13		3-Q2	11	8	1.600		
		9	3.85	1.073			9	0.668	2.395	6.6
2-Q1	6	8	4.19		3-Q3	12	8	1.804		
		9	3.83	1.094			9	0.762	2.367	6.5
2-Q3	7	8	3.58		3-Q4	13	8	1.612		
		9	3.18	1.220			9	0.676	2.385	6.5
					4-Q1	14	8	0.984		
							9	0.720	1.367	1.71
					4-Q2	15	8	0.984		
							9	0.832	1.183	0.45
					4-Q3	16	8	5.01		
							9	4.41	1.136	0.10
					4-Q4	17	8	0.716		
							9	0.568	1.261	1.01
					5-Q1	18	8			
							9	0.544		
					5-Q3	19	8	0.712		
							9	0.468	1.521	2.63
					5-Q2	20	8	0.666		
							9	0.426	1.563	2.87
					5-Q4	21	8	0.572		
							9	0.462	1.238	0.85
					6-Q1	22	8	0.542		
							9	0.388	1.90	2.29
					6-Q2	23	8	2.83		
							9	2.37	1.194	1.35
					6-Q3	24	8	2.90		
							9	2.58	1.124	0.01
					6-Q4	25	8	0.510		
							9	0.446	1.143	0.16
					7-Q1	26	8	0.391		
							9	0.365	1.071	−0.41
					7-Q2	27	8	2.98		
							9	2.27	1.31	1.36
					7-Q4	29	8	4.24		
							9	3.38	1.254	0.96
					8-Q2	31	8	3.70		
							9	2.79	1.33	1.44

[a]Average in-water ratio = 1.123 ± 0.057.

T27

Table 28. Calculated absorption loss at 92 kHz in all hydrophone intervals for acoustic transmissions on runs 26, 27, and 29.

Hydrophone Interval	1-2	2-3	3-4	4-5	5-6	6-7	7-8	8-9
Run 2 (in-water calibration)								
20 log A'/B'	0.36	0.54	0.76	1.24	1.07	2.99	1.14	1.07
Run 26								
20 log AB'/A'B			5.78	4.98	0.30	4.47	2.89	1.15
Sum			5.78	10.76	11.06	15.53	18.42	19.57
d			0.8	2.6	2.6	5.1	5.0	5.1
T_1			-2.5	-4.1	-5.6	-8.6	-11.5	-14.7
T_2			-2.4	-2.5	-4.1	-5.6	-8.6	-11.5
f q			167	139	106	83	65	55
f q d			134	361	276	423	325	281
Sum (f q d)			134	495	771	1194	1519	1800
Run 27								
20 log AB'/A'B			7.00	3.03	0.45	4.58	2.61	1.35
Sum			7.00	10.03	10.48	15.06	17.67	19.02
d			2.7	2.6	2.6	5.1	5.0	5.1
T_1			-3.1	-4.71	-6.0	-8.5	-10.8	-13.1
T_2			-2.0	-3.1	-4.71	-6.0	-8.5	-10.8
f q			164	123	99	82	67	58
f q d			443	320	257	418	335	296
Sum (f q d)			443	763	1020	1438	1773	2069
Run 29								
20 log AB'/A'B		5.0	2.89	3.60	-1.42	4.47	1.40	1.61
Sum		5.0	7.89	11.49	10.07	14.54	15.94	17.55
d		1.7	2.7	2.6	2.6	5.1	5.0	5.1
T_1		-2.5	-3.7	-5.1	-6.3	-8.4	-10.4	-12.3
T_2		-1.9	-2.5	-3.7	-5.1	-6.3	-8.4	-10.4
f q		180	144	114	95	81	68	60
f q d		306	389	296	247	413	340	306
Sum (f q d)		306	695	991	1238	1651	1991	2297
Run 31								
20 log AB'/A'B	1.83	-1.07	2.24	4.27	-0.67	2.14	0.60	0.67

Table 29. *Calculated absorption loss at 92 kHz in the skeletal layer when using the lower two or three hydrophones in the ice.*

Hydrophone No.	Run No.	Loss (dB)	s (cm)	T_1 (°C)	T_2 (°C)	fq	fqs
4–5	23	10.90	1.2	−1.9	−2.6	178	214
	24	8.93	2.1	−2.1	−3.2	160	336
5–6	19	3.52	0.5	−2.2	−2.4	174	87
	20	4.52	0.5	−2.2	−2.4	174	87
6–7	16	2.86	0.5	−2.3	−2.6	167	83
	17	6.40	2.2	−2.5	−3.5	147	323
7–8	12	6.17	0.5	−2.5	−2.2	172	86
	13	6.80	1.5	−2.2	−3.1	159	239
	14	11.60	3.3	−2.7	−4.7	129	426
	15	11.30	4.1	−4.9	−2.4	131	537
8–9	8	8.50	1.6	−3.4	−2.5	148	237
	9	8.91	2.6	−3.7	−2.3	148	385
	10	9.70	3.5	−3.8	−2.2	148	518
Skipping to next hydrophone above							
7–9	12	12.67	5.5	−5.2	−2.2	131	721
6–8	17	14.00	7.3	−6.3	−2.5	117	854
7–9	13	13.30	6.5	−6.5	−2.2	120	780
7–9	14	13.30	8.3	−7.8	−2.7	106	880
5–7	19	8.08	5.5	−5.0	−2.2	133	730
4–6	23	9.15	3.9	−1.9	−3.8	154	601
4–6	24	7.98	4.8	−2.1	−4.4	142	682

Table 30. Times of returns from sensors and ice at 220 kHz, using the platter transducer.

Disk	Date March	Time (local)	Frame No.	Time of Return Sensors (ms)	Ice (ms)	Ice – Sensors (µs)	Ice Change (µs)
Pla-4	19	2100	H2-10	13.611	14.232	621	0
	20	0625	H2-15	13.6l9	14.169	550	71
		1040	H2-20	13.625	14.153	528	93
Pla-5		1425	H1-15	13.619	14.138	517	104
		1915	H1-20	13.656	14.148	492	129
		2315	H2-5	13.658	14.135	477	144
	21	0625	H2-10	13.657	14.111	454	167
		1115	H2-15		14.100		
Pla-6		2144	All-5	13.696	14.099	403	218
	22	0737	All-10	13.691	14.068	377	244
		1316	All-15	13.683	14.046	363	258
		2125	All-20	13.688	14.041	353	268
Pla-7	23	1230	All-5	13.732	14.053	321	300
		2057	All-10	13.723	14.030	307	314
	24	0615	All-15	13.728	14.009	281	340
		1104	All-20	13.739	14.010	271	350
Pla-8		2025	All-5	13.744	13.998	254	367
	25	0740	All-10	13.729	13.954	225	396
		1815	All-15	13.747	13.954	207	414
	26	0750	All-20	11.760			
Pla-9		1054	All-5	13.746			
		1951	All-10	13.747			
	27	0210	All-15	13.749	13.891	142	479
		1311	All-20	13.753			

Note: On 26 March, interference started between sensor and ice reflections.

Table 31. Times of returns from transducer arm and ice at 92 kHz, using the platter transducer.

Disk	Date March	Time (local)	Frame No.	Time of Return Arm (ms)	Time of Return Ice (ms)	Ice – Arm (ms)	Equivalent Ice – Sensors (μs)	Ice Change (μs)
Pla-7	24	1104	18	12.299	14.008	1.709	273	348
Pla-8		2025	3	12.304	13.990	1.686	250	371
	25	0740	8	12.284	13.948	1.664	228	393
		1815	13	12.311	13.951	1.640	204	417
	25	0750	18	12.320	13.936	1.616	180	441
Pla-9		1054	3	12.304	13.915	1.611	175	446
		1951	8	12.306	13.901	1.595	159	462
	27	0210	13	12.308	13.897	1.589	153	468
		1311	18	12.315	13.887	1.572	136	485
Pla-10		2052	3		13.873			
	28	0215	8	12.318	13.864	1.546	110	511
		0720	13	12.293	13.831	1.538	102	519
		1942	18	12.296	13.809	1.513	77	544
Pla-11	29	0530	3	12.303	13.796	1.493	57	564
		1222	8	12.299	13.788	1.489	53	568

Notes: The first four entries overlap those in Table 30.
The arm-sensor difference was established at –1.436 ms.
The block was cut and submerged shortly after the last measurement.

Table 32. Reflection coefficients calculated from measurements of returns from growing ice. Correction factor 1/10 = −20 dB

Date March	Time (local)	Frequency (kHz)					
		37	37[a]	52	92	150	220
19	2100	0.03		0.03	0.03	0.00	0.01
20	0625	0.22		0.09	0.08	0.05	0.13
	1040	0.06	0.15	0.19	0.09	0.07	0.18
	1425	0.06	0.05	0.08	0.04	0.05	0.22
	1915	0.06	0.15	0.12	0.06	0.04	0.16
	2315	0.06	0.15	0.11	0.06	0.05	0.12
21	0625	0.04	0.06	0.08	0.06	0.04	0.40
	1115	0.04	0.14	0.11	0.06	0.06	0.40
Correction factor 1/10 was applied starting here							
	2144	0.06	0.12	0.11	0.06	0.06	0.40
22	0737	0.08	0.14	0.07	0.02	0.08	0.11
	1316	0.32	0.49	0.10	0.17	0.20	0.23
	2125	0.06	0.12	0.17	0.10	0.03	0.16
23	1230	0.18	0.21	0.22	0.05	0.04	0.20
	2057	0.17	0.18	0.05	0.01	0.01	0.17
24	0615	0.14		0.17	0.07	0.03	0.38
	1104	0.07		0.09	0.04	0.06	0.09
	2025	0.15	0.14	0.16	0.05	0.11	0.25
25	0740	0.13	0.16	0.13	0.06	0.06	0.41
	1815	0.12	0.17	0.08	0.08	0.06	0.18
26	0750	0.10		0.11	0.11	0.08	0.22
	1054	0.15		0.11	0.03	0.05	0.04
	1951	0.15		0.02	0.03	0.05	0.06
27	0210	0.18		0.05	0.04	0.06	0.04
	1311[b]	0.07		0.07	0.03	0.06	0.02
	2052	0.19		0.20	0.11	0.04	0.02
28	0215	0.16		0.18	0.08	0.05	0.14
	0720	0.11		0.12	0.04	0.02	0.20
	1942	0.18		0.13	0.02	0.02	0.28
29	0530	0.19		0.16	0.27	0.05	0.03
	1222	0.22		0.13	0.14	0.08	0.45
Average		0.13		0.12	0.07	0.06	0.19
Std dev of mean		0.01		0.01	0.01	0.01	0.02

[a]Combination of two pulses.
[b]Correction factor 1/10 was not used for this time.

Table 33. Travel times of returns from the ice for the 92-kHz ice-erosion sonar.

Date March	Time (local)	Frame No.	Travel Time (ms)	Difference (µs)	Notes
19	1800	1	2.046	0	water surface
	2100	2	2.053	−7	
20	0628	3	1.981	65	
	1200	4	1.943	103	
	1428	5	1.948	98	
	1920	6	1.915	131	
	2320	7	1.910	136	
21	0620	8	1.879	167	
	1007	9	1.843	203	
	2030	10	1.827	219	
22	0630	11	1.821	225	
	1254	12	1.790	256	
	1712	13	1.768	278	
23	0922	14	1.752	294	
	2028	15	1.734	312	
24	0540	16	1.725	321	
	2010	17	1.678	368	
25	0800	18	1.642	404	
	1920	19	1.629	417	
26	1036	20	1.606	440	
	1933	1	1.580	466	
27	0225	2	1.561	485	
	1130	3	1.555	491	
28	1947	4	1.496	550	
29	0830	5	1.472	574	

Table 34. Temperatures recorded during warming of the ice block after submersion.

Thermistor distance from upper ice surface, cm

46.0	44.2	42.0	39.9	37.9	36.0	34.1	32.0	29.9	27.9
25.9	24.0	20.0	17.9	13.9	12.0	7.9	3.8	2.0	0.0

Temperature, °C

29 March 1990　　0835 HR　　　　before melt-out (A)　-6.6 hr

-1.72	-1.72	-1.88	-2.61	-3.50	-4.43	-5.47	-6.37	-7.26	-8.01
-8.94	-9.73	-11.23	-11.94	-13.32	-13.83	-14.81	-15.66	-16.07	-16.69

29 March 1990　　1205 HR　　　　before melt-out (B)　-3.1 hr

-1.72	-1.72	-2.01	-2.76	-3.56	-4.40	-5.34	-6.18	-6.97	-7.61
-8.42	-9.09	-10.35	-10.94	-12.03	-12.40	-13.06	-13.58	-13.79	-14.16

29 March 1990　　1446 HR　　　　before melt-out (C)　-0.4 hr

-1.72	-1.73	-2.11	-2.83	-3.57	-4.34	-5.20	-5.97	-6.67	-7.22
-7.93	-8.49	-9.58	-10.09	-10.99	-11.23	-11.80	-12.21	-12.35	-12.67

29 March 1990　　1534 HR　　　　0.4 hr after melt-out

-1.72	-1.83	-2.00	-3.03	-3.37	-4.16	-4.99	-5.76	-6.45	-7.00
-7.70	-8.26	-9.31	-9.78	-10.50	-10.45	-9.52	-5.89	-2.83	-1.72

29 March 1990　　1540 HR　　　　0.5 hr after melt-out

-1.73	-1.73	-2.00	-2.67	-3.39	-4.18	-5.02	-5.78	-6.46	-7.00
-7.69	-8.23	-9.26	-9.68	-10.30	-10.14	-9.04	-5.56	-2.96	-1.78

29 March 1990　　1555 HR　　　　0.8 hr after melt-out

-1.73	-1.73	-2.03	-2.70	-3.42	-4.19	-5.03	-5.78	-6.45	-6.97
-7.65	-8.18	-9.15	-9.52	-9.91	-9.68	-8.46	-5.34	-3.10	-1.80

29 March 1990　　1610 HR　　　　1.0 hr after melt-out

-1.73	-1.74	-2.05	-2.71	-3.42	-4.19	-5.01	-5.76	-6.42	-6.93
-7.59	-8.09	-8.99	-9.31	-9.52	-9.20	-7.94	-5.12	-3.20	-1.85

29 March 1990　　1625 HR　　　　1.3 hr after melt-out

-1.73	-1.73	-2.07	-2.73	-3.43	-4.19	-5.00	-5.74	-6.39	-6.88
-7.52	-7.98	-8.77	-9.04	-9.15	-8.77	-7.52	-4.95	-3.23	-1.87

29 March 1990　　1640 HR　　　　1.5 hr after melt-out

-1.73	-1.74	-2.12	-2.76	-3.44	-4.17	-4.95	-5.64	-6.24	-6.66
-7.21	-7.55	-8.10	-8.27	-8.15	-7.75	-6.62	-4.53	-3.19	-2.01

29 March 1990　　1737 HR　　　　2.5 hr after melt-out

-1.74	-1.74	-2.14	-2.79	-3.46	-4.16	-4.90	-5.56	-6.12	-6.49
-6.98	-7.26	-7.76	-7.82	-7.66	-7.26	-6.21	-4.34	-3.16	-2.08

29 March 1990　　1748 HR　　　　2.7 hr after melt-out

-1.73	-1.74	-2.15	-2.79	-3.46	-4.15	-4.88	-5.52	-6.07	-6.41
-6.88	-7.15	-7.59	-7.65	-7.48	-7.08	-6.06	-4.27	-3.15	-2.10

29 March 1990　　1810 HR　　　　3.0 hr after melt-out

-1.73	-1.74	-2.19	-2.82	-3.47	-4.14	-4.84	-5.45	-5.95	-6.27
-6.70	-6.92	-7.29	-7.35	-7.16	-6.77	-5.81	-4.17	-3.12	-2.14

29 March 1990　　1835 HR　　　　3.5 hr after melt-out

-1.73	-1.74	-2.23	-2.90	-3.53	-4.17	-4.81	-5.38	-5.85	-6.12
-6.52	-6.70	-7.03	-7.07	-6.84	-6.47	-5.56	-4.03	-3.08	-2.18

29 March 1990　　1855 HR　　　　3.8 hr after melt-out

-1.73	-1.75	-2.24	-2.83	-3.47	-4.10	-4.74	-5.29	-5.74	-5.99
-6.34	-6.50	-6.80	-6.82	-6.60	-6.23	-5.38	-3.93	-3.04	-2.20

```
29 March 1990    1914 HR        4.1 hr after melt-out
  -1.74  -1.75  -2.22  -2.85  -3.47  -4.07  -4.68  -5.23  -5.67  -5.88
  -6.21  -6.35  -6.57  -6.63  -6.39  -6.04  -5.23  -3.85  -3.01  -2.21

29 March 1990    2017 HR        5.2 hr after melt-out
  -1.74  -1.75  -2.20  -2.84  -3.35  -3.93  -4.50  -5.02  -5.37  -5.50
  -5.79  -5.88  -6.07  -6.07  -5.85  -5.53  -4.81  -3.62  -2.90  -2.22

29 March 1990    2055 HR        5.8 hr after melt-out
  -1.74  -1.76  -2.23  -2.80  -3.35  -3.85  -4.41  -4.88  -5.18  -5.30
  -5.56  -5.63  -5.80  -5.80  -5.58  -5.26  -4.60  -3.49  -2.83  -2.20

29 March 1990    2133 HR        6.4 hr after melt-out
  -1.73  -1.75  -2.23  -2.79  -3.28  -3.79  -4.28  -4.67  -4.99  -5.11
  -5.36  -5.42  -5.56  -5.55  -5.34  -5.04  -4.41  -3.38  -2.76  -2.18

29 March 1990    2215 HR        7.1 hr after melt-out
  -1.75  -1.75  -2.22  -2.73  -3.23  -3.69  -4.20  -4.56  -4.83  -4.92
  -5.16  -5.19  -5.32  -5.31  -5.11  -4.81  -4.22  -3.26  -2.68  -2.15

29 March 1990                    8 hr after melt-out
  -1.74  -1.75  -2.23  -2.73  -3.19  -3.64  -4.14  -4.47  -4.73  -4.81
  -5.03  -5.06  -5.19  -5.17  -4.97  -4.69  -4.12  -3.18  -2.63  -2.13

30 March 1990    0415 HR       13.1 hr after melt-out
  -1.74  -1.81  -2.17  -2.39  -2.71  -3.03  -3.31  -3.63  -3.81  -3.81
  -3.96  -3.96  -4.03  -4.01  -3.85  -3.62  -3.19  -2.55  -2.17  -1.96

30 March 1990                   16 hr after melt-out
  -1.74  -1.80  -2.06  -2.31  -2.61  -2.90  -3.16  -3.47  -3.64  -3.62
  -3.78  -3.76  -3.84  -3.81  -3.66  -3.44  -3.04  -2.45  -2.13  -1.95

30 March 1990    1200 HR       20.9 hr after melt-out
  -1.73  -1.79  -1.98  -2.15  -2.33  -2.54  -2.75  -3.02  -3.15  -3.11
  -3.23  -3.20  -3.26  -3.24  -3.12  -2.92  -2.61  -2.20  -2.00  -1.92

30 March 1990    1745 HR       26.6 hr after melt-out
  -1.74  -1.80  -1.96  -2.02  -2.15  -2.34  -2.50  -2.74  -2.84  -2.79
  -2.88  -2.84  -2.90  -2.90  -2.79  -2.61  -2.37  -2.05  -1.90  -1.89

30 March 1990    2139 HR       30.5 hr after melt-out
  -1.73  -1.79  -1.92  -1.95  -2.08  -2.24  -2.39  -2.61  -2.70  -2.62
  -2.71  -2.67  -2.73  -2.73  -2.64  -2.46  -2.25  -1.98  -1.86  -1.86

31 March 1990    0830 HR       41.4 hr after melt-out
  -1.73  -1.76  -1.82  -1.83  -1.91  -2.03  -2.15  -2.34  -2.40  -2.31
  -2.39  -2.34  -2.40  -2.40  -2.34  -2.19  -2.04  -1.86  -1.78  -1.83

31 March 1990    1820 HR       51.2 hr after melt-out
  -1.73  -1.76  -1.79  -1.79  -1.86  -1.93  -2.06  -2.18  -2.23  -2.11
  -2.20  -2.15  -2.21  -2.22  -2.17  -2.03  -1.92  -1.78  -1.73  -1.80

01 April 1990    1415 HR       71.1 hr after melt-out
  -1.73  -1.75  -1.76  -1.72  -1.74  -1.80  -1.90  -2.00  -2.03  -1.90
  -1.97  -1.93  -1.99  -2.01  -1.98  -1.86  -1.79  -1.69  -1.67  -1.77

01 April 1990    1830 HR       75.4 hr after melt-out
  -1.73  -1.74  -1.75  -1.71  -1.72  -1.78  -1.87  -1.97  -2.00  -1.87
  -1.94  -1.89  -1.96  -1.97  -1.96  -1.83  -1.76  -1.68  -1.66  -1.76

01 April 1990    2100 HR       77.9 hr after melt-out
  -1.72  -1.74  -1.75  -1.70  -1.72  -1.76  -1.86  -1.95  -1.97  -1.85
  -1.92  -1.87  -1.93  -1.96  -1.93  -1.82  -1.75  -1.67  -1.65  -1.75

02 April 1990    0615 HR       87.1 hr after melt-out
  -1.73  -1.73  -1.74  -1.69  -1.69  -1.74  -1.82  -1.91  -1.93  -1.80
  -1.87  -1.82  -1.89  -1.91  -1.89  -1.79  -1.73  -1.65  -1.64  -1.75
```

Table 35. Sound speeds (m/s) computed from travel times measured in the hydrophone intervals after the ice block was submerged.

Date March	Time (local)	Run No.	Type[a]	Hydrophone Interval										
				1–2	2–3	3–4	4–5	5–6	6–7	7–8	8–9	9–10	10–11	11–12
29	1650	33	AB	1378	2287	3628	3858	4379	3896	4039	4272	3738	3927	3565
	1800[b]	34	B	1378	2191	3322	3446	4047	3751	3882	4136	3822	3989	
	1835	35	AB	1419	2534	3829	3590	4527	3927	3882	4007	3555	3696	3539
	1900[b]	36	B	1406	2492	3777	3703	4251	3818	3822	3977	3540	3477	
	2005	37	AB	1436	2611	3940	3800	4452	3927	3882	4103	3482	3779	3490
	2100	38	B	1402	2585	3726	3693	4240	3837	3793	3946	3301	3808	
	2130	39	AB	1445	2665	3883	3746	4527	3896	3852	4007	3389	3927	3515
	2200[b]	40	B	1427	2534	3939	3640	4308	3808	3736	3746	3458	3696	
	2230	41	AB	1454	2693	3830	3640	4452	3837	3822	3916	3605	4120	3442
30	0400[b]	42	A	1436	2611	3883	4535	4379	3779	3736	3916	3435	3490	
	0415	43	AB	1509	3041	4308	3746	4527	3808	3793	3916			3307
	1140	44	B		3114	3777	3800	4308	3837	3575	3565			
	1539	45	AB	1779	3272	3581	4169	4308	3808	3653	3719	3119	3490	3285
	1721	46	AB	1703	3357	3581	4169	4452	3957	3575	3541		3242	3222
	1721	47	B	1679	3114	3581	4381	3816	3866	3708	3517	3009		
	2158	48	AB	1740	3231	3628	3977	4173	3896	3627	3693	3531	3659	3181
	2158	49	B	1242	2872	4055	3590	4452	3837	3708	3517	3027		
31	0808	50	B	1892	2971	4520	3400	4173	3866	3627	5068	2972	3751	
	0808	51	AB	1907	3231	3883	3916	4452	3957	3680	3666	2905	3751	3065
	1801	52	AB	1892	3272	3777	3858	4452	3896	3575	3641	3138	3515	3141
	1801	53	B	2110	3114	3676	3746	4173	3837	3475	3565	3044	3515	
1	1400	53'	AB	1986	3231	3777	3916	4308	3896	3524	3565	2938	3696	3028
	2055	54	AB	2314	3314	3940	3916	4173	3927	3575	3590	4034[c]	2659[c]	3083
	2055	55	B	2292	3152	3676	3746	3928	3808	3542	3400			
2	0605	56	AB	2337	3272	3777	3858	4173	3957	3500	3446	3941[c]	2777[c]	3102
	1130	57	AB	2073	3314	3777	3977	4109	3957	3450	3517			3046
	1130	58	B	1986	3231	3676	3693	3987	3808	3427	3446	2990	3565	

[a]Type AB compares measurements at two adjacent hydrophones for the same ping.
 Type B compares times for different pings and thus is less accurate.

[b]Approximate

[c]Questionable division between the two speeds

T35

Table 36. *Average sound speeds and temperatures for selected time intervals after submersion of the ice block. Each hydrophone interval has three listings: sound speed (m/s), standard deviation (m/s), and temperature (°C).*

Run. Nos.	Time after Melt-Out (h:min)	Hydrophone Interval										
		1-2	2-3	3-4	4-5	5-6	6-7	7-8	8-9	9-10	10-11	11-12
33-36	1:40-3:50	1395	2376	3639	3649	4301	3848	3906	4098	3664	3772	3552
		21	164	228	174	203	79	93	135	139	234	18
		-2.0	-2.8	-3.7	-4.7	-5.6	-6.8	-8.1	-9.0	-8.8	-7.2	-3.7
37-41	4:55-7:20	1433	2618	3863	3704	4396	3861	3817	3984	3447	3866	3479
		20	63	89	69	118	49	56	75	113	164	52
		-2.2	-2.8	-3.5	-4.2	-4.7	-5.3	-5.7	-5.8	-5.4	-4.5	-3.0
42-43	13:00-13:15	1473	2826	4096	4141	4297	3794	3765	3916	3435	3490	3307
		52	304	301	558	374	21	40	0			
		-2.2	-2.4	-2.8	-3.2	-3.5	-3.8	-4.0	-4.0	-3.8	-3.1	-2.5
44-53	21:00-51:00	1838	3155	3806	3901	4276	3876	3620	3602	3093	3562	3179
		142	149	294	291	203	51	73	78	192	180	83
		-1.9	-2.0	-2.1	-2.3	-2.5	-2.6	-2.7	-2.7	-2.5	-2.2	-1.9
53'-58	71:00-87:00	2165	3252	3771	3851	4113	3892	3500	3494	2964	3631	3065
		168	62	97	110	138	69	54	75	37	93	34
		-1.7	-1.7	-1.7	-1.8	-1.9	-1.9	-1.9	-1.9	-1.9	-1.8	-1.7

Table 37. *Amplitude reflection coefficients measured for the submerged ice block during several days of warming.*

Date	Time (local)	Frequency (kHz)				
		37	52	92	150	220
March						
29	2139	0.24	0.27	0.11	0.09	0.43
	2243	0.22	0.14	0.13	0.08	0.16
30	0400	0.19	0.16	0.11	0.14	0.11
	1110	0.46	0.24	0.23	0.26	0.50
	1731	0.11	0.09	0.08	0.10	0.15
	2154	0.11	0.07	0.06	0.09	0.09
31	0820	0.08	0.08	0.03	0.10	0.12
	1815	0.08	0.02			
April						
1	1230	0.03	0.08	0.02	0.10	0.22
	2100	0.06	0.07	0.02	0.12	0.05
2	0600	0.06	0.05	0.02	0.12	0.20
	1145	0.03	0.07	0.02	0.04	0.11

Table 38. *First-cycle amplitude readings for each pair of hydrophones and their ratios, measured in water. A is the amplitude of the pulse at the first hydrophone, and B is the amplitude of the pulse at the second hydrophone.*

Run No.	Pulse	Hydrophones							
		1&2	2&3	3&4	4&5	5&6	6&7	7&8	8&9
6	A						2.97	2.56	2.80
	B						2.29	2.33	2.49
	A/B						1.30	1.10	1.12
7	A						2.87	2.53	2.49
	B						2.18	2.25	2.14
	A/B						1.32	1.12	1.16
12	A						2.49	2.27	
	B						2.00	1.20	
	A/B						1.25	1.89[a]	
14	A	1.24	1.43	1.51	1.42	1.49	1.32	2.20	
	B	1.19	1.42	1.28	1.37	1.23	1.05	0.67	
	A/B	1.04	1.01	1.18	1.04	1.21	1.26	3.28[a]	
15	A	2.52	1.54	1.55	1.45	2.88	2.62	2.30	
	B	2.40	1.47	1.29	1.36	2.42	1.97	0.65	
	A/B	1.05	1.05	1.20	1.07	1.19	1.33	3.54[a]	
16	A	10.7	11.3	12.3	11.7	21.6	20.6		
	B	10.2	11.1	10.5	11.0	18.4	11.4		
	A/B	1.05	1.02	1.17	1.06	1.17	1.81[a]		
Average	A/B	1.05	1.02	1.18	1.06	1.19	1.30	1.11	1.14

[a]Excluded because ice was present.

Table 39. *First-cycle amplitude readings for each pair of hydrophones in the submerged ice block, their ratios, and the correction obtained by dividing by the in-water ratio. A/B in water from Table 38 is A'/B' here.*

Diskette No.	Run No.	Pulse	Hydrophones							
			1&2	2&3	3&4	4&5	5&6	6&7	7&8	8&9
8-Q4	33	A	2.18	2.63	2.44	2.02	1.36	3.68	2.03	1.88
		B	2.33	2.16	1.84	1.14	1.54	1.75	1.65	1.03
		A/B	0.94	1.22	1.33	1.77	0.88	2.10	1.23	1.83
		AB'/A'B	0.89	1.19	1.12	1.67	0.74	1.62	1.11	1.60
9-Q2	35	A	5.62	5.34	4.74	4.40	3.51	5.50	3.60	3.06
		B	4.45	4.34	4.02	3.26	4.32	3.24	2.80	1.50
		A/B	1.26	1.23	1.18	1.35	0.81	1.70	1.29	2.04
		AB'/A'B	1.20	1.21	1.00	1.27	0.68	1.31	1.16	1.79
9-Q1	37	A	6.48	1.92	4.78	3.78	3.02	3.95	2.61	2.42
		B	4.50	1.48	4.10	2.75	3.71	2.30	1.89	1.19
		A/B	1.44	1.30	1.17	1.37	0.81	1.72	1.38	2.03
		AB'/A'B	1.37	1.27	0.99	1.30	0.68	1.32	1.24	1.78
10-Q2	39	A	7.78	6.28	5.10	4.74	4.08	5.21	2.68	2.30
		B	6.04	3.98	4.45	3.39	4.92	3.14	1.97	1.17
		A/B	1.29	1.58	1.15	1.40	0.83	1.66	1.36	1.97
		AB'/A'B	1.23	1.55	0.97	1.32	0.70	1.28	1.23	1.72
10-Q4	41	A	9.76	5.44	3.96	4.84	3.68	3.17	3.15	1.36
		B	6.75	2.93	3.53	3.39	4.24	1.84	2.22	0.61
		A/B	1.45	1.86	1.12	1.43	0.87	1.72	1.42	2.23
		AB'/A'B	1.38	1.84	0.95	1.35	0.73	1.33	1.28	1.96
11-Q3	43	A	10.96	5.39	2.36	2.52	1.70	1.92	1.95	1.66
		B	4.98	2.02	2.10	1.68	1.87	1.48	1.28	0.93
		A/B	2.20	2.69	1.12	1.50	0.91	1.30	1.52	1.78
		AB'/A'B	2.10	2.62	0.95	1.42	0.76	1.00	1.37	1.57
11-Q4	45	A	29.4	5.13	2.52	1.39	1.79	2.48	1.25	1.09
		B	4.59	2.85	1.10	1.56	1.86	1.69	0.66	0.64
		A/B	6.40	1.80	2.29	0.89	0.98	1.47	1.89	1.86
		AB'/A'B	6.10	1.76	1.94	0.84	0.81	1.13	1.71	1.63

T39a

Diskette No.	Run No.	Pulse	Hydrophones							
			1&2	2&3	3&4	4&5	5&6	6&7	7&8	8&9
12-Q1	46	A	18.49	3.35	2.34	0.53	0.52	2.11	2.26	1.41
		B	3.34	2.29	1.43	0.77	0.55	1.60	1.29	0.86
		A/B	5.53	1.46	1.64	0.69	0.95	1.32	1.75	1.64
		AB´/A´B	5.27	1.43	1.39	0.65	0.79	1.01	1.58	1.44
12-Q3	48	A	14.76	1.07	1.08	0.54	7.86	8.70	7.94	4.53
		B	1.62	1.00	0.52	0.62	7.78	7.12	4.02	2.28
		A/B	9.11	1.07	2.08	0.87	1.01	1.22	1.98	1.99
		AB´/A´B	8.68	1.05	1.76	0.82	0.85	0.94	1.78	1.74
12-Q?	51	A	15.92	1.83	1.94	1.78	1.38	1.20	1.20	0.57
		B	1.71	1.71	1.64	1.27	1.09	1.11	0.55	0.26
		A/B	9.30	1.07	1.18	1.40	1.27	1.08	2.18	2.19
		AB´/A´B	8.90	1.05	1.00	1.32	1.06	0.83	1.97	1.92
12-Q?	52	A	8.20	3.24	3.74	3.09	2.99	2.66	2.82	1.43
		B	1.17		2.82	2.69	2.40	2.57	1.23	0.69
		A/B	7.01		1.33	1.15	1.25	1.04	2.29	2.07
		AB´/A´B	6.67		1.12	1.08	1.05	0.80	2.07	1.82
14-Q2	54	A		2.10	4.83	1.79	4.02	3.82	1.54	2.40
		B		1.83	2.04	1.90	3.26	3.66	0.51	1.10
		A/B		1.15	2.37	0.94	1.23	1.04	3.02	2.18
		AB´/A´B		1.13	2.01	0.89	1.03	0.80	2.72	1.91
14-Q1	56	A		3.14	3.64	1.85	2.63	2.42	2.46	0.96
		B		3.30	1.69	2.40	2.22	2.23	0.94	0.48
		A/B		0.95	2.15	0.77	1.18	1.09	2.62	2.00
		AB´/A´B		0.93	1.82	0.73	0.99	0.84	2.36	1.75
15-Q1	57	A	7.44	0.96	1.43	0.88	1.13	1.06	1.06	2.13
		B	0.94	1.23	0.74	1.00	0.94	1.00	0.37	1.09
		A/B	7.91	0.78	1.93	0.88	1.20	1.06	2.86	1.95
		AB´/A´B	7.53	0.76	1.64	0.83	1.01	0.82	2.58	1.71

Table 40. Corrected first-cycle amplitude ratios AB´/A´B shown in Table 39.

Date	Time (local)	Run No.	Hydrophones							
			1&2	2&3	3&4	4&5	5&6	6&7	7&8	8&9
March										
29	1650	33	0.89	1.19	1.12	1.67	0.74	1.62	1.11	1.60
	1835	35	1.20	1.21	1.00	1.27	0.68	1.31	1.16	1.79
	2005	37	1.37	1.27	0.99	1.30	0.68	1.32	1.24	1.78
	2130	39	1.23	1.55	0.97	1.32	0.70	1.28	1.23	1.72
	2230	41	1.38	1.84	0.95	1.35	0.73	1.33	1.28	1.96
30	0415	43	2.10	2.62	0.95	1.42	0.76	1.00	1.37	1.57
	1539	45	6.10	1.76	1.94	0.84	0.81	1.13	1.71	1.63
	1721	46	5.27	1.43	1.39	0.65	0.79	1.01	1.58	1.44
	2158	48	8.68	1.05	1.76	0.82	0.85	0.94	1.78	1.74
31	0808	51	8.90	1.05	1.00	1.32	1.06	0.83	1.97	1.92
	1805	52	6.67		1.12	1.08	1.05	0.80	2.02	1.82
April										
1	2055	54		1.13	2.01	0.89	1.03	0.80	2.95	1.91
2	0605	56		0.93	1.82	0.73	0.99	0.84	2.36	1.75
	1130	57	7.53	0.76	1.64	0.83	1.01	0.82	2.58	1.71

Table 41. *Values used in calculating the absorption for each run, including the tem-*
perature effect. The loss is computed from a hydrophone at depth d to the
next hydrophone at s meters above; fqs is computed for each interval, and
the sums of the losses and fqs are tabulated.

	Hydrophone								
	1	2	3	4	5	6	7	8	9
	Run 33 on 29 March at 1650 h								
d	45	42.5	40	37.5	35	32.5	27.5	22.5	17.5
20 log Aᵣ	−1.01	1.51	0.98	4.45	−2.62	4.19	0.91	4.08	
Sum		0.50	1.48	5.93	3.31	7.50	8.41	12.4?	
T	−2.0	−2.8	−3.6	−4.6	−5.5	−6.2	−7.4	−8.	−8.2
fc	170	140	119	103	94	85	78	75	
s	0.025	0.025	0.025	0.025	0.025	0.05	0.05	0.05	
fqs	4.25	3.5	3.0	2.6	2.4	4.2	3.9	3.8	
Sum fqs		7.75	10.75	13.35	15.75	19.95	23.85	27.65	
	Run 35 on 29 March at 1835 h								
Aᵣ	1.20	1.21	1.00	1.27	0.68	1.31	1.16	1.79	
20 log Aᵣ	1.58	1.66	0	2.08	−3.35	2.35	1.29	5.06	
Sum		3.24	3.24	5.32	1.97	4.32	5.61	10.67	
T	−2.2	−2.9	−3.6	−4.5	−5.2	−5.8	−6.6	−7.0	−6.8
fq	163	139	120	106	98	90	85	84	
fqs	4.08	3.48	3.00	2.65	2.45	4.50	4.25	4.20	
Sum fqs		7.56	10.56	13.21	15.66	20.16	24.41	28.61	
	Run 37 on 29 March at 2005 h								
Aᵣ	1.37	1.27	0.99	1.30	0.68	1.32	1.24	1.78	
20 log Aᵣ	2.73	2.08	−0.09	2.28	−3.35	2.41	1.87	5.01	
Sum		4.81	4.72	7.00	3.65	6.06	7.93	12.94	
T	−2.1	−2.8	−3.5	−4.2	−4.9	−5.4	−5.85	−6.1	−5.95
fq	167	141	123	110	101	96	92	91	
fqs	4.18	3.53	3.08	2.75	2.53	4.80	4.60	4.55	
Sum fqs		7.71	10.79	13.54	16.07	20.87	25.47	30.02	
	Run 39 on 29 March at 2130 h								
Aᵣ	1.23	1.55	0.97	1.32	0.70	1.28	1.23	1.72	
20 log Aᵣ	1.80	3.81	−0.26	2.41	−3.10	2.14	1.80	4.71	
Sum		5.61	5.35	7.76	4.66	6.80	8.60	13.31	
T	−2.1	−2.8	−3.9	−4.1	−4.6	−4.9	−5.4	−5.6	−5.4
fq	168	136	121	114	107	102	97	97	
fqs	4.20	3.40	3.03	2.85	2.68	5.10	4.85	4.85	
Sum fqs		7.60	10.63	13.48	16.16	21.26	26.11	30.96	

Table 41, cont.

	Hydrophone								
	1	2	3	4	5	6	7	8	9
	Run 41 on 29 March at 2230 h								
A_r	1.38	1.84	0.95	1.35	0.73	1.33	1.28	1.96	
20 log A_r	2.80	5.30	−0.45	2.61	−2.73	2.48	2.14	5.85	
Sum		8.10	7.65	10.26	7.53	10.01	12.15	18.00	
T	−2.1	−2.7	−3.3	−3.9	−4.5	−4.8	−5.2	−5.3	−5.2
fq	170	146	129	117	109	104	101	101	
fqs	4.25	3.65	3.23	2.93	2.73	5.20	5.05	5.05	
Sum fqs		7.90	11.13	14.06	16.79	22.00	27.04	32.09	
	Run 43 on 30 March at 0415 h								
A_r	2.10	2.62	0.95	1.42	0.76	1.00	1.37	1.57	
20 log A_r	6.44	8.37	−0.45	3.05	−2.38	0	2.73	3.92	
Sum		14.81	14.36	17.41	15.03	15.03	17.76	21.68	
T	−2.1	−2.4	−2.8	−3.2	−3.5	−3.8	−3.96	−4.0	−3.9
fq	177	161	146	136	128	123	121	122	
fqs	4.43	4.03	3.65	3.40	3.20	6.16	6.05	6.10	
Sum fqs		8.46	12.11	15.51	18.71	24.87	30.92	37.02	
	Run 45 on 30 March at 1539 h								
A_r	6.10	1.76	1.94	0.84	0.81	1.13	1.71	1.63	
20 log A_r	15.7	4.91	5.76	−1.51	−1.83	1.06	4.66	4.24	
Sum		20.61	26.4	24.9	23.0	24.1	28.8	33.0	
T	−1.94	−2.1	−2.3	−2.5	−2.8	−3.0	−3.05	−3.1	−3.0
fq	190	180	169	159	149	145	144	144	
fqs	4.75	4.50	4.23	3.98	3.73	7.25	7.20	7.20	
Sum fqs		9.25	13.5	17.5	21.2	28.4	35.6	42.8	
	Run 46 on 30 March at 1721 h								
A_r	5.27	1.43	1.39	0.65	0.79	1.01	1.58	1.44	
20 log A_r	14.4	3.11	2.86	−3.74	−2.05	0.09	3.97	3.17	
Sum		17.5	20.4	16.6	14.6	14.7	18.6	21.8	
T	−1.92	−2.0	−2.2	−2.4	−2.7	−2.8	−2.86	−2.9	−2.82
fq	194	185	174	163	155	152	150	151	
fqs	4.85	4.63	4.35	4.08	3.88	7.60	7.50	7.55	
Sum fqs		9.48	13.83	17.91	21.8	29.4	36.9	44.4	

Table 41, cont.

	Hydrophone								
	1	2	3	4	5	6	7	8	9
	Run 48 on 30 March at 2158 h								
A_r	8.68	1.05	1.76	0.82	0.85	0.94	1.78	1.74	
20 log A_r	18.8	0.42	4.91	−1.72	−1.41	−0.54	5.01	4.81	
Sum		19.2	24.1	22.4	21.3	20.7	25.7	30.6	
T	−1.9	−1.94	−2.1	−2.3	−2.55	−2.7	−2.69	−2.73	−2.66
fq	197	190	180	168	160	157	156	157	
fqs	4.93	4.75	4.50	4.20	4.00	7.86	7.8	7.86	
Sum fqs		9.68	14.2	18.4	22.4	30.3	38.1	45.9	
	Run 51 on 31 March at 0808 h								
A_r	8.90	1.05	1.00	1.32	1.06	0.83	1.97	1.92	
20 log A_r	19.0	0.42	0	2.41	0.51	−1.62	5.89	5.67	
Sum		19.4	19.4	21.8	22.3	20.7	26.6	32.3	
T	−1.8	−1.83	−1.95	−2.1	−2.3	−2.4	−2.37	−2.4	−2.36
fq	204	199	190	180	172	170	170	170	
fqs	5.1	4.98	4.75	4.5	4.3	8.5	8.5	8.5	
Sum fqs		10.1	14.8	19.3	23.6	32.1	40.6	49.1	
	Run 52 on 31 March at 1805 h								
A_r			1.12	1.08	1.05	0.80	2.07	1.82	
20 log A_r			0.98	0.67	0.42	−1.94	6.32	5.2	
Sum			1.65	2.07	0.13	6.45	11.65		
T			−1.88	−2.0	−2.15	−2.23	−2.18	−2.21	−2.19
fq			195	187	180	179	180	180	
fqs			4.88	4.68	4.5	8.95	9.0	9.0	
Sum fqs			4.88	9.56	14.1	23.0	32.0	41.0	
	Run 54 on 1 April at 2055 h								
A_r		1.13	2.01	0.89	1.03	0.80	2.95	1.91	
20 log A_r		1.06	6.06	−1.0	0.26	−1.94	9.4	5.62	
Sum			7.12	6.12	6.38	4.44	13.8	19.5	
T		−1.7	−1.73	−1.81	−1.93	−1.97	−1.90	−1.93	−1.94
fq		212	208	200	195	196	197	196	
fqs		5.3	5.2	5.0	4.80	4.90	4.93	4.90	
Sum fqs			10.5	15.5	20.38	25.28	30.21	35.11	

T41c

Table 41, cont.

	Hydrophone								
	1	2	3	4	5	6	7	8	9
				Run 56 on 2 April at 0605 h					
A_r		0.93	1.82	0.73	0.99	0.84	2.36	1.75	
20 log A_r		−0.63	5.2	−2.73	−0.09	−1.51	7.46	4.86	
Sum			4.57	1.84	1.75	0.24	7.70	12.56	
T		−1.69	−1.70	−1.78	−1.89	−1.93	−1.85	−1.89	−1.90
fq		214	210	203	197	199	200	198	
fqs		5.35	5.25	5.08	4.93	9.95	10.00	9.90	
Sum fqs			10.6	15.7	20.6	30.6	40.6	50.5	
				Run 57 on 2 April at 1130 h					
A_r	7.53	0.76	1.64	0.83	1.01	0.82	2.58	1.71	
20 log A_r	17.5	−2.38	4.30	−1.62	0.09	−1.72	8.23	4.66	
Sum		15.1	19.4	17.8	17.9	16.2	24.4	29.06	
T		−1.69	−1.70	−1.78	−1.89	−1.93	−1.85	−1.89	−1.90
fq		214	210	203	197	199	200	198	
fqs	5.35	5.35	5.25	5.08	4.93	9.95	10.00	9.90	
Sum fqs		10.7	15.95	21.03	26.0	35.9	45.9	55.4	

T41d

Table 42. Summary of Table 41 data used to plot Figure 64.

Run No.	Hyd. Nos.	Sum fqs	Loss (dB)	Run No.	Hyd. Nos.	Sum fqs	Loss (dB)	Run No.	Hyd. Nos.	Sum fqs	Loss (dB)
33	1&2	4.25	-1.01	43	1&2	4.43	6.44	52	1&2	4.88	0.98
	2&3	7.75	0.50		2&3	8.46	14.81		2&3	9.56	1.65
	3&4	10.75	1.48		3&4	12.11	14.36		3&4	14.1	2.07
	4&5	13.35	5.93		4&5	15.51	17.41		4&5	23.0	0.13
	5&6	15.75	3.31		5&6	18.71	15.03		5&6	32.0	6.45
	6&7	19.95	7.50		6&7	24.87	15.03		6&7	41.0	11.65
	7&8	23.85	8.41		7&8	30.92	17.76				
	8&9	27.65	12.49		8&9	37.02	21.68				
35	1&2	4.08	1.58	45	1&2	4.75	15.7	54	1&2	15.3	1.06
	2&3	7.56	3.24		2&3	9.25	20.6		2&3	10.5	7.12
	3&4	10.56	3.24		3&4	13.5	26.4		3&4	15.5	6.12
	4&5	13.21	5.32		4&5	17.5	24.9		4&5	20.38	6.38
	5&6	15.66	1.97		5&6	21.2	23.0		5&6	25.28	4.44
	6&7	20.16	4.32		6&7	28.4	24.1		6&7	30.21	13.8
	7&8	24.41	5.61		7&8	35.6	28.8		7&8	35.11	19.5
	8&9	28.61	10.67		8&9	42.8	33.0				
37	1&2	4.18	2.73	46	1&2	4.85	14.4	56	1&2	5.35	-0.63
	2&3	7.71	4.81		2&3	9.48	17.5		2&3	10.6	4.57
	3&4	10.79	4.72		3&4	13.83	20.4		3&4	15.7	1.84
	4&5	13.54	7.00		4&5	17.91	16.6		4&5	20.6	1.75
	5&6	16.07	3.65		5&6	21.8	14.6		5&6	30.6	0.24
	6&7	20.87	6.06		6&7	29.4	14.7		6&7	40.6	7.70
	7&8	25.47	7.93		7&8	36.9	18.6		7&8	50.5	12.56
	8&9	30.02	12.94		8&9	44.4	21.8				
39	1&2	4.20	1.80	48	1&2	4.93	18.8	57	1&2	5.35	17.5
	2&3	7.60	5.61		2&3	9.68	19.2		2&3	10.70	15.1
	3&4	10.63	5.35		3&4	14.2	24.1		3&4	15.95	19.4
	4&5	13.48	7.76		4&5	18.4	22.4		4&5	21.03	17.8
	5&6	16.16	4.66		5&6	22.4	21.3		5&6	26.0	17.9
	6&7	21.26	6.80		6&7	30.3	20.7		6&7	35.9	16.2
	7&8	26.11	8.60		7&8	38.1	25.7		7&8	45.9	24.4
	8&9	30.96	13.31		8&9	45.9	30.6		8&9	55.4	29.1
41	1&2	4.25	2.80	51	1&2	5.1	19.0				
	2&3	7.90	8.10		2&3	10.1	19.4				
	3&4	11.13	7.65		3&4	14.8	19.4				
	4&5	14.06	10.26		4&5	19.3	21.8				
	5&6	16.79	7.53		5&6	23.6	22.3				
	6&7	22.00	10.01		6&7	32.1	20.7				
	7&8	27.04	12.15		7&8	40.6	26.6				
	8&9	32.09	18.00		8&9	49.1	32.3				

Table 43. *Values of absorption coefficient* k *determined from the best-fit lines in Figure 64.*

Date	Time	Run	Intercept	Slope k	Standard deviation
March 29	1650	33	−3.6	0.55	0.01
	1835	35	0.2	0.28	0.02
	2005	37	1.32	0.31	0.02
	2130	39	1.56	0.32	0.02
	2230	41	2.59	0.41	0.02
March 30	0415	43	9.38	0.31	0.03
	1539	45	17.1	0.34	0.03
	1721	46	15.2	0.10	0.03
	2158	48	17.6	0.23	0.02
March 31	0808	51	16.1	0.27	0.02
	1805	52	−1.8	0.27	0.03
April 1	2055	54	−1.5	0.48	0.06
April 2	0605	56	−1.6	0.23	0.03
	1130	57	13.8	0.22	0.03

Average k (unweighted) = 0.32
Average k (weighted by 1/std dev) = 0.31 ± 0.11

Table 44. *Measurements of ice core temperatures and salinities, and the calcu-*
lated sound speeds and porosities. See Figure 54 for a plot of these
values.

Depth (m)	Sound speed (m/s)	Salinity (ppt)	Temperature (°C)	Porosity (%)
A core taken from the 30 m triad				
9.35	3605	0.85	−12.4	0.4
16.71	3415	3.20	−12.6	1.4
24.27	3549	4.49	−12.4	2.0
31.14	3550	4.19	−11.7	2.0
37.99	3577	2.93	−12.2	1.3
45.57	3491	4.62	−11.5	2.2
53.13	3559	4.69	−12.0	2.2
60.71	3602	4.76	−11.3	2.3
68.29	3478	4.65	−11.0	2.3
75.85	3594	4.14	−10.8	2.1
83.39	3581	4.42	−10.5	2.3
90.97	3531	4.23	−10.5	2.2
97.03	3426	4.09	−9.8	2.3
103.09	3598	3.77	−9.6	2.1
110.73	3556	3.77	−9.3	2.2
118.33	3561	3.81	−8.8	2.3
125.66	3570	3.73	−9.1	2.2
133.42	3507	3.24	−8.9	2.0
141.01	3575	3.18	−8.6	2.0
156.13	3484	3.52	−7.5	2.5
163.66	3586	3.63	−7.7	2.5
171.18	3540	3.40	−6.7	2.7
178.48	3437	3.48	−4.7	3.6
A core taken at the end of the ice growth experiment				
3.87	3605	8.15	−15.5	3.3
11.56	3632	7.48	−13.6	3.3
19.23	3541	6.44	−11.0	3.3
26.84	3605	7.38	−8.0	4.9
33.73	3470	6.36	−4.7	7.2

REPORT DOCUMENTATION PAGE

Public reporting burden for this collection of information is estimated to average 1 hour per response, including the time for reviewing instructions, searching existing data sources, gathering and maintaining the data needed, and reviewing the collection of information. Send comments regarding this burden estimate or any other aspect of this collection of information, including suggestions for reducing this burden, to Washington Headquarters Services, Directorate for Information Operations and Reports, 1215 Jefferson Davis Highway, Suite 1204, Arlington, VA 22202-4302, and to the Office of Information and Regulatory Affairs, Office of Management and Budget, Washington, DC 20503.

1. AGENCY USE ONLY *(Leave blank)*	2. REPORT DATE November 1993	3. REPORT TYPE AND DATES COVERED Technical

4. TITLE AND SUBTITLE

Sound Speed, Reflectivity, Absorption, and Thermal Diffusivity Measurements in Arctic Ice in 1990

5. FUNDING NUMBERS

Contract N00039-91-C-0072

6. AUTHOR(S)

G.R. Garrison, K.L. Williams, P.D. Mourad, R.E. Francois, T. Wen, and W.J. Felton

7. PERFORMING ORGANIZATION NAME(S) AND ADDRESS(ES)

Applied Physics Laboratory
University of Washington
1013 NE 40th Street
Seattle, WA 98105-6698

8. PERFORMING ORGANIZATION REPORT NUMBER

APL-UW TR9208

9. SPONSORING / MONITORING AGENCY NAME(S) AND ADDRESS(ES)

Code 1125AR (T. Curtin)
Office of the Chief of Naval Research, Department of the Navy
Ballston Center Tower #1
800 N. Quincy Street
Arlington, VA 22217-5000

10. SPONSORING / MONITORING AGENCY REPORT NUMBER

11. SUPPLEMENTARY NOTES

12a. DISTRIBUTION / AVAILABILITY STATEMENT

Distribution Unlimited

12b. DISTRIBUTION CODE

13. ABSTRACT *(Maximum 200 words)*

Detailed measurements of internal properties of Arctic ice were made in Spring 1990 to relate acoustic properties to the physical properties of the ice. This report presents the procedures, analyses, and results of those studies. Some basic parameters measured in previous field studies were remeasured; consistency between individual experiments strengthens our confidence in the results and the techniques used. Novel techniques were used to measure properties of growing ice, which was later cored, submerged, and remeasured. Results reported here have been summarized in the open literature [Williams et al., *J. Acoust. Soc. Am.*, 92, 2075, 1992]. The basic data and their processing are described here in detail.

In the ice-growth and submergence study, a 2-m-square hole was cut though the ice canopy. Strings of hydrophones and thermistors were then suspended vertically in the hole, and the water froze around them. Frequent monitoring of ice temperature and the receipt of sound pulses from below, along with salinities determined from ice cores obtained a short distance away, gave insight into the freezing process and the formation of a skeletal layer above the ice/water interface. Periodic measurements of the reflectivity of the growing ice at 37–150 kHz gave further information on the skeletal structure. The sound speed in the skeletal layer varied from that of the water at the ice/water interface to that of bulk ice at about 3 cm into the ice. Absorption of sound (in decibels per meter) was about three times greater near the interface, decreasing to that for bulk ice at 15–20 cm into the ice. When an ice block was cored from the new ice and forced downward 1 m, it warmed to the water temperature in about 3 days. During this time, sound speed, absorption, and reflectivity were monitored and showed effects of the added pressure and higher temperature. The average thermal diffusivity of the ice was between 0.0015 and 0.0035 cm^2/s, with the lower values being obtained when more of the ice was at a temperature near the melting point.

14. SUBJECT TERMS

Ice acoustic properties — reflection, sound speed, attenuation
Ice bulk properties — porosity, thermal conductivity

15. NUMBER OF PAGES
170

16. PRICE CODE

17. SECURITY CLASSIFICATION OF REPORT	18. SECURITY CLASSIFICATION OF THIS PAGE	19. SECURITY CLASSIFICATION OF ABSTRACT	20. LIMITATION OF ABSTRACT
Unclassified	Unclassified	Unclassified	SAR